

Mutational and functional investigation of hemolysin A secretion in *Escherichia coli*

Inaugural-Dissertation

zur Erlangung des Doktorgrades

der Mathematisch-Naturwissenschaftlichen Fakultät

der Heinrich-Heine-Universität Düsseldorf

vorgelegt von

Manuel Tobias Anlauf

aus Duisburg

Düsseldorf, November 2023

aus dem Institut für Biochemie
der Heinrich-Heine-Universität Düsseldorf

Gedruckt mit der Genehmigung
der Mathematisch-Naturwissenschaftlichen Fakultät der
Heinrich-Heine-Universität Düsseldorf

Berichtersteller:

1. Prof. Dr. rer. nat. Lutz Schmitt

2. Prof. Dr. rer. nat. Michael Feldbrügge

Tag der mündlichen Prüfung: 18.12.2023

„Progress is made by trial and failure; the failures are generally a hundred times more numerous than the successes, yet they are usually left unchronicled.”

William Ramsay

Abstract

Gram-negative bacteria have developed a variety of secretion systems to transport molecules and communicate with their environment. One of the simplest arrangements is the Type I Secretion System (T1SS), whose hallmark is the transport of substrates across the inner and outer bacterial membrane in an unfolded state without the occurrence of a periplasmic intermediate. Translocation is mediated via a C-terminal secretion signal and accomplished by a tripartite protein complex consisting of an ATP-binding cassette (ABC) transporter and a membrane fusion protein (MFP) in the inner membrane and an outer membrane protein (OMP). One prominent example is the hemolysin A (HlyA) secretion system of uropathogenic *Escherichia coli*, in which the ABC transporter hemolysin B (HlyB) and MFP hemolysin D (HlyD) together with the OMP TolC transport the 1024 amino acid long HlyA, a member of the repeats in toxin (RTX) protein superfamily. In addition to the conserved nucleotide binding domain (NBD) and transmembrane domain (TMD), HlyB features an N-terminal C39 peptidase-like domain (CLD).

During this thesis, the identity and interplay of the domains of HlyB in respect to secretion were investigated. The CLD, TMD and/or NBD of HlyB were exchanged with the respective domain of the homologous ABC transporter RtxB from *Kingella kingae* and the ability of the chimeric transporters to transport HlyA was quantified. It was shown, that all three domains confer specificity for the secreted substrate and play closely together during secretion. The CLD is the most important specificity determinant, as an exchange led to complete abolishment of secretion. Single substitutions of either the TMD or NBD were tolerated but showed a threefold reduced secretion, while a simultaneous exchange also inhibited secretion of HlyA.

Furthermore unnatural amino acids were successfully introduced into proteins of the hemolysin system for photo-crosslinking. In the stalled complex, p-benzoyl-L-phenylalanine incorporated into eGFP-HlyA crosslinked to HlyB upon UV irradiation. The molecular weight of crosslinked species suggests the presence of two copies of HlyA at the transporter during secretion. With this, the means to map the translocation pathway of HlyA through the transporter are finally in hand.

Zusammenfassung

Gram-negative Bakterien haben eine Vielzahl an Sekretionssystemen entwickelt, um Moleküle zu transportieren und mit ihrer Umgebung zu kommunizieren. Eines der einfachsten Systeme ist das Typ I Sekretionssystem (T1SS), dessen Kennzeichen der Transport von Substraten über die innere und äußere bakterielle Membran in einem ungefalteten Zustand und ohne ein periplasmatisches Zwischenprodukt ist. Die Translokation wird über ein C-terminales Sekretionssignal vermittelt und von einem dreiteiligen Proteinkomplex ausgeführt, welcher aus einem *ATP-binding cassette* (ABC) Transporter und einem Membranfusionsprotein (MFP) in der inneren Membran sowie einem äußeren Membranprotein (OMP) besteht. Ein bekanntes Beispiel ist das Hämolyisin A (HlyA) Sekretionssystem uropathogener *Escherichia coli*, in welchem der ABC Transporter Hämolyisin B (HlyB) und das MFP Hämolyisin D (HlyD) zusammen mit dem OMP TolC das 1024 Aminosäuren lange HlyA transportieren, ein Mitglied aus der *repeats in toxins* (RTX) Protein-Superfamilie. Zusätzlich zu der konservierten Nukleotid-bindenden Domäne (NBD) und Transmembrandomäne (TMD) weist HlyB eine N-terminale C39 Peptidase-ähnliche Domäne (CLD) auf.

In dieser Dissertation wurde die Identität und das Zusammenspiel der Domänen von HlyB in Bezug auf die Sekretion untersucht. Die CLD, TMD und/oder NBD von HlyB wurden mit der entsprechenden Domäne des homologen ABC Transporters RtxB aus *Kingella kingae* ausgetauscht und die Fähigkeit der chimären Transporter, HlyA zu transportieren, quantifiziert. Es konnte gezeigt werden, dass alle drei Domänen Spezifität für das sekretierte Substrat verleihen und während der Sekretion eng zusammenspielen. Die CLD ist die wichtigste Spezifitätsdeterminante, da ein Austausch zum vollständigen Wegfall der Sekretion führte. Einzelne Substitutionen der TMD oder NBD wurden toleriert, führten aber zu einer dreifach reduzierten Sekretion, während ein gleichzeitiger Austausch ebenfalls die Sekretion von HlyA verhinderte.

Darüber hinaus wurden unnatürliche Aminosäuren erfolgreich in Proteine des Hämolyisin Systems zur Photo-Quervernetzung eingeführt. Im arretierten Zustand vernetzte sich das in eGFP-HlyA eingebaute p-Benzoyl-L-Phenylalanin bei UV-Bestrahlung mit HlyB. Das Molekulargewicht der vernetzten Spezies lässt darauf schließen, dass sich während der Sekretion zwei Kopien von HlyA am Transporter befinden. Damit stehen nun die Mittel zur Verfügung, um den Translokationsweg von HlyA durch den Transporter zu kartieren.

Table of Contents

Abstract	I
Zusammenfassung	II
1. Introduction	1
1.1. Transport across biological membranes	1
1.2. Protein secretion in Gram-negative bacteria.....	2
1.2.1. The Sec dependent pathway	3
1.2.2. The twin-arginine translocation pathway	5
1.3. Dedicated secretion systems in Gram-negative bacteria.....	6
1.3.1. RND efflux pumps.....	6
1.3.2. Type I secretion systems (T1SS).....	8
1.3.3. Type II secretion systems (T2SS).....	11
1.3.4. Type III secretion systems (T3SS).....	12
1.3.5. Type IV secretion systems (T4SS)	14
1.3.6. Type V secretion systems (T5SS)	16
1.3.7. Type VI secretion systems (T6SS)	18
1.3.8. Type VII secretion systems (T7SS)	19
1.3.9. Type VIII secretion systems (T8SS)	21
1.3.10. Type IX secretion systems (T9SS)	21
1.3.11. Chaperone-usher pathway	23
1.4. The hemolysin A type I secretion system.....	24
1.4.1. The toxin HlyA	25
1.4.2. The ABC transporter HlyB	27
1.4.3. The membrane fusion protein HlyD	32
1.4.4. The outer membrane protein TolC.....	34
1.4.5. The secretion mechanism.....	35
2. Aims	37

3.	Publications.....	39
3.1.	Chapter 1: ABC Transporters in Bacterial Nanomachineries.....	39
3.2.	Chapter 2: Subcellular localization of HlyA mRNA in <i>Escherichia coli</i>	70
3.3.	Chapter 3: Photo-crosslinking of the hemolysin A type 1 secretion system using unnatural amino acids	107
3.4.	Chapter 4: Type 1 secretion necessitates a tight interplay between all domains of the ABC transporter.....	171
4.	Discussion.....	212
4.1.	What keeps HlyA stable in the cytoplasm?	212
4.2.	The HlyB CLD is a key player during HlyA secretion	216
4.3.	The HlyB TMD as an additional interaction site	219
4.4.	The NBD: more than a powerhouse.....	223
4.5.	Secretion of HlyA and the multiple interactions between hemolysin proteins... ..	224
5.	Bibliography	228
6.	List of Abbreviations.....	252
7.	List of Figures.....	258
8.	Acknowledgements	259
9.	Curriculum vitae	265
10.	Declaration	267

1. Introduction

1.1. Transport across biological membranes

Cells are considered to be the structural and functional units of life. They are able to perform a multitude of metabolic reactions, transport molecules, sense and communicate with their surroundings and replicate themselves. Be it eukaryotes, archaea or bacteria, all cells and their cellular contents are separated from each other and the extracellular space by at least one cell membrane. Usually, these membranes are synthesized from fatty acids ester-bound to glycerol-3-phosphate and build double-layered structures. One exception are archaea, which produce membranes using isoprenoid lipids ether-linked to glycerol-1-phosphate, which are able to form lipid monolayers as well (Siliakus *et al.* 2017). The cell membrane is only permeable for small hydrophobic and neutral molecules like oxygen and impermeable for ions and other hydrophilic and larger compounds like glucose or amino acids (Alberts *et al.* 2002). Because of this, cells developed a multitude of options for the uptake of metabolites and ions on the one hand and to export e.g. signalling molecules, scavenging proteins and toxins into their surrounding environment (Stillwell 2013).

In Gram-negative bacteria, which possess a double membrane envelope, the diffusion of molecules into and out of the cell is mediated by two types of proteins (Hancock 1987, Nikaido 1992, Nikaido 2003). Porins on the one hand are transmembrane β -barrel proteins that allow the passage of water or a range of small charged molecules. Channels on the other hand contain specific binding sites and catalyze the transport of a class of nutrients, e.g. oligosaccharides of the maltose series. Both transport types allow only the transport of solutes alongside a concentration gradient, often referred to as “facilitated diffusion” (Carruthers 1990). The transport of molecules against a concentration gradient is called active transport and can be achieved in two ways (Albers *et al.* 2012): one option is to couple the transport of a substrate to the movement of other solutes from existing concentration gradients. This so called secondary active transport occurs either in the form of symport, where the substrate is transported in the same direction as the ion - the lactose permease LacY being a prominent example - or in the form of antiport, where substrate and ion are transported in opposing directions e.g. the Na^+/H^+ antiporter NhaA (Abramson *et al.* 2004, Hunte *et al.* 2005). Another option is primary active transport, where the pumping of a solute

is facilitated directly by the usage of energy, which is in most cases the hydrolysis of ATP, as in the case of the Na⁺/K⁺ ATPase (Shinoda *et al.* 2009).

1.2. Protein secretion in Gram-negative bacteria

The bacterial domain of life can be subdivided into two groups, depending on their properties displayed during Gram staining (Gram 1884). While Gram-positive bacteria exhibit a thick cell wall consisting of peptidoglycan on top of their cell membrane, Gram-negative bacteria possess two membranes, an inner membrane (IM) and an outer membrane (OM) separated by a periplasm with a considerably thinner cell wall (Perkins 2012). The building blocks of biological membranes are amphipathic lipids, which are in most cases glycerophospholipids. Two hydrophobic fatty acids are connected via a glycerol moiety to a hydrophilic phosphate group and a variable head group. Depending on the organism or compartment, those can be e.g. phosphatidylethanolamine (PE), phosphatidylglycerol (PG), cardiolipin (CL), phosphatidylinositol (PI), phosphatidic acid (PA) or phosphatidylserine (PS). In *Escherichia coli* (*E. coli*) the first three named headgroups are predominantly found with ~75% for PE, ~20% for PG and ~5% for CL (Raetz and Dowhan 1990, Sohlenkamp and Geiger 2015). The OM of Gram-negative bacteria is unusual, as it is highly asymmetrical. The inner leaflet consists of glycerophospholipids while the outer leaflet is comprised of mainly lipopolysaccharides (LPS) (Beveridge 1999).

LPS in the outer leaflet of the OM forms a stable network containing divalent cations and displays a potent permeability barrier against xenobiotics. Although its structure varies between different bacteria, the general architecture involves three parts: the anchoring to the membrane is ensured by β -1'-6-linked glucosamine disaccharides, called Lipid A. Every sugar moiety of Lipid A is acylated with fatty acid chains and in *E. coli* the glucosamine moiety is additionally phosphorylated. 3-deoxy-D-manno-oct-2-ulosonic acid connects Lipid A to the core oligosaccharide, which in turn is linked to the O antigen, a highly diverse oligosaccharide polymer (Whitfield and Trent 2014, Bertani and Ruiz 2018).

The fundamental structural features of the peptidoglycan layer are identical for Gram-positive and Gram-negative bacteria. The cell walls peptidoglycan strands are composed of alternating residues of *N*-acetylglucosamine (NAG) and *N*-acetylmuramic

acid (NAM) joint by β -1-4 bonds. In the mature polymer, single strands are crosslinked at the NAM residue via tetrapeptides. In Gram-negative bacteria this peptide is usually made up of L-Ala, D-Glu, 2,6-diaminopimelic acid (DAP) and D-Ala with the crosslink formed between DAP of one peptide and D-Ala of an opposing peptide (Vollmer *et al.* 2008).

Considering the mechanical barrier posed by the membranes and cell wall, secretion of molecules displays a challenge particularly for Gram-negative bacteria. The transport across one membrane results in the release of the molecule into the extracellular space for Gram-positive bacteria, while the same process leaves the substrate in the periplasm of Gram-negative bacteria. Evolution provided bacteria with a spectrum of different secretion systems capable to transport molecules in one or two steps across one, two or even three membranes for some pathogenic organisms.

1.2.1. The Sec dependent pathway

Over one third of the bacterial proteome is synthesized at ribosomes in the cytoplasm but carry out their function on the opposing side of the membrane either as soluble or membrane-embedded proteins (Orfanoudaki and Economou 2014). A lot of those proteins are transported by the general secretion (Sec) pathway, also known as Sec61 dependent pathway in eukaryotes or SecY dependent pathway in archaea and bacteria; this section will only cover the bacterial pathway. Proteins meant for secretion are targeted to the translocator via their N-terminal signal sequence (Lee and Bernstein 2001, Peterson *et al.* 2003) by two different mechanisms, co-translationally or post-translationally with the participation of different interaction partners in these processes (Figure 1). In both cases, a protein conducting channel consisting of three integral membrane proteins is involved: SecY, which forms the actual channel, SecE, which wraps around it and stabilizes it, and SecG. Interestingly, SecY and SecE are highly conserved and essential for secretion, while SecG is not. The role of SecG is still not fully understood, but was reported to stimulate translocation activity and was postulated to improve the cycle of membrane insertion and dissociation of the ATPase SecA (Nishiyama *et al.* 1993, Duong and Wickner 1997).

Integral proteins of the IM and few secretory proteins are transported using the co-translational pathway (Figure 1). The translocation starts with the signal recognition

particle (SRP), a ribonucleoprotein complex, binding to the hydrophobic signal sequence or transmembrane helix (TMH) of the ribosome nascent chain (RNC) complex, and delivering it to its receptor FtsY in the IM (Grudnik *et al.* 2009). There, the RNC complex is handed over to the SecYEG translocon. Both SRP and FtsY are GTPases, which hydrolyze guanosine triphosphate (GTP) in order to dissociate from each other (Saraogi and Shan 2014). The bound ribosome then translates the polypeptide chain into the SecYEG channel and hydrophobic TMHs are inserted directly into the lipid layer via a lateral gate in SecY with the help of the insertase YidC (Komar *et al.* 2016, Steudle *et al.* 2021).

Most proteins destined to reside in the periplasm or the OM are conversely transported in a post-translational manner (Figure 1) (Saraogi and Shan 2014). There, the chaperone SecB or other universal chaperones bind to fully or partially synthesized proteins and keep them in a secretion-competent state (Wild *et al.* 1992, Driessen *et al.* 2001). The cargo is then delivered to the SecYEG-associated SecA, an essential protein in post-translational secretion which was also shown to participate in some co-translational transport (Cabelli *et al.* 1988, Hartl *et al.* 1990, Deitermann *et al.* 2005). SecA plays a dual role in the secretion process: it acts as receptor for secretory proteins and as an engine, that energizes the translocation by hydrolysis of adenosine triphosphate (ATP). Thereby, 20-30 residues of the protein are pushed stepwise into the SecYEG channel (Schiebel *et al.* 1991). The protein pair SecDF is assisting in translocation using the proton-motive force (PMF) and either captures the secretory protein on the periplasmic side in a ratchet mechanism or pulls it in a power stroke-based manner (Tsukazaki 2018).

In the case of outer membrane proteins, transit through the IM is mediated by the Sec pathway and then handed over to the β -barrel assembly machinery (BAM) complex (Tomasek and Kahne 2021, Troman and Collinson 2021). Aggregation of the cargo is prevented by periplasmic chaperones such as SurA, Skp and DegP (Soltes *et al.* 2017, Wang *et al.* 2021). Recent studies have revealed the multi protein structure consisting of BamABCDE to form a periplasmic traversing supercomplex in conjunction with proteins of the Sec pathway (Wang *et al.* 2016, Alvira *et al.* 2020). Similarly, lipoproteins with the OM as their final destination are transported by the designated Lol (localization of lipoproteins) system. After insertion in the IM by mostly the Sec pathway, lipoproteins are matured, extracted by the ATP-binding cassette (ABC)

transporter LolCDE, transferred to the periplasmic chaperone LolA and shuttled to the OM, where it is integrated to the lipid bilayer by LolB (Grabowicz 2019).

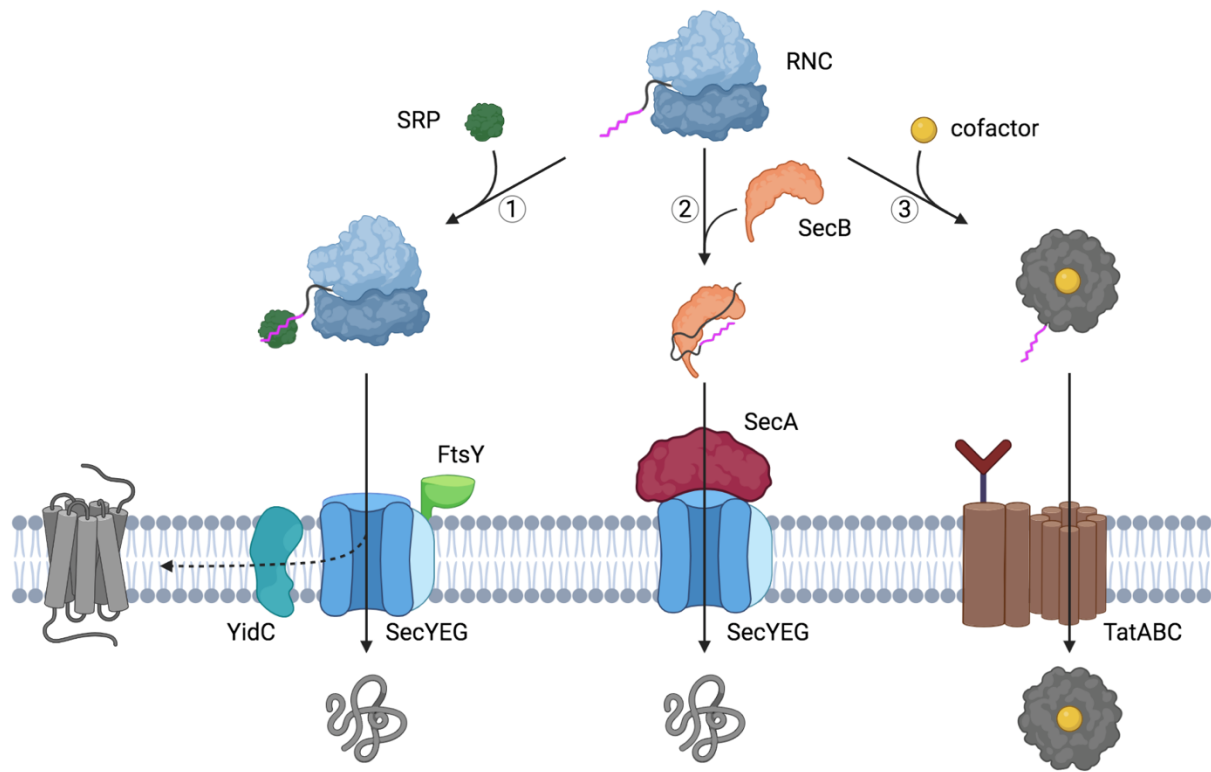


Figure 1: General secretion pathways in bacteria. Translocation occurs either Sec-dependent for unfolded proteins (1 & 2) or Tat-dependent for folded proteins (3). In co-translational targeting (1), the signal recognition particle (SRP, dark green) recognizes the signal peptide (magenta) of the ribosome nascent chain (RNC) complex and directs it to the SecYEG translocon (blue) with the help of its receptor FtsY (bright green). There, the ribosome translates the protein directly into the periplasm or into the membrane via a lateral gate and with the help of the insertase YidC (turquoise). In post-translational targeting (2), the chaperone SecB (orange) recognizes the signal peptide of translated, unfolded proteins and delivers it to the ATPase SecA (red), which translocates the protein through SecYEG. Folded proteins, e.g. cofactor (yellow) containing proteins are transported in *E. coli* to TatBC and recruit TatA (all brown), which oligomerizes and forms the channel for translocation (3). The figure was created with BioRender.com.

1.2.2. The twin-arginine translocation pathway

Contrary to the Sec pathway, which translocates only unfolded proteins, the twin-arginine translocation (Tat) pathway is responsible for the transport of folded proteins across the inner membrane (Figure 1). This route is necessary for proteins which need a controlled environment to fold prior to translocation, mostly because of the introduction of cofactors like [Cu-S] clusters, but also to allow the formation of hetero-oligomeric complexes or to prevent the binding of competing ions to metal-ion containing proteins (Sauvé *et al.* 2007, Tottey *et al.* 2008, Pomowski *et al.* 2011). The

systems name originates from the conserved dual arginine residues found in the signal peptide (Chaddock *et al.* 1995). In *E. coli*, TatC forms a membrane complex with TatB; the former recognizes the signal peptide while the latter is spatially close to the passenger domain (Cline and Mori 2001, Alami *et al.* 2003, Panahandeh *et al.* 2008). Afterwards, PMF-dependent recruitment and oligomerization of the TatB-homologous TatA occurs, which builds the actual channel with a diameter of 20-70 Å (Berks *et al.* 2000, Gohlke *et al.* 2005). After translocation, the signal sequence is cleaved, TatA depolymerizes and dissociates from TatBC (Mori and Cline 2002, Lüke *et al.* 2009).

1.3. Dedicated secretion systems in Gram-negative bacteria

The aforementioned secretion systems are all ubiquitously found in bacteria and used to transport a wide range of substrates across one membrane. Besides those, Gram-negative bacteria developed a range of more specialized secretion systems which either take over substrates transported to the periplasm by the Sec (or Tat) pathway or which transport their substrate from the cytosol directly to the extracellular space or into a host cell. These systems will be briefly introduced in this section.

1.3.1. RND efflux pumps

Transporters of the resistance-nodulation-division (RND) family are commonly found in Gram-negative bacteria. They are capable of secreting a wide range of structurally diverse antibiotics and play a major role in the mediation of multidrug resistance (Nikaido and Pagès 2012). Other protein families related to multidrug efflux are multidrug and toxin extrusion (MATE), major facilitator superfamily (MFS) and small multidrug resistance (SMR), all of which are secondary transporters translocating their substrate across the inner membrane and will not be addressed here (Yan 2015, Bay and Turner 2016, Claxton *et al.* 2021). RND systems utilize ion gradients to energize the translocation, the PMF to be precise, and form multiprotein systems, which span both membranes and secrete their substrate across the inner and outer membrane (Sennhauser *et al.* 2009, Eicher *et al.* 2014). They consist of three proteins: an outer membrane protein (OMP) in the OM as well as a membrane fusion protein (MFP) and

an RND pump both located in the IM (Figure 2). The typical architecture consists of a trimeric RND pump and a trimeric OMP connected by a hexameric MFP with prominent systems being MexAB-OprM from *Pseudomonas aeruginosa* and AcrAB-TolC from *E. coli*, from which the latter will be exemplified (Tsutsumi *et al.* 2019, Glavier *et al.* 2020).

The RND pump AcrB is anchored to the IM with 12 TMHs per protomer and displays two periplasmic domains, being a porter domain and a distal funnel or docking domain. The TMD contains critical residues for the translocation of protons, while the porter domain forms the binding pockets and, together with the TMD, four entrance channels, through which substrates can enter from the periplasm or IM (Seeger *et al.* 2006, Su *et al.* 2006, Sennhauser *et al.* 2007, Oswald *et al.* 2016, Zwama *et al.* 2018, Tam *et al.* 2020). Crosslinking studies hinted the docking domain to directly interact with TolC in a “wrapping model” (Touzé *et al.* 2004, Tamura *et al.* 2005, Lobedanz *et al.* 2007, Symmons *et al.* 2009). However, structures derived from cryogenic electron microscopy (cryo-EM) and cryogenic electron tomography (cryo-ET) as well as structures from similar RND systems suggest that the connection to the OMP is mediated by the MFP AcrA in a tip-to-tip manner (Z. Wang *et al.* 2017, Shi *et al.* 2019, Tsutsumi *et al.* 2019). AcrA exhibits four domains, a membrane proximal domain, a β -barrel domain, a lipoyl domain and an α -helical domain. The α -helical domain is interacting with the hairpin portions of TolC, the membrane proximal domain and β -barrel domain are involved in interactions with AcrB while the lipoyl domain is responsible for inter-MFP interactions (Du *et al.* 2014). The TolC trimer forms a 12-stranded β -barrel in the OM and protrudes 100 Å into the periplasm with 12 α -helices, forming six hairpins for the above mentioned interactions with AcrA (Koronakis *et al.* 2000). AcrZ is an auxiliary, α -helical protein shown to interact with the TMD of AcrB and to be involved in the secretion of some AcrB substrates (Hobbs *et al.* 2012, Du *et al.* 2014). Recent studies revealed AcrA and AcrB to form a stable complex connected to the peptidoglycan layer via AcrA (Shi *et al.* 2019). Complex formation with TolC is stabilized in the presence of substrates, even though recruitment of TolC occurs even in the absence of substrates (Tikhonova and Zgurskaya 2004, Touzé *et al.* 2004).

The transport cycle of the RND pump AcrB resembles the mechanism of the F_1F_0 -ATP synthase, as the three protomers of the pump one by one undergo three asymmetric conformations (Boyer 1997). In the “loose” conformation, the proximal binding pocket

is open to the periplasm and substrates can enter the transporter. Switching to the “tight” conformation leads to the expansion of the distal binding pocket and tighter substrate binding with concomitant constriction of the proximal binding pocket. The exit gate is still closed at this point. Proton-uptake by the TMD leads to the opening of the exit gate while the binding pockets close. The substrate is pushed into the TolC channel in this “open” state. The reset to the “loose” state is achieved after proton-release to the cytoplasm (Kobylka *et al.* 2020).

1.3.2. Type I secretion systems (T1SS)

Judging from the systems architecture, T1SSs are similar to RND efflux systems since they are tripartite systems as well, featuring an OMP, MFP and transporter (Figure 2). Nevertheless, there are two major differences between the two systems. First of all, RND pumps utilize the PMF to translocate substrates, while T1SSs energize the secretion process via an ABC transporter and the hydrolysis of ATP. Furthermore, RND pumps show a pronounced substrate promiscuity, whereas T1SS are usually highly specific and only transport one substrate, which is encoded in an operon together with the MFP and ABC transporter (Thomas *et al.* 2014b). The OMP is not necessarily part of the operon and often used by other transport systems as well with TolC being one example (Costa *et al.* 2015). Substrates are transported unfolded across both membranes in one step without the occurrence of a periplasmic intermediate. The only exception known is the T1SS found in *Pseudomonas fluorescens* Pf0-1, catalyzing the secretion of the giant (>5000 amino acids) adhesin LapA (El-Kirat-Chatel *et al.* 2014). It is unique, as the protein contains an N-terminal retention module, anchoring LapA to the membrane and creating a secretion intermediate arrested in the translocation channel until the retention module is cleaved by the periplasmic protease LapG (Smith *et al.* 2018).

The ABC transporter of T1SSs is a dimer with a TMD, built up by 6 TMHs, and a nucleotide binding domain (NBD) per monomer. Many of those transporters contain an additional domain at the cytosolic N-terminus and can be divided into three groups, depending on the presence and type of the extension (Kanonenberg *et al.* 2013). Transporters of group 1 feature an active C39 peptidase domain cleaving the N-terminal leader peptide before secretion of the substrate, which are small peptides of

the bacteriocin family (Havarstein *et al.* 1995, Duquesne *et al.* 2007, Lecher *et al.* 2012). One example is the colicin V system comprising the transporter CvaB, the MFP CvaA, the OMP TolC and the substrate ColV from *E. coli* (Gilson *et al.* 1990). Translocation of the substrate follows a cycle of conformational changes, where the transporter switches between an inward-facing open and an outward-facing open conformation (Bountra *et al.* 2017).

T1SS transporters of group 2 are structurally very similar to those of group 1 as they contain a peptidase domain as well, albeit inactive and therefore called C39 peptidase-like domain (CLD) (Kanonenberg *et al.* 2013). The missing protease activity does not mean that the domain is not relevant, as it still interacts with the substrate and deletion of the CLD leads to omitted substrate secretion as seen for hemolysin B (HlyB) (Lecher *et al.* 2012). Moreover, the secretion process of the substrate is fundamentally different. First of all, secreted substrates are several magnitudes bigger with the largest ones being from the multifunctional autoprocessing repeats in toxins (MARTX) family and the aforementioned adhesins (Spitz *et al.* 2019). Secondly, substrates of T1SS group 2 transporters feature a C-terminal secretion signal, which reaches the extracellular space first and is not cleaved (Lenders *et al.* 2015). Additionally, all substrates belong to the repeats in toxins (RTX) protein family (Lecher *et al.* 2012). They are characterized by the presence of 10-40 “GG-repeats”, glycine-rich nonapeptides with the consensus sequence “GGxGxDxUx” (with x being any amino acid and U being a large hydrophobic amino acid) (Linhartová *et al.* 2010). These repeats bind to Ca²⁺ with micromolar affinity and induce folding of the protein only after it reached the outside of the cell (Sanchez-Magraner *et al.* 2007, Thomas *et al.* 2014a). In case of the hemolysin A (HlyA) T1SS system, the ABC transporter together with the MFP forms a stable inner membrane complex (IMC) (Pimenta *et al.* 1999, Zhao *et al.* 2022). The outer membrane protein is recruited upon substrate recognition by the IMC (Thanabalu *et al.* 1998, Balakrishnan *et al.* 2001). HlyA interacts with the NBD as well as the CLD via its secretion signal and GG repeats (Benabdelhak *et al.* 2003, Lecher *et al.* 2012, Pourhassan *et al.* 2022). The main focus of this thesis is the HlyA T1SS, one of the best studied T1SS of group 2, and will be exemplified in detail in a later section (section 1.4).

Lastly, T1SS transporters of group 3 lack an additional N-terminal domain and follow the classical domain organization of ABC transporters (Kanonenberg *et al.* 2013). They

convey a C-terminal secretion just like T1SS transporters of group 2 but substrates are not necessarily RTX proteins. A well investigated system is the Has system, responsible for secretion of the 19 kDa hemophore HasA in *Serratia marcescens* (Létoffé *et al.* 1994, Arnoux *et al.* 1999). It is distinct from systems of group 2 as complex formation, the secretion process and the role of the secretion signal are different. On one hand, the substrate is secreted with its N-terminus first. On the other hand, the ABC transporter HasD recognizes its substrate via multiple interaction sites in HasA even without the presence of the secretion signal and forms a stable complex with the MFP HasE (Cescau *et al.* 2007, Masi and Wandersman 2010). The secretion signal is rather involved in the dissociation of the secretion complex once translocation is finished (Cescau *et al.* 2007).

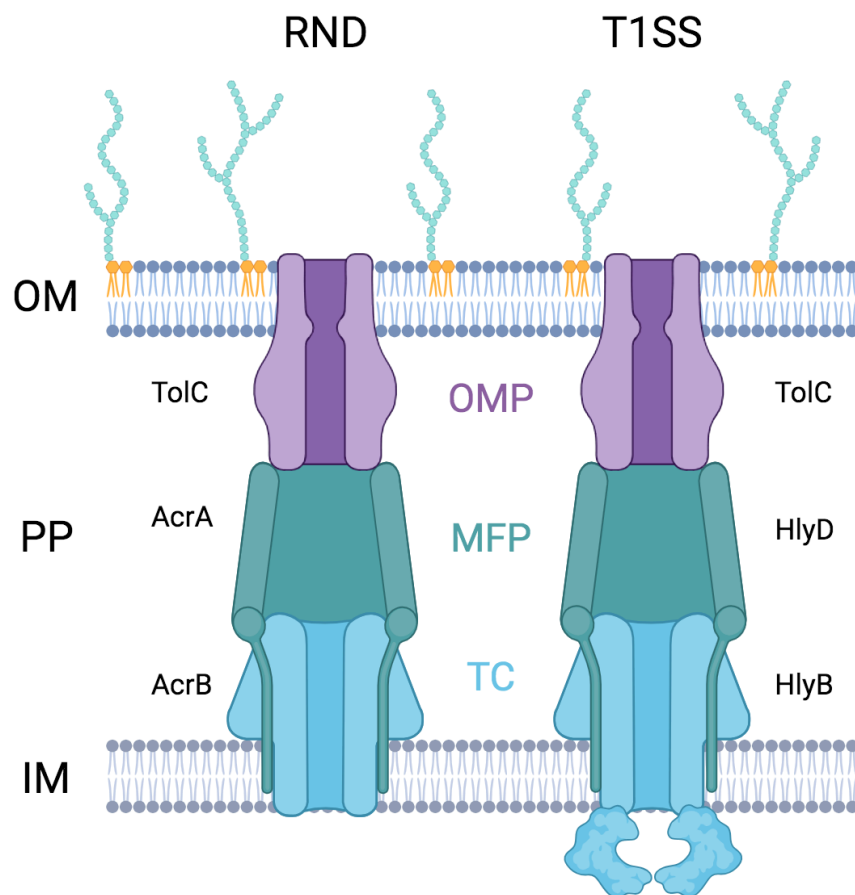


Figure 2: Structural organization of an RND system and T1SS. Resistance-nodulation-division (RND, left) systems and type I secretion systems (T1SS, right) share the same architecture with an outer membrane protein (OMP, purple) in the outer membrane (OM) reaching into the periplasm (PP) and connected to the transporter components (TC, blue) in the inner membrane (IM) via a membrane fusion protein (MFP, turquoise). Protein names of the acridine resistance (Acr) system and the hemolysin (Hly) system from *E. coli* are given as examples for the RND system and T1SS respectively. Both systems transport substrates in one step across both membranes. RND systems utilize the PMF, while T1SS hydrolyze ATP to energize the system. The figure was created with BioRender.com.

1.3.3. Type II secretion systems (T2SS)

T2SS can be found in pathogenic and non-pathogenic Gram-negative bacteria and take over folded substrates transported to the periplasm by the Sec or Tat pathway and execute the transfer across the OM (Costa *et al.* 2015). Substrates are mostly hydrolytic enzymes important for biopolymer degradation and nutrient acquisition (Nivaskumar and Francetic 2014). The secretion complex consists of up to 15 proteins and can be subdivided into four parts (Figure 3): a cytoplasmic ATPase (GspE), an assembly complex in the IM (IMC: GspC, GspF, GspL and GspM), a periplasmic pseudopilus (GspG, GspH, GspI, GspJ, GspK), which in contrast to normal pili remains in the periplasm, and an OM complex (OMC: GspD, GspS) (Costa *et al.* 2015, Naskar *et al.* 2021). The latter is a pentadecameric ring-structure protruding into the periplasm and forming direct contacts with the assembly platform in the IM (Chernyatina and Low 2019). The hexameric ATPase energizes assembly of the pseudopilus and oligomerization of GspG (Patrick *et al.* 2011, Lopez-Castilla *et al.* 2017, Naskar *et al.* 2021). This pushes the substrate through the channel either like a piston or an Archimedes screw (Shevchik *et al.* 1997, Nivaskumar and Francetic 2014). However, targeting and entry of substrates into the secretion system as well as retraction/disassembly of the pseudopilus are still poorly understood. GspC in the IM was shown to be involved in the recognition of some, but not all substrates (Bouley *et al.* 2001, Pineau *et al.* 2014). ATPase activity of GspE is proposed to stall as soon as the pseudopilus tip reaches the OM complex and the pseudopilus disassembles passively (Naskar *et al.* 2021).

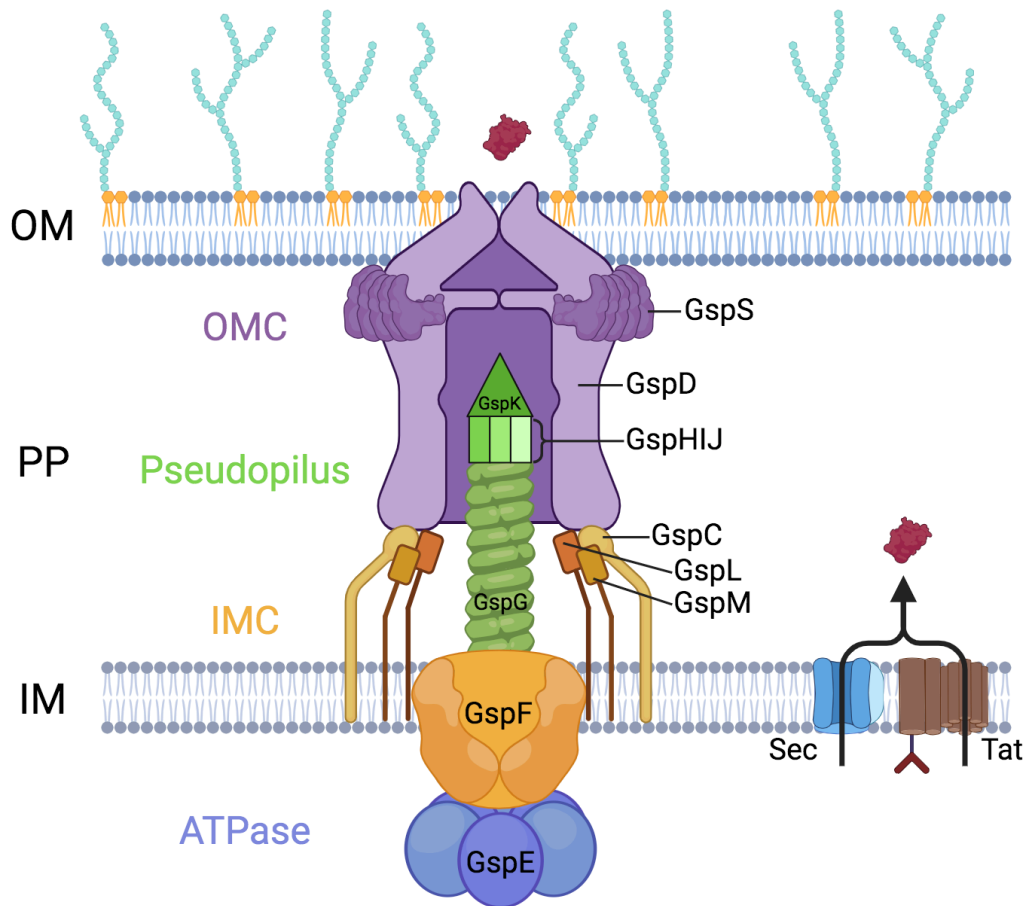


Figure 3: Structural organization of a T2SS. Substrates (red) are first transported by the Sec or Tat pathway across the inner membrane (IM) into the periplasm (PP) where they fold. An assembly consisting of an outer membrane complex (OMC, purple shades) and an inner membrane complex (IMC, orange shades) encase a pseudopilus (green shades) which pushes substrates through the outer membrane (OM). The process is powered by a cytoplasmic ATPase (blue). Protein names of the general secretion pathway (Gsp) from *E. coli* are given as an example. The figure was created with BioRender.com.

1.3.4. Type III secretion systems (T3SS)

Architecture and mechanism of T3SSs are remarkable in comparison to the already introduced systems, as they are able to transport a variety of effector proteins not only across the IM and OM but also through the membrane of eukaryotic cells (Galán and Wolf-Watz 2006). These systems are found in many pathogenic organisms like *Shigella*, enteropathogenic *E. coli* and the well-studied *Salmonella enterica* subsp. *enterica* serovar Typhimurium (Costa *et al.* 2015). The 3.5 MDa complex, often referred to as needle complex or injectisome, consists of over 20 different proteins forming five substructures (Figure 4): a cytosolic ATPase complex (SctN) and ring constituting the so-called sorting platform (SctKLOQ), an export apparatus in the IM (SctRSTUV), a basal body built by two ring structures in the IM (SctDJ) and OM (SctC)

sheathing a needle structure (SctF, SctI, SctA) and a translocator (SctB, SctE) forming a pore in the invaded cells membrane (Deng *et al.* 2017). Secretion of substrates is highly controlled and regulated by several proteins. SctP for example acts as a molecular ruler and regulates the length of the needle, while SctU and SctW switch between early, middle and late substrates (Journet *et al.* 2003, Cherradi *et al.* 2013, Monjarás Feria *et al.* 2015). The substrates contain an N-terminal secretion signal and are kept in a secretion-competent state by chaperones and recruited to the injectisome in a defined order depending on the associated chaperone (Birtalan *et al.* 2002, Samudrala *et al.* 2009, Job *et al.* 2010). Proteins constituting the needle and inner rod belong to the early substrates since they need to be assembled before the transport of further substrates. Translocator-forming proteins are middle substrates, which are secreted next and form the pore in the host membrane before late substrates are transported into the host cell (Deng *et al.* 2017). Those are effectors which suppress the hosts immune response, alter signal cascades and modulate hormone activity (Alfano and Collmer 2004, Espinosa and Alfano 2004, Cunnac *et al.* 2009). Once the needle is assembled and the bacterium senses its host, effectors are secreted utilizing ATP hydrolysis by the ATPase complex and the PMF (Lee and Rietsch 2015). Effectors are either directly injected into the host cell or, at least partly, secreted into the extracellular space before entering the cell in a binary AB toxin-like model (Akopyan *et al.* 2011, Galán *et al.* 2014, Deng *et al.* 2017).

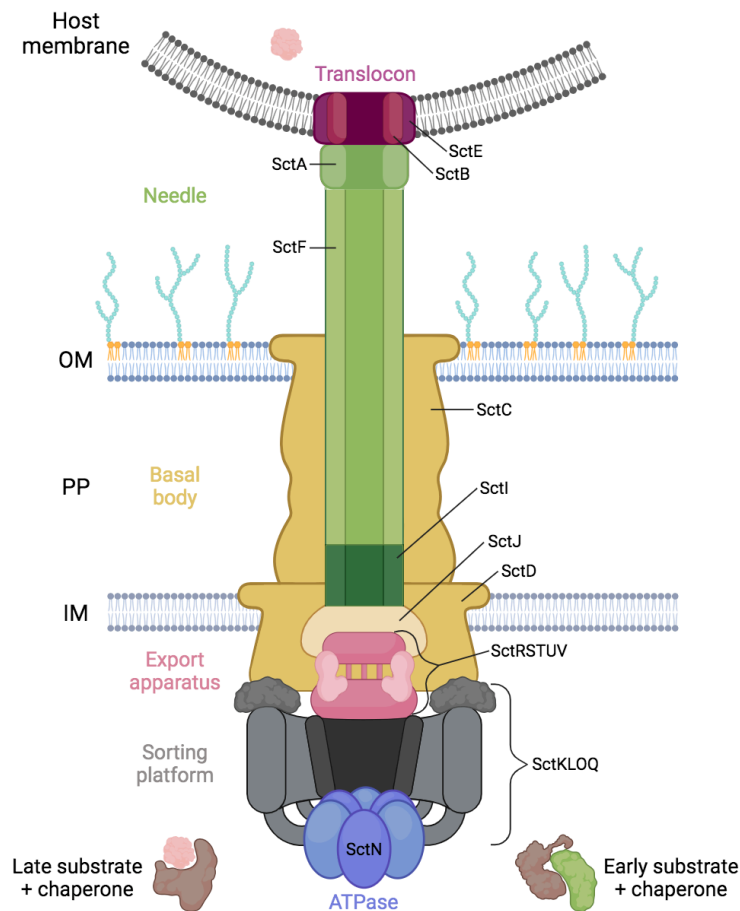


Figure 4: Structural organization of a T3SS. A basal body (yellow) of several ring-like subcomplexes connects the inner (IM) and outer membrane (OM) through the periplasm (PP) and surrounds the needle complex (green shades). The export apparatus (pink shades) at the base of the basal body acts as an entry point for substrates. Those are kept secretion-competent by chaperones (brown) and are recruited in an ordered manner to the sorting platform (grey shades). Early and middle substrates built the needle and translocator (red shades) in the host membrane before late substrates are secreted. The translocation process is energized by an ATPase (blue). Proteins are named using the unified secretion and cellular translocation (Sct) nomenclature. The figure was created with BioRender.com.

1.3.5. Type IV secretion systems (T4SS)

T4SSs are the most ubiquitous secretion system and not only found in Gram-negative bacteria, but also Gram-positive bacteria and archaea with a unique property: besides the secretion of proteins, these systems are able to inject deoxyribonucleic acid (DNA) into eukaryotic host cells or deliver/accept DNA in a process known as conjugation (Costa *et al.* 2015). The widespread use of this secretion system has resulted in a great structural diversity of the system. Still, a minimum amount of 12 so-called “signature subunits” (VirB1-VirB11 and VirD4) is used in Gram-negative bacteria, while this number is reduced to six in Gram-positive bacteria because of the lacking OM (Li *et al.* 2019). Proteins of the T4SS complex form a structure spanning both membranes

in Gram-negative bacteria (Figure 5A). A complex in the IM, formed by VirB3 and VirB8 together with the ATPase VirB4, is connected via a stalk (VirB5 and VirB6) to an outer membrane core complex (OMCC) constituted of ring structures of VirB7, VirB9 and VirB10 (Low *et al.* 2014, Macé *et al.* 2022). VirB8 is forming ring-like arches around the stalk. A periplasmic transglycosylase (VirB1) locally degrades the peptidoglycan layer, necessary for the construction of the protein channel across both membranes (Arends *et al.* 2013). The ATPases VirB4 and VirB11 together with the type IV coupling protein (T4CP) VirD4 are associated to the complex in the IM and energize multiple processes, ranging from the recruitment, processing and translocation of substrates to the biogenesis of the pilus (Li *et al.* 2019). The pilus itself is built up by a VirB5 tip and polymerized VirB2, which is proposed to use VirB6 as a base (Figure 5B) (Aly and Baron 2007, Macé *et al.* 2022, Amro *et al.* 2023). Insertion of substrates into the secretion channel is mediated by the T4CP, a translocation signal and can involve chaperones and additional proteins like a relaxase in the case of DNA substrates (Zechner *et al.* 2012). T4CP recognizes and delivers substrates to the secretion channel by binding to DNA, the relaxase or secreted effectors and energizes the substrate movement by ATP hydrolysis (Zechner *et al.* 2012, Llosa and Alkorta 2017). The translocation signals are in its simplest form hydrophobic or positively charged clusters at the C-terminus but can be more complex e.g. bipartite signals found in *Bartonella henselae* (Nagai *et al.* 2005, Schulein *et al.* 2005, Vergunst *et al.* 2005). Chaperones prevent premature folding and aggregation and help in presenting the translocation signal for recognition (Cambronne and Roy 2007, Alvarez-Martinez and Christie 2009). In case of DNA substrates, a relaxase forms the relaxosome with accessory proteins and processes the DNA destined for transport i.a. by nicking the DNA and covalently binding the 5' end to the relaxase (Zechner *et al.* 2012). This nucleoprotein is recognized via the relaxases translocation signal by T4CP and brought to the secretion complex, through which it is actively pumped into the recipient cell, where the nicking of the DNA is reversed (Cascales and Christie 2004, Zechner *et al.* 2012). Despite the new structural insights into the T4SS, the exact substrate translocation mechanism is still unknown and could either be a one-step secretion from the cytoplasm into another cell or a two-step secretion with a periplasmic intermediate (Trokter *et al.* 2014, Christie 2016).

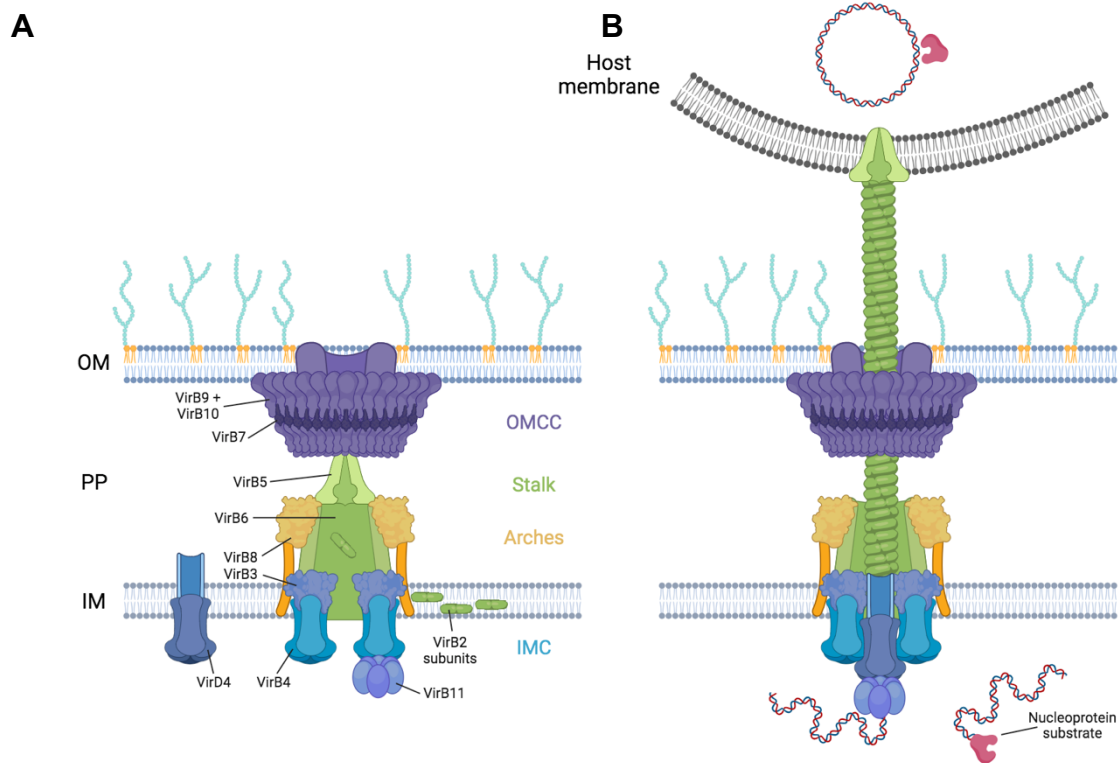


Figure 5: Structural organization of a T4SS. (A) An outer membrane core complex (OMCC, purple shades) is connected to the inner membrane complex (IMC, blue shades) by a stalk (green shades), which is stabilized by arch structures (yellow). In a first step, the pilus is formed using the stalk as a starting point with the process being energized by the ATPases VirB4 and VirB11. (B) Upon completion of the pilus and penetration of the host membrane, substrates (e.g. nucleoproteins) are secreted with the help of the ATPases VirD4 and VirB11. Protein names of the T4SS from *Agrobacterium tumefaciens* are given as an example. The figure was created with BioRender.com.

1.3.6. Type V secretion systems (T5SS)

The autotransporter system, also known as T5SS, form a β -barrel in the OM. Proteins belonging to this group are transported in an unfolded state and are therefore dependent on the Sec pathway and the BAM complex (Leo *et al.* 2012). Depending on the topology of the β -barrel domain and the secreted passenger domain (which function can be very diverse e.g. lipases, proteases, toxins or adhesins (Meuskens *et al.* 2019)) T5SSs can be classified in up to six groups: the classical autotransporters (Va), two-partner secretion systems (Vb), trimeric autotransporters (Vc), fused two-partner secretion systems (Vd), inverted autotransporters (Ve) and type-V-like (Vf) (Bernstein 2019, Meuskens *et al.* 2019). For simplicity, only the classical autotransporters will be described in detail here (Figure 6). After transport into the periplasm by the Sec pathway, autotransporters are kept mainly unfolded and their aggregation prevented by periplasmic chaperones like DegP, Skp and SurA (Baud *et*

al. 2009, Ieva and Bernstein 2009, Weirich *et al.* 2017). Only the C-terminal β -barrel folds partly and is targeted to the BAM complex where it starts to move into the OM (Ieva *et al.* 2008, Pavlova *et al.* 2013). Before complete integration into the membrane, the C-terminal part of the passenger domain forms a hairpin structure inside the β -barrel and is threaded through the pore C-terminus first (Henderson *et al.* 2004, Junker *et al.* 2009). The passenger is secreted by sequentially moving from its chaperone to the BAM complex through the β -barrel pore outside of the cell (Bennion *et al.* 2010, Pavlova *et al.* 2013, Bernstein 2019). Transport takes place without an external energy supply and is proposed to be driven by the vectorial folding of the passenger (Junker *et al.* 2006, Peterson *et al.* 2010). Complete folding resolves the hairpin and the passenger is often autocatalytically cleaved from the autotransporter (Leo *et al.* 2012).

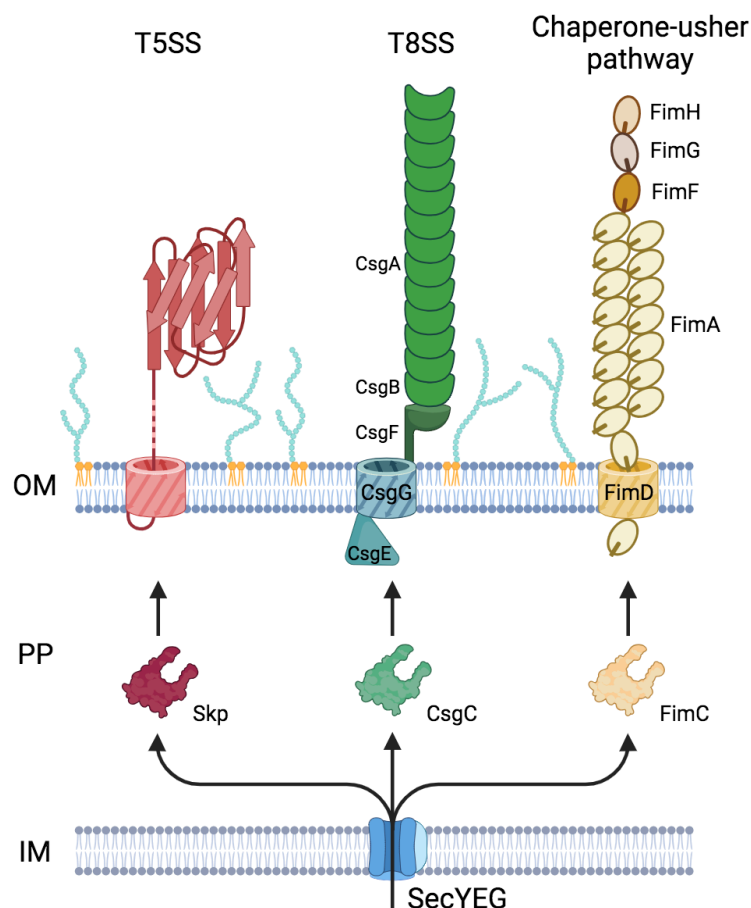


Figure 6: Structural organization of secretion systems spanning the outer membrane. In all cases, substrates are transported into the periplasm (PP) by SecYEG (blue). T5SS autotransporters (left, red shades) are kept unfolded by chaperones like Skp. Insertion into the outer membrane (OM) is mediated by the β -barrel assembly machinery (BAM) complex (not shown). The passenger can be cleaved from the translocator by a signal sequence (dashed line). CsgA is the main component of the T8SS (middle, green shades) and kept unfolded by the chaperone CsgC. It is recognized by CsgE, transported by CsgG and polymerizes on CsgB, which is anchored to the membrane by CsgF. The type I pili assembly is shown as an example for the chaperone-usher pathway (right, yellow shades). The pili subunits (major subunit: FimA, tip subunits: FimFGH) are folded by the chaperone FimC. Polymerization and transport through the membrane occurs through FimD. The figure was created with BioRender.com.

1.3.7. Type VI secretion systems (T6SS)

T6SSs are another system used by Gram-negative bacteria to transport proteins from their cytoplasm through the membrane of competitor or host cells. They are remarkably similar to the contractile injection machineries used by bacteriophages (Durand *et al.* 2015). It consists of 13 essential proteins, of which not all functions are clear, and forms three main complexes (Figure 7A) (Zheng and Leung 2007, Boyer *et al.* 2009, Nguyen *et al.* 2018, Navarro-Garcia *et al.* 2019): a transmembrane complex, a tail tube/sheath complex (TTC) and a baseplate. The transmembrane complex forms a channel through the IM and periplasm (TssL and TssM) and is connected to the OM via a lipoprotein (TssJ) (Rapisarda *et al.* 2019). It is connected to the baseplate (TssEFGK) on its cytoplasmic side, which acts as an adaptor for the TTC (Cherrak *et al.* 2018, Park *et al.* 2018). As the name suggests, the TTC is composed of two polymers, an inner tube (hexameric Hcp) and an outer sheath (hexameric TssBC dimers) (J. Wang *et al.* 2017). The tip of the inner tube is formed by VgrG, which resides in the baseplate and also acts as a nucleation point for Hcp during tail formation (Renault *et al.* 2018). During biogenesis, the metastable polymerizing tail is probably stabilized by the sheath (Zoued *et al.* 2014) and the cap structure of the tail, build by TssA (Santin *et al.* 2018). The latter was shown to play a key role in several stages of the T6SS complex formation, including formation of the membrane complex and recruitment of the baseplate (Zoued *et al.* 2017). Secreted substrates are either bound to the VgrG tip or inside the lumen of the tail built by Hcp (Durand *et al.* 2014, Whitney *et al.* 2014). Polymerization of the tail proceeds in the cytoplasm until the terminal cap reaches the opposite membrane and the associated protein TagA (Santin *et al.* 2018). Upon an unknown extracellular signal, the sheath contracts rapidly, penetrating the preys membrane and delivering substrates in the tube and attached to the tip directly into another cell (Figure 7B) (Costa *et al.* 2015, Cherrak *et al.* 2019). After contraction, the dedicated ATPase ClpV recycles the contracted sheath (Kapitein *et al.* 2013). What remains elusive is the mechanism of how the tip and tail pass the bacterial outer membrane, since structures of the transmembrane complex show no pore-forming component of sufficient size in the outer membrane (Durand *et al.* 2015, Rapisarda *et al.* 2019). It was therefore proposed, that the tip-tail-complex could penetrate the outer membrane together with the host membrane (Durand *et al.* 2015, J. Wang *et al.* 2017).

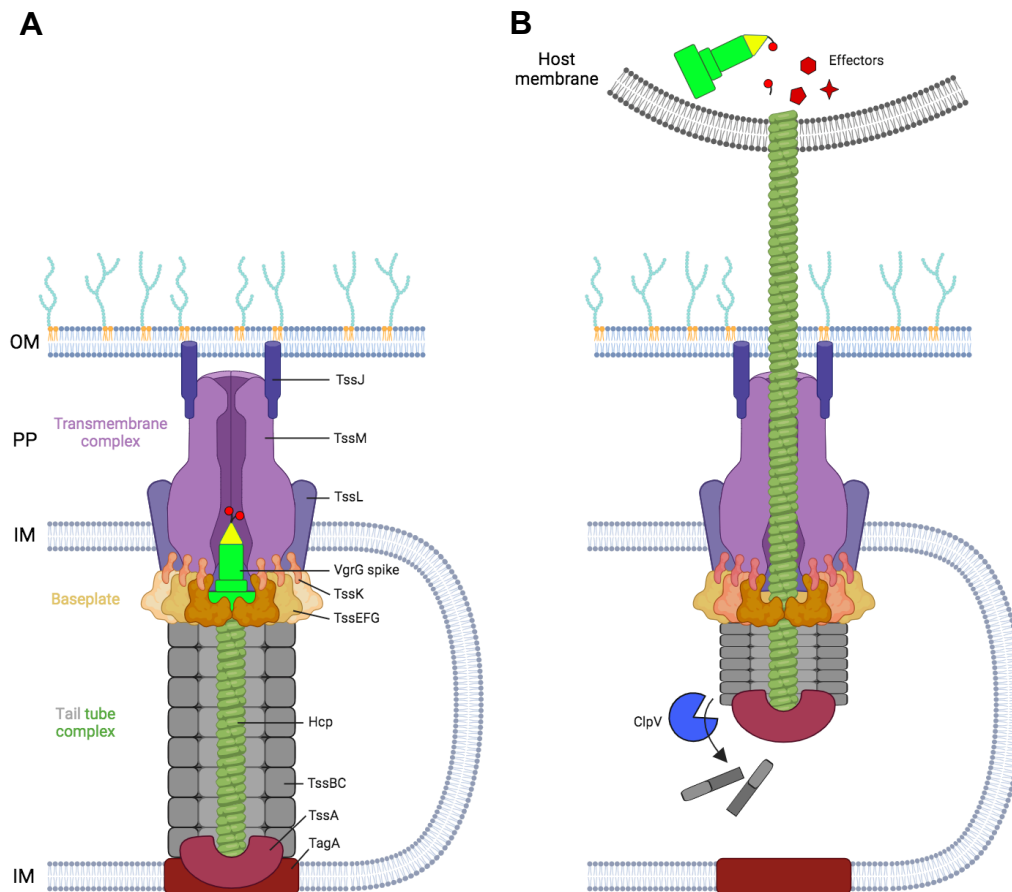


Figure 7: Structural organization of a T6SS. (A) Inner (IM) and outer membrane (OM) are connected by a transmembrane complex (purple shades). A baseplate (yellow shades) docks at the cytoplasmic side and acts as a nucleation point for the polymerization of the tail tube complex (grey and green respectively). Substrates are either associated with the spike protein (bright green and yellow) or loaded as cargo into the tube. Polymerization continues until the tails cap reaches the TagA stopper (both red) on the opposite side of the membrane. (B) Upon host cell recognition, the tail contracts and shoots the tube/spike complex including substrates (red, in the host cell) through the host membrane. A dedicated ATPase (blue) recycles the tails subunits. Protein names of the T6SS from *E. coli* are given as an example. The figure was created with BioRender.com.

1.3.8. Type VII secretion systems (T7SS)

The T7SS is so far not found in Gram-negative bacteria and only present in some Gram-positive bacteria as well as mycobacteria like *Mycobacterium tuberculosis*. Mycobacteria also exhibit a double-membrane envelope with a unique, thick and complex outer membrane containing mycolic acids (Bansal-Mutalik and Nikaido 2014, Rivera-Calzada *et al.* 2021). Therefore, the system will be described only very concise. The core assembly in the inner membrane is a multimeric complex with each protomer composed of four proteins (EccBCDE, Figure 8), which build a channel with a flexible array of four ATPase domains performing different functions (Rivera-Calzada *et al.* 2021). Additionally, a periplasmic protease MycP is associated to the membrane and

was shown to form a complex with EccBCDE (Beckham *et al.* 2021, Bunduc *et al.* 2021), while cytoplasmic chaperones (EspG) and ATPases (EccA) assist in the secretion process (DiGiuseppe Champion *et al.* 2009, Korotkova *et al.* 2014). The exact transport mechanism is still not clear. A universal component in the outer membrane was not identified so far and it remains unknown if transport occurs in one step across both membranes or in two steps with a periplasmic intermediate. Equally debated is the substrates route during secretion, travelling either through a central pore in the complex or through a pore in each individual protomer (Rivera-Calzada *et al.* 2021).

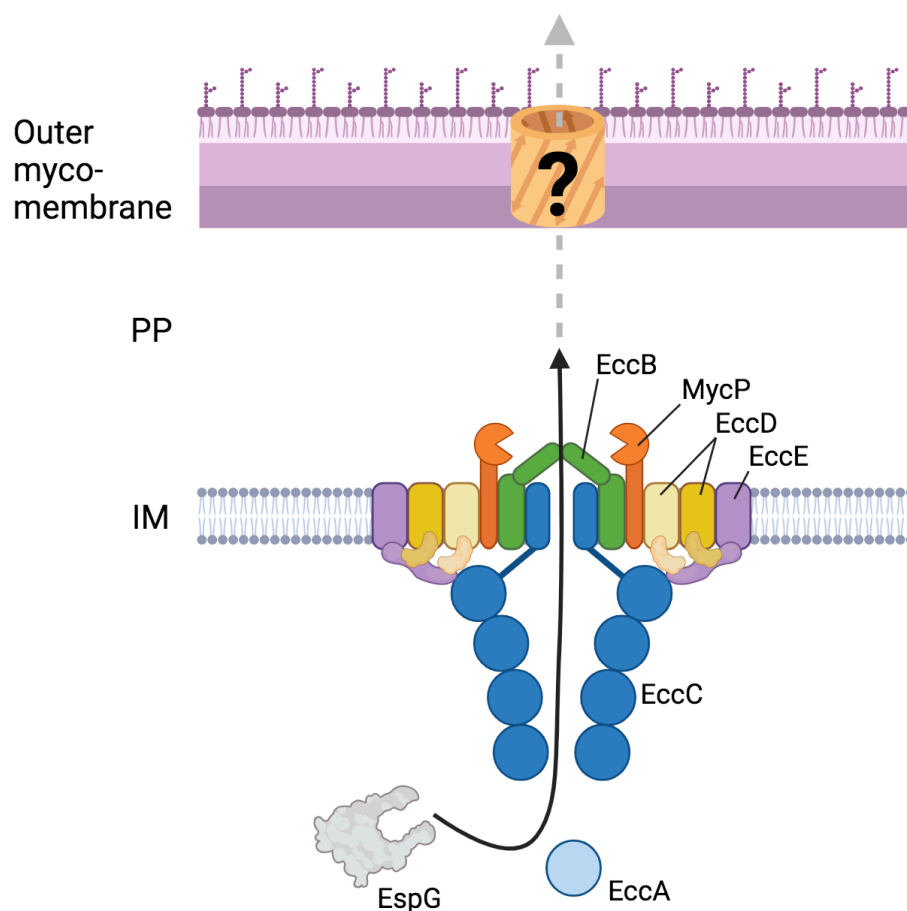


Figure 8: Structural organization of a T7SS. MycP (orange), EccB (green), EccC (blue) EccD (shades of yellow) and EccE (purple) form a complex in the inner membrane (IM). Substrates are translocated with the help of cytoplasmic chaperones (EspG, grey) and ATPases (EccA, light blue). The component in the mycomembrane is unknown as well as if the secretion occurs in one or two steps. Protein names of the T7SS from *Mycobacterium tuberculosis* are given as an example. The figure was created with BioRender.com.

1.3.9. Type VIII secretion systems (T8SS)

The T8SS, also known as the curli biogenesis pathway or nucleation-precipitation pathway, is responsible for the assembly of curli fibres on the cell surface of many Gram-negative bacteria and contributes to biofilm formation and cell adhesion. In *E. coli*, genes of this pathway are regulated by the transcription factor CsgD (Prigent-Combaret *et al.* 2001, Ogasawara *et al.* 2011). The fibres themselves are amyloid-like structures built up by the major subunit CsgA (Figure 6). The nucleation process is initiated by the minor subunit CsgB and the fibres are anchored to the outer membrane by the same protein (Hammar *et al.* 1996, Hammer *et al.* 2007, Wang *et al.* 2007, Hammer *et al.* 2012). Both are secreted in a first step by the SecYEG system and premature polymerization prevented by the periplasmic chaperone CsgC (Evans *et al.* 2015, Taylor *et al.* 2016). The transporter in the OM is composed of CsgG and CsgF in a 9:9 ratio, forming a 36-stranded β -barrel with a diameter of approx. 9 Å (Yan *et al.* 2020, Zhang *et al.* 2020). The accessory protein CsgE was shown to form a cap-like structure on the periplasmic side of CsgG and assists in the secretion of CsgA (Shu *et al.* 2016, Klein *et al.* 2018, Yan *et al.* 2020). Without CsgE, CsgG allows the unselective passage of other small proteins and molecules like erythromycin as well (Nenninger *et al.* 2011, Goyal *et al.* 2014). After transport of CsgA into the extracellular space, it oligomerizes on its own and binds via CsgB to CsgF on the OM (Bhoite *et al.* 2019). The exact driving force of CsgA/B secretion is still unknown, but it is suggested that the locally increased concentration of the substrates by CsgE provides an entropy gradient to facilitate the export (Bhoite *et al.* 2019, Christensen *et al.* 2019).

1.3.10. Type IX secretion systems (T9SS)

The T9SS is a newly identified system restricted to the *Bacteroidetes-Chlorobi-Fibrobacteres* superphylum and associated with periodontitis (Veith *et al.* 2022). Substrates are large (100-650 kDa) multi-domain proteins, which feature an N-terminal secretion signal for transport into the periplasm via the Sec pathway. After folding, a C-terminal domain (CTD) signal recruits them to the T9SS (Veith *et al.* 2013, Kulkarni *et al.* 2017). In *Porphyromonas gingivalis* the transport system itself comprises 20 proteins with a dozen proteins building the attachment complex and over 20 potential substrates with various function (Veith *et al.* 2022). Recent structures of T9SS proteins

shed some light on the mechanistic functioning of the system (Figure 9). The heart of the system is Sov, a single polypeptide with a 36 stranded β -barrel, building the translocon with a 70 Å diameter in the OM (Lauber *et al.* 2018). Two conformations of the translocon were resolved: it is either blocked by a plug or in complex with PorV, the “shuttle protein”. The latter was shown to bind to the CTD of substrates and was therefore suggested to accept cargos directly from the translocon (Glew *et al.* 2017). Most substrates are modified by the attachment complex (PorQUVZ) with A-lipopolysaccharide (A-LPS) and thereby anchored to the OM (Lasica *et al.* 2016, Madej *et al.* 2021, Mizgalska *et al.* 2021). The powerhouse for the translocation process is supposed to be a trans-envelope multi-protein complex (PorKLMN) harnessing the PMF via the TMHs in the IM to move substrates with a rotating motion, of which only a few proteins constituting the motor complex were structurally investigated (Gorasia *et al.* 2016, Leone *et al.* 2018, Hennell James *et al.* 2021, Gorasia *et al.* 2022, Veith *et al.* 2022). Neither the exact transport and modification mechanism and route of the cargo is known in detail, nor the structure of the full complex. A current model proposes the substrate to be transported by SecYEG into the periplasm, where it is delivered to Sov via the trans-envelope complex and PorW. Shuttling to the A-LPS modification complex is performed by PorV, where the CTD is cleaved and A-LPS attached by PorU and PorZ (Veith *et al.* 2022).

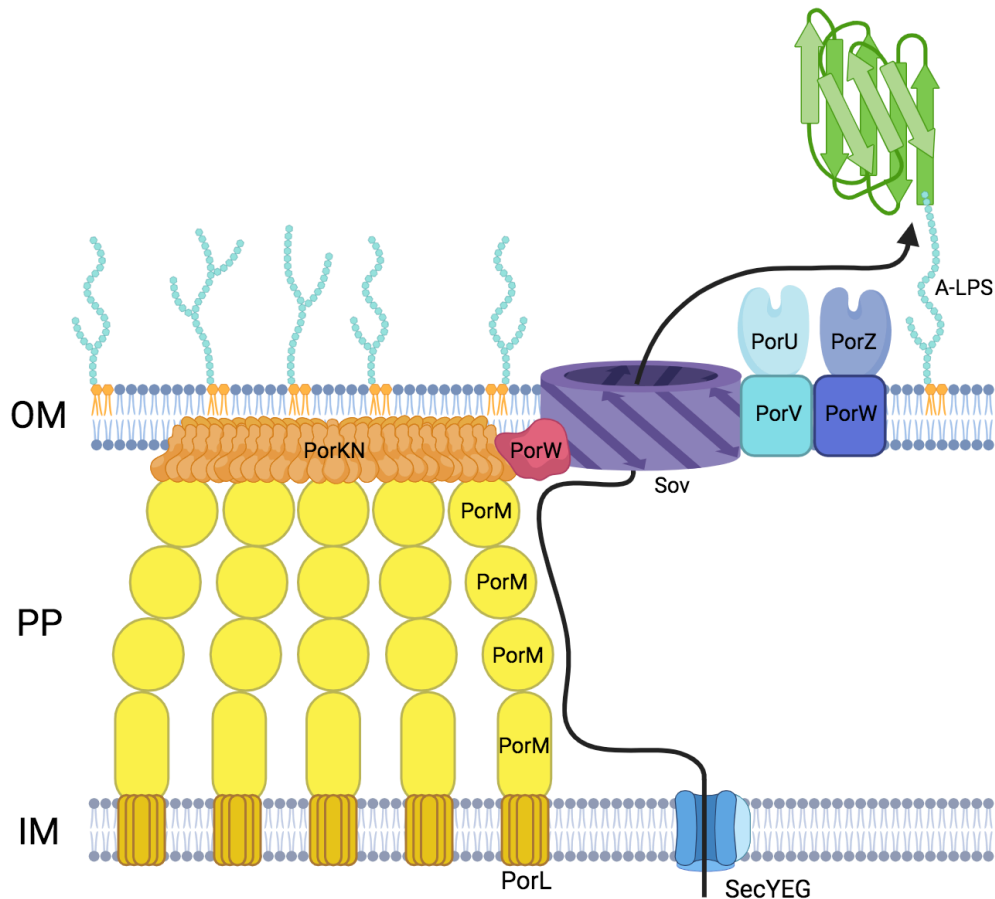


Figure 9: Structural organization of a T9SS. Substrates (green) are transported first across the inner membrane (IM) into the periplasm (PP) by SecYEG (blue). Further transport is energized by PorL and PorM (both shades of yellow). Substrates are supposed to travel along PorM, the PorKN ring (orange) and PorW (red) until being transported through the outer membrane (OM) by Sov (purple). PorU (anchored by PorV) cleaves the C-terminal domain of the substrate and links it to A-Lipopolysaccharide (A-LPS), which is delivered by PorZ (anchored by PorW, all proteins depicted as blue shades in the OM). Protein names of the T9SS from *Porphyromonas gingivalis* are given as an example. The figure was created with BioRender.com.

1.3.11. Chaperone-usher pathway

Pili and fimbriae are found on the surface of many Gram-negative bacteria and are involved in recognition of and attachment to host cells (Costa *et al.* 2015). Even though they appear similar to curli fibres (section 1.3.9), the assembly of these multi-subunit structures is mediated by another secretion system called chaperone-usher pathway (Thanassi *et al.* 1998). The best characterized systems are from type I pili (Fim proteins) and P pili (Pap proteins). Both work similar but differ e.g. in the architecture of the pili tip or termination of the pili biogenesis, which remains unknown for the type I pili (Costa *et al.* 2015). The assembly starts with the transport of the pili subunits (tip subunit: FimFGH/PapEFGK, major subunit: FimA/PapA) into the periplasm by the Sec

pathway (Figure 6). The proper folding of the subunits is assisted by the chaperones FimC and PapD respectively (Lindberg *et al.* 1989, Jones *et al.* 1993). All pili subunits exhibit an incomplete immunoglobulin-like fold with six, instead of the usual seven, β -strands, which generate a destabilizing hydrophobic groove at the C-terminus. In a process called “donor strand complementation” the involved chaperones provide the missing seventh β -strand, stabilizing the protein (Sauer *et al.* 1999). The opening for the pili to the extracellular space is contributed by the so-called “usher” FimD/PapC, a 24-stranded β -barrel in the OM. The usher features a periplasmic plug domain (closing the pore in its resting state) and two binding sites for the aforementioned chaperones (Phan *et al.* 2011, Du *et al.* 2021). In the current model, two loaded chaperones bind to the usher and elongation of the pilus is accomplished by “donor strand exchange” (Choudhury *et al.* 1999, Sauer *et al.* 1999). In a stepwise “zip-in-zip-out” mechanism, the N-terminus of one FimA/PapA copy replaces the β -strand of the chaperone and completes the immunoglobulin-fold of another FimA/PapA copy (Hospenthal *et al.* 2017). For the P pili system, elongation is terminated by PapH, which is unable to perform donor strand exchange and remains bound to the chaperone (Verger *et al.* 2006).

1.4. The hemolysin A type I secretion system

Considering all these secretion systems, the plethora of options for a bacterial cell to transport cargos across membranes is astonishing. All of them developed a unique way of secretion, and the size and complexity of some systems seem overwhelming. Interestingly, not even one of the simplest secretion systems, which is the type I secretion system, is understood completely. Although being relative simple tripartite systems, they catalyze the transport of unfolded substrates, broad in function and size, across both bacterial membranes in one step without a periplasmic intermediate. It is remarkable that this system is capable to transport proteins with a size of several hundred kilodalton by little more than one ABC transporter. One of the best studied and prominent systems is the hemolysin A system of uropathogenic *E. coli*, a T1SS of group 2, whose name originates from the observed secretion of a toxin, able to lyse erythrocytes. It was first mentioned in the 1950s (Robinson 1951) and later identified as HlyA in an operon together with its IM transport components, the ABC transporter

HlyB and the MFP hemolysin D (HlyD) (Noegel *et al.* 1979, Mackman *et al.* 1985). The component in the OM was identified to be TolC in 1990 (Wandersman and Delepelaire 1990). The hemolysin A T1SS is the main focus of this thesis and the proteins involved in secretion will be introduced in detail in the following sections.

1.4.1. The toxin HlyA

The eponymous toxin HlyA comprises 1024 amino acids and is initially synthesized as an inactive pre-protein (pro-HlyA). Hemolytic activity requires the acylation of pro-HlyA at two internal lysins (K564 and K690), preferably with C₁₄-C₁₇ fatty acids (Figure 10A) (Lim *et al.* 2000, Osickova *et al.* 2020, Erenburg *et al.* 2022). This activation is performed by the cytosolic protein HlyC under usage of the acyl carrier protein (ACP) (Issartel *et al.* 1991, Stanley *et al.* 1996). HlyC is also part of the hemolysin operon, but its indispensability is limited to the activation of the pre-toxin, as pro-HlyA is secreted as efficiently as the acylated HlyA (Nicaud *et al.* 1985, Stanley *et al.* 1994). As a member of the RTX protein family, HlyA features at least six conserved RTX domains (GGxGxDxUx, with x being any amino acid and U being a large hydrophobic amino acid) close to its C-terminus (Figure 10A and B). These glycine-rich motifs bind Ca²⁺ ions with an apparent K_D of ~150 μ M (Sanchez-Magraner *et al.* 2007). Since intracellular Ca²⁺ concentrations are several magnitudes lower (approx. 300 nM), Ca²⁺ binding and folding of the protein inside the cell is thereby prevented (Jones *et al.* 1999). This ensures the protein to be in an unfolded and secretion competent state. The fusion of fast folding proteins to HlyA was shown to inhibit the secretion of HlyA by plugging the secretion system (Bakkes *et al.* 2010, Lenders *et al.* 2015). How exactly the unfolded state is stabilized in the cytosol is unclear, as chaperones were not identified yet. Following the RTX domains, the secretion signal of HlyA is located within the last 48-60 amino acids of its C-terminus (Figure 10A) (Koronakis *et al.* 1989, Jarchau *et al.* 1994). Comparison of RTX proteins and their secretion signals did not reveal a conserved sequence and only a few amino acids were shown to be crucial for secretion e.g. F990 (Kenny *et al.* 1992, Kenny *et al.* 1994, Chervaux and Holland 1996, Holland *et al.* 2016). Instead, studies revealed the presence of an amphipathic helix to be essential for the secretion of HlyA and related toxins (Stanley *et al.* 1991, Yin *et al.* 1995, Zhang *et al.* 1995, Hui *et al.* 2000, Hui and Ling 2002, Spitz *et al.* 2022). Recognition of HlyA by the secretion complex seems to be an intricate multi-step

mechanism with several proteins and domains being involved. The secretion signal of HlyA interacts with the NBD of HlyB, while the unfolded C-terminal RTX domains interact with the CLD of HlyB (Benabdelhak *et al.* 2003, Lecher *et al.* 2012, Pourhassan *et al.* 2022). Furthermore, direct interactions of HlyA with the cytoplasmic domain of HlyD are necessary for the recruitment of TolC to the IMC (Thanabalu *et al.* 1998, Balakrishnan *et al.* 2001).

After secretion of HlyA through the HlyBD-TolC complex with its C-terminus first, the RTX motifs of HlyA bind to Ca^{2+} and folding of the protein is induced (Bakkes *et al.* 2010, Thomas *et al.* 2014a, Lenders *et al.* 2015). However, the binding of Ca^{2+} to HlyA and its folding is no driving force for the secretion process and only stabilizes the toxin after secretion in the supernatant (Lenders *et al.* 2016). The structure of HlyA is unknown, but the RTX fold structure of the related bifunctional hemolysin/adenylate cyclase toxin CyaA from *Bordetella pertussis* was resolved recently (Figure 10B). The nonapeptide repeats adopt parallel “ β -rolls” with the Ca^{2+} ion bound between the loops of adjacent β -rolls (Goldsmith *et al.* 2022). The pore-formation mechanism by HlyA and the oligomeric state for this process are unknown as well. Some investigations claim the pore formation to be a “single-hit” event, while complementation and concentration dependent experiments in the 1990s argue the process to involve HlyA oligomers (Short and Kurtz 1971, Jorgensen *et al.* 1980, Benz *et al.* 1992, Ludwig *et al.* 1993, Moayeri and Welch 1994). In any case, the hydrophobic N-terminal part of HlyA as well as the acylation of the aforementioned lysins K564 and K690 are required for membrane binding and pore formation (Ludwig *et al.* 1991, Stanley *et al.* 1994, Hyland *et al.* 2001). Likewise debated is the question, if HlyA binds to membranes in a receptor-dependent or unspecific way. CyaA binds to the β_2 integrin via linker sequences in between RTX blocks, which positions the acylation sites towards the membrane (Figure 10C). This specific linker motif is not present in HlyA (Goldsmith *et al.* 2022). Still, a recent study reported that lysis by HlyA is enhanced in the presence of the integrin β_2 (Ristow *et al.* 2019). The binding to and lysis of erythrocytes by HlyA would need to be facilitated in a different way though, since integrins are absent in erythrocytes. An important factor for the efficient binding of HlyA could be the presence of glycosylated structures in general, which also include integrins. For HlyA, this receptor could be glycophorin, a highly abundant membrane protein in erythrocytes, similar to gangliosides for CyaA (Cortajarena *et al.* 2001, Morova *et al.* 2008). Even though ambiguous, HlyA could also bind to the leukocyte-specific integrin LFA-1. Two

studies reported the interaction with LFA-1, i.a. by the redirection of CyaA-HlyA chimeras to LFA-1, while another study stated the cell-binding of HlyA to be receptor-independent (Lally *et al.* 1997, Valeva *et al.* 2005, Masin *et al.* 2020).

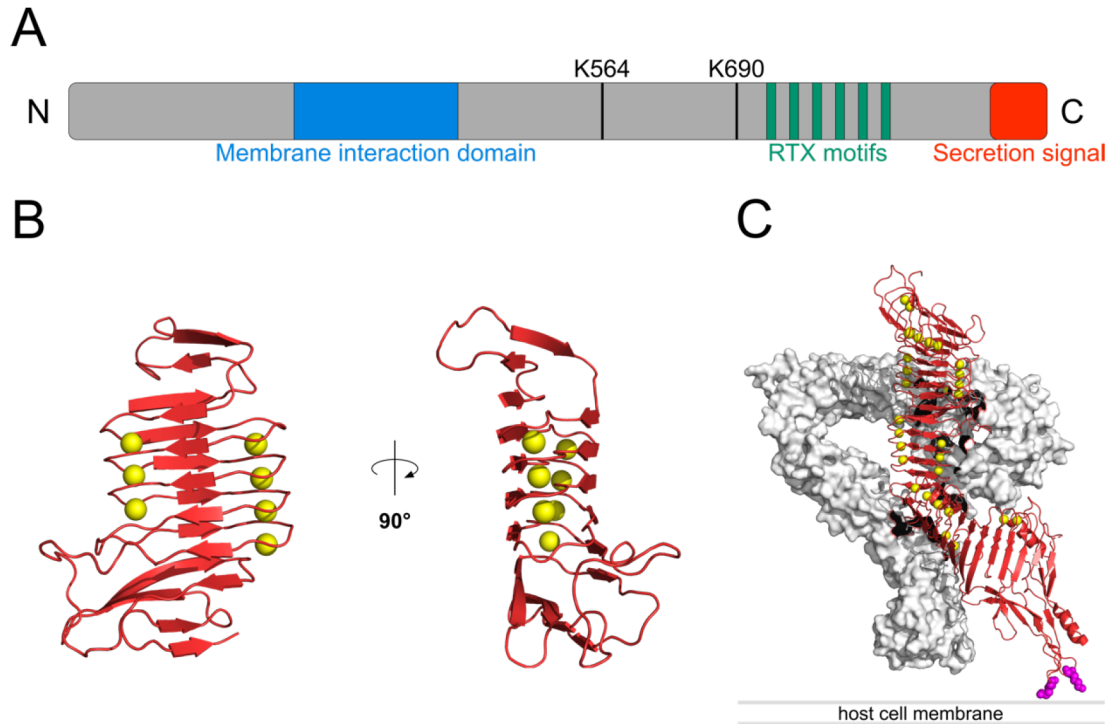


Figure 10: Structural features of HlyA and CyaA. (A) Schematic view on HlyA. The membrane interaction domain is shown in blue, the six highly conserved RTX motifs in green and the C-terminal secretion signal in red. The lysins acylated by HlyC are marked and the N- and C-terminus indicated. (B) Structure of the Repeats in toxins (RTX) β-roll fold from CyaA shown in red (PDB 7USL, residues 1106-1271) with calcium ions as yellow spheres. (C) CyaA (red) bound to α_M integrin (grey, surface representation). Calcium ions are shown as yellow spheres, the side chains of the acylation sites K860 and K983 are shown in magenta with the host cell membrane location approximated. The figure was created with PyMOL and adapted from (Goldsmith *et al.* 2022).

1.4.2. The ABC transporter HlyB

The energizing component of the hemolysin A T1SS in the IM is HlyB. It has a length of 707 amino acids and belongs to the ABC transporter superfamily, one of the largest protein families (Thomas and Tampé 2018). These proteins are found in all three kingdoms of life because they facilitate an essential process: the coupling of ATP hydrolysis to the active transport of molecules across biological membranes irrespective of concentration gradients (Wilkins 2015). The classical architecture of these transporters contains two integral TMDs and two cytosolic NBDs. Older classifications were based on the proteins function and divided into three groups: exporters, non-transporting proteins and substrate binding protein-dependent

transporters, which were mainly importers (Dassa and Bouige 2001). A new approach classifies ABC transporters into seven types, mainly based on the structural features of their TMD, since the NBD is highly conserved (Thomas *et al.* 2020). The two TMDs and two NBDs can either be fused into one polypeptide (full-size transporter) or, as in the case of HlyB, separated into two TMD-NBD polypeptides (half-size transporter), where the functional unit is a dimer (Oswald *et al.* 2006).

The TMD anchors the ABC transporter to the membrane and provides the scaffold through which the substrate is translocated. ABC transporters of the TMD fold type IV, to which HlyB belongs, exhibit a total of 12 TMHs (six TMHs per monomer) and have a so-called domain-swapped arrangement. There, two TMHs are kinked and swap from one monomer into the TMD of the other monomer (Thomas *et al.* 2020). Most ABC transporters with smaller substrates have three main conformational states during the transport cycle, in which the TMD forms a V-shaped opening towards the cytoplasm (inward-facing), followed by an occluded state, where the substrate pocket is closed to both sides of the membrane, and a final outward-facing conformation, in which the TMD is opened towards the periplasm (Kopcho *et al.* 2019). This sequence of structural changes is accompanied by the switch of a high-affinity binding site to a low-affinity binding site, resulting in the release of the bound substrate.

The switch between conformations is energized by the binding of ATP to the NBDs, and hydrolysis to ADP and phosphate. Two NBDs dimerize in a head-to-tail order and create two nucleotide binding sites (NBS) in their interface (Figure 11) (Vergani *et al.* 2005). They contain highly conserved sequence motifs necessary for the interaction with ATP and the NBD cofactor Mg^{2+} (Oswald *et al.* 2006, Zaitseva *et al.* 2006). ATP is coordinated by the Walker A motif (GxxGxGKS/T, with x being any amino acid), Walker B motif ($\phi\phi\phi\phi$ DE, with ϕ being any hydrophobic amino acid) and the conserved glutamine of the Q-loop of one monomer and the ABC protein defining signature motif (LSGGQ) of the other monomer. Additional contacts are provided by a conserved histidine of the H-loop to the γ -phosphate and by a conserved aromatic residue in the A-loop to the adenosine moiety. The D-loop (SALD) just after the Walker B motif serves as a contact point for communication between the NBD monomers (Schmitt and Tampé 2002, Schmitt *et al.* 2003, Oswald *et al.* 2006, Zaitseva *et al.* 2006). Hydrolysis of the γ -phosphate is accomplished by a nucleophilic attack of a coordinating water molecule, from which a proton is abstracted by a glutamate of the Walker B motif,

which acts as a catalytic base (Prieß *et al.* 2018). The histidine of the H-loop might participate and form a catalytic dyad, stabilizing the process (Zaitseva *et al.* 2005). Molecular dynamic simulation suggest, that binding of ATP provides the power stroke and not the hydrolysis of the phosphate-bond (Prieß *et al.* 2018). For the opening and closure of the NBDs two mechanisms are proposed. In the processive clamp model two ATP bind to the two open NBS. Closure of the dimer interface leads to concomitant hydrolysis of both ATP molecules and dissociation of both NBDs (Smith *et al.* 2002, Janas *et al.* 2003). In contrast, the alternating access model proposes that in an ATP bound NBD dimer hydrolysis occurs in only one NBS. Opening and exchange of ADP with a new ATP molecule leads to hydrolysis in the other NBS, leaving the two NBDs always in contact at one NBS (Senior *et al.* 1995, Urbatsch *et al.* 1995, Davidson and Sharma 1997, Tomblin *et al.* 2004). In any case, conformational changes created in the NBD are transferred to the TMD via coupling helices, which extend from the TMD into the cytoplasm and interact with a groove on the NBD (Luo *et al.* 2017, Thomas *et al.* 2020). HlyB transports its substrate with a speed of approx. 16 amino acids per transporter and second, but the number of hydrolyzed ATP molecules for this process remains elusive (Lenders *et al.* 2016).

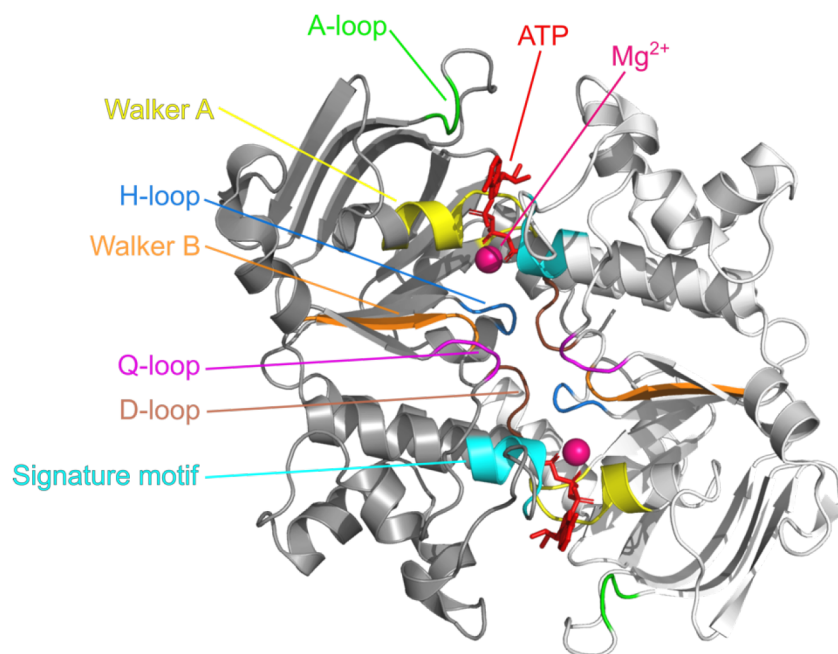


Figure 11: Conserved motifs of the HlyB-NBD (PDB: 1XEF). The two monomers are colored in white and grey respectively. Bound molecules and conserved motifs are colored in both monomers. ATP is shown as red sticks and Mg²⁺ ions as magenta-colored spheres. ATP is coordinated by the Walker A (yellow), Walker B (orange), Q-loop (pink) and A-loop (green) of one more monomer and the signature motif (cyan) of the other monomer. The H-loop (blue) is critical for ATP hydrolysis while the D-loop (brown) mediates communication between the two monomers. The figure was created with PyMOL.

As a member of the T1SS ABC transporter group 2, HlyB contains an N-terminal accessory domain in form of a CLD. This peptidase domain is inactive due to the cysteine of its catalytic triad being replaced by a tyrosine and the histidine being flipped out of the active site (Lecher *et al.* 2012, Kanonenberg *et al.* 2013). Even though inactive, presence of the CLD is indispensable for the secretion process as deletion of this domain leads to abolished secretion (Lecher *et al.* 2012). HlyA interacts via its unfolded RTX domain with the CLD. Combined with the fact that no chaperones were identified, which could stabilize unfolded HlyA in the cytoplasm, it was suggested that the CLD could prevent the aggregation during secretion (Holland *et al.* 2005). Furthermore, ATPase measurements suggest the CLD to play a regulatory role and to modulate the NBDs activity (Reimann *et al.* 2016).

The structure of the TMD and the stoichiometry of the secretion complex were unknown and debated for a long time. A dimeric ABC transporter in the IM and a trimeric OMP would suggest a hexameric MFP (HlyD) as the least common multiple to solve this symmetry mismatch, similar to the MacAB-TolC system (Figure 12B) (Lee *et al.* 2012). Structural information on HlyB was restricted to the isolated NBD and CLD (Schmitt *et al.* 2003, Lecher *et al.* 2012). This changed in 2022, when Zhao *et al.* solved the structure of the IMC, containing HlyB and partly HlyD, via cryo-EM (Figure 12A) (Zhao *et al.* 2022). There, HlyB forms an intriguing hetero-dodecameric complex consisting of three HlyB dimers and six HlyD, the MFP. One HlyB dimer forms an inward-facing conformation with the two NBDs separated, while the other two protomers are in an occluded state with the NBDs in close contact despite the absence of ATP. In all three protomers only one CLD was resolved and is positioned at the interface of neighboring HlyB protomers and not in front of the lateral gate formed by the TMD as observed in the related transporter PCAT1 (Lin *et al.* 2015, Kieuvongngam *et al.* 2020). The complex is stabilized by electrostatic interactions between acidic residues in a helix of HlyD and basic residues on the surface of the CLD. These interactions were shown to be essential for the oligomeric assembly and secretion (Zhao *et al.* 2022). Interestingly, even though all three HlyB dimers hydrolyze ATP, only one protomer showed larger conformational changes in the presence of ATP. The authors hypothesized that only one protomer of the complex would translocate HlyA while the other two protomers assist allosterically in the secretion by hydrolyzing ATP, although how this is accomplished mechanistically is unknown.

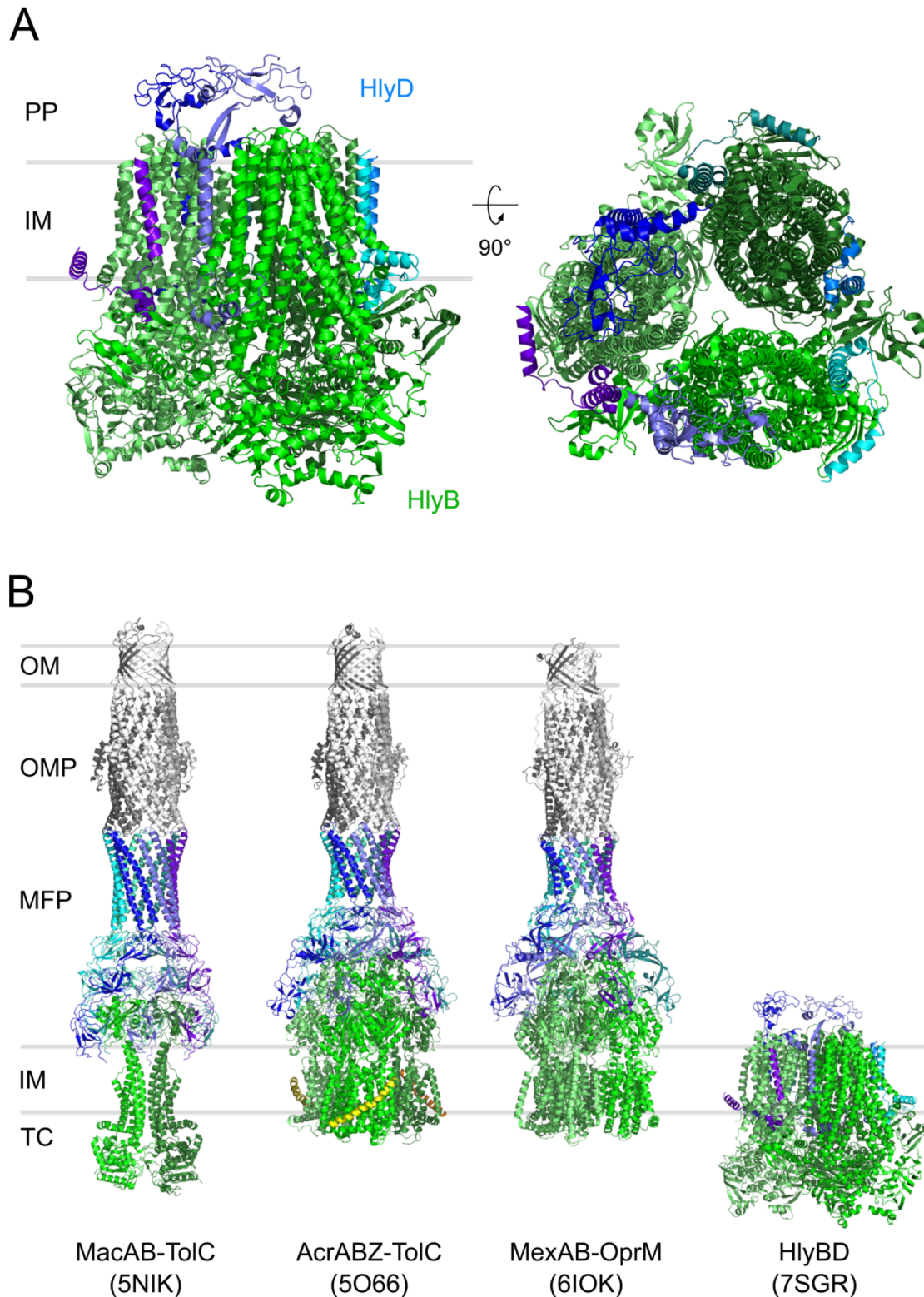


Figure 12: Architecture of the HlyB-HlyD complex and related transport systems. (A) Structure of the HlyB-HlyD complex (PDB: 7SGR). The three HlyB dimers are colored in green shades and the six HlyD are colored in blue shades either viewed parallel to the membrane (left) or from the periplasm (PP, right). The boundaries of the inner membrane (IM) are outlined as grey lines. (B) Current structural information on the HlyA T1SS and related systems viewed parallel to the membrane. The systems names and PDB entries are indicated below. The trimeric outer membrane protein (OMP) is shown in grey shades, the hexameric membrane fusion protein (MFP) in blue shades and the transporter component (TC) in green shades. In case of the Acr system, the auxiliary protein AcrZ is shown in yellow and orange shades. Boundaries of the IM and outer membrane (OM) are shown as grey lines. The figure was created with PyMOL.

Photo-crosslinking verified former results of HlyA to travel through the HlyB dimer interface and not the central pore formed by three protomers (Reimann *et al.* 2016). A complete map of the translocation path and interacting amino acids in HlyA during the secretion are unknown.

The structures of HlyD were only partly resolved and limited to the N-terminal amphipathic helix and TMH and the very C-terminal β -barrel in case of two of the six HlyD. Albeit the exact structure of the complex with TolC remains unknown, it is likely to be similar to the architecture of the RND efflux system MexAB-OprM and AcrAB-TolC, where three pumps are connected via six MFPs to the trimeric OMP in a tip-to-tip manner (Figure 12B) (Du *et al.* 2014, Tsutsumi *et al.* 2019).

1.4.3. The membrane fusion protein HlyD

The connection of the ABC transporter HlyB in the IM and the OMP is provided by the 478 amino acid comprising MFP HlyD. Early studies already showed HlyD to be essential for secretion of HlyA and to form a stable complex with HlyB even without the presence of the substrate (Mackman *et al.* 1985, Thanabalu *et al.* 1998). HlyD interacts via its N-terminus directly with HlyA and recruits the OMP TolC (Thanabalu *et al.* 1998, Balakrishnan *et al.* 2001). Classical MFPs feature a conserved architecture, which includes a membrane proximal domain, a β -barrel domain, a lipoyl domain (two half-motifs, each consisting of four β -strands forming a β -sandwich) and a coiled-coil α -helical domain of varying length (Figure 13A) (Alav *et al.* 2021). Major structural insight on HlyD is derived from a soluble fragment of the periplasmic part (residues 96-372) (Kim *et al.* 2016). As an MFP associated with T1SS, the domain organization of HlyD deviates from the canonical one and is similar to EmrA. Although missing in the crystal structure, HlyD is very likely lacking the membrane proximal domain (Kim *et al.* 2016, Alav *et al.* 2021). Furthermore, the α -helical domain of HlyD is unusual as it is not only particularly elongated (115 Å long) when compared to other MFPs like AcrA or MacA, it is also comprised of three helices instead of the usual two helices (Figure 13A). Early sequence comparisons and mutational studies of MFPs suggested an RLS/T motif in HlyD to be important for the tip-to-tip interaction with TolC as in the case of AcrA and MacA (Lee *et al.* 2012). The structure of Kim *et al.* revealed that motif to be a DLA motif instead and to be shifted to a region downstream of where Lee *et al.* suggested,

in order to enable a similar tip-to-tip interaction as observed for AcrA and TolC (Figure 13B) (Lee *et al.* 2012, Kim *et al.* 2016, Z. Wang *et al.* 2017).

Before revelation of the (partial) HlyB-HlyD structure, the oligomeric state of the MFP in the IMC was debated. Crosslinking data suggested a trimeric form, but structures of efflux systems with a similar architecture (like AcrAB-TolC, MexAB-OprM and MacAB-TolC) showed a hexameric organization of their MFP (Thanabalu *et al.* 1998, Fitzpatrick *et al.* 2017, Z. Wang *et al.* 2017, Tsutsumi *et al.* 2019). The HlyB complex structure shows the hexameric assembly of HlyD in the IMC (Zhao *et al.* 2022). The partially resolved HlyD structure in this complex complements the structure of the soluble part with its N-terminus as well as its C-terminal β -barrel domain.

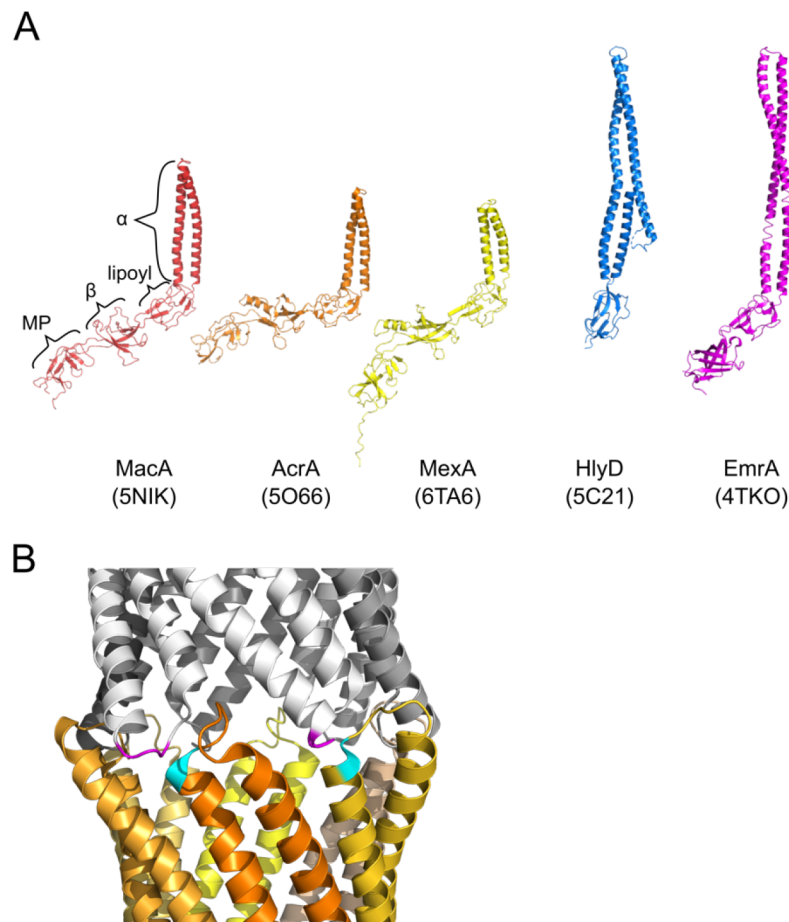


Figure 13: Architecture and interaction of membrane fusion proteins (MFP). (A) Domain organization of different MFPs. The classical organization with an α -helical domain (α), a lipoyl domain (lipoyl), a β -barrel domain (β) and a membrane proximal domain (MP) is exemplified on MacA (red). AcrA is shown in orange, MexA in yellow, HlyD in blue and EmrA in magenta. The PDB entry is given in parentheses below the structure. The MP domain is missing in HlyD and EmrA. The β -barrel domain was not resolved in the structure of HlyD. (B) Tip-to-tip interaction between MFP and the outer membrane protein (OMP) using the examples of AcrA (yellow and orange shades) and TolC (grey shades, 5O66). The conserved VGL/T motif of TolC (residues 146-148 and 364-366) is colored in magenta and the interaction side in AcrA formed by S139 and K140 is colored in cyan. The figure was created with PyMOL.

1.4.4. The outer membrane protein TolC

The HlyA T1SS component in the OM is TolC, a trimeric channel forming protein with a size of 493 amino acids. As an integral protein of the OM, it features a β -barrel domain with each monomer contributing four β -strands, forming a pore with a diameter of 35 Å. The structure of TolC was solved by Koronakis *et al.* in 2000 (Koronakis *et al.* 2000). It extends 100 Å into the periplasm, forming a 12-stranded hollow α -helical barrel with an inner diameter of ~20 Å and is filled with water. Every monomer displays four α -helices and two helix-turn-helix motifs. In its resting state, the α -helices are twisted and almost completely closed towards the periplasm. Molecular dynamics simulations suggest a global constriction of the pore, accompanied by a twisted, iris-like opening of the α -helical barrel (Figure 14) (Vaccaro *et al.* 2008). The structures of tripartite transport systems utilizing TolC (AcrAB-TolC, MacAB-TolC, EmrAB-TolC) or a related protein like OprM (MexAB-OprM) all show complexes with a similar length, suggesting a conserved interaction of the MFP and OMP in a tip-to-tip fashion (Figure 13B) (Du *et al.* 2014, Fitzpatrick *et al.* 2017, Tsutsumi *et al.* 2019, Yousefian *et al.* 2021). The symmetry of TolC and oligomeric organization with its MFP allow two different orientations of TolC in respect to the transporter, differing by a 60° rotation. Recent investigations of the AcrAB-TolC system using cryo-ET revealed both these orientations to occur to the same extent (Chen *et al.* 2022). Due to its length, TolC protrudes far enough into the periplasm to interact with the peptidoglycan layer via its tip region (Shi *et al.* 2019, Chen *et al.* 2022). The components in the IM are only transiently connected to TolC as demonstrated for AcrAB using cryo-ET and for HlyBD by biochemical data (Thanabalu *et al.* 1998, Balakrishnan *et al.* 2001, Shi *et al.* 2019). This could be necessary because of the limited number of TolC in the bacterial cell with approx. 4500 in *E. coli* BL21(DE3) (Beer *et al.* 2021). Due to its promiscuous nature being used by several secretion machineries, a temporary formation of the secretion system allows TolC to also be used by other efflux systems. In case of the hemolysin system, TolC is recruited by HlyD to the IMC after the substrate is recognized by the MFP (Balakrishnan *et al.* 2001).

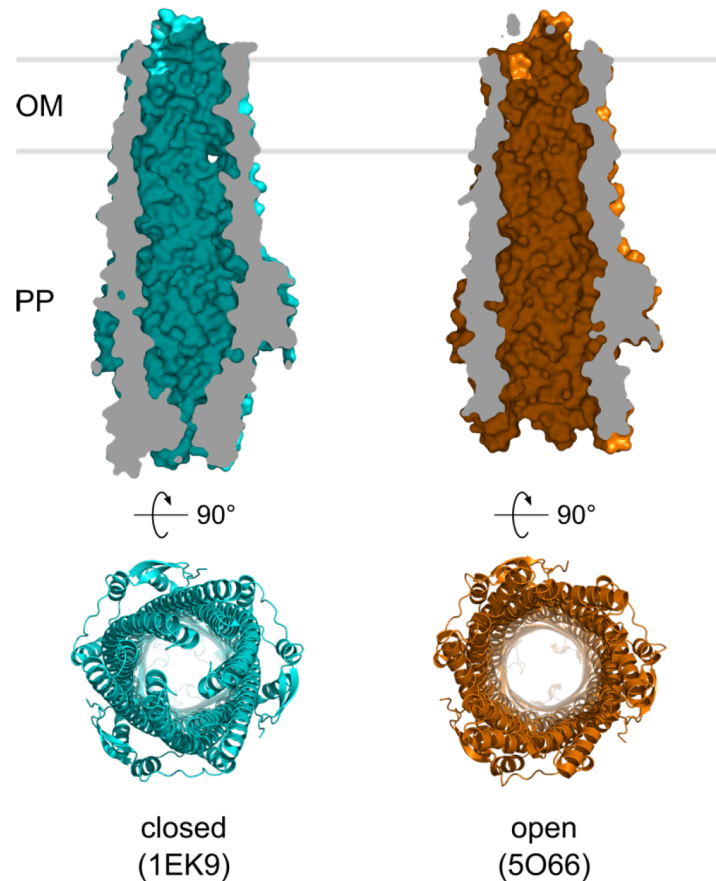


Figure 14: Conformational changes of the outer membrane protein TolC. Shown are cross sections in surface presentation viewed parallel to the outer membrane (OM, top) and cartoon presentations viewed from the periplasm (PP, bottom) of TolC, both in a closed state (cyan, left) and open state (right, orange). Borders of the OM are outlined as grey bars. The PDB entry of the structures is given below. The figure was created with PyMOL.

1.4.5. The secretion mechanism

In summary, the structural and biochemical data available suggest the following secretion mechanism (Figure 15):

The IM components HlyB and HlyD form a stable complex in a ratio of 6:6 even without the presence of the substrate (Thanabalu *et al.* 1998, Balakrishnan *et al.* 2001, Zhao *et al.* 2022). HlyA is completely translated and kept in an unfolded state by unknown means. It is recognized by both the CLD and NBD of HlyB as well as the cytoplasmic part of HlyD (Thanabalu *et al.* 1998, Balakrishnan *et al.* 2001, Benabdelhak *et al.* 2003, Lecher *et al.* 2012). Crucial for the interactions are the RTX domains and especially the C-terminal secretion signal of HlyA (Nicaud *et al.* 1986, Pourhassan *et al.* 2022, Spitz *et al.* 2022). The interaction of HlyA with HlyD recruits TolC in the OM and forms

the continuous secretion channel, supposedly with only one of the three HlyB dimers actually secreting HlyA, while the other two dimers assist in the translocation process by hydrolyzing ATP (Thanabalu *et al.* 1998, Balakrishnan *et al.* 2001, Zhao *et al.* 2022). HlyA is then ATP-dependently secreted with its C-terminus first through the HlyB dimer interface, HlyD and TolC in one step without a periplasmic intermediate (Lenders *et al.* 2015, Reimann *et al.* 2016). Once the RTX motifs reach the extracellular space, binding of Ca^{2+} ions promote the binding of HlyA (Bakkes *et al.* 2010, Thomas *et al.* 2014a). After secretion of one HlyA molecule, either the next one is secreted or the complex dissociates into TolC and the IMC.

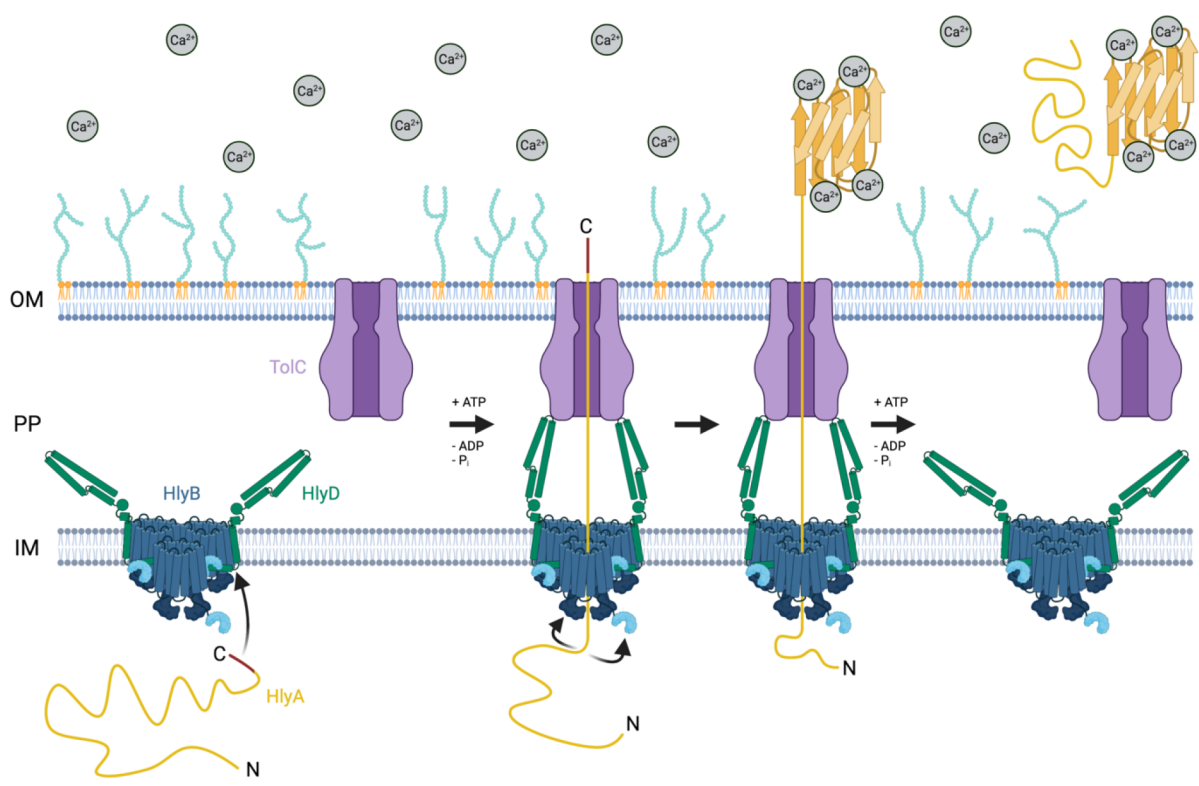


Figure 15: Schematic overview of the HlyA secretion mechanism. Three HlyB dimers (blue shades) and hexameric HlyD (green) form a stable complex in the inner membrane (IM). Note that only two HlyD are shown for simplicity. TolC (purple) in the outer membrane (OM) is recruited upon recognition of unfolded HlyA (yellow) by the cytoplasmic part of HlyD. HlyA then interacts with the nucleotide binding domain (dark blue) of HlyB via its secretion signal (red) and with the C39 peptidase-like domain (light blue) of HlyB via its repeats in toxins (RTX) motifs. The toxin is then transported through the periplasm (PP) and across both membranes in one step with its C-terminus first through one of the HlyB dimer interfaces. During secretion, all three HlyB dimers bind ATP and hydrolyze it to ADP and P_i to energize the process. Reaching the extracellular space, HlyA begins to fold, as highly abundant Ca^{2+} ions bind to the RTX motifs. Once secretion is completed, the next HlyA molecule can be secreted or, as depicted here, TolC dissociates from the HlyB-HlyD complex again. The figure was created with BioRender.com.

2. Aims

Gram-negative bacteria developed a remarkable repertoire of secretion systems to interact with their environment. T1SSs represent one of the architecturally more simple systems, comprising only three proteins in the inner and outer membrane: an ABC transporter, a membrane fusion protein and an outer membrane protein. With this system, bacteria secrete toxins and cause e.g. urinary tract infections, one of the most common infections in humans (Bien *et al.* 2012). The primary cause of those infections are uropathogenic *E. coli*, with the HlyA T1SS as the main reason for the pathogenicity (Al-Dulaimi *et al.* 2022). The HlyA secretion system is one of the best studied T1SS and the focus of this thesis. Although structurally and functionally investigated for several decades, questions revolving the secretion mechanism remain.

One open question revolves around the stability of unfolded HlyA in the cytoplasm and targeting to the IMC. So far, no chaperones for HlyA could be identified. One option might be, that the mRNA of HlyA localizes to the inner membrane as observed for other proteins like LacY (Nevo-Dinur *et al.* 2011). With a localized translation near the secretion system, HlyA would be present in the cytoplasm for only a short time before being secreted. One aim was therefore the localization of *hlyA* mRNA utilizing protein-nucleotide interaction tools and microscopy techniques.

At the start of this thesis, structural information on the ABC transporter HlyB was limited to the isolated C39 peptidase-like domain (CLD) and nucleotide binding domain (NBD) (Zaitseva *et al.* 2005, Lecher *et al.* 2012). Those two domains were known to interact with the substrate *in vitro*, and previous lysine-specific crosslinking suggested HlyA to pass through the HlyB TMD dimer interface (Benabdelhak *et al.* 2003, Lecher *et al.* 2012, Reimann *et al.* 2016). Still, structural information on the transmembrane domain (TMD) was missing. If the TMD of HlyB plays an active role during secretion by directly interacting with HlyA is unknown. One aim was to map the translocation pathway of HlyA through the transporter. For this, unnatural amino acids acting as photo-activatable crosslinkers should be integrated into HlyA and HlyB. This would not only identify possible interacting residues in HlyA and HlyB, but would also provide first structural insights on the TMD by determining residues, which build the inner conduit.

As already mentioned, NBD and CLD of HlyB were shown to individually interact with parts of HlyA. If the TMD plays a more important role than simply providing a framework

through which HlyA can pass, possibly by providing further recognition or interaction sides, is unknown, just like the influence of the three ABC transporter domains on the substrate specificity. Thus, a part of this thesis aimed to deepen the understanding of the role and interplay of HlyB's domains in the secretion process. For this, chimeric proteins with domains of HlyB from *E. coli* and a homologous transporter, RtxB from *Kingella kingae*, were analyzed towards their ability to secrete HlyA.

3. Publications

3.1. Chapter 1: ABC Transporters in Bacterial Nanomachineries

Title:	ABC Transporters in Bacterial Nanomachineries
Authors:	Florestan L. Bilsing, Manuel T. Anlauf , Eymen Hachani, Sakshi Khosa, Lutz Schmitt
Published in:	<i>International Journal of Molecular Sciences</i> (2023) Impact factor 5.6 (2022)
Own work:	15% Writing of the manuscript



International Journal of
Molecular Sciences



Review

ABC Transporters in Bacterial Nanomachineries

Florestan L. Bilsing, Manuel T. Anlauf, Eymen Hachani, Sakshi Khosa and Lutz Schmitt

Special Issue

ABC Transporters: Where Are We 45 Years On?

Edited by

Prof. Dr. Anthony M George



<https://doi.org/10.3390/ijms24076227>



Review

ABC Transporters in Bacterial Nanomachineries

Florestan L. Bilsing, Manuel T. Anlauf, Eymen Hachani , Sakshi Khosa and Lutz Schmitt *

Institute of Biochemistry, Heinrich Heine University, Universitätsstr. 1, 40225 Düsseldorf, Germany

* Correspondence: lutz.schmitt@hhu.de; Tel.: +49-211-81-10773; Fax: +49-211-81-15310

Abstract: Members of the superfamily of ABC transporters are found in all domains of life. Most of these primary active transporters act as isolated entities and export or import their substrates in an ATP-dependent manner across biological membranes. However, some ABC transporters are also part of larger protein complexes, so-called nanomachineries that catalyze the vectorial transport of their substrates. Here, we will focus on four bacterial examples of such nanomachineries: the Mac system providing drug resistance, the Lpt system catalyzing vectorial LPS transport, the Mla system responsible for phospholipid transport, and the Lol system, which is required for lipoprotein transport to the outer membrane of Gram-negative bacteria. For all four systems, we tried to summarize the existing data and provide a structure-function analysis highlighting the mechanistical aspect of the coupling of ATP hydrolysis to substrate translocation.

Keywords: ABC transporter; nanomachineries; Mac system; Lpt system; Mla system; Lol system



Citation: Bilsing, F.L.; Anlauf, M.T.; Hachani, E.; Khosa, S.; Schmitt, L. ABC Transporters in Bacterial Nanomachineries. *Int. J. Mol. Sci.* **2023**, *24*, 6227. <https://doi.org/10.3390/ijms24076227>

Academic Editor: Anthony M George

Received: 24 February 2023

Revised: 18 March 2023

Accepted: 23 March 2023

Published: 25 March 2023



Copyright: © 2023 by the authors. Licensee MDPI, Basel, Switzerland. This article is an open access article distributed under the terms and conditions of the Creative Commons Attribution (CC BY) license (<https://creativecommons.org/licenses/by/4.0/>).

1. The Classical View of an ABC Exporter

ATP-Binding Cassette (ABC) transporters are present in all domains of life, from prokaryotes to eukaryotes [1]. ABC exporters consist of two nucleotide-binding domains (NBDs) and two transmembrane domains (TMDs) [2,3]. The NBDs are responsible for binding and hydrolyzing ATP, and the TMDs allow substrate translocation across the membrane [4]. The conformational changes of the NBDs, due to ATP binding and hydrolysis, are translated via coupling helices to the TMDs [5,6]. While the NBDs are highly conserved among all ABC transporters, the TMDs show a huge variety that goes in line with the huge variety of ABC transporter substrates [7]. Within this review, we will focus on prokaryotic ABC exporters functioning in nanomachineries. Some of the prokaryotic ABC exporters are “half-size” transporters with one NBD and one TMD fused together on a single polypeptide chain, while most harbor NBDs and TMDs as separate polypeptide chains allowing heterooligomeric assemblies (see Figure 1) [3].

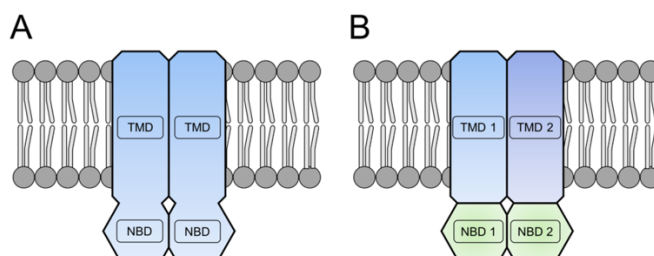


Figure 1. Domain organization of prokaryotic ABC exporters. (A): Half-size homodimer. (B): Single domain heterodimer. TMD = transmembrane domain. NBD = nucleotide-binding domain. The TMD and NBD are either fused on one polypeptide chain (A) or exist as separate polypeptides (B).

Without any structural information, Jardetzky et al. proposed already in 1966 two configurations for a membrane transporter enabling a ‘two-sided access’ to a central cavity

within the transporter [8]. Today we know from multiple protein structures that most of the ABC exporters change during substrate translocation from an inward-facing (IF) state to an outward-facing (OF) state [9–13]. This model of a translocation cycle (see Figure 2) was extended by the outward-occluded state observed for the peptide transporter McjD [14] and for other exporters as well [15]. New findings revealed even more transition states within one translocation cycle [16]. Besides this classical understanding of changing between IF and OF states, there are further models expanding the mechanisms for substrate translocation. On the one hand, there is the alternate access model, where a substrate is not entering from the cytoplasm but from a lateral opening in the TMDs (PCAT1 [17]). On the other hand, there is the outward-only model, where the substrate cavity is open and closing without an inward-facing state (PglK [18]). Similar to this outward-only model, simulations suggested a Constant Contact Model of the NBDs without a wide open IF state [19].

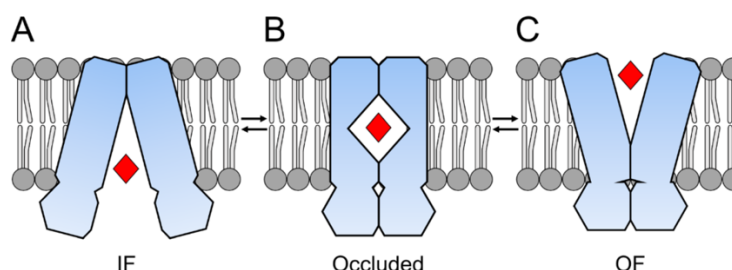


Figure 2. Schematic of a transport cycle of a type IV ABC exporter. (A): In the inward-facing (IF) conformation, the transporter binds the substrate. (B): During substrate translocation across the membrane, the occluded state is formed with the substrate pocket closed to the inside and outside. (C): The transporter adopts the outward-facing (OF) conformation, and the substrate leaves the transporter to the outside.

The power stroke for transmission from IF to OF state, and along with this, the substrate translocation, is supposed to be the binding of ATP. ATP hydrolysis, therefore, only resets the system back into the IF state [20,21]. Moreover, it is conceivable that there is a difference in the power stroke for heterodimeric ABC exporters that contain an intrinsically impaired nucleotide binding site, as it is proposed for BmrCD. Here, turnover from IF to OF state is exclusively attributed to ATP hydrolysis [22]. In addition, novel findings on the homodimeric ABC exporter MacB award at least a part of the power stroke for substrate translocation to the ATP hydrolysis step [23].

Based on the variety of TMDs, a new nomenclature was introduced to categorize ABC transporters on the basis of the different TMD folds into seven different types [24]. Type I–III cover classical ABC importers, and type IV to VII mostly cover ABC exporters. A large number of structures and functional information are known for the type IV ABC transporters that are defined by the architecture of Sav1866. Type V also includes a few ABC transporters with importer functions. Type VI ABC transporters are defined by the fold of LptB₂FG and Type VII by the fold of MacB [24]. These classes of Type VI and VII are of special interest for this review and are complemented by the MlaFEDB system (recently assigned as founding member of type VIII [25]) and the LolCDE system (type VII). Although the classical understanding of the transport cycle from an IF state to an OF state with an occluded state trapping the substrate in a binding pocket is feasible for small substrates such as ions, amino acids, or even smaller peptides, this model cannot apply to large substrates such as lipopolysaccharide (LPS) or lipoproteins. In the following sections, we will summarize the recent findings with respect to the structure and function of these selected ABC transporter systems of MacB, LptB₂FGC, MlaFEDB, and LolCDE (Figure 3) as a wide range of information is available for these nanomachineries.

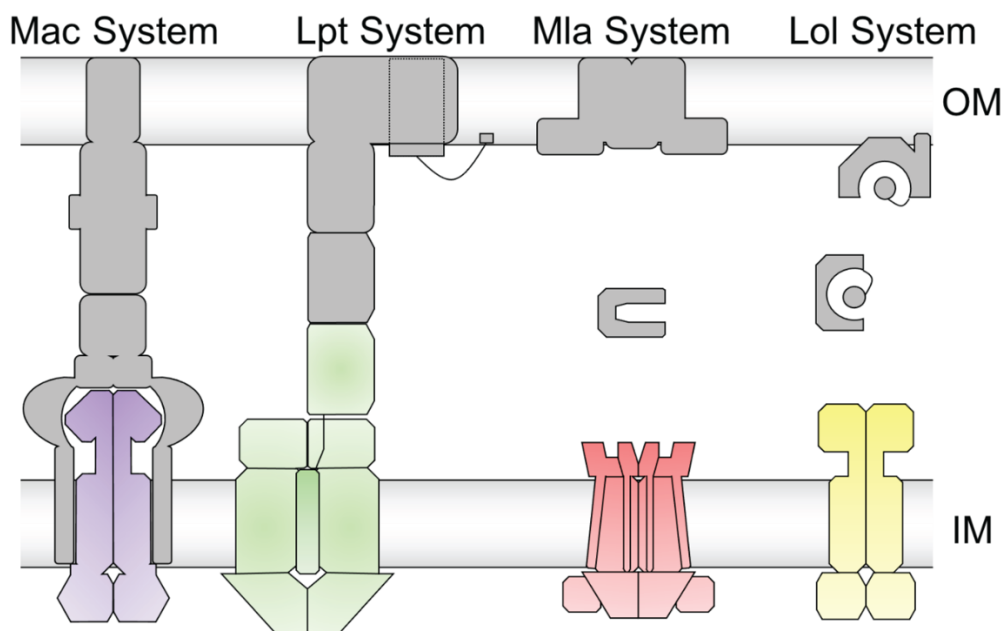


Figure 3. Schematic representation of the Mac, Lpt, Mla, and Lol system. For the Mac system, the ABC transporter MacB is shown in purple. The membrane fusion protein MacA and the outer membrane protein TolC are shown in grey. For the Lpt system, the ABC transporter LptB₂FGC is shown in green. The periplasmic protein LptA and the translocon in the outer membrane LptDE are shown in grey. For the Mla system, the ABC transporter MlaFEDB is shown in red. The periplasmic protein MlaC and the outer membrane protein MlaA, together with OmpF, are shown in grey. For the Lol system, the ABC transporter LolCDE is shown in yellow. The periplasmic protein LolA and the outer membrane protein LolB are shown in grey. Inner membrane (IM) and outer membrane (OM) are depicted as grey bars. The peptidoglycan layer is omitted for reasons of clarity.

2. The MacAB-TolC System

The first experimental evidence of an ABC antibiotic efflux transporter in Gram-negative organisms was published in 2001 by Kobayashi et al. [26]. They investigated a system that gave resistance to erythromycin and other macrolide-type antibiotics and was therefore termed macrolide-specific ABC-type efflux carrier, short “MacAB”. Furthermore, they showed that TolC is necessary for MacAB efflux activity [26]. Today it is known that the MacAB-TolC system also exports the extracellular peptide toxin STII [27], the heme precursor protoporphyrin IX [28], cyclic peptides like bacitracin and colistin [29], and penicillin-type antibiotics as well as arsenite [30]. Furthermore, overexpression of MacAB in *Klebsiella pneumoniae* increased resistance against the synthetic tetracycline-class antibiotic eravacycline [31]. All substrates of the MacAB-TolC system are transported from the periplasm across the outer membrane to the extracellular space [27,29]. Interestingly *macB* homologs can be found in Gram-positive bacteria as well, although they lack a periplasm and a second membrane (reviewed in Greene et al. [32]). The expression of *macA* and *macB* is controlled by the PhoP/PhoQ system [33] and therefore downregulated in case of low Mg²⁺ levels, which was shown using real-time quantitative polymerase chain reaction (rt-qPCR) [34].

The structure of the outer membrane protein TolC was determined in 2000 by Koronakis et al. [35]. Due to DNA sequence analysis, it was already proposed in 2001 without having a high-resolution structure that MacB is a transmembrane protein with four transmembrane helices (TMH) and that MacA is a peripheral membrane protein belonging to the membrane fusion protein (MFP) family [26]. Biochemical and biophysical data by

Lin et al. revealed in 2009 that MacA stabilizes the tripartite assembly of the MacAB-TolC efflux system through specific interactions with MacB as well as TolC. In addition, it was shown that the N-terminal transmembrane helix of MacA, anchoring it into the inner membrane, is not essential for the functional assembly of the system [36]. In contrast, Tikhonova et al. could show that a MacA mutant lacking the N-terminal transmembrane helix was not able to confer an increase in erythromycin resistance in vivo, although in vitro studies showed that this mutant can still interact with MacB [37]. Furthermore, MacA increases MacB's affinity for ATP and the substrate erythromycin. Mass spectrometry (MS) and atomic force microscopy (AFM) revealed a dimeric organization of MacB [36]. Bound lipids such as phosphatidylethanolamine (PE) and cardiolipin could only be observed for the dimeric protein using detailed MS analysis [38]. In 2009, the first crystal structure of the periplasmic domain of MacB [39], as well as the crystal structure of a hexameric arrangement of the periplasmic part of MacA from *Actinobacillus actinomycetemcomitans* [40], became available. Further analysis of the interface between MacA and TolC supported a strongly conserved tip-to-tip interaction between those two proteins [41–43]. In 2017, the single-particle cryo-EM structure of the fully assembled MacAB-TolC efflux system (see Figure 4) from *Escherichia coli* (*E. coli*) was published in a nucleotide- and substrate-free conformation by Fitzpatrick et al. [44]. This structural information on the MacAB-TolC system was complemented by an ADP-bound crystal structure of MacB from *Acinetobacter baumannii* published by Okada et al. [45] and an ATP-bound crystal structure of MacB from *Aggregatibacter actinomycetemcomitans* published by Crow et al. [29] in the same year (see Figure 5). Moreover, the crystal structure of a Gram-positive MacAB-like efflux pump from *Streptococcus pneumoniae* was published by Yang et al. in 2018 [46].

The structure of the full MacAB-TolC efflux system was derived by Fitzpatrick et al. [44] from a hybrid electron density map combining density maps from two different stabilizing approaches of the tripartite assembly. The first approach was a fusion of the C-terminus of MacB to the N-terminus of MacA as they were expected to be in close proximity. Interestingly, the fusion construct resolved only two copies of MacB, which were forming the dimer in the inner membrane. The other four copies of MacB, each fused to one MacA, were not resolved in the electron density map but produced diffuse density in the two-dimensional classifications. The second approach was a stabilization using disulfide bonds between MacA and MacB introduced via cysteine mutations. Only two of the MacA protomers formed a disulfide bond with MacB. Both approaches stabilized MacAB-TolC sufficiently for the acquisition of high-resolution structural data without loss of functionality in vivo [44]. This confirmed the overall organization of the MacAB-TolC system comprising a dimer of MacB in the inner membrane linked to a hexamer of MacA in the periplasm, which in turn is connected to a trimer of TolC in the outer membrane. This tripartite assembly with approximately 320 Å spans the inner and outer membrane in vivo [44].

Within the fully assembled complex, MacA adopts a hexameric structure, as seen for MacA alone [40], with four domains: a cylindrical α -helical hairpin domain, a ring-forming lipoyl domain, a ring-forming β -barrel domain, and a membrane-proximal domain. A density for the N-terminal transmembrane helix was missing, just as for the already existing crystal structure [40]. The already proposed tip-to-tip interaction between the trimeric TolC and MacA [41,42] was located between the α -helical hairpin region of MacA and the intra- and inter-protomer grooves of TolC [44]. A loop in the lipoyl domain of MacA allows highly conserved glutamine residues [40] to form an inter-protomer hydrogen-bond network that acts like a gating ring. Molecular dynamics simulations suggested that this gating ring acts as a one-way valve for the outward-directed transfer of the substrate [44]. The β -barrel domain and the membrane-proximal domain from three MacA protomers interact with the periplasmic domain of one MacB protomer [44].

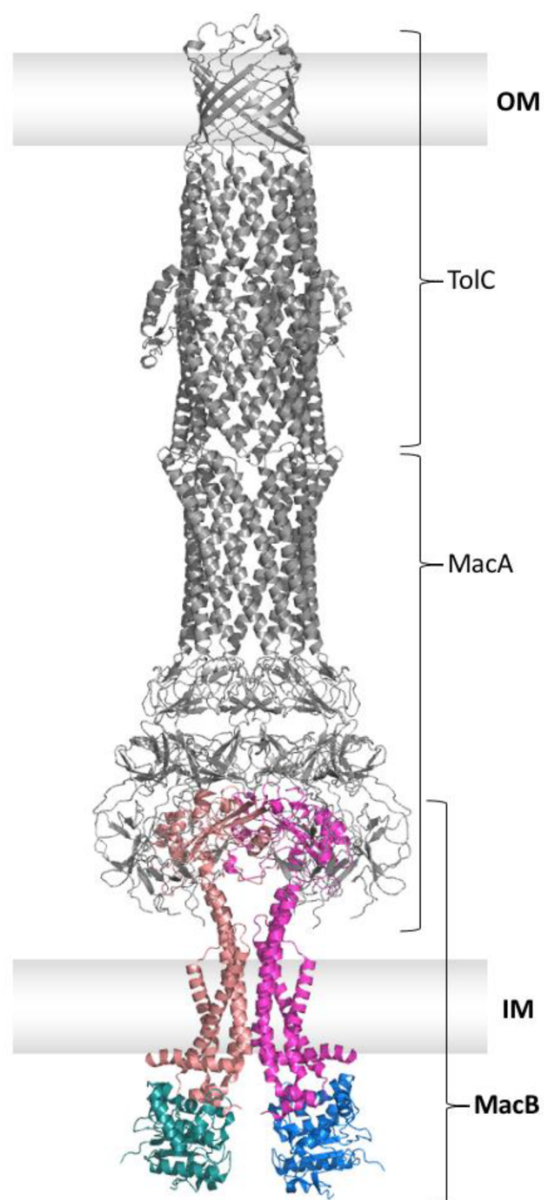


Figure 4. Single particle cryo-EM structure of the assembled MacAB-TolC efflux system (PDB entry 5NIL). Trimeric TolC and hexameric MacA are shown in grey and dimeric MacB in color. The nucleotide-binding domains of MacB are shown in deep teal and marine, and the transmembrane domains, plus the periplasmic part, are shown in salmon and light magenta. The outer membrane (OM) and inner membrane (IM) are displayed as grey boxes. The peptidoglycan layer is omitted for reasons of clarity.

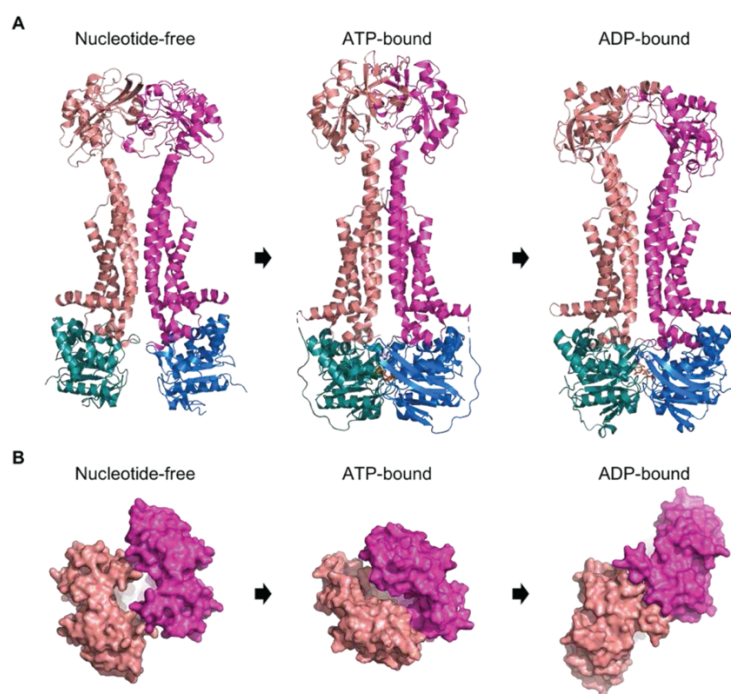


Figure 5. Structures of MacB in a nucleotide-free (PDB entry 5NIL), ATP-bound (PDB entry 5LIL), and ADP-bound (PDB entry 5WS4) state. NBDs are shown in deep teal and marine, and the TMDs with the periplasmic part are shown in salmon and light magenta. (A): Side view of MacB in the different nucleotide-free/-bound states. (B): Top view of the periplasmic part of MacB in the different nucleotide-free/-bound states.

MacB forms a homodimer in the tripartite assembly, with each protomer consisting of a NBD, a TMD, and a periplasmic domain (PD). The NBD is connected to the TMD via a long loop and an amphipathic helix. The TMD of MacB is unlike other ABC transporters, built up by only four TMH. TMH1 and TMH2 are elongated and reach above the membrane plane into the periplasm. In between these two helices, the PD is located. This PD contains a so-called porter domain that is a structural homolog to the AcrB “porter domain” and a sabre (small alpha beta-rich extracytoplasmic) domain. The porter domain is formed by two subunits that are located before and after the sabre domain. TMH3 and TMH4 are shorter than TMH1 and TMH2 and are connected via the so-called shoulder loop [29]. The major coupling helix is located in between TMH2 and TMH3; the minor coupling helix is located C-terminal of TMH4 [44]. The major and minor coupling helix interact with the NBD from the same protomer as there is no domain swapping [29]. The role of the minor coupling helix is not fully understood as, according to Crow et al. [29], the deletion of this helix did not influence MacB activity significantly, but for Okada et al. [45], deletion of the minor coupling helix resulted in the loss of drug export.

Although substrate-bound structures are lacking, the nucleotide-free MacAB-TolC cryo-EM structure [44], together with the ATP-bound crystal structure [29] and the ADP-bound crystal structure [45], allow prediction about the function of MacAB-TolC mediated efflux.

In the nucleotide-free state (see Figure 5A, left panel), the transmembrane dimer interface adopts a V-shape form having the periplasmic parts of TMH1 and TMH2 of one protomer far away from the other protomer and thereby forming a cavity on the periplasmic site margined by the periplasmic domains of MacB. This arrangement also brings the periplasmic domains into an open conformation forming a small gap towards

the periplasm (see Figure 5B, left panel). In the cryo-EM structure, an additional electron density was observed in this periplasmic cavity between the periplasmic elongations of the TMHs. The orientation of this additional density already indicates a lateral substrate entrance. Nevertheless, it was not possible to examine the identity of this molecule. The NBDs are also separated and far away from each other in the nucleotide-free structure [44]. In the ATP-bound state (see Figure 5A, middle panel), the NBDs are dimerized and form a tightly packed classical head-to-tail arrangement. TMH1 and TMH2 of each protomer align parallel to each other in a rigid dimer interface, omitting the V-shaped form but adopting a so-called “zipped stalk” conformation. The PD adopts a closed form without an opening towards the periplasmic side (see Figure 5B, middle panel). The NBDs dimerization is supposed to mediate the “zipping” of the stalk and closure of the PD via the major coupling helix and movement of TMH2, which changes the dimer interface favoring close proximity of TMH1 and TMH2 of each protomer. This transfer of structural movements from one side of the membrane to the other via the transmembrane helices is referred to as mechanotransmission. The mechanotransmission mechanism was investigated *in vivo* by using cysteine mutants that lock MacB TMH1 and TMH2 in the zipped conformation. Those mutants showed decreased resistance to erythromycin [29]. In the ADP-bound state (see Figure 5A, right panel), the NBDs are dimerized but not as tight as in the ATP-bound state. TMH1 and TMH2 adopt a V-shape-like open conformation as in the nucleotide-free state, but the PDs arrange differently, and the opening towards the periplasm is absent (see Figure 5B, right panel) [45].

Biochemical data of Tikhonova et al. showed that MacB exhibits basal ATPase activity in detergent, which is little to none affected by the addition of either substrates or MacA or TolC [37]. When reconstituted into proteoliposomes, the basal ATPase activity of MacB is reduced about 10-fold but is strongly stimulated in the presence of MacA. MacA mutants missing either an N- or C-terminal part of MacA could not stimulate MacB ATPase activity in proteoliposomes *in vitro* and were also not able to increase erythromycin resistance *in vivo*, although the N-terminal truncated mutant was capable of binding MacB *in vitro* [37]. Modali et al. revealed that MacA stabilizes the ATP-bound state of MacB, and a single mutation in the membrane-proximal domain of MacA abolishes the macrolide efflux function of MacAB-TolC [47]. Lu et al. discovered that the periplasmic domain of MacB is essential for MacA-dependent stimulation of MacB ATPase activity. Furthermore, ATP binding of MacB increases affinity towards MacA [48]. In 2021, Souabni et al. determined a transport rate of three molecules per hydrolyzed ATP molecule for the substrate roxithromycin [23]. Recently, Batista dos Santos et al. [49] showed that the presence of TolC increases MacB ATPase activity in detergent as well as in lipid nanodiscs. Furthermore, they could also show a substrate-induced increase in MacB ATPase activity for the fully assembled MacAB-TolC system in a lipid environment [49].

Based on the available structures, Crow et al. [29] postulated a mechanism for substrate efflux of the MacAB-TolC system in 2017 termed the “molecular bellows” mechanism. In the nucleotide-free state, the cavity between the periplasmic part of TMH1 and TMH2 of MacB and MacA is open to the membrane, and substrates can enter. Upon ATP binding, the dimerization of the NBDs on the cytosolic side causes closure of the TMDs of MacB and constrains the volume of the cavity. This generates pressure and pushes the substrate through MacA towards TolC. The gating ring inside MacA prevents backflow of the substrate once the pressure is balanced. After ATP hydrolysis, the system switches back to the nucleotide-free open state [29]. This mechanism was further expanded by Souabni et al. [23] in 2021, investigating the role of ATP hydrolysis using a quantum dots-based real-time analysis of substrate transport and ATP turnover. They suggested a “modified bellows mechanism” where ATP hydrolysis is additionally energizing the transport of the substrate across the MacA gating ring towards TolC. In this modified mechanism, MacA and its transmembrane helix act as a mediator for the additional energetic input. In their study, substrate translocation and ATP hydrolysis are shown to be synchronous events [23].

Although much is known due to biochemical and structural data, many open questions remain regarding the function of the MacAB-TolC system. Examples are: How is the substrate recognized? Is there a specific substrate binding site? Is there a feedback mechanism from the periplasm to the NBDs? How is lateral substrate leakage prevented? These questions require further research using intermediate or substrate-bound structures.

3. The Lpt System

The cell envelope of Gram-negative bacteria exhibits a complex architecture. It not only consists of an inner membrane (IM), made up of phospholipids in the inner and outer leaflet, and an additional outer membrane (OM) but also a periplasm in between with a cell wall formed by crosslinked peptidoglycan. The OM protects the cell from the environment and serves as a potent barrier for hydrophobic molecules. Its composition is highly asymmetrical, with glycerophospholipids in the inner leaflet and mainly LPS molecules in the outer leaflet [50,51]. The interested reader is referred to comprehensive reviews focusing on the structure and synthesis of LPS [52–54], as it will be only briefly described here. The LPS structure can vary among different bacteria; typically, it can be divided into three parts: LPS is anchored to the membrane via its Lipid A moiety, a β -1'-6-linked glucosamine disaccharide, every sugar being acylated with fatty acid chains. Additionally, in *E. coli*, the glucosamine is phosphorylated at positions 1 and 4' and can be further modified, e.g., upon polymyxin exposure with ethanolamine or 4-amino-4-deoxy-L-arabinose to decrease the negative net charge [55,56]. The core oligosaccharide moiety is connected to Lipid A via 3-deoxy-D-manno-oct-2-ulosonic acid (Kdo), which itself is linked with several heptose and hexose molecules. On top of the core oligosaccharide is the O antigen, also called O-antigenic polysaccharide (O-PS); it represents the terminal part of LPS and, as the name suggests, is a polymer made up of different kinds of oligosaccharides. The composition of the O antigen varies greatly, not only between different but also within the same species. *E. coli*, as one example, displays over one hundred different serotypes [52]. LPS is found in most, but not all, Gram-negative bacteria, with exceptions like *Sphingomonas paucimobilis* and *Treponema pallidum* [57,58]. In *E. coli* and *Salmonella*, the presence of LPS is essential, although this is not the case for all LPS-containing bacteria. Certain strains of *Neisseria*, *Moraxella*, and *Acinetobacter* can live without genes necessary for the synthesis or transport of LPS to the OM [59].

The LPS homeostasis displays a delicate challenge. Even though it is exclusively present in the outer leaflet of the OM, the biogenesis starts on the complete opposite side of the cell envelope: The inner leaflet of the IM (and the cytoplasm). Therefore, it does not only need to be extracted from the IM—an energy-consuming process—but the amphipathic LPS molecule also needs to traverse the aqueous periplasm on its route to the OM. Ultimately, the LPS needs to be incorporated into the outer leaflet of the OM. This process must occur repetitively during the life cycle of the cell in a highly ordered manner, as processes in the periplasm and outer membrane cannot be energized directly through ATP hydrolysis.

This part of the review will deal with the LPS transport (Lpt) machinery (see Figure 6), which mediates the extraction of LPS from the IM, its transport across the periplasm, and insertion into the OM. A special focus lies on the ABC transporter, including a step-by-step examination of its functionality and recent discoveries.

Intensive research on the LPS transport over more than five decades, starting with genetic approaches along with biochemical and structural studies, gradually revealed the Lpt system to be a multiprotein assembly with an ABC transporter LptB₂FGC in the inner membrane [60] and a translocon LptDE in the outer membrane [61] which are connected by a periplasmic bridge built up by (most likely) oligomeric LptA [62] (see Figure 6). In this complex, LptB₂FGC provides the energy for the extraction and transport of LPS by ATP binding and hydrolysis. Although its TMD fold is reminiscent to type V ABC transporters, LptB₂GFC is considered to be the first member of the new type VI ABC transporter family, as there are several aspects that led researchers to classify this transporter into its distinct group [24,63].

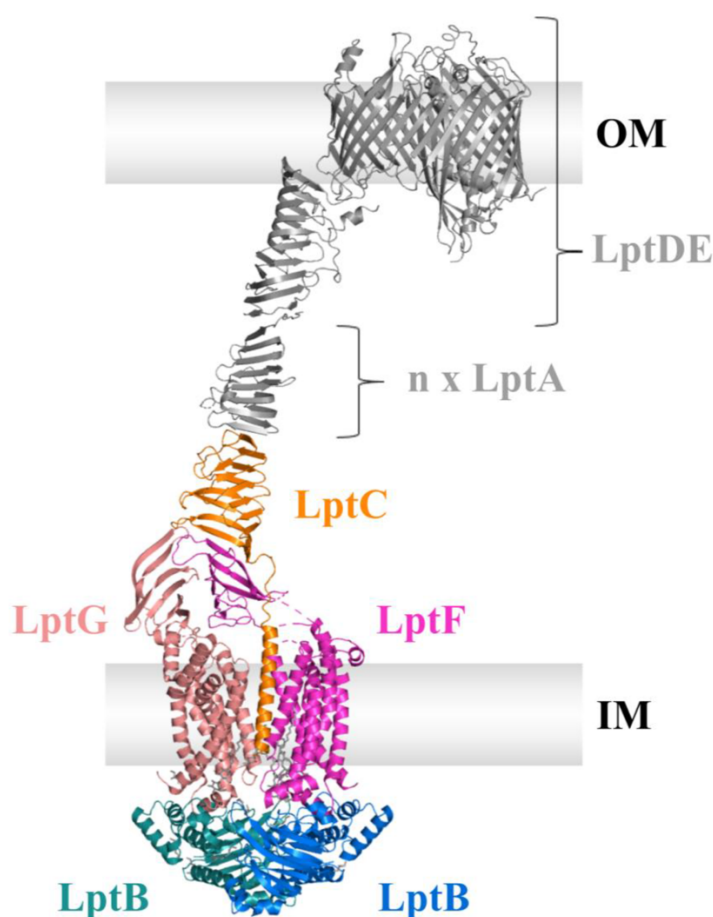


Figure 6. Overview of the Lpt machinery spanning both membranes and the periplasm. Note that the number of LptA oligomers forming the periplasmic bridge is unknown. The figure was created using PyMOL and the PDB entries of LptDE (5IV9, grey in the outer membrane), LptA (2R19, grey in the periplasm), and LptB₂FGC (6MJP, orange, salmon, light magenta, deep teal and marine in the inner membrane). The outer membrane (OM) and inner membrane (IM) are displayed as grey boxes. The peptidoglycan layer is omitted for reasons of clarity.

In the domain organization of the LPS extractor, the two homologous proteins, LptF and LptG, form the TMD [64,65]. Both proteins have an additional periplasmic domain, the so-called β -jellyroll domain. This protein fold is a hallmark of the Lpt system, as it occurs in five of the seven Lpt proteins (LptA, LptC, LptD, LptF, and LptG; see Figure 6). The homo-dimeric LptB shows the fold of a canonical NBD and serves as the motor domain of the extractor. Its structure as an isolated protein was resolved by two independent groups in the same year, Sherman et al. and Wang et al. [66,67]. It is present as a dimer in the cytoplasm, where it binds and hydrolyzes ATP to energize the LPS translocation and forms the functional transporter with LptFG [60]. What makes the LPS transporter complex unique is the presence of a mysterious protein within the inner membrane complex: LptC. It is a small protein, only consisting of an N-terminal TMH and a periplasmic β -jellyroll domain [68]. Like all other Lpt proteins, it is essential for LPS transport, as deletion strains show phenotypes attributed to defective LPS transport, such as increased sensitivity to hydrophobic compounds [69].

LptD and LptE build the translocon in the outer membrane [61,70–73]. LptD is a large, 26-stranded β -barrel protein in which the lipoprotein LptE resides, forming a barrel-and-plug complex. The N-terminal part of LptD features a β -jellyroll domain as well and is connected to the jellyrolls of LptB₂FGC via the periplasmic LptA, in which this protein fold was first discovered [74]. The N-terminal part of LptA's β -jellyroll domain interacts with LptC, while its C-terminal part showed crosslinks to the β -jellyroll domain of LptD. Studies also showed that LptA is capable of forming oligomeric structures in vivo and in vitro, although the exact number of LptA molecules necessary for establishing the periplasmic bridge between the complexes in the IM and OM remains unknown [74–76].

Early models based on initial structures of LptB₂FG by Dong et al. and Luo et al., who only had the transporter in a single functional state available, proposed a sequence in which ATP binding would open the cavity, allowing LPS to enter and subsequent ATP hydrolysis and release of ADP would push LPS out of the transporter [65,77]. Today, additional structures of LptB₂FG together with LptC, bound LPS, and/or bound nucleotide by the groups of Li, Luo, Tang, and Owens suggest the following model [78–81]: In the initial state of the transport cycle, the TMH of LptC (LptCTM) resides between LptF and LptG (see Figure 7, state i). LPS enters the cavity first (see Figure 7, state ii) and triggers in a not completely understood manner the release of LptCTM. Here, a strict NBD-TMD coupling is apparently involved (see Figure 7, state iii). By this, the cavity narrows, and its residues bind tightly to the LPS molecule and elevate it inside the cavity. The NBDs of LptB₂ bind tightly to each other, which results in a complete collapse of the cavity and expulsion of LPS (see Figure 7, state iv). ATP, which can bind before ejection of LptCTM, as new data suggest, is hydrolyzed to ADP and released from the NBDs. This reopens the cavity, and LptCTM can bind again between TMH5 of LptF (TMH5_F) and TMH1 of LptG (TMH1_G) to allow the next transport cycle (see Figure 7, state v) [82].

Together, LptF and LptG are adopting a V-shaped fold with an opening to the periplasm and only a few contacts between their interfaces, namely TMH1 and TMH5 (see Figure 7B and C). The limited interaction sites suggested early on that one, or both interfaces may open further to allow the lateral entry of LPS into the cavity [65,77]. The formed cavity is covered with residues of hydrophobic amino acids, which was confirmed by the structures of LptB₂FG(C) with bound LPS. Additional charged residues stabilize bound LPS via salt bridges to the phosphate groups and glucosamine disaccharides of the lipid A moiety as well as the core oligosaccharide [78,79]. Even before the structure of LptB₂FGC with LPS was revealed, Hamad et al. and Bertano et al. used mutational studies and bacterial strains, which constitutively modify lipid A phosphates to show that a cluster of charged residues in the TMH1 of LptG is important for LPS transport, most likely by binding LPS through establishing contact sites with the phosphate moieties of lipid A [83,84]. The first step in the LPS transport is the entry of the LPS molecule into this cavity for extraction, and this process already raises two questions: (i) From which side of the transporter does LPS enter? The structure of LptB₂FGC allows LPS entry in principle from both LptFG interfaces, TMH1_F:TMH5_G or TMH5_F:TMH1_G. (ii) How does the transporter differentiate between LPS and other phospholipids, which are also present in the outer leaflet of the inner membrane?

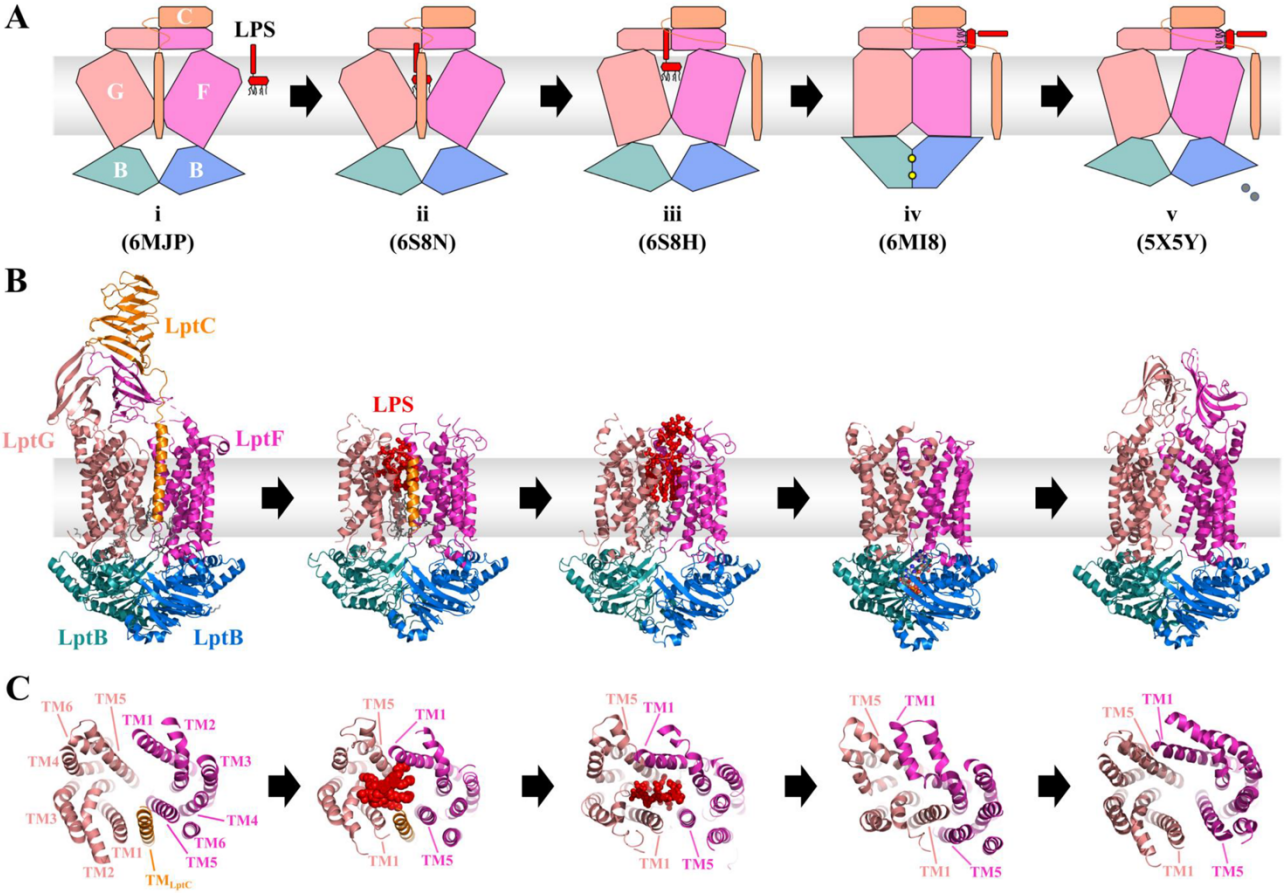


Figure 7. Model and structures of the Lpt systems transport cycle. LptC is shown in orange, while LptF and LptG are shown in light magenta and salmon, respectively. Both LptB protomers are shown in marine and deep teal. LPS is shown in red. Lipids and detergent molecules in the structure are shown as grey sticks,

while nucleotides are shown as spheres. **(A)**: Schematic model of LPS extraction by the extractor LptB₂FGC. The different states of the transporter are labeled i-v with the PDB entry for the respective structure. i,ii: LPS enters the LptB₂FGC cavity from the reader's side. ii,iii: The LptC TMH leaves the LptFG interface, the cavity tightens and elevates LPS, forming tighter contacts. iii,iv: The LptB₂ dimer closes, causing the cavity to collapse and pushes LPS upwards to the β-jellyroll domain of LptF. iv,v: ATP (yellow dots) is hydrolyzed to ADP (grey circles) and P_i, thereby opening LptB₂ and the cavity for a new extraction cycle. **(B)**: Crystal structures and single particle cryo-EM structures according to the different states **(C)**: View on the cavity from the periplasmic side (β-jellyroll domains are omitted for clarity). Note that only structures of states ii and iii show LPS. Even though only the structure of state iv shows bound nucleotides, latest data suggest that ATP can bind already during earlier states. Structures of states ii–iv did not resolve the β-jellyroll domain of LptFG. The structure of state ii did not resolve the β-jellyroll domain of LptC, while the structures of states iii–v were lacking LptC completely.

The first question was answered by crosslinking studies using unnatural amino acids as photo-crosslinkers, together with structures of LptB₂FGC, in which the periplasmic domains of LptF and LptG were resolved. Owens et al. detected crosslinks of LPS to residues in TMH1 of LptG and TMH5 of LptF as well as LptC, but not with the possible cavity opening formed by TMH1 of LptF and TMH5 of LptG [81]. Moreover, structures of the LPS ABC transporter with LptC revealed that the LptCTM is positioned between the interface of TMH5_F:TMH1_G, which is in line with the aforementioned crosslinking studies. So far, no data supported the proposal that LPS might enter from the TMH5_G:TMH1_F interface or LptC to reside in that position. Additionally, the structure of LptB₂FGC showed that the β -jellyroll domains of the transporter are placed above the interface formed by TMH1_F and TMH5_G, possibly blocking the entry of LPS from this side due to the bulky core oligosaccharide and O-antigen moieties [81].

The second question, why phospholipids are not transported by the Lpt system, is not easily answered. The aforementioned study by Owens et al. showed that even in the absence of ATP, LPS is able to enter the cavity of the transporter [81]. One possibility is that phospholipids can enter the cavity through the TMD interface as well but are not recognized by the transporter as a substrate due to the lack of interactions mentioned above. Since the simplest LPS structure, enabling cell viability, contains lipid A and Kdo, it is likely, that the presence of these key components is necessary for substrate recognition by the Lpt transporter [52,85].

We know now that the TMH5_F:TMH1_G interface—in which LptCTM, at least at some point of the transport cycle, resides—is the entry for LPS. However, how does LPS enter the cavity of LptFG with a TMH of another protein in its way? The LptB₂FG(C) structures of Li et al. revealed that LptCTM pushes away TMH1-3 of LptG, preventing the interaction of bound LPS with the charged residues mentioned above (see Figure 7B and C). The tighter binding of LPS might therefore push LptCTM out of the cavity [79]. The constriction of the cavity ultimately results in its full collapse and the transfer of LPS from the cavity to the β -jellyroll domains. This movement, as well as the reopening of the cavity, is performed by the NBDs LptB₂, which bind and hydrolyze ATP. Closure and opening of the NBD interface are thought to be tied to the collapse and opening of the TMD cavity by a rigid body mechanism, as suggested for other transporters as well [5,86,87]. The LptB structure features a groove region in which the coupling helices of LptF and LptG are embedded [66]. These coupling helices are conserved in the TMD of ABC transporters and are crucial for the TMD-NBD interaction and can be found between TMH2 and TMH3 in LptFG [7,65,77]. They were identified using photo-crosslinking and mutational studies, in which defects induced by substituting a conserved glutamate in both LptF (E84) and LptG (E88) could be suppressed by altering an amino acid in the groove region of LptB (R91) [88]. Interestingly, the same study showed that LptF and LptG do not act symmetrically, as identical changes at equivalent positions led to different defects. Following the signature motif is the signature helix, in which Simpson et al. identified an arginine residue (R144) to be important for forming contacts with the Q-Loop and Walker B motif. Altering this residue led to reduced LPS extraction due to a lower ATP binding affinity, favoring the open conformation of the transporter. Strikingly, an alteration in the C-terminal domain (CTD) of LptB (F239), a domain unique to this transporter, is usually lethal but could complement the change in the signature helix. The data for this mutation showed a decreased ATP hydrolysis, indicating that this mutant is favoring the closed conformation, and the combination of these two defects complement each other, resulting in a functional transporter with decreased ATPase activity. Since full restoration of ATP hydrolysis in this double mutant is not necessary for LPS transport, the researchers proposed that the binding of ATP leads to the collapse of the LptFG cavity and hydrolysis to its reopening [89]. This correlation is supported by structures of the transporter in its closed form with bound β - γ -imidoadenosine 5'-triphosphate (AMP-PNP), a nonhydrolyzable ATP analog, and with bound ADP-vanadate [78,79]. ATP binding leads to the closure of the LptB₂ dimer interface

and the concomitant anti-clockwise rotation of the LptFG TMH1-5, ultimately closing its cavity [78].

Since this review focuses on the transporter of the Lpt system, subsequent transport steps will be only briefly described here. At the end of each transport cycle, a new LPS molecule is placed into the β -jellyroll domains of the transporter. The functionality of the transport system is often compared with a PEZ candy dispenser, where the LptB₂FGC transporter acts like a spring, with each cycle loading a new LPS “candy” onto the bridge, pushing the former one further ahead on the LptA bridge towards LptDE and the OM [90]. Although both LptF and LptG feature β -jellyroll domains, structural, mutational, and crosslinking studies so far only showed that LPS travels from the cavity to the β -jellyroll domain of LptF, but not LptG, and further to the one of LptC [81]. The backflow into the cavity must be prevented if the entry of new LPS is not much faster since LPS does not diffuse away from the transporter. Owens et al. proposed on the basis of their LptB₂FGC structure that the β -jellyroll domain of LptF can adopt a closed conformation, preventing a backward flow much like a valve [81]. Another possibility for the unidirectional flow might be different binding affinities of LPS for the different proteins, as this was at least shown for the transfer of LPS from LptC to LptA [68]. Even though LptA is known to form oligomers in vivo and in vitro, the exact number forming the bridge is unknown [62,74]. Sherman et al. succeeded with the in vitro reconstitution of the complete system, proving that LptA physically connects LptB₂FGC with LptDE [91]. Once LPS reaches LptDE in the outer membrane, it is first placed into the β -jellyroll domain of LptD. The lipid A moiety of LPS is proposed to enter the membrane directly through a cavity between its β -jellyroll domain and the 26-strand β -barrel. The hydrophilic part of LPS would then first enter the β -barrel from the periplasmic side before exiting it through a lateral gate between helices 1 and 26, which showed to have only a few interacting residues [73,92,93]. LptE, the barrel’s plug, is not only important for the biogenesis and proper folding of LptD but was also shown to bind LPS and extract it from aggregates, suggesting that its role is to accept LPS coming from the periplasm, weaken neighboring LPS-LPS interactions and assisting its insertion into the OM [61,93–97]. Once the hydrophilic part of LPS has passed the lateral gate, it becomes part of the already existing LPS network. Intriguingly, there is evidence that the activity of the LPS transporter LptB₂FGC in the inner membrane is influenced by the translocon LptDE. For an in vitro setup, inhibition of LPS transport and ATPase activity of LptB₂FGC in liposomes was observed when adding LPS-preloaded LptDE-containing liposomes [98]. Lately, LptB₂FGC has been shown to exhibit an adenylate kinase activity in addition to the ATPase activity, as it was reported for other ABC transporters like MsbA and CFTR [99–101].

Due to recent advances in structural biology, many answers regarding LPS transport could be answered. However, still some key questions remain, especially regarding the enigmatic LptC: What role does LptC play in the transport process since no other ABC transporter features a protein alike? Even though LptC is found in structures with LptB₂FG, its TMH is neither required for LPS to enter the cavity nor for transport in general. Studies showed that LptC variants, in which the TMH was deleted, are still able to form a complex with the other Lpt proteins to transport LPS [102]. Experimental data suggest that the LptCTM plays a regulatory role in the ATPase activity of the transporter. In vitro, LptB₂FG displays an increased ATP hydrolysis when no LptC or only variants without TM helix (LptC^{ΔTM}) are present. Therefore, the helix might reduce futile ATP hydrolysis by coupling it efficiently to substrate extraction [78,79,81]. Lethal LptC deletions can be suppressed when the arginine residue R212 in the β -jellyroll domain of LptF is substituted with glycine, restoring wildtype LPS transport and ATPase activity of the transporter, even though affinity to LptA is reduced [103,104]. Interestingly, this point mutation is still able to form a complex with LptC when it is present. This indicates that the periplasmic β -jellyroll domain of LptC is responsible for the interaction with the other Lpt components and enhances the stability of the transporter to the periplasmic bridge. The availability of LPS-bound LptB₂FG structures with and without LptC allows a comparison of the cavity

and interactions with the LPS molecule. With the LptCTM missing, the transporter cavity is significantly smaller (see Figure 7C). Simultaneously, the LPS structure in those structures is better resolved, indicating an improved binding of LPS once the LptCTM is removed from the transporter. When, how, and why the LptCTM is removed during the transport cycle is still not completely clear.

Recently, Wilson et al. approached these questions by combining LptC^{ΔTM} with mutations in other Lpt transporter components and searched for synergistic or suppressive effects on the phenotypes. They aimed to elucidate the exact role of LptCTM in the different steps of the extraction cycle, as deletion of the TM helix should strengthen or weaken the phenotype when a mutant is affected in the same step, while no change to the phenotype was expected when LptC^{ΔTM} was combined with mutants, in which the TM helix plays no role. Two observations were made: (i) The presence of the LptCTM increases the stability of the protein, possibly by benefiting from a complex formation with LptB₂FG, and (ii) the phenotype of LptB and LptF/G mutants with defects in ATP binding and NBD-TMD coupling were affected, indicating that the LptCTM plays a role in these steps. This new data hints that i) binding of ATP to LptB can occur with the LptCTM associated with LptFG (although it is not obligatory) and (ii) the coupling helices in LptFG, as well as the corresponding groove region in LptB, take part in LptCTM displacement from the transporters cavity, meaning that the sole entry of LPS into the cavity is not sufficient for this process [82]. The proposal that ATP can bind to LptB₂FG with LptCTM still present is contrary to former models, in which LPS binding and formation of tighter contacts to LptFG is displacing LptCTM with ATP binding afterwards, particularly as structures of LptB₂FG with bound LPS and displaced LptCTM were lacking nucleotides so far [79]. It is surprising that the essential process of LPS extraction, which takes place countless times during the lifetime of a cell, features an apparently useless step. One possible explanation is that the intercalation of LptCTM slows down ATP hydrolysis [78,79,81,87,99] to synchronize the hydrolysis of ATP with the binding of LPS to the cavity of the extractor, preventing futile ATP hydrolysis. It also remains enigmatic if the placement of LptCTM is a step that is not performed during active LPS transport but rather to slow it down before turning it off.

4. The Mla System

As mentioned in the previous section, the OM is an asymmetric bilayer, and all the components for building the OM envelope are synthesized either in the cytoplasm or the IM before being transported across the periplasm to be inserted into the OM [105]. As mentioned in the previous section, LPS is trafficked across the cell envelope via the Lpt system. The maintenance of lipid asymmetry (Mla) pathway is involved in maintaining the asymmetry of the OM by trafficking phospholipids (PLs) between the IM and OM [106–108]. The Mla pathway is a multi-component system and uses a ferry-like mechanism to shuttle phospholipids across the periplasm. Its mutation leads to the accumulation of PLs in the outer leaflet of the OM, increased OM permeability, and increased susceptibility to antibiotics [106–109]. Although translocation of phospholipids between outer and inner membrane was initially discovered in *Salmonella typhimurium* as early as 1977, it was not until 2009 that the components of the phospholipid transport system in Gram-negative bacteria were discovered via homology of conserved transporters in Actinobacteria and chloroplasts [106,110–112]. The orthologous TGD pathway of plants transports phosphatidic acid from the OM to the IM of chloroplasts [110], while the Mce4 pathway in Actinobacteria is paralogous and imports exogenous cholesterol [111,112].

In *E. coli*, the genes representing the Mla system are located on the *mfaFEDCB* operon, which is conserved among Gram-negative bacteria. Although *mfaA* and *ompC/G* are part of the Mla system, these genes are located outside the *mfa* locus [106].

The Mla system is a six-component system with components present in each compartment of the cell envelope. It includes an OM lipoprotein termed MlaA; the OM major porins OmpF/OmpC, which act as a scaffold for MlaA; a soluble periplasmic component known as MlaC, which acts as a carrier of PLs, shuttling them between the membranes; a

mammalian cell entry (MCE) domain protein called MlaD which is anchored in the plasma membrane; the transmembrane domain of the ABC transporter MlaE; a sulphate transporter and anti-sigma factor antagonist (STAS) domain protein called MlaB and the ATPase MlaF. These components create the following three main parts of the Mla system [113,114]: (a) the trimeric porin OmpC, which forms a complex with lipoprotein MlaA at the OM; (b) a soluble lipid-binding protein, MlaC, located in the periplasm; and (c) MlaFEDB, an ABC transporter localized in the plasma membrane (see Figure 8).

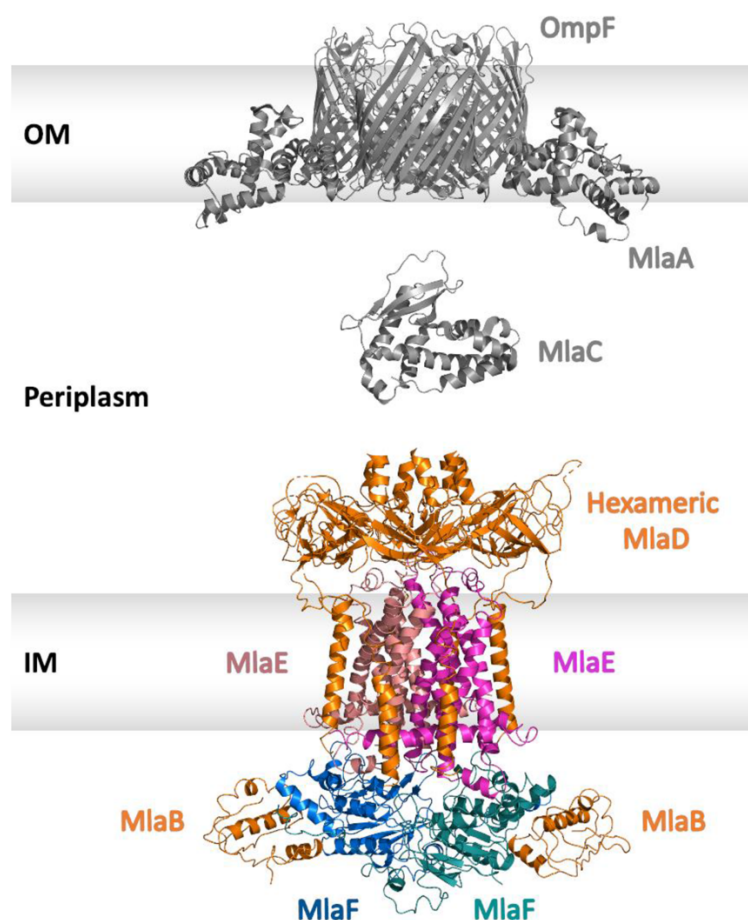


Figure 8. Structural components of the Mla system in a cartoon representation. The homo-trimeric complex of OmpF and MlaA (PDB: 5NUO) situated in the outer membrane is shown in grey color. MlaC (PDB: 6GKI) is shown in the periplasm in grey color. Note: the exact number of MlaC molecules in the periplasm is unknown. The inner membrane complex of MlaFEDB (PDB: 6ZY2) is shown in color: hexameric MlaD, and both MlaB molecules are shown in orange. The two MlaE molecules are shown in salmon and light magenta. The two molecules of MlaF are shown in marine and deep teal. Outer membrane (OM) and inner membrane (IM) are displayed as grey boxes. The peptidoglycan layer is omitted for reasons of clarity.

MlaA is a lipid transport protein and assembles into a ring-shaped α -helical structure that contains a central pore [115]. It forms a complex with both the OM porin proteins, OmpC and OmpF [115,116]. However, the complex of OmpC-MlaA is the active species, as MlaA copurifies with OmpC. MlaA binds in the groove between the two OmpF/C monomers, and the interaction between MlaA and OmpF/C is mainly mediated via van

der Waals forces [115]. Since MlaA might be unstable on its own in the lipid bilayer, the porins might function as a scaffold to ensure the proper functioning of MlaA [115].

MlaC is a periplasmic lipid-binding protein. The crystal structure of MlaC was resolved and comprised four β -sheets and seven helices with a large hydrophobic pocket in the core of the protein. Since MlaC can bind to both IM and OM complexes, it probably exhibits a central role in the transport of PLs between the membranes [117]. MlaC has a high affinity towards phospholipids and can bind three different PLs: phosphatidylglycerol, phosphatidylethanolamine, and cardiolipin [118,119].

MlaD is anchored to the IM through a single N-terminal TMH with its MCE domain residing in the periplasm. The MCE domains have been involved in lipid uptake in Gram-negative bacteria and retrograde transport of PLs in chloroplasts [110,117,120]. MlaD forms a ring-shaped homo-hexamer with a central hydrophobic pore that allows movement of PLs [114,117–119].

MlaE represents the transmembrane domain of the ABC transporter, which forms a homodimer. In contrast to the previously described TMDs of MacB and LptF/G (Sections 3 and 4), MlaE has five TMHs. Recently, it has been assigned as a founding member of the type VIII group of ABC transporters [24,117]. Each subunit contains one elbow helix (EH), five transmembrane helices (TMH1–5), one coupling helix (CH), and one periplasmic helix (PH). TMH1, TMH2 and TMH5 of the two subunits of MlaE form a central hydrophobic cavity. EH runs parallel to the inner membrane plane while the CH connects TMH2 and TMH3 and is involved in interaction with MlaF. The PH is placed between TMH3 and TMH4 and interacts with MlaD [121].

MlaF represents the nucleotide-binding domain of the ABC transporter with a conserved structure representative of the ABC superfamily and is present as a dimer [121]. MlaB contains a STAS domain and represents the accessory protein, which is involved in cross-talk with the NBDs of ABC transporters. The two MlaB subunits are located on the opposite side of the MlaF dimer [122,123] and are involved in stabilizing the complex and ATP hydrolysis [109,124].

The inner membrane complex (IMC) of the Mla pathway is composed of MlaFEDB, which represents the ABC transporter. Overall, the complex comprises of four different proteins: MlaF, MlaE, MlaD, and MlaB in a stoichiometry of 2:2:6:2 [109,117,121,125]. The homodimers of MlaE and MlaF function as the TMDs and the NBDs, respectively. Associated with the homodimers are the unique auxiliary proteins: MlaB and MlaD. While there are two copies of MlaB, MlaD is present as a hexamer in the complex [109]. The two MlaB proteins in the cytoplasm do not contact each other, and each MlaB molecule interacts with one MlaF [121]. The MlaD hexamer rests on top of the periplasmic side of the MlaE dimer [117]. The six α -helices form a hollow hydrophobic channel to allow the transport of lipids. A total of six MlaD TMHs in the MlaFEDB complex are inserted into the membrane [121]. Each three MlaD subunits incorporate one MlaE where the interaction between the TMH of MlaD and the EH of MlaE is critical for the phospholipid transport function of MlaFEDB [121].

Recent cryo-EM structural work on the Mla system has provided further insights into this intriguing complex. The high-resolution structures from *E. coli* [114,121,126], *Pseudomonas aeruginosa* [127], and *Acinetobacter baumannii* [128,129] clearly indicate that the overall architecture of the whole complex is conserved throughout these species.

These structures show that in the absence of ATP, MlaE embraces a V-shaped open conformation to frame a cavity with the wider side confronting the hydrophobic channel of MlaD. In the case of *E. coli*, the lipid binding site has been shown to be the outward-open pocket of MlaE [114,126], while for *A. baumannii*, lipid binding is described to happen at the pore of MlaD and in between the pore loops of the MCE domain of the MlaD hexamer [128]. A few of the structures contain residual electron density in the cavity and in different locations and could represent PLs or bound detergent [114,121,126–129] (see Figure 9A). The direction of lipid transport by the Mla system is discussed as controversial. A retrograde transport mechanism was originally described for the Mla system, where it maintained

the lipid asymmetry by removing mislocated phospholipids from the outer leaflet of the OM and importing them back to the plasma membrane [106–109,113,115,116,130]. However, there is also data that supports the export of phospholipids (anterograde transport) from the IM to the OM [119,125,126,131] or even a bi-directional transport between both membranes [114].

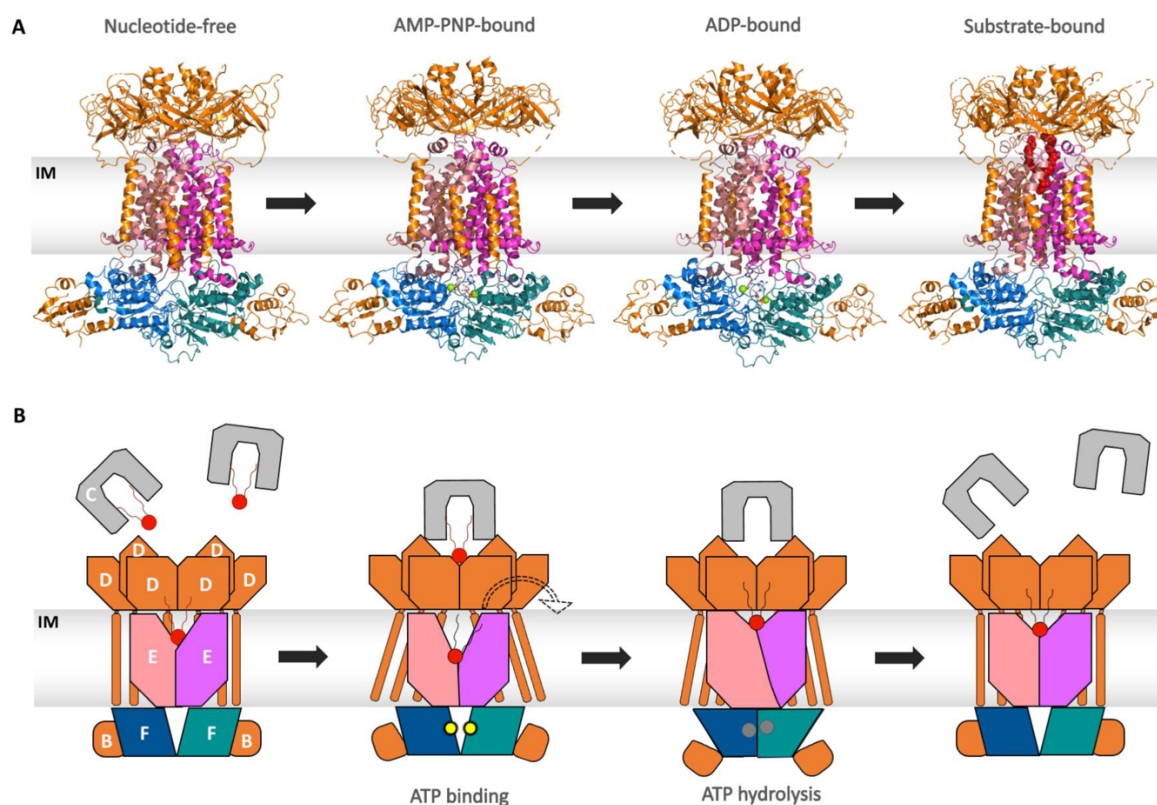


Figure 9. Structures and model representing the transport cycle of the Mla pathway. MlaC is shown in grey. The hexameric MlaD and both MlaB are shown in orange. MlaE is shown in salmon and light magenta. MlaF is shown in marine and deep teal. Lipid molecules are shown in red, and nucleotides are shown as spheres. The IM is displayed as a grey box. The peptidoglycan layer is omitted for reasons of clarity. (A): Different states of the ABC transporter during the transport cycle: nucleotide-free (PDB: 6ZY2), AMP-PNP-bound (PDB: 6ZY9), ADP-bound (PDB: 6ZY4), and substrate-bound (PDB: 6ZY3). (B): A schematic model of the retrograde transport of the lipid via MlaFEDB. Lipid-loaded MlaC binds to MlaD in the resting state of MlaFEDB. Binding of ATP (yellow dots) prompts the exit of the lipid molecule present in the cavity of MlaE from the last transport cycle. ATP hydrolysis to ADP (grey circles) and P_i prompts dimerization of MlaF and conformational changes in MlaE, which ultimately lead to the extraction of lipid from MlaD-MlaC into the cavity of MlaE. Upon release of hydrolyzed products, the conformation gets back to the resting state.

For simplicity, we only describe here the proposed retrograde transport mechanism in the context of phospholipid import (see Figure 9B). However, reversing the outlined steps could result in anterograde transport of phospholipids, as also described [119,125].

As part of the OmpF/C complex, MlaA is embedded inside the OM, and together they form a channel across the membrane [115]. Phospholipids are extracted from the outer leaflet of the OM into the channel via a lateral pathway. Interaction of MlaC to the MlaA-OmpC/OmpF complex results in phospholipid transfer to the hydrophobic pocket of MlaC [114,117,118]. Then, MlaC diffuses across the periplasm to deliver the lipids to

the MlaFEDB complex in the IM. A hexameric ring formed by MlaD subunits creates a central hydrophobic tunnel for the transport of lipids [117]. MlaC acts as a chaperone and directly binds to MlaD [117], transferring the lipid into a continuous channel from MlaD to an outward-facing MlaE [114,121,127–129]. ATP binding induces a conformational change in MlaE, resulting in the collapse of the lipid-binding pocket, thereby facilitating the incorporation of the lipids into the IM [121]. The auxiliary protein MlaB is known to regulate the transport [109,124].

Although the recent advances in research have added a plethora of information about the Mla system, a major unresolved question is still the directionality of lipid transport. MCEs are usually involved in the retrograde transport of misplaced phospholipids; however, there are still crucial details missing regarding the transfer of PLs from MlaC to MlaD.

Another open question is the reason behind the formation of stable complexes of MlaA with both OmpF and OmpC. Interestingly only one of these assemblies is functional, although functionality towards the transport of PLs lies within MlaA. These questions need to be addressed in the future to better understand the system.

5. The Lol System

Lipoproteins are crucial elements in bacteria. They are either located in the outer leaflet of the cytoplasmic membrane or in the leaflets of the OM. The latter case is most often true for Gram-negative bacteria, which is also the focus of this section. Lipoproteins are a compelling object of study for many reasons. One of them is their strong involvement in building and maintaining the OM of Gram-negative bacteria. As the OM is the first line of defense against xenobiotics, lipoproteins, their synthesis, and their transport pathway are attractive targets for novel antibiotics [132,133]. This section focuses specifically on the ABC transporter, which is involved in the transport of lipoproteins, and shows a transport mechanism differing from the classical ABC transporter mechanism. For a better overview regarding the synthesis, sorting, and function of lipoproteins, the interested reader is referred to other reviews [132,133], as these aspects will only be briefly mentioned here.

Lipoproteins are synthesized in the cytoplasm together with a cleavable signal peptide, which contains a consensus sequence that is highly conserved among lipoproteins, called the lipobox. The consensus sequence is L-A/S-G/A-C and was confirmed by various sequence analyses [134,135]. After translocation to the IM via the Sec [132,136] or, in some cases, via the Tat machinery [132,137], lipoproteins undergo further maturation steps in the outer leaflet of the IM. In the first step, the enzyme Lgt attaches a diacyl moiety to the cysteine in the aforementioned consensus sequence [138]. Subsequently, the enzyme Lsp [139,140] cleaves the signal sequence from the cysteine, and therefore this residue is named Cys⁺ and becomes the new N-Terminus of the lipoprotein. In the last maturation step, another acyl group is attached to the free amino group of the cysteine by Lnt [141,142]. The sorting of lipoproteins either to the IM or the OM is determined in *E. coli* by the amino acid next to the N-terminal cysteine of mature lipoproteins (the +2 position). If this amino acid is aspartate, the lipoprotein is retained in the IM [143]. In the case of most other naturally occurring residues, the lipoprotein is localized to the OM [144].

The trafficking of lipoproteins to the OM of Gram-negative bacteria is mediated by the localization of lipoproteins (Lol) system [133]. The discovery of the Lol system started with the discovery of the periplasmic chaperone LolA (called p20 at that time), which was found to form a soluble complex with a lipoprotein [145]. Soon, the interaction partner of LolA, namely LolB, was also discovered [146]. LolB was localized to the OM and was identified as an essential protein for *E. coli*, as depletion of LolB is lethal. It was further shown that the incubation of a lipoprotein-LolA complex with a soluble LolB derivative led to the transfer of the lipoprotein to the OM. Through these findings, an initial mechanism for lipoprotein localization was already emerging. Soon after that, the crystal structures of LolA and LolB were solved [147]. Remarkably, both proteins showed a similar overall structure, despite their different amino acid sequences. Both proteins show a beta-barrel structure with a hydrophobic inside and alpha-helical lid. The hydrophobic cavities were identified as the

possible binding sites for the acyl chains of the transported lipoproteins. This was further supported by finding polyethylene glycol 2000 monomethyl ether (PEGMME2000), which was used for the crystallization, in the hydrophobic cavity in one of the LolB structures [147].

It was later discovered that the detachment of lipoproteins from the membrane is ATP-dependent, and the corresponding protein is an ABC transporter [148]. Yakushi et al. solved the stoichiometry of this transporter termed LolCDE. It is a tetrameric and asymmetric ABC transporter composed of the proteins LolC and LolE, which make up the TMDs, and two copies of LolD, which form the NBDs. It was predicted that both proteins, LolC and LolE, each possess four transmembrane helices and a large periplasmic domain [148]. Due to the topology of LolCDE, the transporter can be assigned to the group of type VII ABC transporters [24]. Taking together all main findings, a general transport cycle, as shown in Figure 10, was derived.

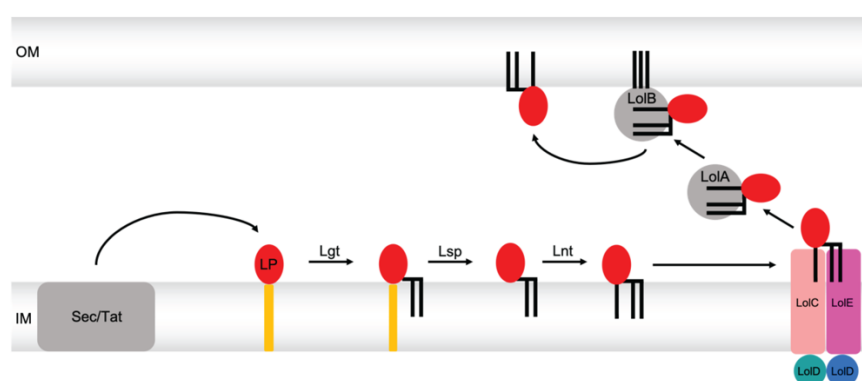


Figure 10. Overview of the Lol pathway. After insertion of lipoproteins (red, labeled one time with LP) via the Sec or the Tat pathway into the IM, they are diacylated (black) by Lgt in a first modification step. This is followed by cleavage of the N-terminal signal sequence (orange) by Lsp. Subsequently, Lnt acylates the newly N-terminally located cysteine, which makes the now mature lipoprotein ready for transport via the Lol machinery. This starts with the extraction of the lipoprotein from the cytoplasmic membrane via the ABC transporter LolCDE (salmon, light magenta, deep teal, and marine), which leads to the delivery of the lipoprotein to the periplasmic chaperone LolA (grey). LolA shuffles the lipoprotein to the last checkpoint LolB (grey), which finally inserts the lipoprotein into the outer membrane.

One major unknown factor was certainly the ABC transporter LolCDE. Its mechanism has to surely differ from the mechanism of classical ABC transporter, as the substrate is located in the outer leaflet of the inner membrane and not in the cytoplasm. However, for a relatively long time after the discovery of the Lol pathway, the ABC transporter LolCDE lacked structural analysis, and thus, a detailed understanding of its molecular mechanisms was missing. The first published structure related to LolCDE comprised a crystal structure of a soluble periplasmic domain of LolC solved by the Koronakis lab [29]. This structural analysis was done to confirm the structural similarity of the periplasmic domain of LolC to that of the homologous ABC transporter MacB, which is involved inter alia in the efflux of antibiotic macrolides (described in Section 2). The confirmation of the similarity of the two periplasmic domains of LolC and MacB led to the conclusion that LolC could also follow the mechanotransmission mechanism. This characteristic periplasmic domain is divided into two subdomains named *sabre* and *porter*. The superposition of the *sabre* domains of LolC and MacB showed a prominent loop in LolC which is not present in MacB. Accordingly, this loop was investigated further by the Koronakis lab, and they solved the crystal structure of the periplasmic domain of LolC in complex with the periplasmic chaperone LolA [149]. This structure sheds light on the molecular details of the interactions within the complex and highlights the importance of this loop, which was termed “hook”.

Furthermore, an additional important interacting domain was found in LolC, which was termed “pad”. The hook and the pad were determined to be essential for the recruitment of LolA. These findings further underpin the assignment of LolCDE into the group of type VII ABC transporters, as MacB is the founding member of this group [24]. In a more recent study, the crystal structure of LolA bound to a ligand was also solved by the Koronakis lab [150]. The structure shows the precise interaction of the acyl chains of the lipoprotein with the hydrophobic cavity in LolA. In addition, an overlap between the acyl binding sites and the LolC binding sites of LolA were found by comparison with other LolC-LolA structures. This indicates that the substrate binding to LolA is inducing the detachment from LolC. These findings further complete our understanding of the Lol system.

Since 2021, major breakthroughs have been made regarding the structural characterization of LolCDE. Tang et al. started this by solving six structures of the transporter representing different states of the transport via cryo-EM [151]. The structures represent LolCDE solubilized in the detergent LMNG. In the apo state, the NBDs show a relaxed conformation, whereas the rest of the transporter shows a rather compact conformation. More precisely, the transmembrane (TM) segments of LolC twist around the TM segments of LolE, and the PD of LolC rotates to the front of the PD of LolE. In the substrate-bound conformation, the TMDs of LolCDE are outward-opened, leading to a V-shaped central channel. In addition, two lateral gates are observable, which are formed by TMH1 and TMH2 of each of the proteins, LolC and LolE. The triacyl chains and a small N-terminal segment of the lipoprotein were resolved in a vertical arrangement in the upper part of the V-shaped channel. This suggests that the lipoprotein was extracted laterally from the periplasmic side of the IM, as this is also the arrangement of the lipoprotein in the IM. Furthermore, two AMP-PNP-bound LolCDE structures were solved by Tang et al. [151]. Only one of these structures contains a bound lipoprotein. Since AMP-PNP is a non-hydrolyzable ATP analog, these structures represent LolCDE after ATP binding. In the lipoprotein-bound structure, the transporter maintains its V-shaped cavity, and the NBDs are open. In the structure without the lipoprotein, the NBDs are closed. The closure of the NBDs leads to conformational changes in the TMDs, which leads to the closure of the central channel. In particular, TMH1 and TMH2 of LolE are shifted towards LolC. Additionally, the TMH2 of LolE clashes with the triacylcysteine of the lipoprotein of the ligand-bound state, which leads to the extrusion of the lipoprotein.

Sharma and colleagues published cryo-EM structures of LolCDE in a nucleotide-free and a nucleotide-bound state reconstituted in nanodiscs, which represent a native-like lipid environment [152]. In summary, the two determined structures show a very high similarity to the structural counterparts determined by Tang et al. [151]. The nucleotide-bound state was determined using an ADP-vanadate complex trapped in the ATP binding site. In addition, in the vanadate-trapped structure, the two LolD proteins come into close contact, which leads to the uplifting of the TMH2. Thus, ATP-binding leads to the extrusion of the lipoproteins from the TMDs to LolA. Sharma et al. further points out that in this conformation, TMH2 closes the lateral opening between LolC and LolE [152]. This could serve as a further mechanism for preventing substrate entry before the completion of a full transport cycle. In comparison to the structures of Tang et al. [151], the nucleotide-free structure of Sharma et al. [152] shows a significant difference in the binding of the lipoproteins. In the structure of Sharma et al. [152], the N-terminally linked acyl chain of the lipoprotein adopts a rather horizontal conformation in the cavity of LolCDE compared to the rather vertical arrangement of this acyl chain in the structure of Tang et al. [151].

In a relatively recent study, Bei et al. presented cryo-EM structures of nanodisc-reconstituted LolCDE in the apo, lipoprotein-bound, and AMP-PNP-bound states [153]. In general, the structures are highly similar to the corresponding structures published by Tang et al. [151] and Sharma et al. [152]. However, Bei et al. [153] pointed out a remarkable difference in the distances of the periplasmic domains of LolC and LolE in the apo state compared to the apo state determined by Tang et al. [151]. Nevertheless, the structures of Bei et al. [153] also suggested that the binding of ATP leads to the closure

of the central cavity and to the extrusion of the lipoprotein. The three structures determined by Bei et al. [153] are depicted exemplarily for the LolCDE transport mechanism in Figure 11. Panel B shows how the movement of TMH2 of LolE leads to the blockage of the central cavity and, thus, to the extrusion of the lipoprotein.

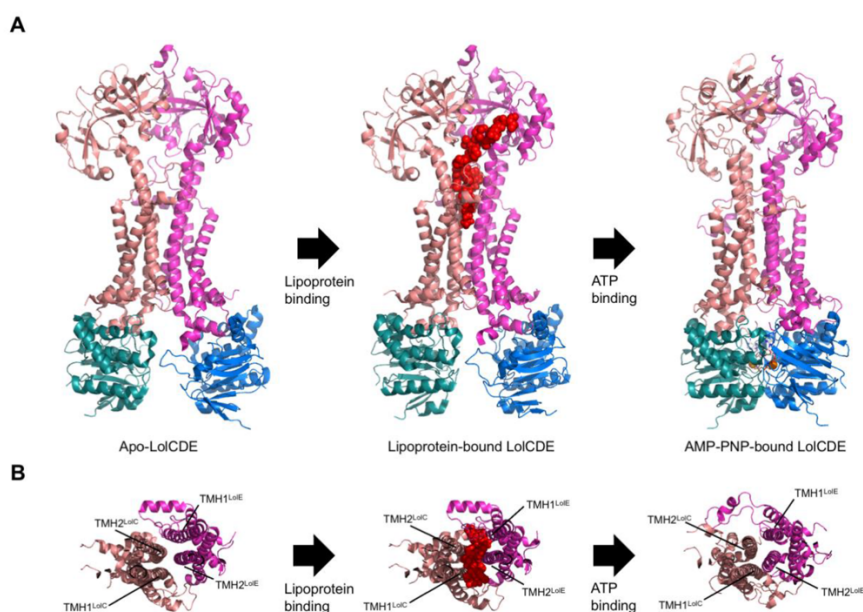


Figure 11. Structures of LolCDE in the Apo (PDB: 7V8M), lipoprotein-bound (PDB: 7V8L), and AMP-PNP-bound (PDB: 7V8I) form. LolC is shown in salmon, LolE is shown in light magenta, one LolD monomer is shown in deep teal, and the other LolD monomer is shown in marine. The lipoprotein is shown in red spheres. **(A):** Side-view of LolCDE. In the Apo state, LolCDE exhibits a V-shaped cavity that the lipoprotein enters from the membrane. Upon ATP binding (AMP-PNP-bound state), the central cavity is closed, and the substrate is shuffled out of LolCDE to LolA. **(B):** Cross-sectional view of the TMDs of LolCDE in the different substrate- or nucleotide-bound states. Movement of TMH2 of LolE upon ATP-binding into the central cavity extrudes the substrate out of the transporter.

Putting it all together, the published LolCDE structures in different transport states show a high similarity and correspond well with each other, especially regarding the connection of ATP-binding and release of the substrate to the periplasmic chaperone LolA [152,153]. All studies suggested a similar transport mechanism. In the apo state, the lipoprotein is extracted from the outer leaflet of the IM in an energy-independent manner into the V-shaped cavity inside LolCDE. Through ATP-binding, the NBDs dimerize, which leads to movements in the TMDs, resulting in the shuffling of the lipoprotein to LolA. After the dissociation of ADP and the lipoprotein-LolA complex, the central cavity opens again, and the transporter is primed for the next transport cycle. Despite the vast similarities, slight differences exist between specific structures. There are also differences between the ATPase activities of the different structures. For instance, LolCDE prepared in nanodiscs by Sharma and colleagues shows a several-fold higher activity than LolCDE purified in LMNG by Tang et al. [151,152]. The differences could be attributed to the different detergent and lipid environments in which the structures were solved. This further emphasizes the significance and involvement of lipids in the function of membrane transporters and membrane proteins in general. The ABC transporter LolCDE falls in line with a group of emerging ABC transporters, which show a non-classical transport mechanism. The initial suggestion that LolCDE also follows a mechanotransmission mechanism due to the resemblance to MacB [29] was confirmed by the various discussed LolCDE structures. The study of such ABC transporters with non-conventional transport mechanisms enhances

our understanding of living systems and could pave the way for novel drug targets and biotechnological applications.

6. Conclusions

Here, we have reviewed four ABC transporters that form the energizing component of four bacterial nanomachineries. We also tried to highlight how the use of ATP deviates from the classic “two-side access” [8] and how these machineries adapted to the particular needs of transporting quite different substrates. Although we have witnessed a tremendous increase in knowledge about the function and structure of the nanomachineries, we have also summarized the obvious questions.

Despite the availability of structural information on the whole MacAB-TolC nanomachinery, detailed insights about substrate binding and recognition are still lacking, including intermediate or substrate-bound structures. Especially the role of ATP hydrolysis in substrate translocation and possible feedback from the putative binding site to the NBDs require further investigations.

Similarly, there are still some intriguing features of the Lpt system, such as the role of LptC during the inactive state or the influence of LptC on the binding of LptB₂FG to ATP and substrate, that need to be studied in detail towards an in-depth understanding of the Lpt system. Additionally, the oligomeric organization of LptA forming the periplasmic bridge is still unknown.

For the Mla system, the fundamental question regarding the directionality of the transport remains open. The influence of the cell wall on the movement of MlaC is also unknown. Furthermore, the role of a non-functional OMP-MlaA assembly remains elusive.

In terms of the Lol system, the variety of structures is impressive though a detailed functional understanding of the shuttling process between IM and OM remains unclear. This emphasizes the necessity of a combination of all kinds of structural, biochemical, and biophysical data to understand these complex systems in detail.

These questions need to be addressed in the future to fully understand and maybe even exploit the beautiful variety of these different nanomachineries in prokaryotes.

Author Contributions: All authors wrote, drafted, and revised the review and searched for literature. L.S. was responsible for the ideation. All authors have read and agreed to the published version of the manuscript.

Funding: Work on ABC transporters is funded by the DFG (CRC 1208 project A01 and Schm1279/17-1 to L.S.).

Institutional Review Board Statement: Not applicable.

Informed Consent Statement: Not applicable.

Data Availability Statement: No new data were created or analyzed in this study. Data sharing is not applicable to this article.

Acknowledgments: We thank all current and former members of the Institute of Biochemistry for their support and many stimulating discussions. Apologies to all our colleagues whose work was not referenced. We thank the Center for Structural Sciences (CSS) at Heinrich Heine University for excellent support and infrastructure, which enables structural studies of our ABC systems.

Conflicts of Interest: The authors declare no conflict of interest.

References

1. Higgins, C.F. ABC transporters: Physiology, structure and mechanism—an overview. *Res. Microbiol.* **2001**, *152*, 205–210. [[CrossRef](#)] [[PubMed](#)]
2. Davidson, A.L.; Dassa, E.; Orelle, C.; Chen, J. Structure, function, and evolution of bacterial ATP-binding cassette systems. *Microbiol. Mol. Biol. Rev.* **2008**, *72*, 317–364. [[CrossRef](#)] [[PubMed](#)]
3. Biemans-Oldehinkel, E.; Doeven, M.K.; Poolman, B. ABC transporter architecture and regulatory roles of accessory domains. *FEBS Lett.* **2006**, *580*, 1023–1035. [[CrossRef](#)] [[PubMed](#)]

4. Thomas, C.; Tampe, R. Structural and Mechanistic Principles of ABC Transporters. *Annu. Rev. Biochem.* **2020**, *89*, 605–636. [[CrossRef](#)] [[PubMed](#)]
5. Oldham, M.L.; Davidson, A.L.; Chen, J. Structural insights into ABC transporter mechanism. *Curr. Opin. Struct. Biol.* **2008**, *18*, 726–733. [[CrossRef](#)]
6. Higgins, C.F.; Linton, K.J. The ATP switch model for ABC transporters. *Nat. Struct. Mol. Biol.* **2004**, *11*, 918–926. [[CrossRef](#)]
7. Hollenstein, K.; Dawson, R.J.; Locher, K.P. Structure and mechanism of ABC transporter proteins. *Curr. Opin. Struct. Biol.* **2007**, *17*, 412–418. [[CrossRef](#)]
8. Jardetzky, O. Simple allosteric model for membrane pumps. *Nature* **1966**, *211*, 969–970. [[CrossRef](#)]
9. Dawson, R.J.; Locher, K.P. Structure of a bacterial multidrug ABC transporter. *Nature* **2006**, *443*, 180–185. [[CrossRef](#)]
10. Bonifer, C.; Glaubit, C. MsbA: An ABC transporter paradigm. *Biochem. Soc. Trans.* **2021**, *49*, 2917–2927. [[CrossRef](#)]
11. Liu, F.; Zhang, Z.; Csanády, L.; Gadsby, D.C.; Chen, J. Molecular Structure of the Human CFTR Ion Channel. *Cell* **2017**, *169*, 85–95.e8. [[CrossRef](#)]
12. Chen, S.; Oldham, M.L.; Davidson, A.L.; Chen, J. Carbon catabolite repression of the maltose transporter revealed by X-ray crystallography. *Nature* **2013**, *499*, 364–368. [[CrossRef](#)]
13. Aller, S.G.; Yu, J.; Ward, A.; Weng, Y.; Chittaboina, S.; Zhuo, R.; Harrell, P.M.; Trinh, Y.T.; Zhang, Q.; Urbatsch, I.L.; et al. Structure of P-glycoprotein reveals a molecular basis for poly-specific drug binding. *Science* **2009**, *323*, 1718–1722. [[CrossRef](#)] [[PubMed](#)]
14. Choudhury, H.G.; Tong, Z.; Mathavan, I.; Li, Y.; Iwata, S.; Zirah, S.; Rebuffat, S.; Van Veen, H.W.; Beis, K. Structure of an antibacterial peptide ATP-binding cassette transporter in a novel outward occluded state. *Proc. Natl. Acad. Sci. USA* **2014**, *111*, 9145–9150. [[CrossRef](#)] [[PubMed](#)]
15. Kopcho, N.; Chang Gand Komives, E.A. Dynamics of ABC Transporter P-glycoprotein in Three Conformational States. *Sci. Rep.* **2019**, *9*, 15092. [[CrossRef](#)] [[PubMed](#)]
16. Hofmann, S.; Janulien, D.; Mehdipour, A.R.; Thomas, C.; Stefan, E.; Brüchert, S.; Kuhn, B.T.; Geertsma, E.R.; Hummer, G.; Tampé, R.; et al. Conformation space of a heterodimeric ABC exporter under turnover conditions. *Nature* **2019**, *571*, 580–583. [[CrossRef](#)]
17. Lin, D.Y.; Huang, S.; Chen, J. Crystal structures of a polypeptide processing and secretion transporter. *Nature* **2015**, *523*, 425–430. [[CrossRef](#)]
18. Perez, C.; Mehdipour, A.R.; Hummer, G.; Locher, K.P. Structure of Outward-Facing PglK and Molecular Dynamics of Lipid-Linked Oligosaccharide Recognition and Translocation. *Structure* **2019**, *27*, 669–678.e5. [[CrossRef](#)]
19. George, A.M.; Jones, P.M. An asymmetric post-hydrolysis state of the ABC transporter ATPase dimer. *PLoS ONE* **2013**, *8*, e59854. [[CrossRef](#)]
20. Prieß, M.; Göddeke, H.; Groenhof, G.; Schäfer, L.V. Molecular Mechanism of ATP Hydrolysis in an ABC Transporter. *ACS Cent. Sci.* **2018**, *4*, 1334–1343. [[CrossRef](#)]
21. Stefan, E.; Hofmann, S.; Tampé, R. A single power stroke by ATP binding drives substrate translocation in a heterodimeric ABC Transporter. *Elife* **2020**, *9*, e55943. [[CrossRef](#)] [[PubMed](#)]
22. Mishra, S.; Verhalen, B.; Stein, R.A.; Wen, P.C.; Tajkhorshid, E.; Mchaourab, H.S. Conformational dynamics of the nucleotide binding domains and the power stroke of a heterodimeric ABC transporter. *Elife* **2014**, *3*, e02740. [[CrossRef](#)] [[PubMed](#)]
23. Souabni, H.; Batista dos Santos, W.; Cece, Q.; Catoire, L.J.; Puvanendran, D.; Bavro, V.N.; Picard, M. Quantitative real-time analysis of the efflux by the MacAB-TolC tripartite efflux pump clarifies the role of ATP hydrolysis within mechanotransmission mechanism. *Commun. Biol.* **2021**, *4*, 493. [[CrossRef](#)] [[PubMed](#)]
24. Thomas, C.; Aller, S.G.; Beis, K.; Carpenter, E.P.; Chang, G.; Chen, L.; Dassa, E.; Dean, M.; Duong Van Hoa, F.; Ekiert, D.; et al. Structural and functional diversity calls for a new classification of ABC transporters. *FEBS Lett.* **2020**, *594*, 3767–3775. [[CrossRef](#)]
25. Ekiert, D.C.; Coudray, N.; Bhabha, G. Structure and mechanism of the bacterial lipid ABC transporter, MlaFEDB. *Curr. Opin. Struct. Biol.* **2022**, *76*, 102429. [[CrossRef](#)] [[PubMed](#)]
26. Kobayashi, N.; Nishino, K.; Yamaguchi, A. Novel macrolide-specific ABC-type efflux transporter in Escherichia coli. *J. Bacteriol.* **2001**, *183*, 5639–5644. [[CrossRef](#)]
27. Yamanaka, H.; Kobayashi, H.; Takahashi, E.; Okamoto, K. MacAB is involved in the secretion of Escherichia coli heat-stable enterotoxin II. *J. Bacteriol.* **2008**, *190*, 7693–7698. [[CrossRef](#)]
28. Turlin, E.; Heuck, G.; Simões Brandão, M.I.; Szili, N.; Mellin, J.R.; Lange, N.; Wandersman, C. Protoporphyrin (PPIX) efflux by the MacAB-TolC pump in Escherichia coli. *Microbiologyopen* **2014**, *3*, 849–859. [[CrossRef](#)]
29. Crow, A.; Greene, N.P.; Kaplan, E.; Koronakis, V. Structure and mechanotransmission mechanism of the MacB ABC transporter superfamily. *Proc. Natl. Acad. Sci. USA* **2017**, *114*, 12572–12577. [[CrossRef](#)]
30. Shi, K.; Cao, M.; Li, C.; Huang, J.; Zheng, S.; Wang, G. Efflux proteins MacAB confer resistance to arsenite and penicillin/macrolide-type antibiotics in Agrobacterium tumefaciens 5A. *World J. Microbiol. Biotechnol.* **2019**, *35*, 115. [[CrossRef](#)]
31. Zheng, J.X.; Lin, Z.W.; Sun, X.; Lin, W.H.; Chen, Z.; Wu, Y.; Qi, G.B.; Deng, Q.W.; Qu, D.; Yu, Z.J. Overexpression of OqxAB and MacAB efflux pumps contributes to eravacycline resistance and heteroresistance in clinical isolates of Klebsiella pneumoniae. *Emerg. Microbes. Infect.* **2018**, *7*, 139. [[CrossRef](#)]
32. Greene, N.P.; Kaplan, E.; Crow, A.; Koronakis, V. Antibiotic Resistance Mediated by the MacB ABC Transporter Family: A Structural and Functional Perspective. *Front. Microbiol.* **2018**, *9*, 950. [[CrossRef](#)] [[PubMed](#)]
33. Groisman, E.A. The pleiotropic two-component regulatory system PhoP-PhoQ. *J. Bacteriol.* **2001**, *183*, 1835–1842. [[CrossRef](#)] [[PubMed](#)]

34. Nishino, K.; Latifi, T.; Groisman, E.A. Virulence and drug resistance roles of multidrug efflux systems of *Salmonella enterica* serovar Typhimurium. *Mol. Microbiol.* **2006**, *59*, 126–141. [\[CrossRef\]](#) [\[PubMed\]](#)
35. Koronakis, V.; Sharff, A.; Koronakis, E.; Luisi, B.; Hughes, C. Crystal structure of the bacterial membrane protein TolC central to multidrug efflux and protein export. *Nature* **2000**, *405*, 914–919. [\[CrossRef\]](#)
36. Lin, H.T.; Bavro, V.N.; Barrera, N.P.; Frankish, H.M.; Velamakanni, S.; van Veen, H.W.; Robinson, C.V.; Borges-Walmsley, M.I.; Walmsley, A.R. MacB ABC transporter is a dimer whose ATPase activity and macrolide-binding capacity are regulated by the membrane fusion protein MacA. *J. Biol. Chem.* **2009**, *284*, 1145–1154. [\[CrossRef\]](#)
37. Tikhonova, E.B.; Devroy, V.K.; Lau, S.Y.; Zgurskaya, H.I. Reconstitution of the *Escherichia coli* macrolide transporter: The periplasmic membrane fusion protein MacA stimulates the ATPase activity of MacB. *Mol. Microbiol.* **2007**, *63*, 895–910. [\[CrossRef\]](#)
38. Barrera, N.P.; Isaacson, S.C.; Zhou, M.; Bavro, V.N.; Welch, A.; Schaedler, T.A.; Seeger, M.A.; Miguel, R.N.; Korkhov, V.M.; Van Veen, H.W.; et al. Mass spectrometry of membrane transporters reveals subunit stoichiometry and interactions. *Nat. Methods* **2009**, *6*, 585–587. [\[CrossRef\]](#)
39. Xu, Y.; Sim, S.H.; Nam, K.H.; Jin, X.L.; Kim, H.M.; Hwang, K.Y.; Lee, K.; Ha, N.C. Crystal structure of the periplasmic region of MacB, a noncanonic ABC transporter. *Biochemistry* **2009**, *48*, 5218–5225. [\[CrossRef\]](#)
40. Yum, S.; Xu, Y.; Piao, S.; Sim, S.H.; Kim, H.M.; Jo, W.S.; Kim, K.J.; Kweon, H.S.; Jeong, M.H.; Jeon, H.; et al. Crystal structure of the periplasmic component of a tripartite macrolide-specific efflux pump. *J. Mol. Biol.* **2009**, *387*, 1286–1297. [\[CrossRef\]](#)
41. Xu, Y.; Sim, S.H.; Song, S.; Piao, S.; Kim, H.M.; Jin, X.L.; Lee, K.; Ha, N.C. The tip region of the MacA alpha-hairpin is important for the binding to TolC to the *Escherichia coli* MacAB-TolC pump. *Biochem. Biophys. Res. Commun.* **2010**, *394*, 962–965. [\[CrossRef\]](#) [\[PubMed\]](#)
42. Xu, Y.; Song, S.; Moeller, A.; Kim, N.; Piao, S.; Sim, S.H.; Kang, M.; Yu, W.; Cho, H.S.; Chang, I.; et al. Functional implications of an intermeshing cogwheel-like interaction between TolC and MacA in the action of macrolide-specific efflux pump MacAB-TolC. *J. Biol. Chem.* **2011**, *286*, 13541–13549. [\[CrossRef\]](#) [\[PubMed\]](#)
43. Lee, M.; Kim, H.L.; Song, S.; Joo, M.; Lee, S.; Kim, D.; Hahn, Y.; Ha, N.C.; Lee, K. The alpha-barrel tip region of *Escherichia coli* TolC homologs of *Vibrio vulnificus* interacts with the MacA protein to form the functional macrolide-specific efflux pump MacAB-TolC. *J. Microbiol.* **2013**, *51*, 154–159. [\[CrossRef\]](#) [\[PubMed\]](#)
44. Fitzpatrick, A.W.; Llabrés, S.; Neuberger, A.; Blaza, J.N.; Bai, X.C.; Okada, U.; Murakami, S.; Van Veen, H.W.; Zachariae, U.; Scheres, S.H.; et al. Structure of the MacAB-TolC ABC-type tripartite multidrug efflux pump. *Nat. Microbiol.* **2017**, *2*, 17070. [\[CrossRef\]](#)
45. Okada, U.; Yamashita, E.; Neuberger, A.; Morimoto, M.; van Veen, H.W.; Murakami, S. Crystal structure of tripartite-type ABC transporter MacB from *Acinetobacter baumannii*. *Nat. Commun.* **2017**, *8*, 1336. [\[CrossRef\]](#) [\[PubMed\]](#)
46. Yang, H.B.; Hou, W.T.; Cheng, M.T.; Jiang, Y.L.; Chen, Y.; Zhou, C.Z. Structure of a MacAB-like efflux pump from *Streptococcus pneumoniae*. *Nat. Commun.* **2018**, *9*, 196. [\[CrossRef\]](#) [\[PubMed\]](#)
47. Modali, S.D.; Zgurskaya, H.I. The periplasmic membrane proximal domain of MacA acts as a switch in stimulation of ATP hydrolysis by MacB transporter. *Mol. Microbiol.* **2011**, *81*, 937–951. [\[CrossRef\]](#)
48. Lu, S.; Zgurskaya, H.I. Role of ATP binding and hydrolysis in assembly of MacAB-TolC macrolide transporter. *Mol. Microbiol.* **2012**, *86*, 1132–1143. [\[CrossRef\]](#)
49. Batista Dos Santos, W.; Souabni, H.; Picard, M. Corseting a tripartite ABC transporter to make it fit for transport. *Biochimie* **2022**, *205*, 117–123. [\[CrossRef\]](#)
50. Mühlradt, P.F.; Golecki, J.R. Asymmetrical distribution and artifactual reorientation of lipopolysaccharide in the outer membrane bilayer of *Salmonella typhimurium*. *Eur. J. Biochem.* **1975**, *51*, 343–352. [\[CrossRef\]](#)
51. Beveridge, T.J. Structures of gram-negative cell walls and their derived membrane vesicles. *J. Bacteriol.* **1999**, *181*, 4725–4733. [\[CrossRef\]](#)
52. Raetz, C.R.; Whitfield, C. Lipopolysaccharide endotoxins. *Annu. Rev. Biochem.* **2002**, *71*, 635. [\[CrossRef\]](#) [\[PubMed\]](#)
53. Whitfield, C.; Trent, M.S. Biosynthesis and export of bacterial lipopolysaccharides. *Annu. Rev. Biochem.* **2014**, *83*, 99–128. [\[CrossRef\]](#) [\[PubMed\]](#)
54. Bertani, B.; Ruiz, N. Function and biogenesis of lipopolysaccharides. *EcoSal Plus* **2018**, *8*. [\[CrossRef\]](#) [\[PubMed\]](#)
55. Trent, M.S.; Ribeiro, A.A.; Lin, S.; Cotter, R.J.; Raetz, C.R. An Inner Membrane Enzyme in *Salmonella* and *Escherichia coli* That Transfers 4-Amino-4-deoxy-L-arabinose to Lipid A: Induction in Polymyxin-Resistant Mutants and Role of a Novel Lipid-Linked Donor. *J. Biol. Chem.* **2001**, *276*, 43122–43131. [\[CrossRef\]](#) [\[PubMed\]](#)
56. Nummala, K.; Kilpeläinen, I.; Zähringer, U.; Vaara, M.; Helander, I.M. Lipopolysaccharides of polymyxin B-resistant mutants of *Escherichia coli* are extensively substituted by 2-aminoethyl pyrophosphate and contain aminoarabinose in lipid A. *Mol. Microbiol.* **1995**, *16*, 271–278. [\[CrossRef\]](#) [\[PubMed\]](#)
57. Kawasaki, S.; Moriguchi, R.; Sekiya, K.; Nakai, T.; Ono, E.; Kume, K.; Kawahara, K. The cell envelope structure of the lipopolysaccharide-lacking gram-negative bacterium *Sphingomonas paucimobilis*. *J. Bacteriol.* **1994**, *176*, 284–290. [\[CrossRef\]](#)
58. Salazar, J.C.; Hazlett, K.R.; Radolf, J.D. The immune response to infection with *Treponema pallidum*, the stealth pathogen. *Microbes Infect.* **2002**, *4*, 1133–1140. [\[CrossRef\]](#)
59. Zhang, G.; Meredith, T.C.; Kahne, D. On the essentiality of lipopolysaccharide to Gram-negative bacteria. *Curr. Opin. Microbiol.* **2013**, *16*, 779–785. [\[CrossRef\]](#)

60. Narita S-i Tokuda, H. Biochemical characterization of an ABC transporter LptBFGC complex required for the outer membrane sorting of lipopolysaccharides. *FEBS Lett.* **2009**, *583*, 2160–2164. [[CrossRef](#)]
61. Freinkman, E.; Chng, S.-S.; Kahne, D. The complex that inserts lipopolysaccharide into the bacterial outer membrane forms a two-protein plug-and-barrel. *Proc. Natl. Acad. Sci. USA* **2011**, *108*, 2486–2491. [[CrossRef](#)] [[PubMed](#)]
62. Freinkman, E.; Okuda, S.; Ruiz, N.; Kahne, D. Regulated Assembly of the Transenvelope Protein Complex Required for Lipopolysaccharide Export. *Biochemistry* **2012**, *51*, 4800–4806. [[CrossRef](#)] [[PubMed](#)]
63. Thomas, C.; Tampé, R. Multifaceted structures and mechanisms of ABC transport systems in health and disease. *Curr. Opin. Struct. Biol.* **2018**, *51*, 116–128. [[CrossRef](#)] [[PubMed](#)]
64. Ruiz, N.; Gronenberg, L.S.; Kahne, D.; Silhavy, T.J. Identification of two inner-membrane proteins required for the transport of lipopolysaccharide to the outer membrane of *Escherichia coli*. *Proc. Natl. Acad. Sci. USA* **2008**, *105*, 5537–5542. [[CrossRef](#)]
65. Luo, Q.; Yang, X.; Yu, S.; Shi, H.; Wang, K.; Xiao, L.; Zhu, G.; Sun, C.; Li, T.; Li, D.; et al. Structural basis for lipopolysaccharide extraction by ABC transporter LptB2FG. *Nat. Struct. Mol. Biol.* **2017**, *24*, 469–474. [[CrossRef](#)]
66. Sherman, D.J.; Lazarus, M.B.; Murphy, L.; Liu, C.; Walker, S.; Ruiz, N.; Kahne, D. Decoupling catalytic activity from biological function of the ATPase that powers lipopolysaccharide transport. *Proc. Natl. Acad. Sci. USA* **2014**, *111*, 4982–4987. [[CrossRef](#)]
67. Wang, Z.; Xiang, Q.; Zhu, X.; Dong, H.; He, C.; Wang, H.; Zhang, Y.; Wang, W.; Dong, C. Structural and functional studies of conserved nucleotide-binding protein LptB in lipopolysaccharide transport. *Biochem. Biophys. Res. Commun.* **2014**, *452*, 443–449. [[CrossRef](#)]
68. Tran, A.X.; Dong, C.; Whitfield, C. Structure and functional analysis of LptC, a conserved membrane protein involved in the lipopolysaccharide export pathway in *Escherichia coli*. *J. Biol. Chem.* **2010**, *285*, 33529–33539. [[CrossRef](#)]
69. Sperandio, P.; Lau, F.K.; Carpentieri, A.; De Castro, C.; Molinaro, A.; Deho, G.; Silhavy, T.J.; Polissi, A. Functional analysis of the protein machinery required for transport of lipopolysaccharide to the outer membrane of *Escherichia coli*. *J. Bacteriol.* **2008**, *190*, 4460–4469. [[CrossRef](#)]
70. Bos, M.P.; Tefsen, B.; Geurtsen, J.; Tommassen, J. Identification of an outer membrane protein required for the transport of lipopolysaccharide to the bacterial cell surface. *Proc. Natl. Acad. Sci. USA* **2004**, *101*, 9417–9422. [[CrossRef](#)]
71. Wu, T.; McCandlish, A.C.; Gronenberg, L.S.; Chng, S.S.; Silhavy, T.J.; Kahne, D. Identification of a protein complex that assembles lipopolysaccharide in the outer membrane of *Escherichia coli*. *Proc. Natl. Acad. Sci. USA* **2006**, *103*, 11754–11759. [[CrossRef](#)]
72. Dong, H.; Xiang, Q.; Gu, Y.; Wang, Z.; Paterson, N.G.; Stansfeld, P.J.; He, C.; Zhang, Y.; Wang, W.; Dong, C. Structural basis for outer membrane lipopolysaccharide insertion. *Nature* **2014**, *511*, 52–56. [[CrossRef](#)] [[PubMed](#)]
73. Qiao, S.; Luo, Q.; Zhao, Y.; Zhang, X.C.; Huang, Y. Structural basis for lipopolysaccharide insertion in the bacterial outer membrane. *Nature* **2014**, *511*, 108–111. [[CrossRef](#)]
74. Suits, M.D.; Sperandio, P.; Deho, G.; Polissi, A.; Jia, Z. Novel structure of the conserved gram-negative lipopolysaccharide transport protein A and mutagenesis analysis. *J. Mol. Biol.* **2008**, *380*, 476–488. [[CrossRef](#)]
75. Bowyer, A.; Baardsnes, J.; Ajamian, E.; Zhang, L.; Cygler, M. Characterization of interactions between LPS transport proteins of the Lpt system. *Biochem. Biophys. Res. Commun.* **2011**, *404*, 1093–1098. [[CrossRef](#)] [[PubMed](#)]
76. Sperandio, P.; Villa, R.; Martorana, A.M.; Šamalikova, M.; Grandori, R.; Deho, G.; Polissi, A. New insights into the Lpt machinery for lipopolysaccharide transport to the cell surface: LptA-LptC interaction and LptA stability as sensors of a properly assembled transenvelope complex. *J. Bacteriol.* **2011**, *193*, 1042–1053. [[CrossRef](#)] [[PubMed](#)]
77. Dong, H.; Zhang, Z.; Tang, X.; Paterson, N.G.; Dong, C. Structural and functional insights into the lipopolysaccharide ABC transporter LptB2FG. *Nat. Commun.* **2017**, *8*, 1–11. [[CrossRef](#)] [[PubMed](#)]
78. Tang, X.; Chang, S.; Luo, Q.; Zhang, Z.; Qiao, W.; Xu, C.; Zhang, C.; Niu, Y.; Yang, W.; Wang, T.; et al. Cryo-EM structures of lipopolysaccharide transporter LptB(2)FGC in lipopolysaccharide or AMP-PNP-bound states reveal its transport mechanism. *Nat. Commun.* **2019**, *10*, 4175. [[CrossRef](#)]
79. Li, Y.; Orlando, B.J.; Liao, M. Structural basis of lipopolysaccharide extraction by the LptB2FGC complex. *Nature* **2019**, *567*, 486–490. [[CrossRef](#)]
80. Luo, Q.; Shi, H.; Xu, X. Cryo-EM structures of LptB2FG and LptB2FGC from *Klebsiella pneumoniae* in complex with lipopolysaccharide. *Biochem. Biophys. Res. Commun.* **2021**, *571*, 20–25. [[CrossRef](#)]
81. Owens, T.W.; Taylor, R.J.; Pahil, K.S.; Bertani, B.R.; Ruiz, N.; Kruse, A.C.; Kahne, D. Structural basis of unidirectional export of lipopolysaccharide to the cell surface. *Nature* **2019**, *567*, 550–553. [[CrossRef](#)] [[PubMed](#)]
82. Wilson, A.; Ruiz, N. The transmembrane alpha-helix of LptC participates in LPS extraction by the LptB2 FGC transporter. *Mol. Microbiol.* **2022**, *118*, 61–76. [[CrossRef](#)] [[PubMed](#)]
83. Bertani, B.R.; Taylor, R.J.; Nagy, E.; Kahne, D.; Ruiz, N. A cluster of residues in the lipopolysaccharide exporter that selects substrate variants for transport to the outer membrane. *Mol. Microbiol.* **2018**, *109*, 541–554. [[CrossRef](#)] [[PubMed](#)]
84. Hamad, M.A.; Di Lorenzo, F.; Molinaro, A.; Valvano, M.A. Aminoarabinose is essential for lipopolysaccharide export and intrinsic antimicrobial peptide resistance in *Burkholderia cenocepacia*. *Mol. Microbiol.* **2012**, *85*, 962–974. [[CrossRef](#)] [[PubMed](#)]
85. Gronow, S.; Brade, H. Invited review: Lipopolysaccharide biosynthesis: Which steps do bacteria need to survive? *J. Endotoxin Res.* **2001**, *7*, 3–23. [[CrossRef](#)]
86. Khare, D.; Oldham, M.L.; Orelle, C.; Davidson, A.L.; Chen, J. Alternating access in maltose transporter mediated by rigid-body rotations. *Mol. Cell* **2009**, *33*, 528–536. [[CrossRef](#)]

87. Lundstedt, E.A.; Simpson, B.W.; Ruiz, N. LptB-LptF coupling mediates the closure of the substrate-binding cavity in the LptB2FGC transporter through a rigid-body mechanism to extract LPS. *Mol. Microbiol.* **2020**, *114*, 200–213. [\[CrossRef\]](#)
88. Simpson, B.W.; Owens, T.W.; Orabella, M.J.; Davis, R.M.; May, J.M.; Trauger, S.A.; Kahne, D.; Ruiz, N. Identification of residues in the lipopolysaccharide ABC transporter that coordinate ATPase activity with extractor function. *MBio* **2016**, *7*, e01729-16. [\[CrossRef\]](#)
89. Simpson, B.W.; Pahil, K.S.; Owens, T.W.; Lundstedt, E.A.; Davis, R.M.; Kahne, D.; Ruiz, N. Combining mutations that inhibit two distinct steps of the ATP hydrolysis cycle restores wild-type function in the lipopolysaccharide transporter and shows that ATP binding triggers transport. *MBio* **2019**, *10*, e01931-19. [\[CrossRef\]](#)
90. Okuda, S.; Sherman, D.J.; Silhavy, T.J.; Ruiz, N.; Kahne, D. Lipopolysaccharide transport and assembly at the outer membrane: The PEZ model. *Nat. Rev. Microbiol.* **2016**, *14*, 337–345. [\[CrossRef\]](#)
91. Sherman, D.J.; Xie, R.; Taylor, R.J.; George, A.H.; Okuda, S.; Foster, P.J.; Needleman, D.J.; Kahne, D. Lipopolysaccharide is transported to the cell surface by a membrane-to-membrane protein bridge. *Science* **2018**, *359*, 798–801. [\[CrossRef\]](#)
92. Botte, M.; Ni, D.; Schenck, S.; Zimmermann, I.; Chami, M.; Bocquet, N.; Egloff, P.; Bucher, D.; Trabuco, M.; Cheng, R.K.; et al. Cryo-EM structures of a LptDE transporter in complex with Pro-macrobodies offer insight into lipopolysaccharide translocation. *Nat. Commun.* **2022**, *13*, 1–10. [\[CrossRef\]](#) [\[PubMed\]](#)
93. Gu, Y.; Stansfeld, P.J.; Zeng, Y.; Dong, H.; Wang, W.; Dong, C. Lipopolysaccharide is inserted into the outer membrane through an intramembrane hole, a lumen gate, and the lateral opening of LptD. *Structure* **2015**, *23*, 496–504. [\[CrossRef\]](#) [\[PubMed\]](#)
94. Malojčić, G.; Andres, D.; Grabowicz, M.; George, A.H.; Ruiz, N.; Silhavy, T.J.; Kahne, D. LptE binds to and alters the physical state of LPS to catalyze its assembly at the cell surface. *Proc. Natl. Acad. Sci. USA* **2014**, *111*, 9467–9472. [\[CrossRef\]](#) [\[PubMed\]](#)
95. Chng, S.S.; Ruiz, N.; Chimalakonda, G.; Silhavy, T.J.; Kahne, D. Characterization of the two-protein complex in Escherichia coli responsible for lipopolysaccharide assembly at the outer membrane. *Proc. Natl. Acad. Sci. USA* **2010**, *107*, 5363–5368. [\[CrossRef\]](#) [\[PubMed\]](#)
96. Ruiz, N.; Chng, S.S.; Hiniker, A.; Kahne, D.; Silhavy, T.J. Nonconsecutive disulfide bond formation in an essential integral outer membrane protein. *Proc. Natl. Acad. Sci. USA* **2010**, *107*, 12245–12250. [\[CrossRef\]](#) [\[PubMed\]](#)
97. Chimalakonda, G.; Ruiz, N.; Chng, S.S.; Garner, R.A.; Kahne, D.; Silhavy, T.J. Lipoprotein LptE is required for the assembly of LptD by the β -barrel assembly machine in the outer membrane of Escherichia coli. *Proc. Natl. Acad. Sci. USA* **2011**, *108*, 2492–2497. [\[CrossRef\]](#)
98. Xie, R.; Taylor, R.J.; Kahne, D. Outer Membrane Translocon Communicates with Inner Membrane ATPase To Stop Lipopolysaccharide Transport. *J. Am. Chem. Soc.* **2018**, *140*, 12691–12694. [\[CrossRef\]](#)
99. Baeta, T.; Giandoreggio-Barranco, K.; Ayala, I.; Moura, E.C.; Sperandio, P.; Polissi, A.; Simorre, J.P.; Laguri, C. The lipopolysaccharide-transporter complex LptB2FG also displays adenylate kinase activity in vitro dependent on the binding partners LptC/LptA. *J. Biol. Chem.* **2021**, *297*, 101313. [\[CrossRef\]](#)
100. Randak, C.; Welsh, M.J. An intrinsic adenylate kinase activity regulates gating of the ABC transporter CFTR. *Cell* **2003**, *115*, 837–850. [\[CrossRef\]](#)
101. Kaur, H.; Lakatos-Karoly, A.; Vogel, R.; Nöll, A.; Tampé, R.; Glaubitz, C. Coupled ATPase-adenylate kinase activity in ABC transporters. *Nat. Commun.* **2016**, *7*, 13864. [\[CrossRef\]](#) [\[PubMed\]](#)
102. Villa, R.; Martorana, A.M.; Okuda, S.; Gourlay, L.J.; Nardini, M.; Sperandio, P.; Dehò, G.; Bolognesi, M.; Kahne, D.; Polissi, A. The Escherichia coli Lpt transenvelope protein complex for lipopolysaccharide export is assembled via conserved structurally homologous domains. *J. Bacteriol.* **2013**, *195*, 1100–1108. [\[CrossRef\]](#) [\[PubMed\]](#)
103. Falchi, F.A.; Taylor, R.J.; Rowe, S.J.; Moura, E.C.; Baeta, T.; Laguri, C.; Simorre, J.P.; Kahne, D.E.; Polissi, A.; Sperandio, P. Suppressor Mutations in LptF Bypass Essentiality of LptC by Forming a Six-Protein Transenvelope Bridge That Efficiently Transports Lipopolysaccharide. *mBio* **2022**, *0*, e02202-22. [\[CrossRef\]](#) [\[PubMed\]](#)
104. Benedet, M.; Falchi, F.A.; Puccio, S.; Di Benedetto, C.; Peano, C.; Polissi, A.; Deho, G. The lack of the essential LptC protein in the trans-envelope lipopolysaccharide transport machine is circumvented by suppressor mutations in LptF, an inner membrane component of the Escherichia coli transporter. *PLoS ONE* **2016**, *11*, e0161354. [\[CrossRef\]](#)
105. Silhavy, T.J.; Kahne, D.; Walker, S. The bacterial cell envelope. *Cold Spring Harb Perspect. Biol.* **2010**, *2*, a000414. [\[CrossRef\]](#)
106. Malinverni, J.C.; Silhavy, T.J. An ABC transport system that maintains lipid asymmetry in the gram-negative outer membrane. *Proc. Natl. Acad. Sci. USA* **2009**, *106*, 8009–8014. [\[CrossRef\]](#)
107. Powers, M.J.; Trent, M.S. Phospholipid retention in the absence of asymmetry strengthens the outer membrane permeability barrier to last-resort antibiotics. *Proc. Natl. Acad. Sci. USA* **2018**, *115*, E8518–E8527. [\[CrossRef\]](#)
108. Sutterlin, H.A.; Shi, H.; May, K.L.; Miguel, A.; Khare, S.; Huang, K.C.; Silhavy, T.J. Disruption of lipid homeostasis in the Gram-negative cell envelope activates a novel cell death pathway. *Proc. Natl. Acad. Sci. USA* **2016**, *113*, E1565–E1574. [\[CrossRef\]](#)
109. Thong, S.; Ercan, B.; Torta, F.; Fong, Z.Y.; Wong, H.Y.A.; Wenk, M.R.; Chng, S.S. Defining key roles for auxiliary proteins in an ABC transporter that maintains bacterial outer membrane lipid asymmetry. *Elife* **2016**, *5*, e19042. [\[CrossRef\]](#)
110. Benning, C. A role for lipid trafficking in chloroplast biogenesis. *Prog. Lipid Res.* **2008**, *47*, 381–389. [\[CrossRef\]](#)
111. Mohn, W.W.; Van Der Geize, R.; Stewart, G.R.; Okamoto, S.; Liu, J.; Dijkhuizen, L.; Eltis, L.D. The actinobacterial mce4 locus encodes a steroid transporter. *J. Biol. Chem.* **2008**, *283*, 35368–35374. [\[CrossRef\]](#)
112. Pandey, A.K.; Sasseti, C.M. Mycobacterial persistence requires the utilization of host cholesterol. *Proc. Natl. Acad. Sci. USA* **2008**, *105*, 4376–4380. [\[CrossRef\]](#) [\[PubMed\]](#)

113. Low, W.-Y.; Thong, S.; Chng, S.-S. ATP disrupts lipid-binding equilibrium to drive retrograde transport critical for bacterial outer membrane asymmetry. *Proc. Natl. Acad. Sci. USA* **2021**, *118*, e2110055118. [[CrossRef](#)] [[PubMed](#)]
114. Tang, X.; Chang, S.; Qiao, W.; Luo, Q.; Chen, Y.; Jia, Z.; Coleman, J.; Zhang, K.; Wang, T.; Zhang, Z.; et al. Structural insights into outer membrane asymmetry maintenance in Gram-negative bacteria by MlaFEDB. *Nat. Struct. Mol. Biol.* **2021**, *28*, 81–91. [[CrossRef](#)] [[PubMed](#)]
115. Abellón-Ruiz, J.; Kaptan, S.S.; Baslé, A.; Claudi, B.; Bumann, D.; Kleinekathöfer, U.; van den Berg, B. Structural basis for maintenance of bacterial outer membrane lipid asymmetry. *Nat. Microbiol.* **2017**, *2*, 1616–1623. [[CrossRef](#)] [[PubMed](#)]
116. Chong, Z.S.; Woo, W.F.; Chng, S.S. Osmoporin OmpC forms a complex with MlaA to maintain outer membrane lipid asymmetry in *Escherichia coli*. *Mol. Microbiol.* **2015**, *98*, 1133–1146. [[CrossRef](#)]
117. Ekiert, D.C.; Bhabha, G.; Isom, G.L.; Greenan, G.; Ovchinnikov, S.; Henderson, I.R.; Cox, J.S.; Vale, R.D. Architectures of lipid transport systems for the bacterial outer membrane. *Cell* **2017**, *169*, 273–285.e17. [[CrossRef](#)]
118. Ercan, B.; Low, W.Y.; Liu, X.; Chng, S.S. Characterization of interactions and phospholipid transfer between substrate binding proteins of the OmpC-Mla system. *Biochemistry* **2018**, *58*, 114–119. [[CrossRef](#)]
119. Hughes, G.W.; Hall, S.C.; Laxton, C.S.; Sridhar, P.; Mahadi, A.H.; Hatton, C.; Piggot, T.J.; Wotherspoon, P.J.; Leney, A.C.; Ward, D.G.; et al. Evidence for phospholipid export from the bacterial inner membrane by the Mla ABC transport system. *Nat. Microbiol.* **2019**, *4*, 1692–1705. [[CrossRef](#)]
120. Isom, G.L.; Davies, N.J.; Chong, Z.S.; Bryant, J.A.; Jamshad, M.; Sharif, M.; Cunningham, A.F.; Knowles, T.J.; Chng, S.S.; Cole, J.A.; et al. MCE domain proteins: Conserved inner membrane lipid-binding proteins required for outer membrane homeostasis. *Sci. Rep.* **2017**, *7*, 8608. [[CrossRef](#)]
121. Chi, X.; Fan, Q.; Zhang, Y.; Liang, K.; Wan, L.; Zhou, Q.; Li, Y. Structural mechanism of phospholipids translocation by MlaFEDB complex. *Cell Res.* **2020**, *30*, 1127–1135. [[CrossRef](#)] [[PubMed](#)]
122. Oldham, M.L.; Chen, J. Crystal structure of the maltose transporter in a pretranslocation intermediate state. *Science* **2011**, *332*, 1202–1205. [[CrossRef](#)] [[PubMed](#)]
123. Shibagaki, N.; Grossman, A.R. The role of the STAS domain in the function and biogenesis of a sulfate transporter as probed by random mutagenesis. *J. Biol. Chem.* **2006**, *281*, 22964–22973. [[CrossRef](#)] [[PubMed](#)]
124. Kolich, L.R.; Chang, Y.T.; Coudray, N.; Giacometti, S.I.; MacRae, M.R.; Isom, G.L.; Teran, E.M.; Bhabha, G.; Ekiert, D.C. Structure of MlaFB uncovers novel mechanisms of ABC transporter regulation. *Elife* **2020**, *9*, e60030. [[CrossRef](#)] [[PubMed](#)]
125. Kamischke, C.; Fan, J.; Bergeron, J.; Kulasekara, H.D.; Dalebroux, Z.D.; Burrell, A.; Kollman, J.M.; Miller, S.I. The *Acinetobacter baumannii* Mla system and glycerophospholipid transport to the outer membrane. *Elife* **2019**, *8*, e40171. [[CrossRef](#)]
126. Coudray, N.; Isom, G.L.; MacRae, M.R.; Saiduddin, M.N.; Bhabha, G.; Ekiert, D.C. Structure of bacterial phospholipid transporter MlaFEDB with substrate bound. *Elife* **2020**, *9*, e62518. [[CrossRef](#)]
127. Zhou, C.; Shi, H.; Zhang, M.; Zhou, L.; Xiao, L.; Feng, S.; Im, W.; Zhou, M.; Zhang, X.; Huang, Y. Structural insight into phospholipid transport by the MlaFEBD complex from *P. aeruginosa*. *J. Mol. Biol.* **2021**, *433*, 166986. [[CrossRef](#)]
128. Mann, D.; Fan, J.; Somboon, K.; Farrell, D.P.; Muenks, A.; Tzokov, S.B.; DiMaio, F.; Khalid, S.; Miller, S.I.; Bergeron, J.R. Structure and lipid dynamics in the maintenance of lipid asymmetry inner membrane complex of *A. baumannii*. *Commun. Biol.* **2021**, *4*, 1–9. [[CrossRef](#)]
129. Zhang, Y.; Fan, Q.; Chi, X.; Zhou, Q.; Li, Y. Cryo-EM structures of *Acinetobacter baumannii* glycerophospholipid transporter. *Cell Discov.* **2020**, *6*, 86. [[CrossRef](#)]
130. Yeow, J.; Tan, K.W.; Holdbrook, D.A.; Chong, Z.S.; Marzinek, J.K.; Bond, P.J.; Chng, S.S. The architecture of the OmpC–MlaA complex sheds light on the maintenance of outer membrane lipid asymmetry in *Escherichia coli*. *J. Biol. Chem.* **2018**, *293*, 11325–11340. [[CrossRef](#)]
131. Hughes, G.W.; Sridhar, P.; Nestorow, S.A.; Wotherspoon, P.J.; Cooper, B.F.; Knowles, T.J. MlaFEDB displays flippase activity to promote phospholipid transport towards the outer membrane of Gram-negative bacteria. *bioRxiv* **2020**. [[CrossRef](#)]
132. Narita, S.I.; Tokuda, H. Bacterial lipoproteins; biogenesis, sorting and quality control. *Biochim. Biophys. Acta. Mol. Cell Biol. Lipids.* **2017**, *1862*, 1414–1423. [[CrossRef](#)]
133. Grabowicz, M. Lipoproteins and Their Trafficking to the Outer Membrane. *EcoSal Plus* **2019**, *8*. [[CrossRef](#)] [[PubMed](#)]
134. Hayashi, S.; Wu, H.C. Lipoproteins in bacteria. *J. Bioenerg. Biomembr.* **1990**, *22*, 451–471. [[CrossRef](#)] [[PubMed](#)]
135. Babu, M.M.; Priya, M.L.; Selvan, A.T.; Madera, M.; Gough, J.; Aravind, L.; Sankaran, K. A database of bacterial lipoproteins (DOLOP) with functional assignments to predicted lipoproteins. *J. Bacteriol.* **2006**, *188*, 2761–2773. [[CrossRef](#)] [[PubMed](#)]
136. Pugsley, A.P. The complete general secretory pathway in gram-negative bacteria. *Microbiol. Rev.* **1993**, *57*, 50–108. [[CrossRef](#)]
137. Giménez, M.I.; Dilks, K.; Pohlschröder, M. Haloferax volcanii twin-arginine translocation substates include secreted soluble, C-terminally anchored and lipoproteins. *Mol. Microbiol.* **2007**, *66*, 1597–1606. [[CrossRef](#)]
138. Sankaran, K.; Wu, H.C. Lipid modification of bacterial prolipoprotein. Transfer of diacylglycerol moiety from phosphatidylglycerol. *J. Biol. Chem.* **1994**, *269*, 19701–19706. [[CrossRef](#)]
139. Inouye, S.; Franceschini, T.; Sato, M.; Itakura, K.; Inouye, M. Prolipoprotein signal peptidase of *Escherichia coli* requires a cysteine residue at the cleavage site. *EMBO J.* **1983**, *2*, 87–91. [[CrossRef](#)]
140. Vogeley, L.; El Arnaout, T.; Bailey, J.; Stansfeld, P.J.; Boland, C.; Caffrey, M. Structural basis of lipoprotein signal peptidase II action and inhibition by the antibiotic globomycin. *Science* **2016**, *351*, 876–880. [[CrossRef](#)]

141. Jackowski, S.; Rock, C.O. Transfer of fatty acids from the 1-position of phosphatidylethanolamine to the major outer membrane lipoprotein of *Escherichia coli*. *J. Biol. Chem.* **1986**, *261*, 11328–11333. [[CrossRef](#)] [[PubMed](#)]
142. Gupta, S.D.; Wu, H.C. Identification and subcellular localization of apolipoprotein N-acyltransferase in *Escherichia coli*. *FEMS Microbiol. Lett.* **1991**, *62*, 37–41. [[CrossRef](#)] [[PubMed](#)]
143. Yamaguchi, K.; Yu, F.; Inouye, M. A single amino acid determinant of the membrane localization of lipoproteins in *E. coli*. *Cell* **1988**, *53*, 423–432. [[CrossRef](#)] [[PubMed](#)]
144. Gennity, J.M.; Inouye, M. The protein sequence responsible for lipoprotein membrane localization in *Escherichia coli* exhibits remarkable specificity. *J. Biol. Chem.* **1991**, *266*, 16458–16464. [[CrossRef](#)] [[PubMed](#)]
145. Matsuyama, S.; Tajima, T.; Tokuda, H. A novel periplasmic carrier protein involved in the sorting and transport of *Escherichia coli* lipoproteins destined for the outer membrane. *EMBO J.* **1995**, *14*, 3365–3372. [[CrossRef](#)]
146. Matsuyama, S.; Yokota, N.; Tokuda, H. A novel outer membrane lipoprotein, LolB (HemM), involved in the LolA (p20)-dependent localization of lipoproteins to the outer membrane of *Escherichia coli*. *EMBO J.* **1997**, *16*, 6947–6955. [[CrossRef](#)]
147. Takeda, K.; Miyatake, H.; Yokota, N.; Matsuyama, S.I.; Tokuda, H.; Miki, K. Crystal structures of bacterial lipoprotein localization factors, LolA and LolB. *EMBO J.* **2003**, *22*, 3199–3209. [[CrossRef](#)]
148. Yakushi, T.; Masuda, K.; Narita, S.I.; Matsuyama, S.I.; Tokuda, H. A new ABC transporter mediating the detachment of lipid-modified proteins from membranes. *Nat. Cell Biol.* **2000**, *2*, 212–218. [[CrossRef](#)]
149. Kaplan, E.; Greene, N.P.; Crow, A.; Koronakis, V. Insights into bacterial lipoprotein trafficking from a structure of LolA bound to the LolC periplasmic domain. *Proc. Natl. Acad. Sci. USA* **2018**, *115*, E7389–E7397. [[CrossRef](#)]
150. Kaplan, E.; Greene, N.P.; Jepson, A.E.; Koronakis, V. Structural basis of lipoprotein recognition by the bacterial Lol trafficking chaperone LolA. *Proc. Natl. Acad. Sci. USA* **2022**, *119*, e2208662119. [[CrossRef](#)]
151. Tang, X.; Chang, S.; Zhang, K.; Luo, Q.; Zhang, Z.; Wang, T.; Qiao, W.; Wang, C.; Shen, C.; Zhang, Z.; et al. Structural basis for bacterial lipoprotein relocation by the transporter LolCDE. *Nat. Struct. Mol. Biol.* **2021**, *28*, 347–355. [[CrossRef](#)] [[PubMed](#)]
152. Sharma, S.; Zhou, R.; Wan, L.; Feng, S.; Song, K.; Xu, C.; Li, Y.; Liao, M. Mechanism of LolCDE as a molecular extruder of bacterial triacylated lipoproteins. *Nat. Commun.* **2021**, *12*, 4687. [[CrossRef](#)] [[PubMed](#)]
153. Bei, W.; Luo, Q.; Shi, H.; Zhou, H.; Zhou, M.; Zhang, X.; Huang, Y. Cryo-EM structures of LolCDE reveal the molecular mechanism of bacterial lipoprotein sorting in *Escherichia coli*. *PLoS Biol.* **2022**, *20*, e3001823. [[CrossRef](#)] [[PubMed](#)]

Disclaimer/Publisher's Note: The statements, opinions and data contained in all publications are solely those of the individual author(s) and contributor(s) and not of MDPI and/or the editor(s). MDPI and/or the editor(s) disclaim responsibility for any injury to people or property resulting from any ideas, methods, instructions or products referred to in the content.

3.2. Chapter 2: Subcellular localization of HlyA mRNA in *Escherichia coli*

Title:	Subcellular localization of HlyA mRNA in <i>Escherichia coli</i>
Authors:	Manuel T. Anlauf , Stefanie Weidtkamp-Peters, Lutz Schmitt
Published in:	(to be submitted)
Own proportion on this work:	80%
	Designing and cloning of plasmids
	Expression of proteins
	Preparation of microscopy samples
	Data analysis
	Preparation of figures
	Writing of the manuscript

Subcellular localization of HlyA mRNA in *Escherichia coli*

Manuel T. Anlauf¹, Stefanie Weidtkamp-Peters², Lutz Schmitt^{1*}

¹: Heinrich Heine University Düsseldorf, Faculty of Mathematics and Natural Sciences, Institute of Biochemistry, Universitätsstraße 1, 40225 Düsseldorf, Germany

²: Heinrich Heine University Düsseldorf, Faculty of Mathematics and Natural Sciences, Center for Advanced Imaging (CAi), Universitätsstraße 1, 40225 Düsseldorf, Germany

*: To whom correspondence should be addressed: Lutz Schmitt, Heinrich Heine University Düsseldorf, Faculty of Mathematics and Natural Sciences, Institute of Biochemistry, Universitätsstraße 1, 40225 Düsseldorf, Germany, Tel.: +49 211 81-10773, E-Mail: lutz.schmitt@hhu.de

Abstract

Secretion of substrates in Gram-negative bacteria is often mediated through dedicated secretion systems, which are classified by their structural features and molecular mechanisms. The type I secretion system (T1SS) is a simple system, consisting of three membrane components which form a channel that passes through the inner and outer membrane of the bacterial cell. The ABC transporter hemolysin B provides the energy for the translocation of the toxin hemolysin A (HlyA). It forms a complex in the inner membrane with the membrane fusion protein hemolysin D (HlyD), which connects the transporter with the outer membrane protein TolC. HlyA is recognized and transported via its C-terminal secretion signal in an unfolded state. Surprisingly, unfolded HlyA is stable in the cytoplasm and so far no chaperones were identified which could explain the lack of aggregation or degradation. We aimed to deploy the MS2 system and GFP fluorescence to answer the question, whether HlyA mRNA localizes to the membrane as translation may be spatially restricted, minimizing the presence of the unfolded protein in the cytoplasm. Neither the positive control of LacY mRNA nor HlyA mRNA exhibited localized GFP fluorescence at the membrane and problems as well as alternatives will be discussed here.

Abbreviations

ABC: ATP-binding cassette, CLD: C39 peptidase-like protein, eGFP: enhanced green fluorescent protein, hemolysin A: HlyA, hemolysin B: HlyB, hemolysin D: HlyD, IMC: inner membrane complex, IPTG: isopropyl- β -D-thiogalacto-pyranoside, MCP: MS2 coat protein, MFP: membrane fusion protein, MS2d: MS2 coat protein dimer, NBD: nucleotide-binding domain, OMP: outer membrane protein, rtPCR: reverse transcriptase Polymerase Chain Reaction, RTX: repeat in toxins, T1SS: Type 1 secretion system

Keywords

mRNA localization, MS2 coat protein, eGFP, fluorescence microscopy, hemolysin, type I secretion system

Introduction

Over millions of years, Gram-negative bacteria evolved a multitude of protein complexes to facilitate the secretion of substrates across their two membranes. The complexity ranges from the 6 MDa type III secretion system (T3SS) to simple tripartite Resistance-nodulation-division (RND) pumps such as AcrAB-TolC. The T3SS is composed of almost 20 different proteins with up to over hundred copies in one complex, enabling the secretion of dozens of functionally diverse proteins across a third membrane, the plasma membrane of the host, whereas RND pumps are capable of transporting a broad range of small exogenous molecules (Du *et al.* 2014, Wagner *et al.* 2018). Type I secretion systems (T1SS) are very similar to those RND pumps: they are also tripartite systems and use the porin-like TolC as the outer membrane protein (OMP) component. However, other than RND pumps, which utilize the proton motif force to transport the substrate, T1SS hydrolyze ATP to energize the secretion process (Koronakis *et al.* 1991, Koronakis *et al.* 1995, Murakami *et al.* 2002). This is accomplished by an ATP-binding cassette (ABC) transporter, which resides in the inner membrane. It is connected to the aforementioned OMP via a membrane fusion protein (MFP), forming a continuous channel and allowing the transport of substrates from the cytoplasm directly into the extracellular space (Delepelaire 2004).

One of the best studied T1SS is the hemolysin secretion system found in uropathogenic *E. coli* (UPEC) (Noegel *et al.* 1979, Holland *et al.* 2016, Nhu *et al.* 2019, Beer *et al.* 2021). The ABC transporter is hemolysin B (HlyB), a homodimeric protein with an additional C39 peptidase-like domain (CLD) at the N-terminus, commonly found in transporters of T1SS (Lecher *et al.* 2012). Together with the MFP hemolysin D (HlyD) it forms an inner membrane complex (IMC) (Gray *et al.* 1989, Wang *et al.* 1991, Pimenta *et al.* 1999, Balakrishnan *et al.* 2001). Upon recognition of the substrate, the OMP TolC is recruited and the complete transport complex is assembled (Thanabalu *et al.* 1998, Balakrishnan *et al.* 2001). The secreted substrate is hemolysin A (HlyA), a pore-forming toxin with a size of 1024 amino acids, its name originating from the ability to lyse erythrocytes (Springer *et al.* 1980, Bhakdi *et al.* 1986). It is part of the Repeats in ToXin (RTX) protein superfamily, a protein family which is commonly secreted by T1SS (Linhartová *et al.* 2010). Proteins of this family exhibit, often more than one, conserved glycine-rich nonapeptide repeat with the sequence GGxGxDxUx (where x is any amino acid and U a large, hydrophobic amino acid) (Welch 2001). These GG

repeats are able to bind Ca^{2+} ions primarily with the first six residues of the motif, promoting the folding into a β -roll structure (Baumann *et al.* 1993, Bumba *et al.* 2016). The Ca^{2+} ion concentration in the cytoplasm of *E. coli* is within 100-300 nM (Gangola *et al.* 1987, Jones 1999) and too low to bind to the RTX domains of HlyA ($K_D = 150 \mu\text{M}$ (Sanchez-Magraner *et al.* 2007)). The protein is therefore intrinsically disordered prior to secretion and only folds upon reaching the extracellular space. An unfolded state is a prerequisite for the secretion of substrates by T1SS, as it was shown that the transport of fast folding proteins or the fusion of such proteins to a native substrate is not possible (Bakkes *et al.* 2010, Lenders *et al.* 2015). One known bottleneck is the inner diameter of TolC; the narrowest part has a width of 20 Å, only allowing the passage of smaller secondary structures like α -helices (Koronakis *et al.* 2004, Lenders *et al.* 2013). Additionally, the unfolded RTX domain was shown to directly interact with the N-terminal CLD of the ABC transporter (Lecher *et al.* 2011, Lecher *et al.* 2012, Reimann *et al.* 2016). The information necessary for the secretion of HlyA is comprised in the secretion signal sequence located in the last 48-60 amino acids of the C-terminus (Nicaud *et al.* 1986, Mackman *et al.* 1987, Gray *et al.* 1989, Koronakis *et al.* 1989, Kenny *et al.* 1992, Jarchau *et al.* 1994). Although all substrates of T1SS carry such a secretion signal, no conserved primary sequence could be identified (Holland *et al.* 2016). Instead, the presence of an amphipathic helix in the secretion signal is suggested to be crucial for recognition of the toxin by its transporter (Koronakis *et al.* 1989, Stanley *et al.* 1991, Spitz *et al.* 2022). HlyA is interacting directly with HlyD and via its secretion signal with the NBD of HlyB (Thanabalu *et al.* 1998, Balakrishnan *et al.* 2001, Benabdelhak *et al.* 2003). After recognition and assembly of the secretion complex, HlyA is transported with its C-terminus first across both membranes directly into the extracellular space without formation of a periplasmic intermediate (Lenders *et al.* 2015).

Even though the hemolysin system is well investigated, some key questions remain unanswered. One of them is associated with two key characteristics of the secretion system: because HlyA's secretion signal is located at the C-terminus, it needs to be completely translated for the secretion process to start. At the same time, the toxin is in an unfolded state, without any signs of aggregation or degradation until secretion occurs. Another secretion system, the T3SS, solves this problem and keeps the transported proteins in a secretion-competent state by using specialized chaperones (Fu *et al.* 1998, Bronstein *et al.* 2000, Parsot *et al.* 2003, Akeda *et al.* 2005, Darwin *et*

et al. 2001). Neither specific nor universal chaperones were identified to interact with HlyA, e.g. the secretion of HlyA is independent from SecB and GroEL-GroES (Létoffé *et al.* 1992, Bakkes *et al.* 2010). One possible explanation is the guidance of HlyA mRNA to the cytoplasmic membrane. In this case, the translation would then occur in direct proximity to the inner membrane and the transporter complex where it is required, and the unfolded toxin would only be present in the cytoplasm for a very limited time. A similar observation of sub-cellularly localized RNA was made for the *E. coli* membrane-bound lactose permease LacY. The mRNA of this membrane protein was observed at or near the membrane (Nevo-Dinur *et al.* 2011). A similar result was also obtained for the mRNA of BglF, a protein involved in the phosphoenolpyruvate-dependent sugar phosphotransferase system (Nevo-Dinur *et al.* 2011). Additional proteins, for which the mRNA was found to be enriched near the membrane are the Fimbrin-like protein FimI and the 8-amino-7-oxononanoate synthase BioF (Kannaiah *et al.* 2019).

We therefore sought to localize the HlyA mRNA in *E. coli* to elucidate, if the absence of degradation or aggregation for unfolded HlyA in the cytoplasm is due to a spatially constrained translation. For this, we used the binding of the coat protein of the MS2 bacteriophage (henceforth called “MCP” for MS2 coat protein) to its respective RNA binding motif (MS2 stem loops). By fusing a fluorescent protein like eGFP to MS2 and concomitantly linking MS2 loops to the mRNA of interest, it is possible to localize and track the mRNA in the cell. This tool has already been successfully employed in mammalian cells, yeast and *E. coli* (Fouts *et al.* 1997, Valegård *et al.* 1997, Bertrand *et al.* 1998, Fusco *et al.* 2003, Golding *et al.* 2004). We chose LacY mRNA, which was demonstrated to localize to the membrane in *E. coli*, as a positive control for our experiments.

Results

With this project we sought to visualize and localize the mRNA of HlyA in *E. coli* cells. Even though bacterial cells are not compartmentalized, transcripts of some bacterial proteins were shown to localize at specific sites inside the cells (Nevo-Dinur *et al.* 2011, Kannaiah *et al.* 2019). Since chaperones could not be identified to explain the lack of degradation of unfolded HlyA prior to secretion, a localized expression of HlyA at the

membrane is a plausible cause, as it reduces the time of HlyA in the cytoplasm until it reaches the secretion complex by diffusion. Therefore, we applied the system which was used by Nevo-Dinur *et al.* (Nevo-Dinur *et al.* 2011) to localize the mRNA of LacY and used the same protein as a positive control for localization experiments. For this a total of three plasmids were generated: the gene coding for the fusion of *lacY* and the MS2 stem loops 6xMS2v4 was under control of an IPTG (isopropyl- β -D-thiogalacto-pyranoside) inducible *lac* promoter. The respective plasmid (pSU-6xMS2v4-lacY) had an ColE1 ori and conferred an ampicillin (Amp) resistance. For visualization of the mRNA, a gene fusion of an MCP dimer (*ms2d*) and *egfp* was cloned into the plasmid. The gene was under control of the *lac* promoter and included a kanamycin (Kan) resistance gene as well as a p15a ori (pK-MS2d-eGFP). Concomitantly, a second plasmid encoding for *ms2d-egfp* was constructed, as the first plasmid would not have been compatible with a plasmid encoding for *hlyBD*. This plasmid version had the gene for *ms2d-egfp* under control of an arabinose inducible araBAD promoter with an chloramphenicol (Cm) resistance gene and a ColA ori.

E. coli BL21(DE3) cells were transformed either with only one of the MS2d-eGFP coding plasmids or additionally with pSU-6xMS2v4-lacY. In both cases protein expression was induced and cells were incubated for 2 hours at 37°C and 180 rpm. Before preparation of cells for microscopy, a sample of the cultures was taken, diluted to equal optical densities and the presence of eGFP fluorescence was verified using an Amersham Imager 680 (Figure 1).

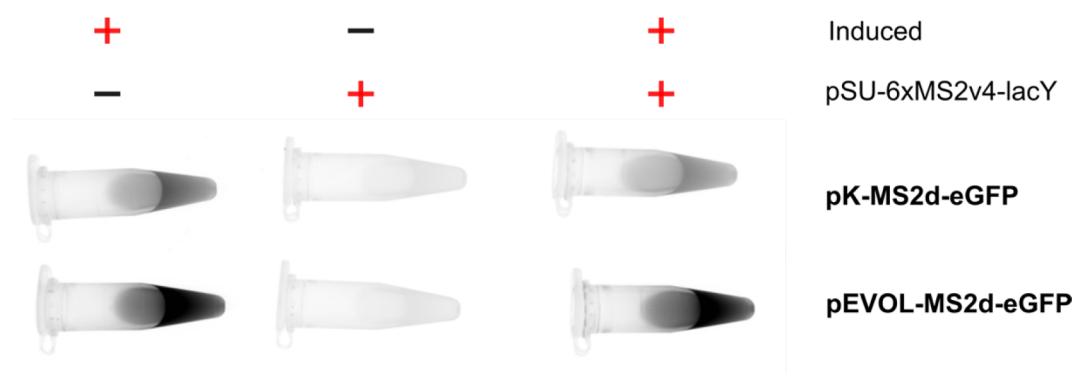


Figure 1: Test for eGFP fluorescence of *E. coli* BL21(DE3) cells expressing MS2d-eGFP 2 h after induction. Expression level of MS2d-eGFP is higher with the pEVOL-MS2d-eGFP plasmid in comparison to the pK-MS2d-eGFP plasmid (left). Both plasmids show no leaky expression (middle) and the presence of the plasmid pSU-6xMS2v4-lacY has no visible influence on the fluorescence. eGFP fluorescence was imaged with excitation at 460 nm using Blue Epi light.

With both plasmid variants, successful expression of MS2d-eGFP could be verified as reaction tubes with cell suspensions showed a fluorescent signal upon excitation at 460 nm. This fluorescence test also indicated, that cells transformed with pEVOL-MS2d-eGFP presented a stronger signal and therefore exhibited a higher expression level of MS2d-eGFP in comparison to cells carrying the pK-MS2d-eGFP plasmid. Nevertheless, since MS2d-eGFP was present, cells were fixated for fluorescence microscopy and localization of LacY mRNA fused to the 6xMS2v4 stem loops. *E. coli* BL21(DE3) transformed with one of the MS2d-eGFP coding plasmids and pSU-6xMS2v4-lacY were imaged 2 h after induction of protein expression (Figure 2). Two control measurements were conducted as well: one control comprised *E. coli* BL21(DE3) containing only the plasmid for expression of MS2d-eGFP, the other control were *E. coli* BL21(DE3) cells containing a plasmid for MS2d-eGFP and 6xMS2v4-LacY, but protein expression was not induced. Independent of the plasmid pSU-6xMS2v4-lacY being present or not (Figure 2, right and left panel respectively), fluorescence of eGFP was not restricted to the membrane of the cells as reported by Nevo-Dinur (Nevo-Dinur *et al.* 2011), but rather homogenously distributed in the cytoplasm of *E. coli*. No addition of IPTG or arabinose (Figure 2, middle panel) lead to very low levels of fluorescence, especially visible by the background fluorescence of the surrounding buffer for the cells transformed with the plasmid pK-MS2d-eGFP which showed the lower MS2d-eGFP expression level (Figure 2, middle upper panel).

Since eGFP fluorescence was not absent overall, there are two possibilities for the lack of localized fluorescence of eGFP: either the MS2d dimer is missing from the fusion protein or the 6xMS2v4-LacY mRNA is missing. The first possibility was assessed by Western blot analysis of expression samples using *E. coli* BL21(DE3) cells transformed with pEVOL-MS2d-eGFP (Figure 3). The antibody used targeted eGFP and resulted in three bands. The most intense band is visible at a height corresponding to approx. 55 kDa which fits to the theoretical mass of MS2d-eGFP with 52,854 Da. Furthermore, the band is only visible after induction of protein expression. The other two bands at approx. 60 and 26 kDa are lower in intensity and are present even before induction of protein expression, likely representing a cross reaction of the antibody with other endogenous proteins of *E. coli*. The lower band at ~26 kDa would potentially fit the size of monomeric eGFP.

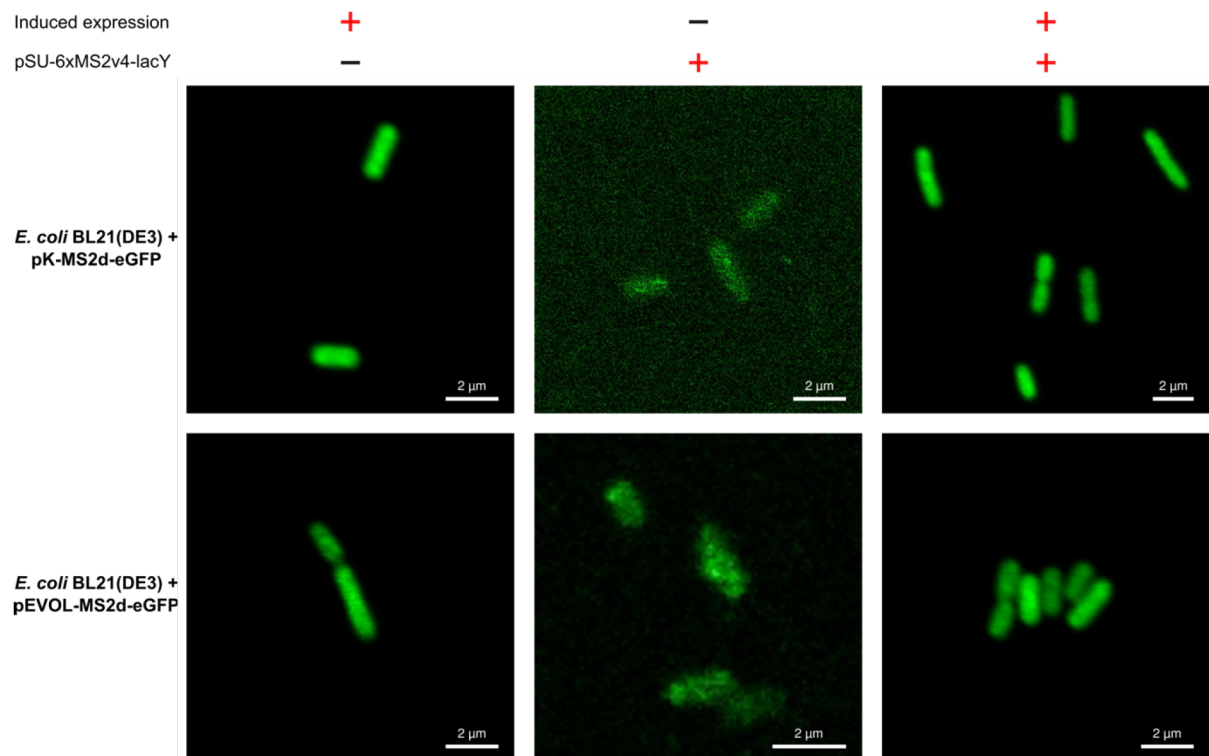


Figure 2: Localization of LacY mRNA in *E. coli* BL21(DE3) using fluorescence microscopy. Shown is the eGFP fluorescence of cells expressing MS2d-eGFP either from the plasmid pK-MS2d-eGFP (upper panel) or pEVOL-MS2d-eGFP (lower panel). The different combinations of induced protein expression and presence of additional plasmids is indicated on the top.

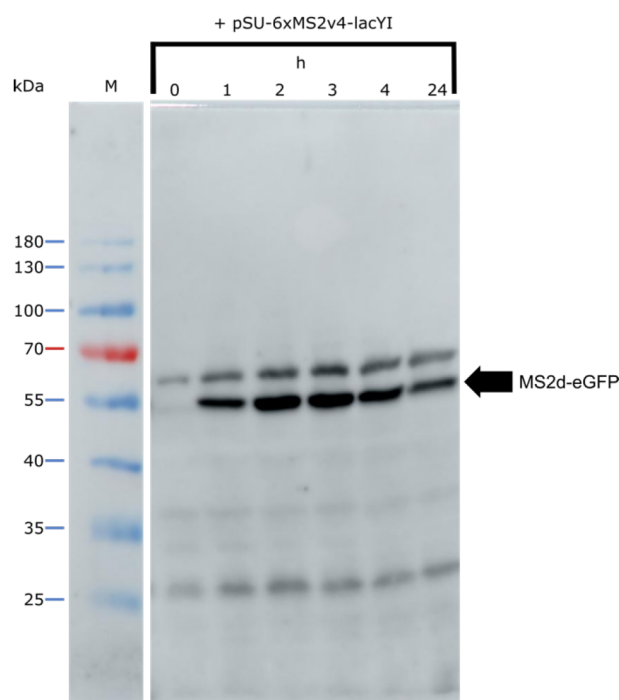


Figure 3: Western blot analysis of whole *E. coli* BL21(DE3) cells expressing MS2d-eGFP from the plasmid pEVOL-MS2d-eGFP. Cells additionally carried the plasmid pSU-6xMS2v4-lacYI. The numbers shown on the top indicate the hours after induction of protein expression. The polyclonal antibody used targeted eGFP. M: Protein marker, the approx. size of the marker proteins is given on the left. The theoretical mass of MS2d-eGFP is 52,854 Da.

As MS2d-eGFP seems to be present in the cells as full-length protein, the potential for the lack of 6xMS2v4-LacY mRNA was examined. For this, *E. coli* BL21(DE3) carrying pK-MS2d-eGFP and pSU-6xMS2v4-lacY were cultivated as described for fluorescence microscopy before. Total RNA was isolated and an agarose gel analysis performed as a quality control (Figure 4A). The gel shows a successful isolation of RNA, as three bands are visible. Ribosomal (rRNA) and transfer (tRNA) ribonucleic acids are the most abundant RNA species in cells. The upper band at ~1500 bp corresponds to the 23S rRNA, while the middle band at ~1000 bp corresponds to the 16S rRNA. The lower and most intense band is most likely comprised out of 5S rRNA and tRNAs.

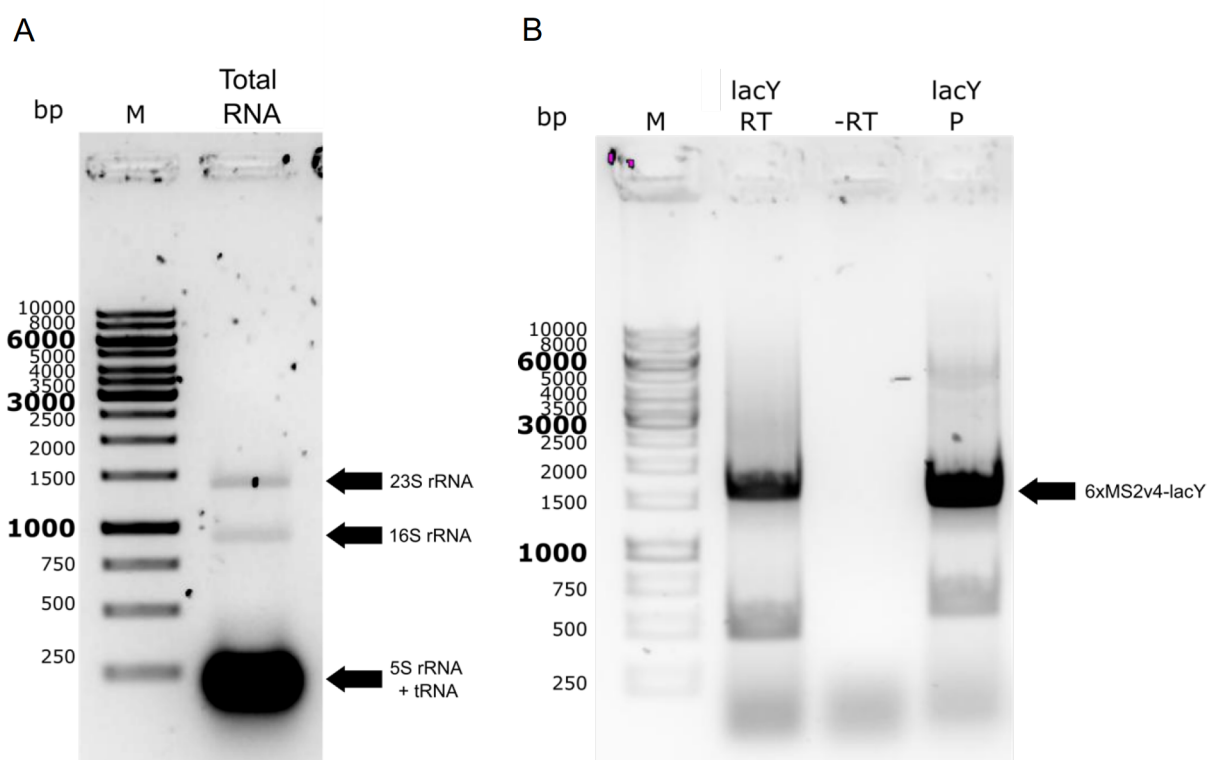


Figure 4: Identification of 6xMS2v4-LacY transcripts. **(A)** Agarose gel analysis of total RNA isolated from *E. coli* BL21(DE3) + pK-MS2d-eGFP + pSU-6xMS2v4-lacY. 10 μ l total RNA were mixed with 10 μ l 2xFA buffer. The upper and middle band correspond to bacterial 16S and 23S rRNA, while the lower band is comprised of 5S RNA and tRNA. **(B)** PCR using 6xMS2v4-lacY specific primers after rtPCR. Templates for the PCR: lacY RT: rtPCR using lacY-rev as a primer; lacY -RT: rtPCR without reverse transcriptase (control for gDNA contamination); lacY P: pSU-6xMS2v4-lacY plasmid (positive control). M: Generuler 1 kb DNA Ladder, the approx. size of the DNA fragments is given on the left side of the gels.

The isolated RNA was transcribed into cDNA using reverse transcriptase Polymerase Chain Reaction (rtPCR) and afterwards used in a PCR reaction using primers specific for *6xMS2v4-lacY* to identify the presence of the transcript in our cells (Figure 4B). Two control templates were used for the PCR: “-RT” is the product of the rtPCR without the reverse transcriptase added to the reaction. Product bands occurring within this sample are an indication for genomic DNA (gDNA) contamination, since no cDNA can be synthesized here and the RNA cannot be used as a template afterwards by the DNA polymerase. Here, no gDNA contamination was detectable. The “lacY P” sample contained the pSU-6xMS2v4-lacY plasmid as a positive control and shows the expected product band at a height of 1612 bp. “lacY RT” included the cDNA from the rtPCR as a template and added reverse transcriptase. A band with an identical size like in the positive control could be detected, indicating the presence of *6xMS2v4-lacY* transcript in cells transformed with pSU-6xMS2v4-lacY after induced expression.

Since no component of the MS2 system was absent in our cells, we varied different parameters in our setup to be as close as possible to the setup used by Nevo-Dinur. First, we changed the expression strain from *E. coli* BL21(DE3) to *E. coli* MG1655 and reduced the temperature during cultivation from 37°C to 30°C (Nevo-Dinur *et al.* 2011). This change did not influence the presence and fluorescence of eGFP in the cells (Figure S1). Neither the change of the expression strain to *E. coli* MG1655 nor the variation in expression time changed the localization of eGFP in the cells, as the eGFP fluorescence was still distributed homogenously in the cytoplasm (Figure S2).

Next, we changed the induction of transcription and protein expression: instead of inducing synthesis of MS2d-eGFP with arabinose and transcription of *6xMS2v4-lacY* with IPTG, we only added arabinose to the medium and transcription of *6xMS2v4-lacY* was not induced, limiting the mRNA production to the leaky expression of the lac operator (Nevo-Dinur *et al.* 2011). By doing this, we avoided the possibility of an overproduction of LacY mRNA, which could cause the mRNA to be not only localized at the membrane, but also to mislocalize in the cytoplasm. However, this did not lead to a change in the localization behavior of eGFP fluorescence (Figure S3).

Even though the localization of LacY mRNA at the membrane could not be reproduced here, a plasmid with the MS2 stem loops 6xMS2v4 upstream of the HlyA was generated to check for a localization of the respective HlyA mRNA in *E. coli* MG1655 cells. Several combinations of MS2d-eGFP plasmid variant, expression time, co-

expression of the HlyA T1SS IMC components HlyB and HlyD as well as adding or omitting IPTG during induction were tested (Figure 5). It should be noted, that omitting IPTG during the induction does not only limit transcription of the 6xMS2v4-HlyA mRNA to very low levels comparable to leaky expression, but also the expression of HlyB and HlyD if present. None of the tested conditions exhibited a localization of eGFP fluorescence at the membrane but rather a homogenously distributed fluorescence within the cytosol as observed before with 6xMS2v4-*lacY* transcripts.

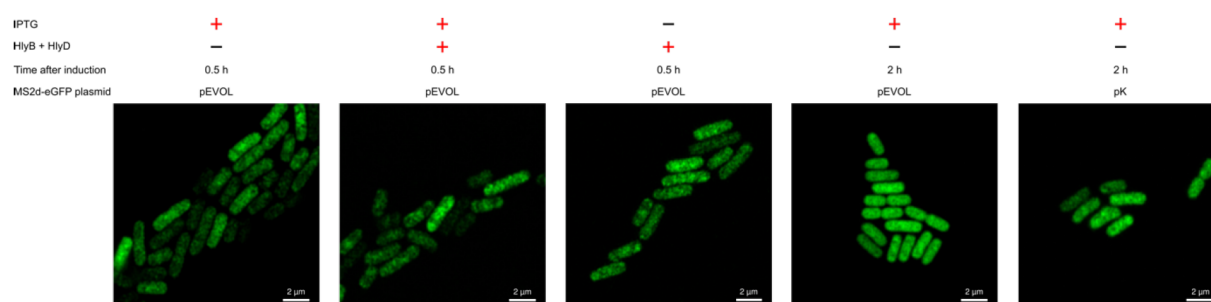


Figure 5: Localization of HlyA mRNA in *E. coli* MG1655 using fluorescence microscopy. Shown is the eGFP fluorescence of cells expressing MS2d-eGFP either from the plasmid pK-MS2d-eGFP (pK) or pEVOL-MS2d-eGFP (pEVOL). The different combinations of expression time (Time after induction), co-expression of HlyB and HlyD (HlyB + HlyD) and addition of IPTG during induction (IPTG) are indicated on the top.

We therefore assessed the presence and functionality of 6xMS2v4-HlyA mRNA in the imaged cells. *E. coli* MG1655 cells transformed with pEVOL-MS2d-eGFP, pK184-HlyBD and pSU-6xMS2v4-HlyA were used in a secretion experiment to test for the successful expression and secretion of non-acylated pro-HlyA with the MS2 stem loops upstream of *hlyA*. The strain *E. coli* BL21(DE3) + pK184-HlyBD + pSU2726-HlyA routinely used in our lab was used as a positive control. An SDS-PAGE of supernatant samples was performed (Figure 6A). Additionally, whole cells samples of strains used during the secretion experiment were used in Western blot analysis with an antibody targeting the secretion signal of pro-HlyA to identify not secreted protein (Figure 6B). Cells expressing MS2d-eGFP, HlyB and HlyD were able to transcribe 6xMS2v4-*hlyA* and subsequently secrete pro-HlyA. However, the amount of secreted pro-HlyA was reduced in comparison to cells expressing HlyB, HlyD and HlyA without the stem loops present upstream of *hlyA*. The latter strain showed a significant amount of not secreted pro-HlyA inside the cells, while no residual pro-HlyA was detectable in cells transcribing *hlyA* with the MS2 stem loop upstream of the gene.

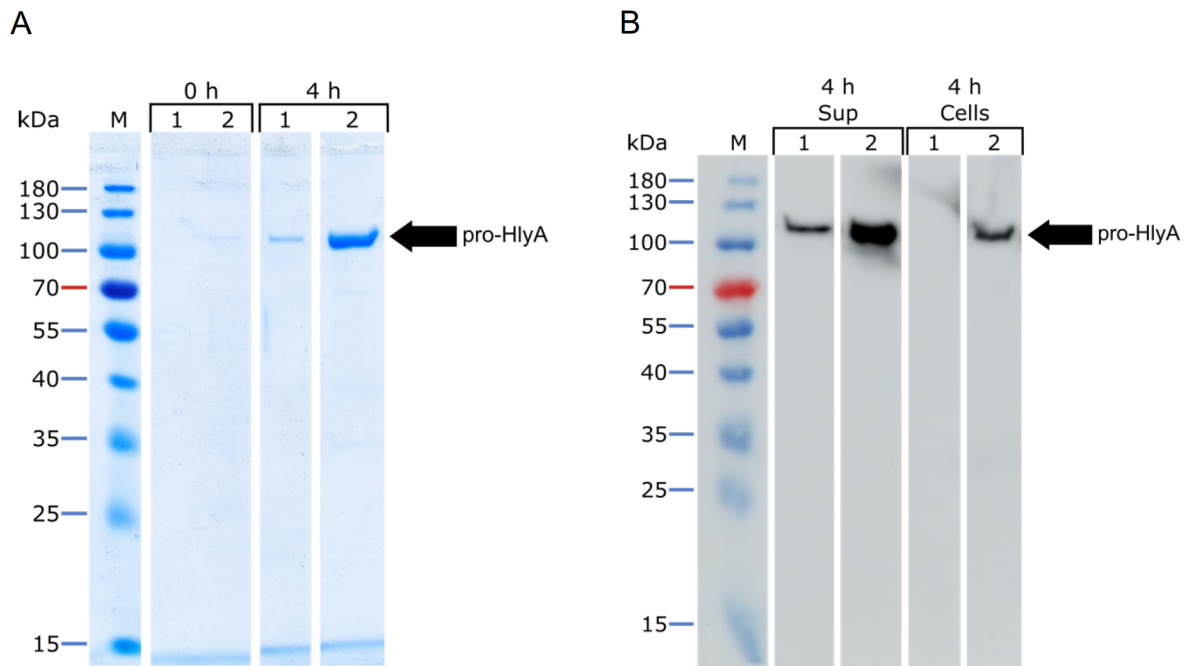


Figure 6: Secretion test of pro-HlyA expressed from pSU-6xMS2v4-HlyA. **(A)** SDS-PAGE of supernatant samples from *E. coli* MG1655 transformed with pEVOL-MS2d-eGFP, pK184-HlyBD and pSU-6xMS2v4-HlyA (1) as well as *E. coli* BL21(DE3) transformed with pK184-HlyBD and pSU2726-HlyA as positive control (2) either 0 h or 4 h after induction of protein expression. **(B)** Western blot analysis of the supernatant samples (Sup) and whole cell samples (Cells) 4 h after induction of protein expression from the strains described under (A).

Discussion

The MS2 bacteriophage, which infects Enterobacteriaceae like *E. coli*, relies on the binding of its coat protein to the dedicated RNA stem loop for proliferation (Peabody 1993, Johansson *et al.* 1997). This specific RNA-protein interaction has been widely and successfully used in biotechnology in conjunction with fluorescent markers to observe and track (m)RNA in living cells (Forrest *et al.* 2003, Fusco *et al.* 2003, Dynes *et al.* 2007). The technique has recently been used in bacteria as well and unveiled the spatial organization of mRNA in prokaryotes even though they are not compartmentalized (Nevo-Dinur *et al.* 2011, Kannaiah *et al.* 2019).

Here we aimed to apply the MS2 system in an attempt to localize the mRNA of HlyA in *E. coli*. We hypothesized, that spatial translation is a potential explanation for the lack of degradation/aggregation of HlyA prior to secretion, although the protein exists in an unfolded state in the cytoplasm. We used the mRNA of LacY as a positive control for the localization experiments, which was shown to localize to the membrane in *E. coli* (Nevo-Dinur *et al.* 2011). We were unable to reproduce the localization pattern

of LacY mRNA shown by Nevo-Dinur and coworkers, as the eGFP fluorescence was distributed equally in the cytoplasm of *E. coli* cells irrespective of expression temperature, expression duration and inducer concentration.

For the cloning of the respective plasmid backbones we followed the characteristics stated in the original publication (Nevo-Dinur *et al.* 2011). We used slightly different versions of the MS2 coat protein and RNA stem loop in comparison to Nevo-Dinur: in case of the MS2 tag the exact nucleotide sequence was not available. The stem loop has a conserved sequence of Pu-N-N-A-N-Py-A (A being an adenine, N any nucleotide, Pu a purine base and Py a pyrimidine base) (Lago *et al.* 1998). Nevo-Dinur used a homo-hexameric high affinity version of the stem loop with the purine being an adenine and the pyridine being a cytosine (complete sequence: A-G-G-A-U-C-A), although the linker length in between the loops was not stated. We also used high affinity hexameric, but non-repetitive stem loops (A-N-N-A-U-C-A) with a 32 bp linker in between the loops. Longer linkers of 40 or 50 bp are usually used to allow the accessibility of nucleases to coat protein-stem loop complexes for visualization of mRNA dynamics (Tutucci *et al.* 2018a, Tutucci *et al.* 2018b, Vera *et al.* 2019).

In case of the MS2 coat protein, a dimer of the wild type protein was used in the original publication. We decided for an optimized version containing the point mutation V29I which confers a tighter binding to the stem loop (Lim *et al.* 1994) as well as a deletion of the FG loop, rendering the coat protein dimers defective in further multimerization and capsid formation, preventing aggregation of MS2d-eGFP (Peabody *et al.* 1992, Peabody *et al.* 2001, Lima *et al.* 2006, Llopis *et al.* 2010). Although those variants were used successfully before (Le *et al.* 2005, Le *et al.* 2006, Guet *et al.* 2008), we cannot exclude this difference as the source for failed LacY mRNA localization at the membrane in our case, and using different combinations of binding partner variants might solve this problem.

We could exclude the absence of 6xMS2v4-LacY mRNA as an error source, as the isolation of total RNA from cells transcribing 6xMS2v4-*lacY* and cDNA synthesis via rtPCR resulted in product bands with coinciding size in the subsequent amplification using 6xMS2v4-*lacY* specific primers. The identification of LacY on the protein level was not practical here, since the lactose permease is expressed endogenously in *E. coli*. The eventuality of a non-functional 6xMS2v4-LacY mRNA can therefore not be ruled out at this point. An artifactual cytoplasmic eGFP fluorescence due to

overexpression of MS2d-eGFP or a too high abundance of 6xMS2v4-LacY mRNA are unlikely. Even short expression times and leaky transcription levels, which were also used by Nevo-Dinur, did not change eGFP localization.

We could confirm the successful expression of MS2d-eGFP, as eGFP fluorescence and a protein of expected molecular weight in GFP-immunoblots was detectable upon induction of protein expression. However, the binding of MS2d-eGFP to the stem loops was not tested here and could be another error source. The presence and integrity of the coat protein could be assessed via mass spectrometry or immunoblotting using a respective antibody. The functionality of the coat protein-stem loop interaction could be verified via an electrophoresis mobility shift assay (EMSA) (Hellman *et al.* 2007).

Since the localization of the LacY mRNA control was not unambiguous, a conclusive statement on the HlyA mRNA cannot be given here. Independent of expression time, IPTG amount and presence of the IMC components HlyB and HlyD, no localized eGFP fluorescence could be observed with HlyA mRNA. The transcribed mRNA is functional, as pro-HlyA is synthesized and secreted. Secretion is unaffected, as no intracellular pro-HlyA could be detected. Still, expression of 6xMS2v4 tagged *hlyA* is affected: the expression level of pro-HlyA from pSU-6xMS2v4-HlyA is lower when compared to the variant without the stem loop sequence. So far it is unclear, if this is due to a lower transcription level, increased mRNA instability or decreased translation level. The impairment may be reduced by shifting the stem loops from the 5' end to the 3' end of *hlyA*. The usage of a plasmid resulting in a polycistronic mRNA of HlyA, HlyB and HlyD, as present in the HlyA operon (Leeds *et al.* 1997, Khosa *et al.* 2018), or even incorporation of the stem loops into the sequence of the parental strain *E. coli* UTI89 would allow the observation in an endogenous environment and circumvent problems with overexpression.

In summary, the MS2 system proved to be not optimal for our objective. The application of alternative systems for mRNA localization represents a promising option. Fluorescence *in situ* hybridization has been used for many years and a multitude of different techniques and protocols are available (Levsky *et al.* 2003, Young *et al.* 2020). The usage of labeled RNA probes with optimized hybridization conditions would result in increased sensitivity and would eliminate problems with overexpression as well. This approach would be more laborious and exhibits its own limitations; the fixation can mask the target nucleotides as one example. Systems similar to the MS2 system could

be deployed as well, e.g. the PP7 or the λ N system. The PP7 system is related to the MS2 system and likewise utilizes the interaction of the coat protein from the PP7 bacteriophage to its RNA aptamer (Chao *et al.* 2008, Wu *et al.* 2012, Lenstra *et al.* 2016). The λ N system is derived from the λ phage, where a 22 amino acid peptide from the λ N peptide binds to a 15 nucleotide RNA loop (Daigle *et al.* 2007, König *et al.* 2009, Schönberger *et al.* 2012), which might reduce the observed impairment in *hlyA* expression. It should be noted though, that both the PP7 and the λ N system are not as widely used as the MS2 system, especially not in bacterial cells. Different approaches for identification and mapping of RNA-protein interactions represent proximity labeling (Branon *et al.* 2018, Qin *et al.* 2021) or the isolation of RNA-protein complexes via immobilized RNA-specific antisense oligonucleotides (Matia-González *et al.* 2017).

Funding

This work was supported by the Deutsche Forschungsgemeinschaft (DFG, CRC 1208 project A01 to LS and Z02 to SWP).

Acknowledgements

We thank all members of the Institute of Biochemistry for fruitful discussions. We are indebted to Prof Dr. Michael Feldbrügge and Dr. Kira Müntjes for their expertise regarding the MS2 system, helpful input for designing of experiments and sharing of plasmids (Heinrich Heine University Düsseldorf, Faculty of Mathematics and Natural Sciences, Institute of Microbiology).

Material and Methods

Bacterial strains and plasmids

Escherichia coli DH5 α cells were used for cloning, *E. coli* BL21(DE3) and *E. coli* MG1655 cells were used for cultivation and expression. Used plasmids are listed in Table 1, oligonucleotides used are listed in Table 2 and gene strands used are listed in Table 3. Genestrands and oligonucleotides were purchased from Eurofins Genomics. The plasmid pUMa2491_12xPBS-24-MBS-v4 encoding for the 6xMS2v4 sequence was a kind gift of Prof. Dr. Michael Feldbrügge (Heinrich Heine University Düsseldorf, Faculty of Mathematics and Natural Sciences, Institute of Microbiology).

Construction of plasmids

All PCRs were performed using Q5 DNA Polymerase according to the manufacturers protocol (New England Biolabs) with subsequent DpnI digestion. DNA was purified using the Monarch PCR & DNA Cleanup Kit (New England Biolabs). The NucleoSpin Plasmid Miniprep Kit was purchased from Macherey Nagel and DNA sequencing performed at Microsynth Seqlab.

The plasmids carrying a fusion of eGFP and a dimer of the MS2 coat protein (MS2d) were cloned to match the characteristics stated in Nevo-Dinur *et al.* 2011. For the construction of pK-MS2d-eGFP, the pK184 plasmid backbone was used, in which the lac promoter from the original pK184-HlyBD plasmid was exchanged with the arabinose-inducible araBAD promoter (pK184-HlyBD-araCBAD). It carries a p15a origin of replication (ori) and a kanamycin resistance gene. The plasmid usually contains the genes coding for HlyB and HlyD. The plasmid was amplified without those genes using the primers pK184-ara-2MCP+eGFP-Ins-fw/-rev, which featured overhangs complementary to the sequence of MS2d-eGFP for the insertion via Gibson assembly (Gibson 2011). The MS2d-eGFP sequence was split up into two gene strands because of repetitive sequences, with one gene strand coding for one copy of MS2 and the other gene strand coding for MS2-eGFP (for sequences see Table 3).

A second plasmid variant with *ms2d-egfp* was constructed, as the first variant was not compatible with the pK184-HlyBD plasmid and simultaneous expression of MS2d-eGFP, HlyA with HlyB and HlyD would not have been possible. Therefore, pEVOL-

MS2d-eGFP was generated, as it contains a ColA ori and a chloramphenicol resistance gene. It is based on pEVOL-Bpa-ColA, which usually codes for an orthogonal tRNA / aminoacyl-tRNA synthetase pair for the insertion of unnatural amino acids into amber stop codons. The plasmid was amplified without those genes using the primers pEVOL-ColA-2MCP+eGFP-Ins-fw/-rev, which featured overhangs complementary to the sequence of MS2d-eGFP for the insertion via Gibson assembly. In this case, three gene strands were used; similar to the plasmid pK-MS2d-eGFP, one gene strand coded for one copy of MS2 and another one coded for MS2-eGFP. A third gene strand encoded for a terminator, as the terminator region present on the plasmid was not amplified during PCR amplification of the pEVOL plasmid backbone for the Gibson assembly. The Gibson assembly was performed with the Gibson Assembly Master Mix (New England Biolabs) and according to the manufacturers protocol. In short, plasmid backbone and inserts were mixed with the insert in threefold molar excess and subsequently incubated at 50°C for 1 h. Next, 50 µl of chemically competent *E. coli* DH5α were transformed with 2 µl of the assembly reaction, plated out on an agar plate containing 30 µg/ml of either kanamycin (pK-MS2d-eGFP) or chloramphenicol (pEVOL-MS2d-eGFP) and incubated at 37°C overnight. Single clones were transferred to 5 ml 2xYT medium supplemented with the respective antibiotic, incubated at 37°C overnight and used for plasmid isolation with subsequent sequencing.

The plasmid pYFP-lacY-1 was ordered from Addgene (#140138) and used as the source for *lacY* as a positive control for mRNA localization (Nevo-Dinur *et al.* 2011). The MS2 loops 6xMS2v4 were amplified from the plasmid pUMa2491_12xPBS-24-MBS-v4 using the primers 6xMS2v4-fw/-rev. This sequence was inserted via complementary overhangs and Gibson assembly into pYFP-lacY-1 upstream of *eyfp*, which was linearized using the primers pYFP-lacY-6xMS2v4-Ins-fw/-rev. Again, the insert was used in threefold molar excess with the backbone, incubated at 50°C for 60 min and 2 µl of the assembly mix were used for transformation of *E. coli* DH5α for plasmid isolation and sequencing, yielding the plasmid pYFP-6xMS2v4-lacYI. Subsequently, 6xMS2v4-*eyfp-lacY-lacI* was amplified using the primers pYFP+lacY+lacI-fw/-rev and inserted into the Multiple Cloning Site (MCS) of the pJET1.2 vector (see below). The plasmid pSU2726-HlyA was used as a backbone for the creation of the positive control plasmid carrying 6xMS2v4-lacY. It contains a ColE1 ori, an ampicillin resistance gene, an IPTG inducible lac promoter and is suitable for

co-expression of plasmids with a pK184 and pEVOL backbone. The plasmid was linearized via PCR amplification using the primers lin-pSU-fw/-rev, thereby deleting the *hlyA* gene usually present on the plasmid. The pSU backbone was inserted into the MCS of the pJET plasmid, using the Blunt-End cloning protocol of the CloneJET PCR Cloning Kit (Thermo Scientific). In short, linearized plasmid and insert were ligated with the insert in a threefold molar excess for 5 min at room temperature (RT) and used for transformation of *E. coli* DH5 α with subsequent plasmid isolation and sequencing (see above). For the digestion of pJET plasmids containing the pSU backbone and 6xMS2v4-eYFP-lacYI fragment with XhoI and XbaI, 1 μ g of each plasmid DNA was used. DNA was purified using the Monarch DNA Gel Extraction Kit (New England Biolabs) and ligated in a 1:1 ratio using T4 DNA Ligase (New England Biolabs) as stated in the manufacturers protocol. The ligation mix was inactivated via incubation at 65°C for 10 min. *E. coli* DH5 α cells were transformed with 3 μ l of the ligation mix. Cells were plated out on 2xYT agar plates supplemented with 100 μ g/ml ampicillin. Plasmids were checked by colony PCR using OneTaq DNA Polymerase (New England Biolabs). Correct plasmids showed a band with a size of 1777 bp via agarose gel electrophoresis. From the resulting plasmid (pSU-6xMS2v4-eYFP-lacYI) both *eyfp* and *lacI* were deleted in two steps using PCR and the primer pairs placY-fw/-rev and pSU-6xMS2v4-del-lacI-fw/-rev respectively. After PCR, the reaction mixture was treated with KLD Enzyme Mix (New England Biolabs) as stated in the manufacturers protocol and used for transformation of *E. coli* DH5 α . Correct sequence of the resulting plasmids pSU-6xMS2v4-eYFP-lacY and pSU-6xMS2v4-lacY was confirmed by sequencing.

In a last step, the 6xMS2v4 stem loop sequence was introduced upstream of *hlyA* in pSU2726-HlyA. For this purpose, 6xMS2v4 was amplified with the primers 6xMS2v4-fw/-rev and the pSU backbone was amplified using the primer pair pSU-HlyA-6xMS2v4-Ins-fw/-rev for application in Gibson assembly. The pSU backbone was purified using the DNA cleanup kit stated above, while the 6xMS2v4 sequence was purified via gel extraction. Both fragments were mixed with the insert in fivefold molar excess and the Gibson assembly was performed as described above. Correct sequence of the resulting plasmid pSU-6xMS2v4-HlyA was confirmed by sequencing.

The expression of HlyB and HlyD in *E. coli* cells transformed with pEVOL-MS2d-eGFP and pSU-6xMS2v4-HlyA was executed using the plasmid pK184-HlyBD (Bakkes *et al.* 2010).

Table 1: Plasmids used in this study.

Plasmid name	Backbone	Encoded genes	Resistance	Origin of replication	Promoter	Source
pYFP-lacY-1	pAN1818	<i>eyfp, lacY, lacI</i>	Kan	p15a	tac	Addgene (#140138)
pYFP-lacYI-6xMS2v4	pAN1818	<i>eyfp, lacY, lacI</i>	Kan	p15a	tac	This study
pJET1.2	pJET	-	Amp	ColE1	T7	Thermo Scientific
pUMa2491_12xPBS-24-MBS-v4	pUC57	-	Amp	ColE1	-	(Halstead <i>et al.</i> 2015)
pK184-HlyBD	pK184	<i>hlyB, hlyD</i>	Kan	p15a	lac	(Bakkes <i>et al.</i> 2010)
pK184-HlyBD-araCBAD	pK184	<i>hlyB, hlyD</i>	Kan	p15a	araBAD	This study
pK-MS2d-eGFP	pK184	<i>ms2d-egfp</i>	Kan	p15a	araBAD	This study
pEVOL-Bpa-ColA	pEVOL	<i>aaRS_{Bpa}, tRNA_{Bpa}</i>	Cm	ColA	araBAD	This study
pEVOL-MS2d-eGFP	pEVOL	<i>ms2d-egfp</i>	Cm	ColA	araBAD	This study
pSU2726-HlyA	pUC19	<i>hlyA</i>	Amp	ColE1	lac	(Thomas <i>et al.</i> 2014)
pSU-6xMS2v4-eYFP-lacYI	pUC19	<i>eyfp, lacY, lacI</i>	Amp	ColE1	lac	This study
pSU-6xMS2v4-lacY	pUC19	<i>lacY</i>	Amp	ColE1	lac	This study
pSU-6xMS2v4-HlyA	pUC19	<i>hlyA</i>	Amp	ColE1	lac	This study

Table 2: Oligonucleotides used in this study. Overhangs for Gibson assembly are underlined.

Name	Details	Sequence (5'→3')	Plasmid
pK184-ara-2MCP+eGFP-Ins-fw pK184-ara-2MCP+eGFP-Ins-rev	Amplification of pK184-ara-HlyBD without <i>hlyB</i> and <i>hlyD</i> with overhangs to the gene strands for <i>ms2d-egfp</i> for Gibson assembly	<u>TGGACGAGCTGTACAAGTAA</u> TCTAGAGCGGCCGGCACG <u>TGAGTAAAGTTAGAAGCCAT</u> GACTGTTTCCTGTGTGAAAATGGAGAAACAG	pK-MS2d-eGFP
pEVOL-ColA-2MCP+eGFP-Ins-fw pEVOL-ColA-2MCP+eGFP-Ins-rev	Amplification of pEVOL-Bpa-ColA without the sequences for tRNA _{Bpa} and aaRS _{Bpa} with overhangs to the gene strands for <i>ms2d-egfp</i> for Gibson assembly	<u>AGCTCCCGGTCATCAATCATCCCCATAATCCTTGTTAGATGCATGCTCGAGCAGCTC</u> AGG <u>TGAGTAAAGTTAGAAGCCAT</u> AGATCTAATTCCTCCTGTTAGCCCCAAAAAACGG	pEVOL-MS2d-eGFP
lin-pSU-fw lin-pSU-rev	Linearization of pSU2726-HlyA without amplifying <i>hlyA</i> for insertion into pJET1.2	TATATTAATTAAATGATAGCAATCTTACTGGGC AATTGTTATCCGCTCACAATTCC	pJET containing the pSU backbone
pYFP+lacY+lacI-fw pYFP+lacY+lacI-rev	Amplification of 6xMS2v4-eYFP-lacY-lacI for insertion into pJET1.2	AGCTGTCACCGGATGTGCTTTC TCACTGCCCGCTTTCCAGTC	pJET containing the 6xMS2v4-eYFP-lacYI fragment
6xMS2v4-fw 6xMS2v4-rev pYFP-lacY-6xMS2v4-Ins-fw pYFP-lacY-6xMS2v4-Ins-rev	Amplification of the 6 repetitions of the MS2 stem loop sequence with a spacer of 32 bp in between each of the loops (6xMS2v4) for Gibson assembly Amplification of pYFP-lacY-1 with overhangs to 6xMS2v4 for Gibson assembly	TACCTACAAACGGCAGAG GGATCTGGTATGTCCGATGTTG <u>ACATCGGACATACCAGATCCATAATTTTGTTTAATACTAGAGAAAGAGG</u> <u>GCTCGTGCCGTTTGTAGGTATTGTAGAGGCTGTTTCGTC</u>	pSU-6xMS2v4-eYFP-lacYI
placY-fw placY-rev	Deletion of <i>eyfp</i> from pSU-6xMS2v4-eYFP-lacYI	ATGTACTATTTAAAAACACAACTTTTGG CTAGTATTTCCCCTCTTTCTC	pSU-6xMS2v4-lacY

Continuation Table 2: Oligonucleotides used in this study. Overhangs for Gibson assembly are underlined.

Name	Details	Sequence (5'→3')	Plasmid
6xMS2v4-fw	Amplification of the 6 repetitions of the MS2 stem loop sequence with a spacer of 32 bp in between each of the loops (6xMS2v4) for Gibson assembly	TACCTACAAACGGCACGAG	pSU-6xMS2v4-eYFP-lacYI
6xMS2v4-rev		GGATCTGGTATGTCCGATGTTG	
pYFP-lacY-6xMS2v4-Ins-fw		<u>ACATCGGACATACCAGATCC</u> ATAATTTTGTTTAATACTAGAGAAAGAGG	
pYFP-lacY-6xMS2v4-Ins-rev		<u>GCTCGTGCCGTTTGTAGGTA</u> TGTAGAGGCTGTTTCGTC	
placY-fw	Deletion of <i>eyfp</i> from pSU-6xMS2v4-eYFP-lacYI	ATGTACTATTTAAAAACACAAACTTTTG	pSU-6xMS2v4-lacY
placY-rev		CTAGTATTTCCCCTCTTTCTC	
pSU-6xMS2v4-del-lacI-fw	Deletion of <i>lacI</i> from pSU-6xMS2v4-eYFP-lacYI	ATCTTTCTAGAAAGATTATATTAATTTAAATG	pSU-6xMS2v4-lacY
pSU-6xMS2v4-del-lacI-rev		TTAAGCGACTTCATTCAC	
6xMS2v4-fw	Amplification of the 6 repetitions of the MS2 stem loop sequence with a spacer of 32 bp in between each of the loops (6xMS2v4) for Gibson assembly	TACCTACAAACGGCACGAG	pSU-6xMS2v4-HlyA
6xMS2v4-rev		GGATCTGGTATGTCCGATGTTG	
pSU-HlyA-6xMS2v4-Ins-fw		<u>ACATCGGACATACCAGATCC</u> CAGATTTTAATTTTTCATTAAGTGG	
pSU-HlyA-6xMS2v4-Ins-rev		<u>GCTCGTGCCGTTTGTAGGTA</u> ACTTTCTTTTACTTCAGTTATTAAC	
lacY-rev	Amplification of <i>6xMS2v4-lacY</i> transcripts during cDNA synthesis from isolated RNA and in the subsequent PCR	TTAAGCGACTTCATTCACCTG	pSU-6xMS2v4-lacY
6xMS2v4-fw	Amplification of <i>6xMS2v4-lacY</i> during PCR after cDNA synthesis from isolated RNA together with the primer lacY-rev (see above)	TACCTACAAACGGCACGAG	pSU-6xMS2v4-lacY

Table 3: Gene strands used in this study. Overhangs for Gibson assembly are underlined.

Name	Details	Sequence (5'→3')	Plasmid
MCP	One copy of the MS2 coat protein	ATGGCTTCTAACTTTACTCAGTTCGTTCTCGTCGACAATGGCGGAACGGCGACGTGACTGT CGCCCCAAGCAACTTCGCTAACGGGATCGCTGAATGGATCAGCTCTAACTCGCGTTCACAG GCTTACAAAGTAACCTGTAGCGTTCGTGAGAGCTCTGCGCAGAATCGCAAATACACCATCAA AGTCGAGGTGCCTAAAGGCGCCTGGCGTTCGTACTTAAATATGGAACATAACCATTCCAATTT TCGCCACGAATTCGACTGCGAGCTTATTGTTAAGGCAATGCAAGGTCTCCTAAAAGATGGA AACCCGATTCCCTCAGCAATCGCAGCAAACCTCCGGCATCTACGCC	pK-MS2d-eGFP
MCP-eGFP	One copy of the MS2 coat protein fused to eGFP with overhangs to the N-terminal copy of the MS2 coat protein for Gibson assembly	<u>AACTCCGGCATCTACGCC</u> ATGGCTTCTAACTTTACTCAGTTCGTTCTCGTCGACAATGGCGG AACTGGCGACGTGACTGTGCCCCAAGCAACTTCGCTAACGGGATCGCTGAATGGATCAGC TCTAACTCGCGTTCACAGGCTTACAAAGTAACCTGTAGCGTTCGTGAGAGCTCTGCGCAGA ATCGCAAATACACCATCAAAGTCGAGGTGCCTAAAGGCGCCTGGCGTTCGTACTTAAATATG GAACTAACCATTTCAATTTTCGCCACGAATTCGACTGCGAGCTTATTGTTAAGGCAATGCA AGGTCTCCTAAAAGATGGAAACCCGATTCCCTCAGCAATCGCAGCAAACCTCCGGCATCTAC GCGGATTCTAGCTCCGCGGCCGCCATGGTGAGCAAGGGCGAGGAGCTGTTACCGGGGGT GGTGCCCATCCTGGTCGAGCTGGACGGCGACGTAACGGCCACAAGTTCAGCGTGTCCGG CGAGGGCGAGGGCGATGCCACCTACGGCAAGCTGACCCTGAAGTTCATCTGCACCACCGG CAAGCTGCCCCTGCCCTGGCCACCCTCGTGACCACCCTGACCTACGGCGTGAGTGCTT CAGCCGCTACCCCGACCACATGAAGCAGCACGACTTCTTCAAGTCCGCCATGCCCGAAGG CTACGTCCAGGAGCGCACCATCTTCTTCAAGGACGACGGCAACTACAAGACCCGCGCCGA GGTGAAGTTCGAGGGCGACACCCTGGTGAACCGCATCGAGCTGAAGGGCATCGACTTCAA GGAGGACGGCAACATCCTGGGGCACAAGCTGGAGTACAACATAACAGCCACAACGTCTAT ATCATGGCCGACAAGCAGAAGAACGGCATCAAGGTGAACTTCAAGATCCGCCACAACATCG AGGACGGCAGCGTGCAGCTCGCCGACCACTACCAGCAGAACACCCCATCGGCGACGGC CCCGTGCTGCTGCCCGACAACCACTACCTGAGCACCCAGTCCGCCCTGAGCAAAGACCCC AACGAGAAGCGCGATCACATGGTCTGCTGGAGTTCGTGACCGCCGCCGGGATCACTCTC GGCATGGACGAGCTGTACAAGTAA	

Continuation Table 3: Gene strands used in this study. Overhangs for Gibson assembly are underlined.

Name	Details	Sequence (5'→3')	Plasmid
MCP	One copy of the MS2 coat protein	ATGGCTTCTAACTTTACTCAGTTCGTTCTCGTCGACAATGGCGGAACTGGCGACGTGACTGTCGCCCCA AGCAACTTCGCTAACGGGATCGCTGAATGGATCAGCTCTAACTCGCGTTCACAGGCTTACAAAGTAACC TGTAGCGTTCGTCAGAGCTCTGCGCAGAATCGCAAATACACCATCAAAGTCGAGGTGCCTAAAGGCGC CTGGCGTTCGTACTTAAATATGGAATAACCATTTCCAAATTTTCGCCACGAATCCGACTGCGAGCTTATT GTTAAGGCAATGCAAGGTCTCCTAAAAGATGGAACCCGATTCCCTCAGCAATCGCAGCAAACCTCCGGC ATCTACGCC	pEVOL-MS2d-eGFP
MCP-eGFP-pEVOL	One copy of the MS2 coat protein fused to eGFP with overhangs to the N-terminal copy of the MS2 coat protein and the terminator region downstream for Gibson assembly	<u>AACTCCGGCATCTACGCC</u> ATGGCTTCTAACTTTACTCAGTTCGTTCTCGTCGACAATGGCGGAACTGGC GACGTGACTGTCGCCCCAAGCAACTTCGCTAACGGGATCGCTGAATGGATCAGCTCTAACTCGCGTTCA CAGGCTTACAAAGTAACCTGTAGCGTTCGTCAGAGCTCTGCGCAGAATCGCAAATACACCATCAAAGTC GAGGTGCCTAAAGGCGCCTGGCGTTCTGACTTAAATATGGAATAACCATTTCCAAATTTTCGCCACGAATT CCGACTGCGAGCTTATTGTTAAGGCAATGCAAGGTCTCCTAAAAGATGGAACCCGATTCCCTCAGCAA TCGCAGCAAACCTCCGGCATCTACGCGGATTCTAGCTCCGCGGCCGCCATGGTGAGCAAGGGCGAGGA GCTGTTACCGGGGTGGTGCCCATCCTGGTCGAGCTGGACGGCGACGTAAACGGCCACAAGTTCAGC GTGTCCGGCGAGGGCGAGGGCGATGCCACCTACGGCAAGCTGACCCTGAAGTTCATCTGCACCACCG GCAAGCTGCCCCGTGCCCTGGCCACCCTCGTGACCACCCTGACCTACGGCGTGAGTGCTTCAGCCG CTACCCCGACCACATGAAGCAGCACGACTTCTTCAAGTCCGCCATGCCCGAAGGCTACGTCCAGGAGC GCACCATCTTCTTCAAGGACGACGGCAACTACAAGACCCGCGCCGAGGTGAAGTTCGAGGGCGACACC CTGGTGAACCGCATCGAGCTGAAGGGCATCGACTTCAAGGAGGACGGCAACATCCTGGGGCACAAGCT GGAGTACAACTACAACAGCCACAACGTCTATATCATGGCCGACAAGCAGAAGAACGGCATCAAGGTGAA CTTCAAGATCCGCCACAACATCGAGGACGGCAGCGTGACGCTCGCCGACCACTACCAGCAGAACACCC CCATCGGCGACGGCCCCGTGCTGCTGCCCCGACAACCACTACCTGAGCACCCAGTCCGCCCTGAGCAA AGACCCCAACGAGAAGCGCGATCACATGGTCCTGCTGGAGTTCGTGACCGCCGCCGGGATCACTCTCG <u>GCATGGACGAGCTGTACAAGTAAGTTTAAACGGTCTCCAGCTTGGCTGTTTTGGCGGATGAGA</u>	
pEVOL-Terminator	Terminator region, which was deleted from the original pEVOL plasmid	GTTTAAACGGTCTCCAGCTTGGCTGTTTTGGCGGATGAGAGAAGATTTTCAGCCTGATACAGATTAAATC AGAACGCAGAAGCGGTCTGATAAAACAGAATTTGCCCTGGCGGCAGTAGCGCGGTGGTCCCACCTGACC CCATGCCGAACTCAGAAGTGAACGCCGTAGCGCCGATGGTAGTGTGGGGTCTCCCCATGCGAGAGTA GGGAACTGCCAGGCATCAAATAAAACGAAAGGCTCAGTCGAAAGACTGGGCCTTGTTGTGAGCTCCC GGTCAATCAATCATCCCCATAATCCTTGTTAGAT	

Cell cultivation and protein expression

Either *E. coli* BL21(DE3) or *E. coli* MG1655 were used for cultivation and protein expression. The stated cells were transformed first with one of the reporter plasmids, either pK-MS2d-eGFP (kanamycin resistance, 30 µg/µl) or pEVOL-MS2d-eGFP (chloramphenicol resistance, 30 µg/µl). After overnight incubation on 2xYT agar plates supplemented with the respective antibiotic at 37°C, 5 ml 2xYT medium supplemented with the respective antibiotic were inoculated with the cells and incubated overnight at 37°C and 180 rpm. The cells transformed before were made competent again to be transformed with one of the target plasmids carrying either the gene 6xMS2v4-lacY or 6xMS2v4-hlyA (ampicillin resistance, 100 µg/µl). The cells were plated on agar plates and grown in liquid media (supplemented with ampicillin and either kanamycin or chloramphenicol) as described above. Cells carrying the plasmids pEVOL-MS2d-eGFP and pSU-6xMS2v4-HlyA were made chemically competent for the transformation with pK184-HlyBD and treated as described above (2xYT medium supplemented with ampicillin, kanamycin and chloramphenicol).

The cells in 5 ml 2xYT medium were used as a preculture to inoculate 20 ml 2xYT supplemented with the respective antibiotics (same concentrations as above) in a 100 ml un baffled flask to an optical density (OD₆₀₀) of 0.1. Cells were cultivated at 180 rpm and 37°C. In some cases, expression of 6xMS2v4-LacY was performed at 30°C instead. When the OD₆₀₀ reached 0.6-0.8, protein expression was induced.

The expression of MS2d-eGFP - and HlyB as well as HlyD when present - was induced with 6.6 mM arabinose (\pm 0.1% (w/v)). Pro-HlyA expression was induced using 1 mM IPTG and the folding of the toxin was induced with the addition of 4 mM CaCl₂ to the culture medium. For LacY, leaky expression (no addition of IPTG) and induction with 1 mM IPTG was tested. Cells were grown at 180 rpm and either 30°C or 37°C (see above). The OD₆₀₀ was measured and two samples of the expressions were taken 0.5 h, 1 h and 2 h after induction; one sample was used for SDS-PAGE and one for fixation with subsequent microscopy imaging. The supernatant was separated from the cells by centrifugation for 2 min at 13,000 xg at room temperature (RT). For SDS-PAGE analysis, the cells were resuspended in MilliQ water to normalize the samples in respect of their OD₆₀₀, the same was performed for the supernatants by dilution with MilliQ water. Both cells and supernatant samples were mixed with SDS sample buffer containing 40 mM DTT.

The samples were subjected to an SDS-PAGE and heated for 5 min at 95°C beforehand. Western blots were performed as semi-dry (Trans-Blot Turbo, Bio-Rad). The SDS-PAGE gels were stained using Quick Coomassie Stain solution (Protein Ark), Western blots of supernatant samples were incubated with a polyclonal antibody targeting full-length HlyA.

Cell preparation for microscopy

PBS buffer was added to the cell samples collected after induction at the time points stated above to dilute them to 1 ml with an OD₆₀₀ of 2.0. Cells were then centrifuged at 13,000 rpm for 1 min at RT and washed twice with 1 ml PBS buffer and centrifuged in between the washing steps. Cells were then resuspended in 1 ml of freshly prepared 4% (v/v) paraformaldehyde (PFA) in PBS buffer and incubated at RT for 1 h under mild agitation (650 rpm). Afterwards, cells were centrifuged and washed with PBS buffer as described above. Next, cells were resuspended in 1 ml of 100 mM NH₄Cl in PBS buffer and incubated at RT and 650 rpm for 20 min to quench any remaining PFA. Cells were again centrifuged and washed twice with 1 ml PBS buffer and finally resuspended in 1 ml PBS buffer.

Fixed cells were immobilized on polysine adhesion slides (Thermo Scientific, J2800AMNZ). For this, 20 µl of cells were added to the polysine-coated side of the microscopy slide and incubated at RT for 30 min to let the cells set. The suspension was removed and carefully washed thrice with 1 ml of PBS buffer. After the last washing step, excess PBS buffer was carefully removed from the microscopy slide and the immobilized cells embedded with one drop (~10 µl) ProLong Diamond Antifade Mountant (Invitrogen) and a cover slide.

Fluorescence microscopy

Two microscope systems were used in this study. Images taken with an Olympus FV3000 confocal laser scanning microscope system (Olympus GmbH) were equipped with a super apochromat 60x / 1.35 oil immersion objective. The pinhole was set to 0.89 AU and the acquisition was performed at a scanspeed of 20 µs/pixel. The eGFP fluorescence was excited at 488 nm and emission of eGFP was detected at 510 nm.

Images taken with a Zeiss LSM 880 Airyscan microscope system (Zeiss Microscopy GmbH) were equipped with a plan apochromat 63x / 1.4 oil immersion objective. The pinhole was set to 1.5 AU and the acquisition was performed at a scanspeed of 10 μ s/pixel. The eGFP fluorescence was excited at 488 nm and emission of eGFP was detected with the Airyscan Filter at 495-550 nm.

RNA isolation

5 ml precultures of *E. coli* BL21(DE3) + pK-MS2d-eGFP + pSU-6xMS2v4-lacY cells were grown overnight at 37°C and 180 rpm. The next day, 20 ml 2xYT medium in a 100 ml unbaffled flask were inoculated to an OD₆₀₀ of 0.1 and grown at 37°C and 180 rpm. At an OD₆₀₀ of ~0.4 expression was induced by the addition of 6.6 mM arabinose and 1 mM IPTG. Cells were further incubated at 37°C and 180 rpm until the OD₆₀₀ reached 1.0. At this point, cells were diluted to an OD₆₀₀ of 2.0 and 625 μ l of the cell suspension taken for subsequent RNA isolation.

RNAs were isolated using the Monarch Total RNA Miniprep Kit according to the manufacturers protocol, including the on-column DNase I treatment (New England Biolabs).

10 μ l of RNA were mixed with 10 μ l 2xFA buffer (95% deionized formamide, 25 mM EDTA pH 8, 0.025% (w/v) bromphenolblue, 0.025% (w/v) xylencyanol) and heated for 10 min at 65°C and placed on ice after that. This RNA sample was applied to an agarose gel electrophoresis for quality control of the isolated RNA.

cDNA synthesis and PCR

For the synthesis of cDNA the Maxima H Minus First Strand cDNA Synthesis Kit (Thermo Scientific) was used according to the manufacturers protocol. The “sample” reaction included the isolated RNA as a template, the “-RT” reaction did not include the reverse transcriptase and was used as a control for gDNA contamination. The “NTC” reaction (no template control) did not include the isolated RNA template. This reaction was used to check all reagents for contamination. Before addition of the reverse transcriptase, reaction mixtures were heat shocked at 65°C for 5 min to avoid

possible secondary structures of the RNA template and problems during amplification. After addition of the reverse transcriptase, reaction mixtures were incubated at 50°C for 30 min and cDNA synthesis terminated by heating at 85°C for 5 min. Generated cDNA was either directly used for PCR or stored at -80°C.

The product of the first strand cDNA synthesis was used as template in a subsequent PCR reaction to amplify LacY-DNA or MS2d-eGFP-DNA, if present. 3 µl of cDNA product were used in a 30 µl reaction mix with 200 µM dNTPs, 1 µM of each primer and 0.04 U/µl Q5 DNA polymerase. For amplification of *6xMS2v4-lacY* the primers 6xMS2v4-fw and lacY-rev were used. A standard PCR program according to the manufacturers protocol was used with an elongation time of 45 sec and an annealing temperature of 48°C for amplification of *6xMS2v4-lacY*.

PCR products were analyzed via agarose gel electrophoresis using a 1% agarose gel.

Literature

1. Akeda, Y. and Galán, J. E. (2005). "Chaperone release and unfolding of substrates in type III secretion." *Nature* **437**(7060): 911-915.
2. Bakkes, P. J., Jenewein, S., Smits, S. H., Holland, I. B. and Schmitt, L. (2010). "The rate of folding dictates substrate secretion by the *Escherichia coli* hemolysin type 1 secretion system." *J. Biol. Chem.* **285**(52): 40573-40580.
3. Balakrishnan, L., Hughes, C. and Koronakis, V. (2001). "Substrate-triggered recruitment of the TolC channel-tunnel during type I export of hemolysin by *Escherichia coli*." *J. Mol. Biol.* **313**(3): 501-510.
4. Baumann, U., Wu, S., Flaherty, K. M. and McKay, D. B. (1993). "Three-dimensional structure of the alkaline protease of *Pseudomonas aeruginosa*: a two-domain protein with a calcium binding parallel beta roll motif." *EMBO J.* **12**(9): 3357-3364.
5. Beer, T., Hänsch, S., Pfeffer, K., Smits, S. H., Weidtkamp-Peters, S. and Schmitt, L. (2021). "Quantification and surface localization of the hemolysin A type 1 secretion system at the endogenous level and under conditions of overexpression." *Appl. Environ. Microbiol.* **88**(3): 01896-01821.
6. Benabdelhak, H., Kiontke, S., Horn, C., Ernst, R., Blight, M. A., Holland, I. B. and Schmitt, L. (2003). "A specific interaction between the NBD of the ABC-transporter HlyB and a C-terminal fragment of its transport substrate haemolysin A." *J. Mol. Biol.* **327**(5): 1169-1179.
7. Bertrand, E., Chartrand, P., Schaefer, M., Shenoy, S. M., Singer, R. H. and Long, R. M. (1998). "Localization of ASH1 mRNA particles in living yeast." *Mol. Cell* **2**(4): 437-445.
8. Bhakdi, S., Mackman, N., Nicaud, J. and Holland, I. (1986). "*Escherichia coli* hemolysin may damage target cell membranes by generating transmembrane pores." *Infect. Immun.* **52**(1): 63-69.
9. Branon, T. C., Bosch, J. A., Sanchez, A. D., Udeshi, N. D., Svinkina, T., Carr, S. A., Feldman, J. L., Perrimon, N. and Ting, A. Y. (2018). "Efficient proximity labeling in living cells and organisms with TurboID." *Nature Biotechnol.* **36**(9): 880-887.
10. Bronstein, P. A., Miao, E. A. and Miller, S. I. (2000). "InvB is a type III secretion chaperone specific for SspA." *J. Bacteriol.* **182**(23): 6638-6644.
11. Bumba, L., Masin, J., Macek, P., Wald, T., Motlova, L., Bibova, I., Klimova, N., Bednarova, L., Veverka, V. and Kachala, M. (2016). "Calcium-driven folding of RTX domain β -rolls ratchets translocation of RTX proteins through type I secretion ducts." *Mol. Cell* **62**(1): 47-62.
12. Chao, J. A., Patskovsky, Y., Almo, S. C. and Singer, R. H. (2008). "Structural basis for the coevolution of a viral RNA–protein complex." *Nat. Struct. Mol. Biol.* **15**(1): 103-105.
13. Daigle, N. and Ellenberg, J. (2007). " λ N-GFP: an RNA reporter system for live-cell imaging." *Nat. Methods* **4**(8): 633-636.

14. Darwin, K. H. and Miller, V. L. (2001). "Type III secretion chaperone-dependent regulation: activation of virulence genes by SicA and InvF in *Salmonella typhimurium*." EMBO J. **20**(8): 1850-1862.
15. Delepelaire, P. (2004). "Type I secretion in Gram-negative bacteria." Biochim. Biophys. Acta, Mol. Cell Res. **1694**(1-3): 149-161.
16. Du, D., Wang, Z., James, N. R., Voss, J. E., Klimont, E., Ohene-Agyei, T., Venter, H., Chiu, W. and Luisi, B. F. (2014). "Structure of the AcrAB–TolC multidrug efflux pump." Nature **509**(7501): 512.
17. Dynes, J. L. and Steward, O. (2007). "Dynamics of bidirectional transport of Arc mRNA in neuronal dendrites." J. Comp. Neurol. **500**(3): 433-447.
18. Forrest, K. M. and Gavis, E. R. (2003). "Live imaging of endogenous RNA reveals a diffusion and entrapment mechanism for nanos mRNA localization in *Drosophila*." Curr. Biol. **13**(14): 1159-1168.
19. Fouts, D. E., True, H. L. and Celandier, D. W. (1997). "Functional recognition of fragmented operator sites by R17/MS2 coat protein, a translational repressor." Nucleic Acids Res. **25**(22): 4464-4473.
20. Fu, Y. and Galán, J. E. (1998). "Identification of a specific chaperone for SptP, a substrate of the centisome 63 type III secretion system of *Salmonella typhimurium*." J. Bacteriol. **180**(13): 3393-3399.
21. Fusco, D., Accornero, N., Lavoie, B., Shenoy, S. M., Blanchard, J.-M., Singer, R. H. and Bertrand, E. (2003). "Single mRNA molecules demonstrate probabilistic movement in living mammalian cells." Curr. Biol. **13**(2): 161-167.
22. Gangola, P. and Rosen, B. (1987). "Maintenance of intracellular calcium in *Escherichia coli*." J. Biol. Chem. **262**(26): 12570-12574.
23. Gibson, D. G. (2011). "Enzymatic assembly of overlapping DNA fragments." Methods Enzymol. **498**: 349-361.
24. Golding, I. and Cox, E. C. (2004). "RNA dynamics in live *Escherichia coli* cells." Proc. Natl. Acad. Sci. **101**(31): 11310-11315.
25. Gray, L., Baker, K., Kenny, B., Mackmann, N., Haigh, R. and Holland, I. B. (1989). "A novel C-terminal signal sequence targets *Escherichia coli* haemolysin directly to the medium." J. Cell Sci. **1989**(Supplement_11): 45-57.
26. Guet, C. C., Bruneaux, L., Min, T. L., Siegal-Gaskins, D., Figueroa, I., Emonet, T. and Cluzel, P. (2008). "Minimally invasive determination of mRNA concentration in single living bacteria." Nucleic Acids Res. **36**(12): e73-e73.
27. Halstead, J. M., Lionnet, T., Wilbertz, J. H., Wippich, F., Ephrussi, A., Singer, R. H. and Chao, J. A. (2015). "An RNA biosensor for imaging the first round of translation from single cells to living animals." Science **347**(6228): 1367-1671.
28. Hellman, L. M. and Fried, M. G. (2007). "Electrophoretic mobility shift assay (EMSA) for detecting protein–nucleic acid interactions." Nat. Protoc. **2**(8): 1849-1861.
29. Holland, I., Peherstorfer, S., Kanonenberg, K., Lenders, M., Reimann, S. and Schmitt, L. (2016). "Type I protein secretion-deceptively simple yet with a wide range of mechanistic variability across the family." EcoSal Plus **7**(1): 1-46.

30. Jarchau, T., Chakraborty, T., Garcia, F. and Goebel, W. (1994). "Selection for transport competence of C-terminal polypeptides derived from *Escherichia coli* hemolysin: the shortest peptide capable of autonomous HlyB/HlyD-dependent secretion comprises the C-terminal 62 amino acids of HlyA." Mol. Gen. Genet. **245**(1): 53-60.
31. Johansson, H. E., Liljas, L. and Uhlenbeck, O. C. (1997). "RNA recognition by the MS2 phage coat protein". Semin. Virol. **8**(3): 176-185.
32. Jones, D. T. (1999). "Protein secondary structure prediction based on position-specific scoring matrices." J. Mol. Biol. **292**(2): 195-202.
33. Kannaiah, S., Livny, J. and Amster-Choder, O. (2019). "Spatiotemporal organization of the *E. coli* transcriptome: translation independence and engagement in regulation." Mol. Cell **76**(4): 574-589.
34. Kenny, B., Taylor, S. and Holland, I. B. (1992). "Identification of individual amino acids required for secretion within the haemolysin (HlyA) C-terminal targeting region." Mol. Microbiol. **6**(11): 1477-1489.
35. Khosa, S., Scholz, R., Schwarz, C., Trilling, M., Hengel, H., Jaeger, K.-E., Smits, S. H. J. and Schmitt, L. (2018). "An A/U-rich enhancer region is required for high-level protein secretion through the HlyA type I secretion system." Appl. Environ. Microbiol. **84**(1): e01163-01117.
36. König, J., Baumann, S., Koepke, J., Pohlmann, T., Zarnack, K. and Feldbrügge, M. (2009). "The fungal RNA-binding protein Rrm4 mediates long-distance transport of ubi1 and rho3 mRNAs." EMBO J. **28**(13): 1855-1866.
37. Koronakis, E., Hughes, C., Milisav, I. and Koronakis, V. (1995). "Protein exporter function and *in vitro* ATPase activity are correlated in ABC-domain mutants of HlyB." Mol. Microbiol. **16**(1): 87-96.
38. Koronakis, V., Eswaran, J. and Hughes, C. (2004). "Structure and function of TolC: the bacterial exit duct for proteins and drugs." Annu. Rev. Biochem. **73**(1): 467-489.
39. Koronakis, V., Hughes, C. and Koronakis, E. (1991). "Energetically distinct early and late stages of HlyB/HlyD-dependent secretion across both *Escherichia coli* membranes." EMBO J. **10**(11): 3263-3272.
40. Koronakis, V., Koronakis, E. and Hughes, C. (1989). "Isolation and analysis of the C-terminal signal directing export of *Escherichia coli* hemolysin protein across both bacterial membranes." EMBO J. **8**(2): 595-605.
41. Lago, H., Fonseca, S. A., Murray, J. B., Stonehouse, N. J. and Stockley, P. G. (1998). "Dissecting the key recognition features of the MS2 bacteriophage translational repression complex." Nucleic Acids Res. **26**(5): 1337-1344.
42. Le, T. T., Emonet, T., Harlepp, S., Guet, C. C. and Cluzel, P. (2006). "Dynamical determinants of drug-inducible gene expression in a single bacterium." Biophys. J. **90**(9): 3315-3321.
43. Le, T. T., Harlepp, S., Guet, C. C., Dittmar, K., Emonet, T., Pan, T. and Cluzel, P. (2005). "Real-time RNA profiling within a single bacterium." Proc. Natl. Acad. Sci. **102**(26): 9160-9164.

44. Lecher, J., Schwarz, C. K., Stoldt, M., Smits, S. H., Willbold, D. and Schmitt, L. (2012). "An RTX transporter tethers its unfolded substrate during secretion via a unique N-terminal domain." Structure **20**(10): 1778-1787.
45. Lecher, J., Stoldt, M., Schwarz, C. K., Smits, S. H., Schmitt, L. and Willbold, D. (2011). "1 H, 15 N and 13 C resonance assignment of the N-terminal C39 peptidase-like domain of the ABC transporter Haemolysin B (HlyB)." Biomol. NMR Assign. **5**(2): 199-201.
46. Leeds, J. A. and Welch, R. A. (1997). "Enhancing transcription through the *Escherichia coli* hemolysin operon, *hlyCABD*: RfaH and upstream JUMPStart DNA sequences function together via a postinitiation mechanism." J. Bacteriol. **179**(11): 3519-3527.
47. Lenders, M. H., Reimann, S., Smits, S. H. and Schmitt, L. (2013). "Molecular insights into type I secretion systems." Biol. Chem. **394**(11): 1371-1384.
48. Lenders, M. H., Weidtkamp-Peters, S., Kleinschrodt, D., Jaeger, K.-E., Smits, S. H. and Schmitt, L. (2015). "Directionality of substrate translocation of the hemolysin A type I secretion system." Sci. Rep. **5**(1): 12470.
49. Lenstra, T. L. and Larson, D. R. (2016). "Single-molecule mRNA detection in live yeast." Curr. Protoc. Mol. Biol. **113**(1): 14.24.1-14.24.15.
50. Létoffé, S. and Wandersman, C. (1992). "Secretion of CyaA-PrtB and HlyA-PrtB fusion proteins in *Escherichia coli*: involvement of the glycine-rich repeat domain of *Erwinia chrysanthemi* protease B." J. Bacteriol. **174**(15): 4920-4927.
51. Levsky, J. M. and Singer, R. H. (2003). "Fluorescence *in situ* hybridization: past, present and future." J. Cell Sci. **116**(14): 2833-2838.
52. Lim, F. and David, S. P. (1994). "Mutations that increase the affinity of a translational repressor for RNA." Nucleic Acids Res. **22**(18): 3748-3752.
53. Lima, S. M., Vaz, A. C. Q., Souza, T. L., Peabody, D. S., Silva, J. L. and Oliveira, A. C. (2006). "Dissecting the role of protein–protein and protein–nucleic acid interactions in MS2 bacteriophage stability." FEBS J. **273**(7): 1463-1475.
54. Linhartová, I., Bumba, L., Mašín, J., Basler, M., Osička, R., Kamanová, J., Procházková, K., Adkins, I., Hejnová-Holubová, J. and Sadílková, L. (2010). "RTX proteins: a highly diverse family secreted by a common mechanism." FEMS Microbiol. Rev. **34**(6): 1076-1112.
55. Llopis, P. M., Jackson, A. F., Sliusarenko, O., Surovtsev, I., Heinritz, J., Emonet, T. and Jacobs-Wagner, C. (2010). "Spatial organization of the flow of genetic information in bacteria." Nature **466**(7302): 77-81.
56. Mackman, N., Baker, K., Gray, L., Haigh, R., Nicaud, J. and Holland, I. (1987). "Release of a chimeric protein into the medium from *Escherichia coli* using the C-terminal secretion signal of haemolysin." EMBO J. **6**(9): 2835-2841.
57. Matia-González, A. M., Iadevaia, V. and Gerber, A. P. (2017). "A versatile tandem RNA isolation procedure to capture *in vivo* formed mRNA-protein complexes." Methods **118**: 93-100.
58. Murakami, S., Nakashima, R., Yamashita, E. and Yamaguchi, A. (2002). "Crystal structure of bacterial multidrug efflux transporter AcrB." Nature **419**(6907): 587-593.

-
59. Nevo-Dinur, K., Nussbaum-Shochat, A., Ben-Yehuda, S. and Amster-Choder, O. (2011). "Translation-independent localization of mRNA in *E. coli*." Science **331**(6020): 1081-1084.
 60. Nhu, N. T. K., Phan, M. D., Forde, B. M., Murthy, A. M. V., Peters, K. M., Day, C. J., Poole, J., Kidd, T. J., Welch, R. A., Jennings, M. P., Ulett, G. C., Sweet, M. J., Beatson, S. A. and Schembri, M. A. (2019). "Complex multilevel control of hemolysin production by uropathogenic *Escherichia coli*." MBio **10**(5): e02248-19.
 61. Nicaud, J.-M., Mackman, N., Gray, L. and Holland, I. (1986). "The C-terminal, 23 kDa peptide of *E. coli* haemolysin 2001 contains all the information necessary for its secretion by the haemolysin (Hly) export machinery." FEBS Lett. **204**(2): 331-335.
 62. Noegel, A., Rdest, U., Springer, W. and Goebel, W. (1979). "Plasmid cistrons controlling synthesis and excretion of the exotoxin α -haemolysin of *Escherichia coli*." Mol. Gen. Genet. **175**(3): 343-350.
 63. Parsot, C., Hamiaux, C. and Page, A.-L. (2003). "The various and varying roles of specific chaperones in type III secretion systems." Curr. Opin. Microbiol. **6**(1): 7-14.
 64. Peabody, D. S. (1993). "The RNA binding site of bacteriophage MS2 coat protein." EMBO J **12**(2): 595-600.
 65. Peabody, D. S. and Al-Bitar, L. (2001). "Isolation of viral coat protein mutants with altered assembly and aggregation properties." Nucleic Acids Res. **29**(22): e113-e113.
 66. Peabody, D. S. and Ely, K. R. (1992). "Control of translational repression by protein-protein interactions." Nucleic Acids Res. **20**(7): 1649-1655.
 67. Pimenta, A., Young, J., Holland, I. and Blight, M. (1999). "Antibody analysis of the localisation, expression and stability of HlyD, the MFP component of the *E. coli* haemolysin translocator." Mol. Gen. Genet. **261**(1): 122-132.
 68. Qin, W., Cho, K. F., Cavanagh, P. E. and Ting, A. Y. (2021). "Deciphering molecular interactions by proximity labeling." Nat. Methods **18**(2): 133-143.
 69. Reimann, S., Poschmann, G., Kanonenberg, K., Stühler, K., Smits, S. H. and Schmitt, L. (2016). "Interdomain regulation of the ATPase activity of the ABC transporter hemolysin B from *E. coli*." Biochem. J. **473**(16): 2471-2483.
 70. Sanchez-Magraner, L., Viguera, A. R., Garcia-Pacios, M., Garcillan, M. P., Arrondo, J.-L. R., de la Cruz, F., Goni, F. M. and Ostolaza, H. (2007). "The calcium-binding C-terminal domain of *Escherichia coli* α -hemolysin is a major determinant in the surface-active properties of the protein." J. Biol. Chem. **282**(16): 11827-11835.
 71. Schönberger, J., Hammes, U. Z. and Dresselhaus, T. (2012). "*In vivo* visualization of RNA in plants cells using the Δ N22 system and a GATEWAY-compatible vector series for candidate RNAs." Plant J. **71**(1): 173-181.
 72. Spitz, O., Erenburg, I. N., Kanonenberg, K., Peherstorfer, S., Lenders, M. H., Reiners, J., Ma, M., Luisi, B. F., Smits, S. H. and Schmitt, L. (2022). "Identity determinants of the translocation signal for a type 1 secretion system." Front. Physiol. **12**: 1-13.

73. Springer, W. and Goebel, W. (1980). "Synthesis and secretion of hemolysin by *Escherichia coli*." J. Bacteriol. **144**(1): 53-59.
74. Stanley, P., Koronakis, V. and Hughes, C. (1991). "Mutational analysis supports a role for multiple structural features in the C-terminal secretion signal of *Escherichia coli* haemolysin." Mol. Microbiol. **5**(10): 2391-2403.
75. Thanabalu, T., Koronakis, E., Hughes, C. and Koronakis, V. (1998). "Substrate-induced assembly of a contiguous channel for protein export from *E. coli*: reversible bridging of an inner-membrane translocase to an outer membrane exit pore." EMBO J. **17**(22): 6487-6496.
76. Thomas, S., Smits, S. H. and Schmitt, L. (2014). "A simple *in vitro* acylation assay based on optimized HlyA and HlyC purification." Anal. Biochem. **464**: 17-23.
77. Tutucci, E., Vera, M., Biswas, J., Garcia, J., Parker, R. and Singer, R. H. (2018a). "An improved MS2 system for accurate reporting of the mRNA life cycle." Nat. Methods **15**(1): 81-89.
78. Tutucci, E., Vera, M. and Singer, R. H. (2018b). "Single-mRNA detection in living *S. cerevisiae* using a re-engineered MS2 system." Nat. Protoc. **13**(10): 2268-2296.
79. Vålegård, K., Murray, J. B., Stonehouse, N. J., van den Worm, S., Stockley, P. G. and Liljas, L. (1997). "The three-dimensional structures of two complexes between recombinant MS2 capsids and RNA operator fragments reveal sequence-specific protein-RNA interactions." J. Mol. Biol. **270**(5): 724-738.
80. Vera, M., Tutucci, E. and Singer, R. H. (2019). "Imaging single mRNA molecules in mammalian cells using an optimized MS2-MCP system." Imaging Gene Expression: Methods and Protocols: 3-20.
81. Wagner, S., Grin, I., Malmshemer, S., Singh, N., Torres-Vargas, C. E. and Westerhausen, S. (2018). "Bacterial type III secretion systems: a complex device for the delivery of bacterial effector proteins into eukaryotic host cells." FEMS Microbiol. Lett. **365**(19): fny201.
82. Wang, R., Seror, S. J., Blight, M., Pratt, J. M., Broome-Smith, J. K. and Holland, I. B. (1991). "Analysis of the membrane organization of an *Escherichia coli* protein translocator, HlyB, a member of a large family of prokaryote and eukaryote surface transport proteins." J. Mol. Biol. **217**(3): 441-454.
83. Welch, R. (2001). "RTX toxin structure and function: a story of numerous anomalies and few analogies in toxin biology." Curr. Top. Microbiol. Immunol. **257**: 85-111.
84. Wu, B., Chao, Jeffrey A. and Singer, Robert H. (2012). "Fluorescence fluctuation spectroscopy enables quantitative imaging of single mRNAs in living cells." Biophys. J. **102**(12): 2936-2944.
85. Young, A. P., Jackson, D. J. and Wyeth, R. C. (2020). "A technical review and guide to RNA fluorescence *in situ* hybridization." PeerJ **8**: e8806.

Supplementary Information

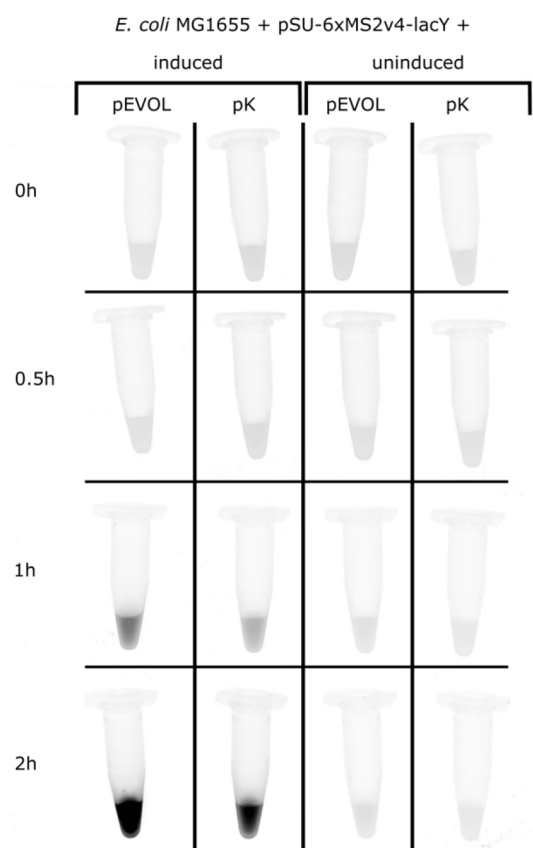


Figure S1: Test for eGFP fluorescence of *E. coli* MG1655 cells expressing 6xMS2v4-lacY and MS2d-eGFP up to 2 h after induction. Expression level of MS2d-eGFP is higher with the pEVOL-MS2d-eGFP plasmid (pEVOL) in comparison to the pK-MS2d-eGFP plasmid (pK). Both plasmids show no leaky expression (right, uninduced). The expression time increases from top to bottom with the time after induction in hours indicated on the left side. eGFP fluorescence was imaged with excitation at 460 nm using Blue Epi light.

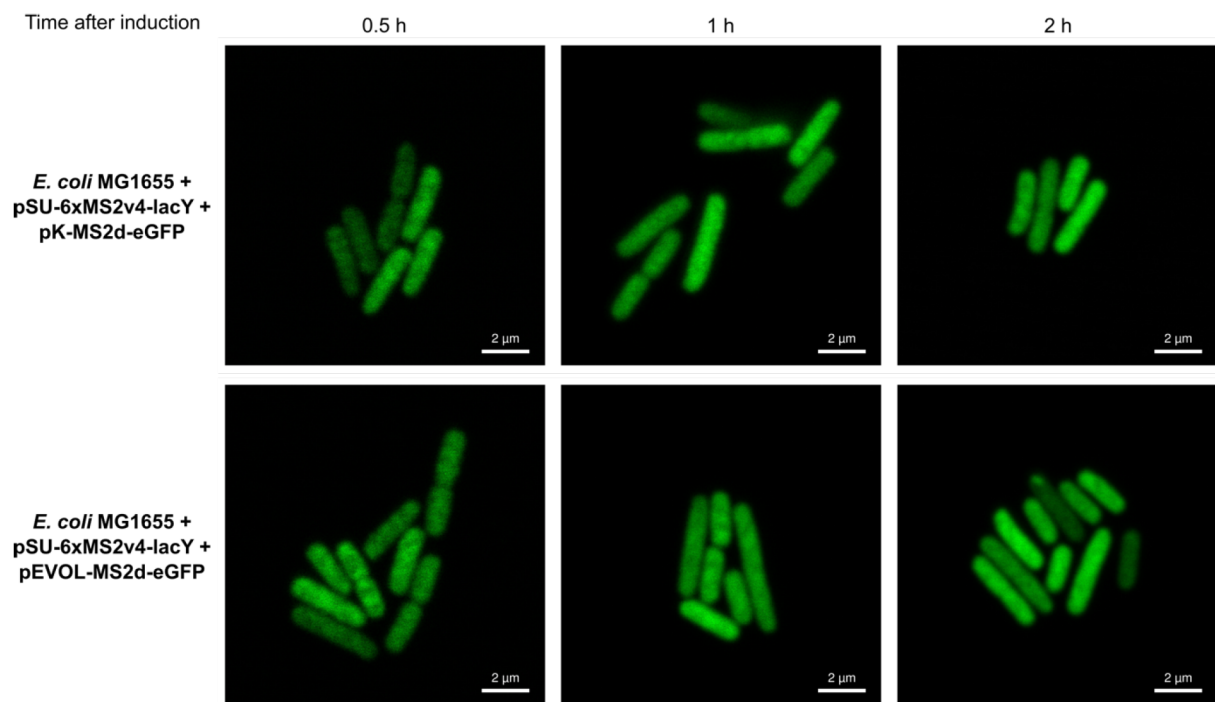


Figure S2: Localization of LacY mRNA in *E. coli* MG1655 using fluorescence microscopy. Shown is the eGFP fluorescence of cells expressing MS2d-eGFP either from the plasmid pK-MS2d-eGFP (upper panel) or pEVOL-MS2d-eGFP (lower panel) co-transformed with pSU-6xMS2v4-lacY. The time after induction when the cell samples were taken is indicated on the top in hours.

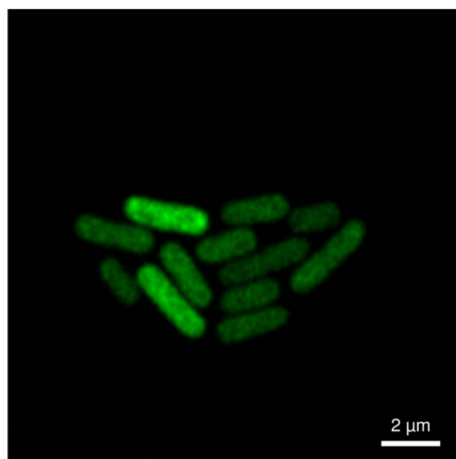


Figure S3: Localization of LacY mRNA in *E. coli* BL21 MG1655 + pK-MS2d-eGFP + pSU-6xMS2v4-lacY using fluorescence microscopy. Shown is the eGFP fluorescence of cells 2 h after addition of 0.1% arabinose (induction of MS2d-eGFP) without addition of IPTG (leaky transcription of 6xMS2v4-lacY mRNA).

3.3. Chapter 3: Photo-crosslinking of the hemolysin A type 1 secretion system using unnatural amino acids

Title:	Photo-crosslinking of the hemolysin A type 1 secretion system using unnatural amino acids
Authors:	Manuel T. Anlauf , Cigdem Günes, Gereon Poschmann, Sven Reimann, Kai Stühler, Sander H.J. Smits, Lutz Schmitt
Published in:	(to be submitted)
Own proportion on this work:	80%
	Designing and cloning of the majority of plasmids (>95%)
	Expression and secretion of proteins with incorporated unnatural amino acids
	Secretion experiments with mutants and proteins with different tags
	Crosslinking experiments
	Pull-down experiments
	Data analysis and quantification
	Writing of the manuscript

Photo-crosslinking of the hemolysin A type 1 secretion system using unnatural amino acids

Manuel T. Anlauf¹, Cigdem Günes¹, Gereon Poschmann², Sven Reimann^{1,3},
Kai Stühler², Sander H.J. Smits^{1,4}, Lutz Schmitt^{1*}

¹: Heinrich Heine University Düsseldorf, Faculty of Mathematics and Natural Sciences, Institute of Biochemistry, Universitätsstraße 1, 40225 Düsseldorf, Germany

²: Heinrich Heine University Düsseldorf, Faculty of Mathematics and Natural Sciences, Molecular Proteomics Laboratory, Biomedical Research Center (BMFZ), Universitätsstraße 1, 40225 Düsseldorf, Germany

³: present address: Bayer, Wuppertal, Germany

⁴: Heinrich Heine University Düsseldorf, Faculty of Mathematics and Natural Sciences, Center for Structural Studies, Universitätsstraße 1, 40225 Düsseldorf, Germany

*: To whom correspondence should be addressed: Lutz Schmitt, Heinrich Heine University Düsseldorf, Faculty of Mathematics and Natural Sciences, Institute of Biochemistry, Universitätsstraße 1, 40225 Düsseldorf, Germany, Tel.: +49 211 81-10773, E-Mail: lutz.schmitt@hhu.de

Abstract

Secretion of toxins in Gram-negative bacteria is often mediated by type 1 secretion systems (T1SS). In *Escherichia coli*, the toxin hemolysin A (HlyA) is recognized by the secretion complex via its C-terminal secretion signal. The secretion complex is composed of the outer membrane protein TolC and an inner membrane complex consisting of the ABC transporter hemolysin B (HlyB) and the membrane fusion protein hemolysin D (HlyD). HlyA was shown to interact with the nucleotide-binding domain and C39 peptidase-like domain of HlyB, resulting in the recruitment of TolC and formation of a secretion-competent channel. However, amino acids forming the translocation channel and possibly interacting with HlyA during the secretion process are unknown. We therefore mapped the translocation pathway by employing the incorporation of unnatural amino acids (UAA) as photo-activatable crosslinkers. We introduced two different unnatural amino acids into HlyB and, more efficiently, into various positions and versions of HlyA. The incorporation of UAA into eGFP-HlyA stalled the secretion process and placed the crosslinking moiety into the translocation channel. By doing so, we verified the formation of higher molecular weight crosslinked species for a multitude of positions upon UV irradiation, even though the exact crosslinked amino acids could not be identified by mass spectrometry. Overall, formation of crosslinks appeared to be independent from the position in HlyA, where the UAA was placed. Additionally, we identified F175 as a position in HlyB dimers to form intermolecular crosslinks when replaced with UAAs. Furthermore, we investigated the ability of differently tagged variants of HlyB to secrete HlyA. However, insertion of affinity tags influenced expression level and/or secretion competency of HlyB, which strongly hinders the use of tagged versions of HlyB for structural analyses.

Keywords

Photo-crosslinking, unnatural amino acid, amber mutation, hemolysin, type I secretion system, ABC transporter, secretion

Introduction

The active transport of compounds from the cytoplasm across biological membranes into the extracellular space is a challenging task, especially for Gram-negative bacteria because of their double membrane organization. In prokaryotes, a multitude of different secretion systems evolved to manage this process, with some pathogenic organisms being able to even penetrate an additional host membrane to inject toxins and other virulence factors (Costa *et al.* 2015). The prototypic type I secretion system (T1SS) displays a rather simple architecture, where the transport of substrates across the inner and outer membrane occurs without the participation of the secretory (Sec) pathway (Delepelaire 2004) and usually in a single step without the formation of a periplasmic intermediate. The transported substrate is in most cases a polypeptide, which can vary in size and function, ranging from the 19 kDa hemophore HasA from *Serratia marcescens* (Létoffé *et al.* 1994) to the adhesion protein LapA from *Pseudomonas fluorescens* with a size of 900 kDa (Hinsa *et al.* 2003). As a tripartite system, its translocation channel consists of three proteins: an ATP binding cassette (ABC) transporter and a membrane fusion protein (MFP) in the inner membrane, connected to an outer membrane protein (OMP) in the outer membrane.

The respective system found in uropathogenic *E. coli* is the hemolysin T1SS: its substrate is hemolysin A (HlyA), a 110 kDa toxin from the Repeats in ToxIns (RTX) superfamily (Welch 1991). These kind of proteins contain a conserved nonapeptide sequence (GGxGxDxUx, with x being any amino acid and U being a large, hydrophobic amino acid), which is able to bind Ca²⁺ ions and induce folding afterwards (Ostolaza *et al.* 1995, Chenal *et al.* 2009). However, the concentration of intracellular Ca²⁺ in *E. coli* is too low for binding and thus the toxin is present in an unfolded state, a prerequisite for the secretion process (Jones *et al.* 1999, Sanchez-Magraner *et al.* 2007, Bakkes *et al.* 2010). Reaching the extracellular space allows binding of Ca²⁺ ions due to the higher concentration, thereby promoting the folding of the toxin and allowing it to hydrolyze erythrocytes (Boehm *et al.* 1990). The energy necessary for the secretion process is provided by the dimeric ATP binding cassette (ABC) transporter hemolysin B (HlyB). The protein features an additional N-terminal C39 peptidase-like domain (CLD), classifying it as a T1SS group 2 transporter (Lecher *et al.* 2012, Kanonenberg *et al.* 2013). Hemolysin D (HlyD), the MFP, is also present in the inner membrane and, together with HlyB, forms an inner membrane complex (IMC) for which

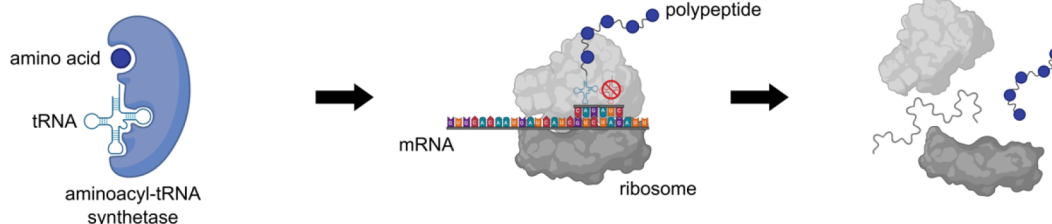
the presence of the substrate is dispensable (Gray *et al.* 1989, Wang *et al.* 1991, Pimenta *et al.* 1999, Balakrishnan *et al.* 2001). HlyA can bind to the cytosolic domain of HlyD (Thanabalu *et al.* 1998, Balakrishnan *et al.* 2001) as well as to the CLD and nucleotide-binding domain (NBD) of HlyB (Benabdelhak *et al.* 2003, Lecher *et al.* 2012, Pourhassan *et al.* 2022). Upon recognition of HlyA by the IMC, the outer membrane component TolC is recruited to form the secretion complex (Thanabalu *et al.* 1998, Balakrishnan *et al.* 2001). TolC is a porin-like protein, which is not exclusively present in the hemolysin system but is also known to interact with other transport systems like the drug efflux systems of AcrAB and MacAB (Kim *et al.* 2010, Xu *et al.* 2011). HlyA is then secreted with its C-terminus first (Lenders *et al.* 2015). All necessary information to secrete HlyA is comprised in its last 48-60 amino acids. This secretion signal is situated at the C-terminus and not cleaved off at any point during the secretion process (Koronakis *et al.* 1989, Jarchau *et al.* 1994). The fusion of fast-folding proteins to the N-terminus of HlyA, like fast-folding eGFP, halts the secretion process: the major portion can still reach the outside of the cell, but the folded eGFP acts like a plug, stalling the complex and effectively anchoring HlyA to the secretion system (Lenders *et al.* 2015).

Although a lot about the regulation and assembly of the secretion complex is known, the secretion process of HlyA itself remains largely elusive. For instance, the exact entry point for HlyA in HlyB is unknown, as well as the existence of recognition/binding sites of HlyA in the transmembrane domain (TMD) of HlyB. We therefore aimed to identify and map the interaction sites between HlyA and HlyB *in vivo*, using unnatural amino acids (UAA) as photo-activatable crosslinkers. This tool has already been successfully used in bacteria such as *Escherichia coli*, yeasts like *Saccharomyces cerevisiae* and *Pichia pastoris* as well as mammalian cells (Hino *et al.* 2005, Chen *et al.* 2007, Young *et al.* 2009, Berg *et al.* 2014, Murray *et al.* 2016, Simpson *et al.* 2016, Choi *et al.* 2019, Torres-Vargas *et al.* 2019). For this, a stop codon is used to incorporate an UAA at any position of choice. To minimize the integration of the UAA in endogenous proteins already carrying the stop codon, the amber stop codon (TAG) is used, as it is the least used stop codon (7%) in *E. coli* (Belin and Puigbò 2022). Normally, a stop codon is lacking a respective tRNA with a matching anticodon (Figure 1, upper panel). By generating a pair of an orthogonal tRNA and aminoacyl-tRNA synthetase (aaRS), this amber stop codon can be reassigned to encode for UAA, ultimately suppressing it (Figure 1, lower panel). Ideally, this tRNA-aaRS pair shows

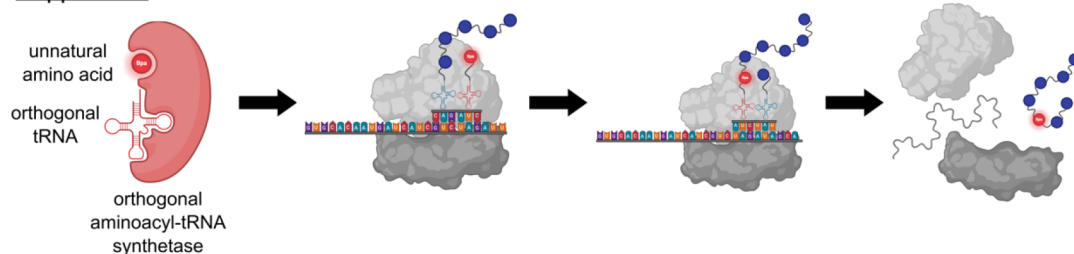
no cross-reactivity with any endogenous tRNAs or aaRSs present in the host organism to ensure a high specificity (Young *et al.* 2010).

A

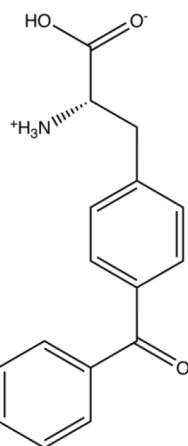
Endogenous



Suppressed



B



C

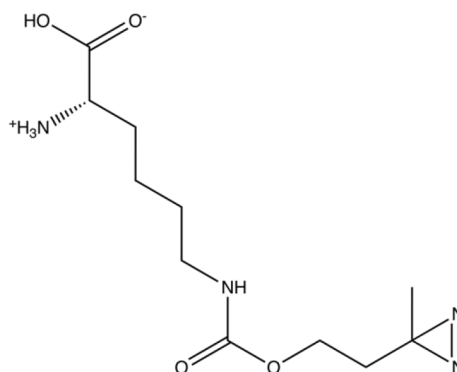


Figure 1: Schematic of UAAs and their incorporation via amber stop codon suppression (**A**) Upper panel: Naturally, only endogenous aminoacyl-tRNA synthetases are present in the cell, which load tRNAs with the respective canonical amino acid (blue). During translation, when the ribosome reaches a stop codon on the mRNA (e.g. amber = UAG), no tRNA with a matching anticodon is available. The ribosome ultimately falls apart, releasing the polypeptide chain. Lower panel: By introducing an orthogonal aminoacyl-tRNA synthetase and tRNA pair (red), amber stop codons can be suppressed. The orthogonal tRNA carries an anticodon matching the amber codon. The translation is not stopped when the ribosome reaches an amber stop codon and the unnatural amino acid (here Bpa in red) is incorporated into the polypeptide chain. (**B**) Chemical structure of the unnatural amino acid p-benzoyl-L-phenylalanine (Bpa). (**C**) Chemical structure of the unnatural amino acid photolysine (AbK). The figure was created with BioRender.com.

Here, we present the successful incorporation of different UAAs, acting as photoactivatable crosslinkers, at varying positions in HlyA (all variants summarized in Figure 2) as well as HlyB. We could show the formation of higher molecular weight crosslinks (>300 kDa) when the hemolysin T1SS was stalled by Bpa-incorporated eGFP-HlyA and was predominantly independent from the position of the unnatural amino acid. Enrichment of crosslinked peptides was not possible, as both termini of HlyA were inaccessible in the stalled secretion complex and did not show any binding to different affinity resins. Substitution of F175 in HlyB with Bpa resulted in the formation of photo-induced, intermolecular HlyB crosslinks. Furthermore, we present a high sensitivity of HlyB expression level and secretion competency for the presence of affinity tags at both termini.

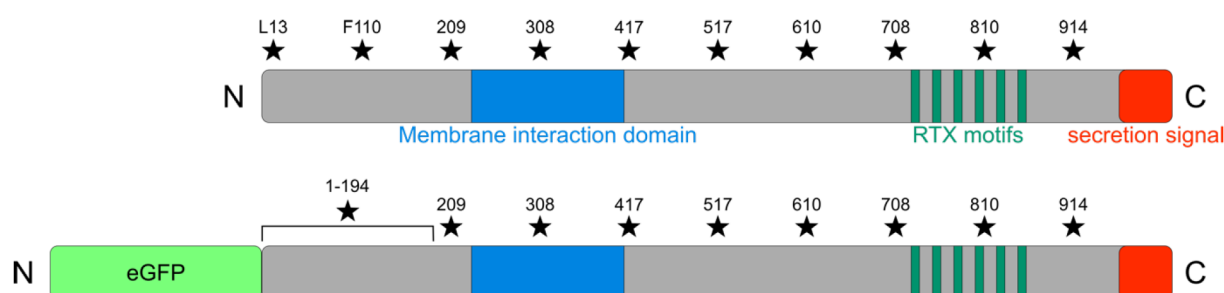


Figure 2: Schematic overview of HlyA variants and positions of amber stop codon mutations used in this study. Top: HlyA, bottom: eGFP-tagged HlyA. The approx. last 60 amino acids at the C-terminus forming the secretion signal are shown in red, while the six glycine rich RTX motifs are shown in dark green. The domain shown to interact with the membrane is highlighted in blue (Ludwig *et al.* 1991). The N-terminal fusions of eGFP is shown in bright green. Amino acid positions for amber codon substitution are indicated with a numbered star.

Results

Incorporation and activation of p-benzoyl-L-phenylalanine

We intended to map specific amino acids involved in the binding and translocation of HlyA by HlyB within this project using unnatural amino acids (UAA). First, we probed the applicability of the UAA photolysine, also known as 3'-Azibutyl-N-carbamoyl-lysine (AbK, Figure 1C), but noticed early on that incorporation efficiency and activation via UV irradiation were not optimal with the hemolysin system (Figure S1). We therefore chose the UAA p-benzoyl-L-phenylalanine (Bpa, Figure 1B) as it is commonly used to crosslink proteins. Upon irradiation with UV light at 365 nm, a carbonyl diradical is

formed, which can abstract protons from primarily C-H bonds near the ketone oxygen, thereby connecting two interacting proteins with a covalent bond (Dorman and Prestwich 1994, Sato *et al.* 2011). This system, and specifically Bpa, has been used to investigate various systems, such as the LPS transport system in *E. coli* (Simpson *et al.* 2016, Owens *et al.* 2019), the type III secretion system of *Salmonella enterica* (Fukumura *et al.* 2017, Torres-Vargas *et al.* 2019) and the interface of arrestin and G protein-coupled receptors (Böttke *et al.* 2020). Proteins with an incorporated UAA are designated with an asterisk from here on, e.g. eGFP-HlyA*.

We assessed the functionality of the crosslinking system in our hands on the basis of two control measurements: First, the photo-activation of Bpa was tested by absorbance measurements at 262 nm (Miller and Kaiser 1988). We could confirm the effective photo-activation of Bpa, as absorption at 262 nm decreased upon irradiation with UV light at 365 nm in a time dependent manner with complete activation after 20 min of irradiation (Figure 3A). Secondly, the formation of crosslinked species of two interacting proteins was tested: the effector protein SptP from *S. enterica* together with its dedicated chaperone SicP, which featured an N-terminal GST tag and an amber stop codon mutation at position F36. Upon UV-irradiation, two signals of crosslinked species could be identified with Bpa-incorporated GST-SicP with molecular weights of ~120 kDa and 200 kDa (Figure 3B), which resemble the formation of SicP-SptP complexes in ratios of 1:1 and 2:1, as two copies of the chaperone SicP can bind to one copy of SptP (Fu and Galán 1998, Stebbins and Galán 2001). Furthermore, expression within Bpa supplemented medium resulted in a clear signal for GST-SicP at ~40 kDa, although weak bands were also visible in the absence of Bpa (Figure 3B). This may be attributed to a readthrough of the stop codon even without the unnatural amino acid being present.

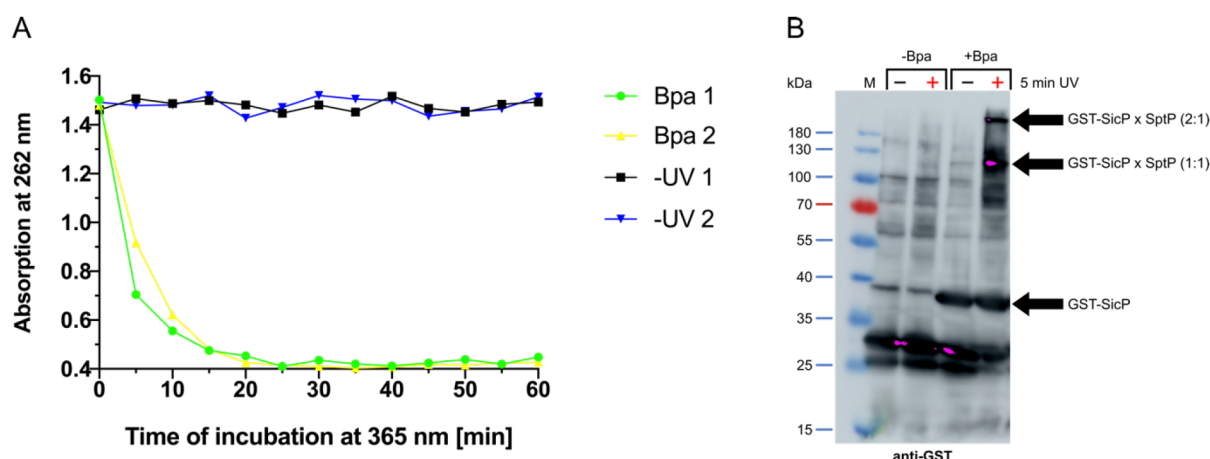


Figure 3: Positive controls for the incorporation of Bpa and UV-induced crosslink formation. **(A)** Photo-activation of the unnatural amino acid Bpa. Green and yellow lines: Absorbance at 262 nm of 1 mM Bpa from two different sources (1 and 2) in PBS buffer. A portion of the same samples was kept in the dark and not UV-irradiated as a negative control (black and blue). Successful photo-activation of Bpa is apparent by a decrease of the absorbance at 262 nm upon prolonged irradiation at 365 nm. **(B)** Crosslink of the Bpa incorporated chaperone GST-SicP* with SptP. After expression of GST-SicP* and SptP with (+Bpa) or without Bpa (-Bpa) in the medium, whole *E. coli* BL21(DE3) cells were resuspended in PBS buffer and UV-irradiated for up to 5 min at 365 nm (+) or kept in the dark and not UV-irradiated as a negative control (-). The immunoblot was analyzed with an antibody targeting the N-terminal GST tag on SicP*. The signals for non-crosslinked GST-SicP* and the crosslinked complexes with SptP in ratios 1:1 and 2:1 are marked with an arrow. M: PageRuler Prestained Protein Ladder.

Photo-crosslinking of eGFP-HlyA* using Bpa

After verifying the functionality of the Bpa crosslinking system, we turned towards the HlyA T1SS. A previously reported N-terminally eGFP tagged version of HlyA was used here, since the eGFP acts like a plug and stalling of the secretion system should decrease the dynamics of the system, thereby aiding in the formation of crosslinks (Lenders *et al.* 2015, Lenders *et al.* 2016, Beer *et al.* 2021). Furthermore, the eGFP and N-terminal 6xHis tag should allow us to enrich and isolate eGFP-HlyA and crosslinked species.

We first tested 10 amber positions in HlyA: L13, F110, L209, G308, M417, P517, I610, K708, L810 and W914, which were at a distance of roughly 100 aa to each other. At the time when these experiments were performed, no structure of a T1SS ABC transporter was available, and PCAT1 from *Clostridium thermocellum* was one of the only ABC transporters with a known structure, which was similar to HlyB (Lin *et al.* 2015, Kieuvongngam *et al.* 2020). In PCAT1, the lateral opening for the cargo is in between the transmembrane helices 3 and 4 with a length of the TMD being approx. 75 Å. If one assumes the lateral opening in HlyB to be at an equivalent position and

identical length of the TMD, Bpa of eGFP-HlyA-L13* should reside within the HlyB-TMD of the stalled complex. Thus, L13* was the most promising amino acid position to form crosslinks with HlyB.

We tested the incorporation of Bpa into these eGFP-HlyA amber mutants. A signal for eGFP-HlyA* was only visible when Bpa was present in the medium during expression and successfully incorporated in the amber codon mutation 4 h after induction (W914 as an exemplary mutant, Figure 4), while in the absence of the UAA, translation stopped before synthesis of the secretion signal and consequently, no signal was detected in the respective expression sample (Figure 4, -Bpa 4 h), confirming the successful suppression of the amber stop codon with eGFP-HlyA as well. Since the eGFP-tagged variant of HlyA was used, it cannot be secreted into the supernatant and is either stalled in the secretion complex or remains in the cytoplasm. Furthermore, the expression of HlyB and HlyD was unaffected by the amber suppression system and Bpa in the medium (Figure S2).

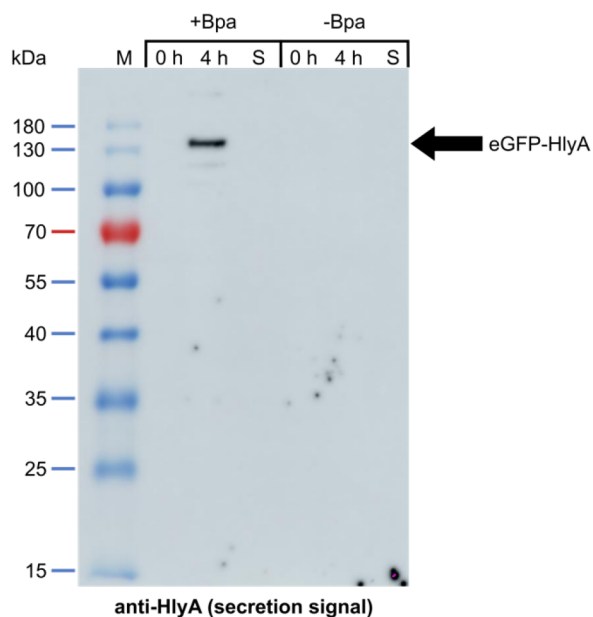


Figure 4: Incorporation of Bpa into eGFP-HlyA-W914*. Whole cell samples were taken before (0 h) and 4 h after induction as well as a supernatant sample taken after 4 h (S), either with (+Bpa) or without Bpa added to the medium (-Bpa). The immunoblot was analyzed with an antibody targeting the C-terminal secretion signal on HlyA. The signal for expressed eGFP-HlyA is marked. M: PageRuler Prestained Protein Ladder.

Antibody-dependent detection of high-molecular eGFP-HlyA* crosslinks

Initial identification of crosslinked eGFP-HlyA species were performed using a HlyA antibody targeting the C-terminal secretion signal. However, no additional signals for crosslinked eGFP-HlyA-L13* were detectable after cells were subjected to UV irradiation. Still, the signal for non-crosslinked eGFP-HlyA-L13* was vanishing (Figure 5A). Two signals for eGFP-HlyA-L13* were visible when cells were not irradiated with UV light, with molecular masses roughly corresponding to a dimer of eGFP-HlyA-L13* (molecular weight of ~280.0 kDa) and monomeric eGFP-HlyA-L13* (140.0 kDa) respectively. Since the samples displayed in Figure 5A were neither cooked before subjection to the SDS-PAGE nor dithiothreitol (DTT) was added, signals with the higher molecular weight represent most likely dimeric species of eGFP-HlyA-L13*. This is further supported by comparing untreated samples to cooked SDS samples of eGFP-HlyA*, in which the higher molecular weight band disappeared (Figure 5B). Already 5 min of UV irradiation resulted in a significant decrease in band intensities for eGFP-HlyA-L13* when compared to the untreated samples, and after 15 min of UV irradiation no signals for eGFP-HlyA-L13* were visible.

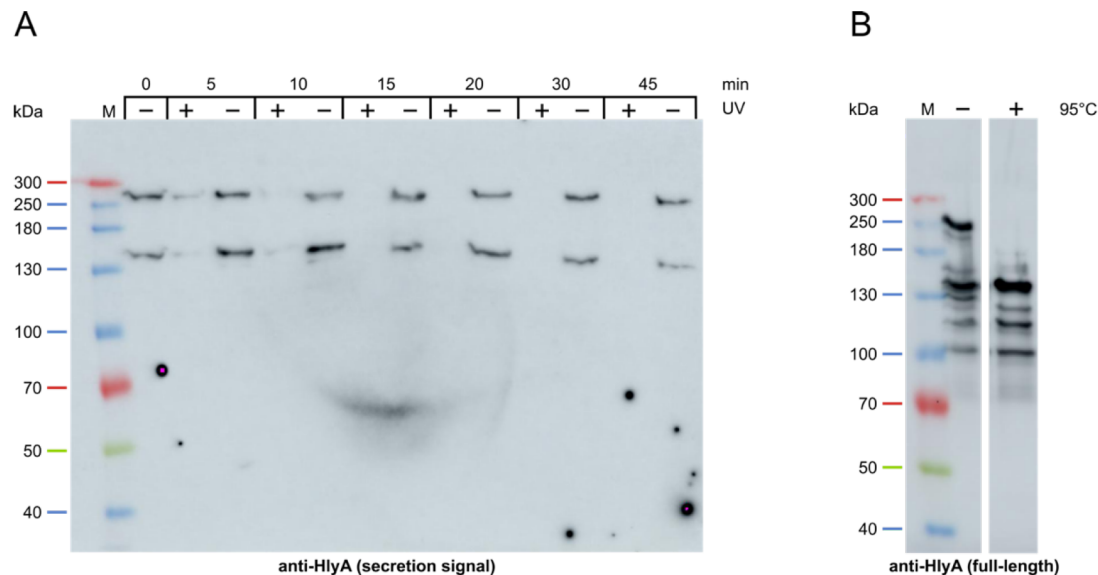


Figure 5: Identification of Bpa-crosslinked eGFP-HlyA using an antibody targeting the secretion signal of HlyA. **(A)** Immunoblot analysis of *E. coli* BL21(DE3) cells expressing HlyB, HlyD and eGFP-HlyA-L13* after *in vivo* photo-crosslinking. Protein expression was performed for 4 h. The antibody used targeted the secretion signal of HlyA. Cells were either irradiated with UV light of 365 nm (+) or left untreated as a control (-) for up to 45 min (indicated above). SDS samples were neither cooked nor DTT added. **(B)** Influence of cooking of the SDS-PAGE sample on signal pattern during immunoblot. *E. coli* BL21(DE3) cells expressed HlyB, HlyD and eGFP-HlyA-L13* for 4 h. Prior to SDS-PAGE, samples were either cooked at 95°C for 5 min (+) or left untreated (-). The antibody used targeted full-length HlyA. M: Spectra Multicolor High Range Protein Ladder.

Next, the presence of crosslinked eGFP-HlyA* was analyzed using a different antibody, targeting the full-length HlyA with the intention, that the increased number of recognized epitopes (in comparison to the single epitope of the secretion single antibody) should reveal any crosslinked eGFP-HlyA*.

The ten previously used amber mutants of eGFP-HlyA* between L13* and W914* were again tested. This time, signals with higher molecular weight were detectable for all ten mutants upon UV irradiation, while the signal for non-crosslinked eGFP-HlyA* diminished simultaneously (exemplary immunoblots shown for L13*, G308* and M417*, Figure 6A and B). Interestingly, these signals occurred as an unfocused smear which intensified to a band-like structure above 300 kDa. However, bands smaller than 140 kDa were detectable as well, most likely caused by truncated versions of eGFP-HlyA. Surprisingly, a similar band pattern at high molecular weight was also visible with the unmodified eGFP-HlyA wildtype control, in which Bpa was present in the medium but no amber codon substitution was introduced (Figure 6C). In the monitored time frame, no increased accumulation of crosslink bands was observed for UV irradiations longer than 5 min, however, the intensity of the non-crosslinked eGFP-HlyA signal at 140 kDa decreased with increasing irradiation time. In the case of eGFP-HlyA without amber stop codon substitution, a prolonged irradiation with UV light even resulted in a decrease of crosslink-band intensity at ~300 kDa (Figure 6C).

E. coli BL21(DE3) cells expressing HlyB, HlyD and eGFP-HlyA-L13*, which were crosslinked via UV irradiation, were further analyzed by isolation of the cell membranes (Figure 6D). For this, cells were disrupted after UV irradiation, membranes isolated by step-wise centrifugation, and solubilized using the detergent Fos-Choline-14 (FC14). The crosslinked eGFP-HlyA-L13* with a molecular weight of >300 kDa observed before could also be detected in the solubilized membrane fraction, indicating that the previously identified eGFP-HlyA-L13* crosslinks were not derived from soluble eGFP-HlyA, and indeed localized to the stalled T1SS complex in the membrane. Upon examining the samples using an antibody targeting the NBD of the ABC transporter HlyB, a faint band for the monomeric transporter at 70 kDa as well as a signal with a molecular weight >300 kDa was visible (Figure 6E). However, similar to HlyA, identification of HlyB involved crosslinks proved to be difficult since samples did not always show the clear formation of higher molecular weight bands after UV irradiation and instead only the signal for the non-crosslinked HlyB vanished.

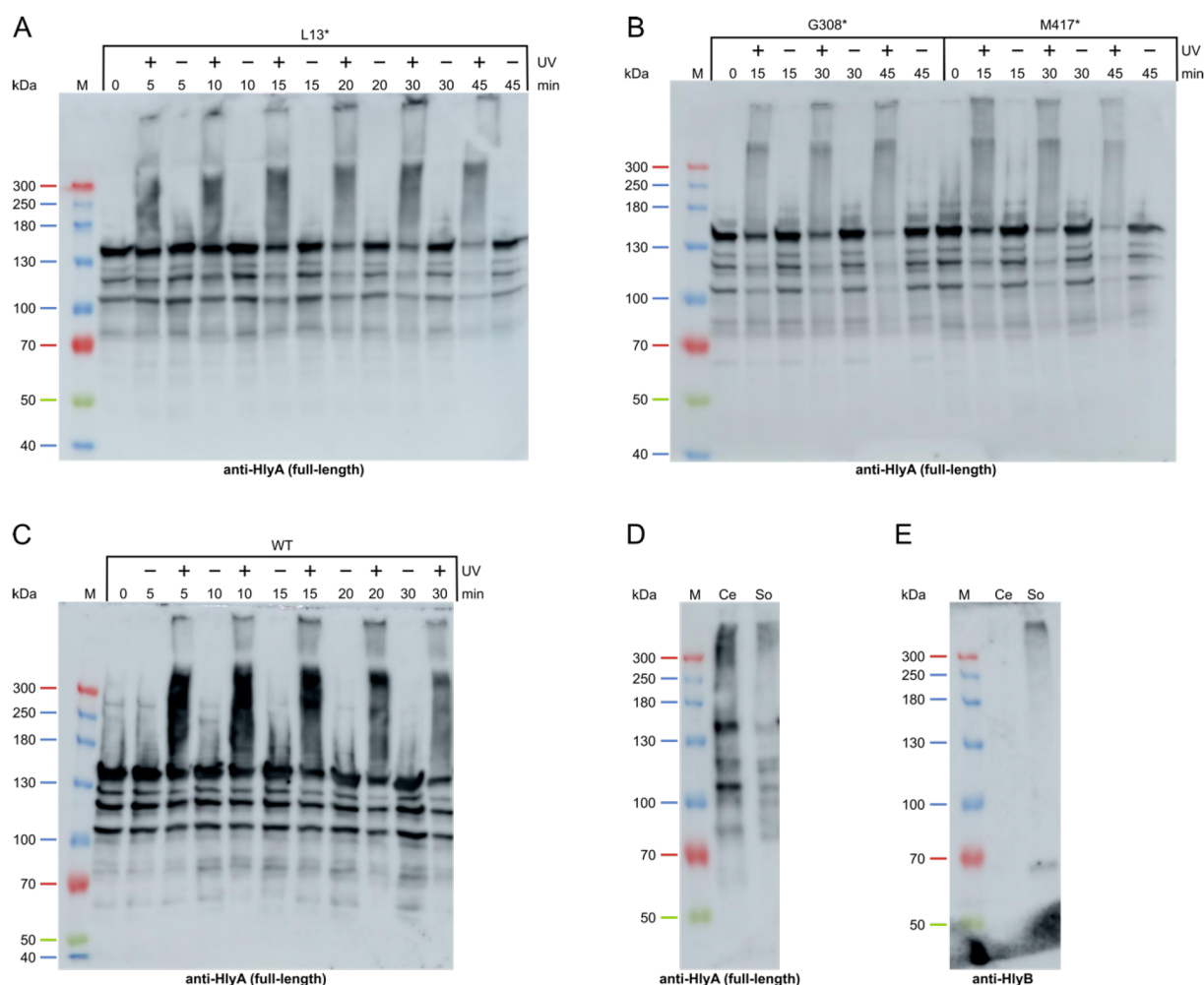


Figure 6: Identification of Bpa-crosslinked eGFP-HlyA using an antibody targeting full-length HlyA. **(A)** Immunoblot analysis of *E. coli* BL21(DE3) cells expressing HlyB, HlyD and eGFP-HlyA-L13* after *in vivo* photo-crosslinking using an antibody targeting full-length HlyA. Protein expression was performed for 4 h. Cells were either irradiated with UV light of 365 nm (+) or left untreated as a control (-) for up to 45 min (indicated above). **(B)** Same as in **(A)**, but instead of eGFP-HlyA-L13* the amber mutants eGFP-HlyA-G308* (G308*) and eGFP-HlyA-M417* (M417*) were used. **(C)** Same as in **(A)**, but instead of eGFP-HlyA-L13* the wildtype eGFP-HlyA (WT) without an amber stop codon substitution was used. **(D)** Immunoblot of whole *E. coli* BL21(DE3) cells expressing HlyB, HlyD and eGFP-HlyA-L13* irradiated with UV light of 365 nm for 45 min (Ce). The cell membranes were isolated, solubilized using 0.5% FC14 and the supernatant (So) analyzed using an antibody targeting full-length HlyA. **(E)** Same as in **(D)**, but an antibody targeting HlyB was used for detection. M: Spectra Multicolor High Range Protein Ladder.

Verification of Bpa-specific formation of crosslinks

Both, Bpa-incorporated HlyA mutants as well as HlyA without amber codon mutation showed higher molecular weight signals after UV irradiation. Hence it was not clear, if the crosslink bands, which are detectable with the full-length HlyA antibody after UV irradiation, were caused solely by non-specific crosslinks e.g. UV-induced crosslinking of aromatic residues or due to crosslinks introduced by Bpa. We hypothesized, that the amount of non-crosslinked eGFP-HlyA* should be reduced in the case of Bpa-

incorporated mutants in comparison to wildtype eGFP-HlyA if Bpa-specific crosslinks were generated. If the UV irradiation resulted only in non-specific crosslinks, the reduction of the band intensity for non-crosslinked eGFP-HlyA should be identical for Bpa-incorporated and wildtype eGFP-HlyA. We therefore repeated the crosslink experiment with the secretion signal specific HlyA antibody, since immunoblots showed only a single band. This allowed a clear identification and quantification of the non-crosslinked species over the course of irradiation time. We analyzed whole *E. coli* BL21(DE3) cells after 4 h of expression and compared wildtype eGFP-HlyA to mutants, in which the amber mutation was positioned at the N-terminal and C-terminal end of HlyA (L13* and W914*). Both the immunoblots using the secretion signal specific HlyA antibody (Figure 7A) as well as the subsequent quantifications (Figure 7B) demonstrate a stronger signal decrease for the Bpa-incorporated mutants of eGFP-HlyA L13* (0.18 ± 0.08) and W914* (0.21 ± 0.23) when compared to non-modified eGFP-HlyA WT (0.59 ± 0.28), albeit the signal intensities of the investigated eGFP-HlyA variants showed some biological variation.

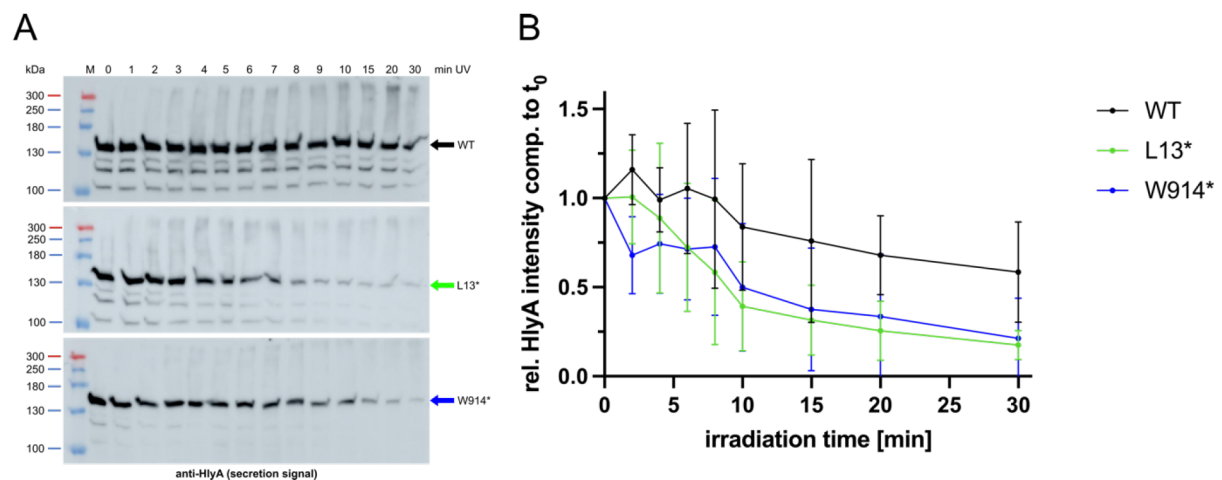


Figure 7: Quantification of UV-induced signal reduction in Immunoblots of eGFP-HlyA. **(A)** Exemplary immunoblots of *E. coli* BL21(DE3) cells expressing HlyB, HlyD and eGFP-HlyA of the indicated variant (black: WT, green: L13*, blue: W914*). *In vivo* photo-crosslinking with Bpa was performed 4 h after induction for up to 30 min. The non-crosslinked eGFP-HlyA signal at 140 kDa, detectable using an antibody targeting the secretion signal of HlyA, was used for quantification (marked with an arrow). The signal intensity was normalized to the signal intensity of eGFP-HlyA before UV irradiation ($t_0 = 0$ min). M: Spectra Multicolor High Range Protein Ladder. **(B)** Quantification of non-crosslinked eGFP-HlyA signal intensity in response to prolonged UV irradiation at 365 nm. A total of 4 individual quantifications were performed.

Enrichment of crosslinked secretion complexes for mass spectrometry

After confirmation that the detected crosslink bands were, at least in part, caused by the introduced photo-crosslinker Bpa, we aimed to further analyze proteins of eGFP-HlyA crosslinked by Bpa to other parts of the hemolysin T1SS using mass spectrometry. To ensure a concentration of crosslinked protein sufficient for reliable detection in mass spectrometry, we applied co-immunoprecipitation (co-IP) utilizing the N-terminally fused eGFP on HlyA, which is commonly used as a target for co-IP with immobilized nanobodies (Vermeulen *et al.* 2010, Harterink *et al.* 2011, Kloet *et al.* 2016). We therefore subjected isolated and solubilized membranes from UV irradiated *E. coli* BL21(DE3) cells expressing HlyB, HlyD and eGFP-HlyA-L13* to GFP-Traps to enrich crosslinked eGFP-HlyA species. However, no signals in the subsequent immunoblot analysis could be detected in the wash (Wa) or elution (El) fraction (Figure 8A). Instead, identical band patterns were observable in the flow through fraction after the binding step (Fl) and the solubilized membrane sample (So) used for the co-IP, indicating that no eGFP-HlyA-L13* could bind to the nanobodies. The functionality of the immunoprecipitation was assessed by applying purified eGFP-HlyA to the GFP-Trap (Figure 8C).

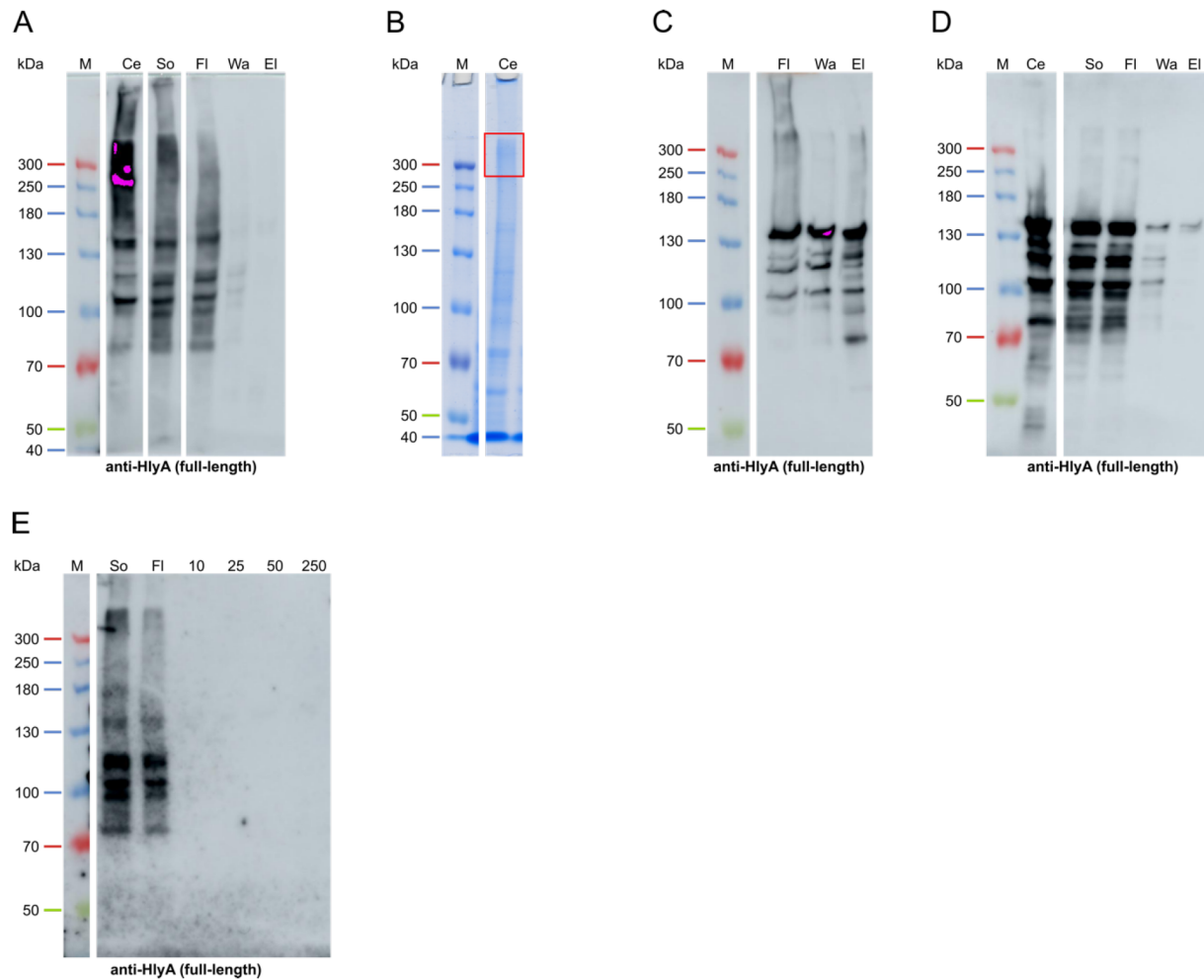


Figure 8: Co-Immunoprecipitation of the hemolysin secretion complex stalled with eGFP. **(A)** Co-IP of Bpa-crosslinked eGFP-HlyA-L13* using GFP-Trap agarose after UV irradiation (365 nm) of cells for 45 min. Ce: Whole cells of *E. coli* BL21(DE3) expressing HlyB, HlyD and eGFP-HlyA-L13* after 45 min of UV irradiation (365 nm), So: Isolated membranes solubilized with 0.5% FC14, FI: Flow through fraction after incubation of solubilized membranes with GFP-Trap agarose, Wa: Wash fraction of GFP-Trap agarose, El: Elution of bound protein from GFP-Trap agarose. **(B)** Coomassie stained SDS gel of the whole cell sample (Ce) shown in **(A)**. The area marked in red was cut out from the gel and analyzed by mass spectrometry. **(C)** Co-IP of purified eGFP-HlyA using GFP-Trap agarose. Abbreviations are the same as in **(A)**. **(D)** Co-IP of non-crosslinked eGFP-HlyA-L13* using GFP-Trap agarose without UV irradiation. Abbreviations are the same as in **(A)**. **(E)** Co-IP of Bpa-crosslinked eGFP-HlyA-L13* using Ni-NTA agarose beads. So: Isolated membranes solubilized with 0.5% FC14, FI: Flow through fraction after incubation of solubilized membranes with Ni-NTA agarose beads, 10: Wash fraction using 10 mM imidazole, 25: Wash fraction using 25 mM imidazole, 50: Wash fraction using 50 mM imidazole, 250: Elution of bound protein using 250 mM imidazole. All immunoblots were analyzed with an antibody targeting full-length HlyA. M: Spectra Multicolor High Range Protein Ladder.

Signals for eGFP-HlyA were detectable in the elution fraction (El), confirming that eGFP-tagged HlyA is in principle able to bind to the nanobodies. The presence of eGFP-HlyA could also be detected in the Wash fraction (Wa) due to subjection of an excess amount of eGFP-HlyA. The co-IP of eGFP-HlyA was further investigated to determine the reason for the inability of the stalled T1SS to bind to GFP-Traps. For this, *E. coli* BL21(DE3) cells were cultivated to express HlyB, HlyD and eGFP-HlyA-

L13* as before, but no UV light was used to induce crosslinks. In the respective immunoblot analysis only very faint bands for eGFP-HlyA-L13* were detectable in the wash and elution fraction at 140 kDa, the majority of the protein remained unbound and was found in the flow through after the binding step (Figure 8D). As a consequence, the UV irradiation could not be the reason for the lack of binding to the GFP-traps. An alternative enrichment approach was tested using the His tag upstream of eGFP-HlyA and nickel nitrilotriacetic acid (Ni-NTA) agarose beads. Still, no binding of eGFP-HlyA-L13* was observed and protein bands for eGFP-HlyA were solely detected in the flow through fraction (Figure 8E).

As enrichment of the crosslinked species containing eGFP-HlyA was not possible, we instead analyzed the region in an SDS gel corresponding to the crosslinked band with a molecular mass >300 kDa visible in immunoblots (Figure 8B) via mass spectrometry. We were able to detect 50 unique peptides, which could be assigned to eGFP-HlyA-L13*, with a total sequence coverage of 51.1% and could thereby confirm the successful incorporation of Bpa. Even though no crosslinked peptides were identified during mass spectrometry analysis, 19 unique peptides of HlyB (sequence coverage 42.3%) and 9 unique peptides of HlyD (sequence coverage 30.5%) were found in the excised region, where proteins of the size of HlyB and HlyD are not found under normal conditions.

Mutational scanning of the N-terminal 194 amino acids in eGFP-HlyA*

In the end, we applied scanning mutagenesis to substitute each codon of the N-terminal 194 amino acids of HlyA with an amber codon to map the N-terminal part of HlyA for crosslinks. Surprisingly, an immunoblot detection using the antibody targeting the secretion signal of HlyA revealed bands with higher molecular weight for the first time (Figure 9A, eGFP-HlyA* amber mutants 28*, 41* and 93* shown as examples). The molecular weight of these crosslinked species observed with the secretion signal specific HlyA antibody coincide with the molecular mass of crosslinked species identified before with the full-length HlyA antibody (e.g. Figure 9B). Also for the first time, a clear difference between crosslinks of eGFP-HlyA-WT and eGFP-HlyA* with incorporated Bpa was visible in immunoblots using the secretion signal specific antibody, as only amber mutants of eGFP-HlyA (28*, 41* and 93*, Figure 9A) exhibited

an UV-induced crosslink band >300 kDa, but not the wildtype control. The usage of the full-length HlyA antibody did not allow such a distinguishment before (Figure 9B) and the results are in agreement with the quantified signal reductions of non-crosslinked eGFP-HlyA (Figure 7). This finally confirmed, that the observed crosslink bands are Bpa-specific and not derived from unspecific crosslinking.

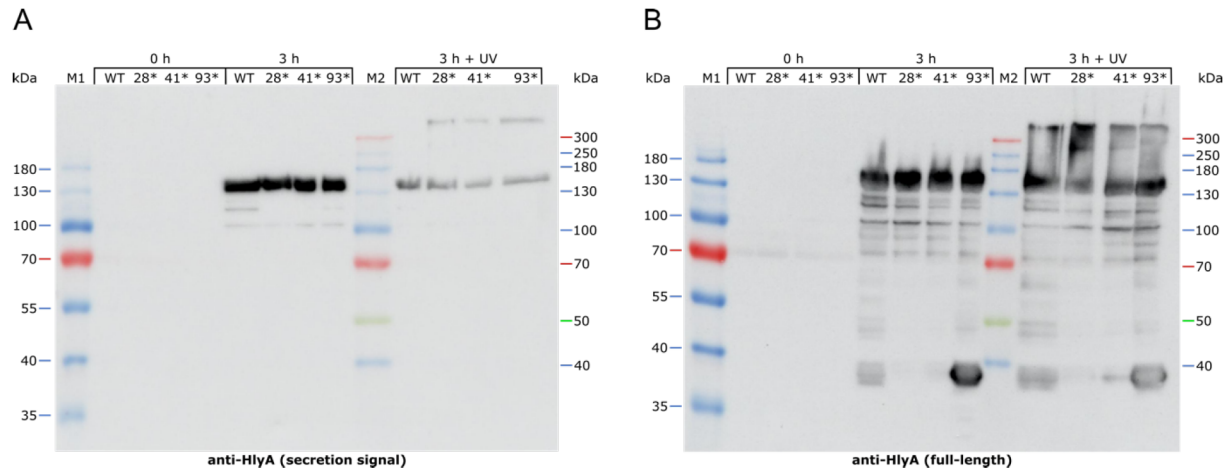


Figure 9: Exemplary photo-crosslinking of Bpa-incorporated eGFP-HlyA* with amber mutations introduced during scanning mutagenesis of the N-terminal 194 amino acids. Immunoblot analysis of whole *E. coli* BL21(DE3) cells expressing HlyB, HlyD and eGFP-HlyA* with an amber mutation at the position indicated above (WT: no amber mutation). Samples were taken before induction (0 h) and after 3 h of expression (3 h). Subsequent UV irradiation was performed at 365 nm for 15 min (3 h + UV). The used antibody targeted either the secretion signal of HlyA (A) or full-length HlyA (B). M1: PageRuler Prestained Protein Ladder, M2: Spectra Multicolor High Range Protein Ladder.

Incorporation of Bpa into HlyB*

Since the amino acids in HlyB, which formed crosslinks with HlyA* could not be identified, we intended to invert the crosslink approach. We aimed to incorporate Bpa into HlyB* for photo-crosslinking to eGFP-HlyA to pinpoint interaction or recognition sites in HlyB for HlyA. At the time of this study, no structural information of the TMD of HlyB was known. We therefore used a homology model of the HlyB dimer based on the transporter PCAT1 from *Clostridium thermocellum* (Lin *et al.* 2015, Kieuvongngam *et al.* 2020) in order to determine residues as promising candidates for substitution with Bpa. We decided to incorporate Bpa at one position in each of the six transmembrane helices (F175*, F216*, Q260*, K322*, I381* and Q435*, Figure 10A and B) located such that Bpa would face to the inside of the translocation channel at different positions in the channel during translocation for crosslinking to HlyA. One of these positions, K322, was already confirmed to form the translocation channel for HlyA (Reimann *et al.* 2016). Additionally, we also introduced an amber codon mutation in the CLD of HlyB

at amino acid Y9, as it faces towards the putative cleft between TMH4 and TMH6 (Figure 10A and B) and, furthermore, is the position at which the catalytically active cysteine of the C39 peptidase domain of PCAT1 is located (identified via sequence alignment, data not shown). Test expressions of these HlyB* amber mutants and HlyD in the presence of Bpa revealed, that the incorporation of Bpa into HlyB was severely less efficient when compared to HlyA. Incorporations at Y9*, F175*, F216* and K322* were slightly better, while almost no signal for HlyB* could be detected for the mutants Q260*, I381* and Q432* (Figure 10C). This trend was further supported by HlyA secretion experiments with the HlyB* amber mutants (Figure 10D). Cells expressing the HlyB-Y9*, HlyB-F175*, HlyB-F216* or HlyB-K322* showed a signal for HlyA at ~110 kDa in the supernatant after 3 h of expression, while no HlyA was detected in supernatants from cells expressing HlyB-Q260*, HlyB-I381* or HlyB-Q432*. Although expression levels of the HlyB* amber mutants was significantly reduced, secretion of HlyA as well as the expression of HlyD was mainly unaffected with the exception of HlyB-Q260* HlyD co-expressions, excluding HlyD as a factor for the reduced HlyA secretion (Figure S3).

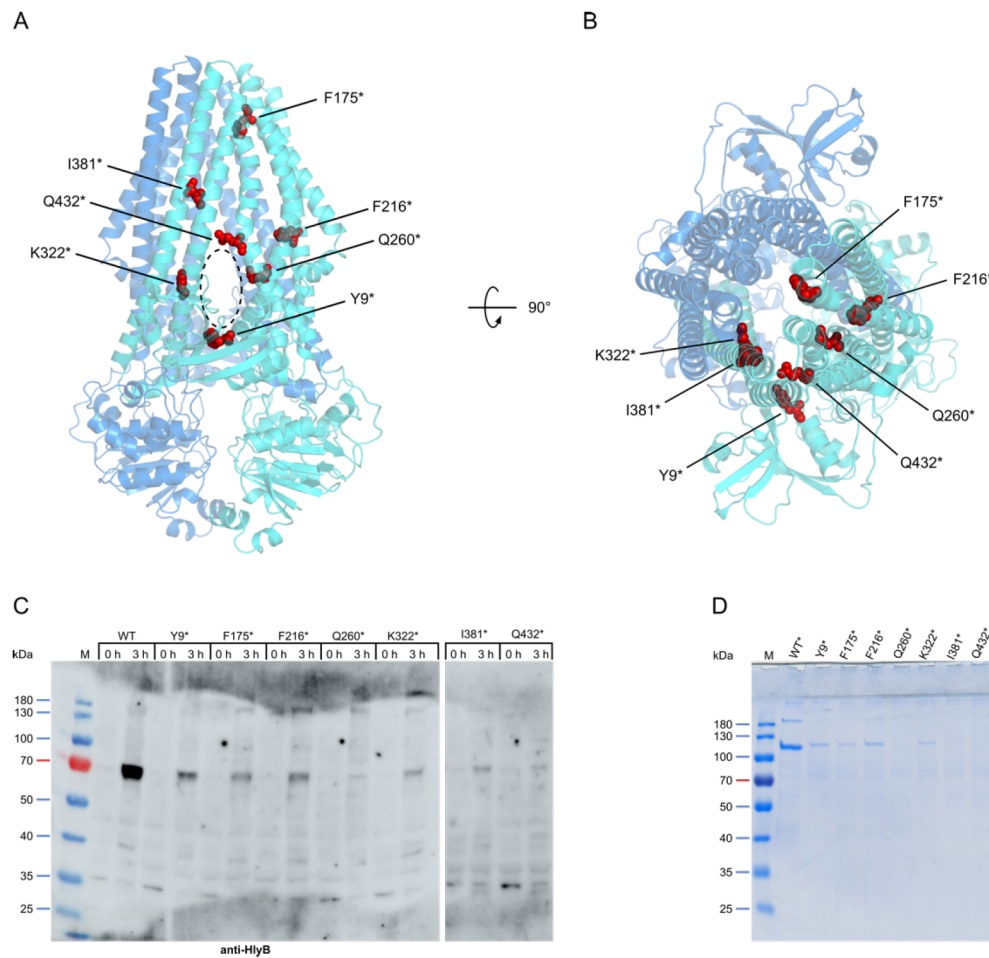


Figure 10: Expression and secretion of HlyB* amber mutants with incorporated Bpa. **(A)** Cartoon representation of a HlyB dimer homology model based on the structure of PCAT1 (Lin *et al.* 2015) created with PyMOL 2.3.4. The two protomers are colored in blue and cyan respectively. Residues substituted with Bpa are shown in only one protomer as red spheres. The possible opening for HlyA in the TMD is marked with a dashed circle. **(B)** Top-down view from the periplasm on the model shown in **(A)**. The incorporated Bpa would face to the inside of the translocation channel in case of the TMD and to the possible entry hole for HlyA in case of the CLD. **(C)** Immunoblot analysis of whole *E. coli* BL21(DE3) cells expressing HlyD and HlyB* with an amber mutation at the position indicated above (WT: no amber mutation). Samples were taken before (0 h) and 3 h after induction (3 h). The used antibody targeted HlyB. **(D)** SDS-PAGE analysis of supernatant samples from **(C)**. M: PageRuler Prestained Protein Ladder.

Despite the low incorporation efficiency of Bpa, photo-crosslinking of HlyB* to HlyA was initiated (Figure 11A): surprisingly, the incorporation of Bpa at position K322, which was previously crosslinked to HlyA using a lysine-specific crosslinker (Reimann *et al.* 2016), did not lead to the formation of crosslinks. In fact, signals with higher molecular weight upon UV irradiation could only be detected with HlyB-F175*, which formed a crosslinked product with a molecular weight of 180-250 kDa, therefore smaller than the crosslinked products observed in experiments using Bpa-incorporated

eGFP-HlyA. Mass spectrometric analysis of an excised HlyB-F175* crosslink band identified a limited amount of HlyB peptides and no crosslinked peptides.

Because of this unexpected result, a control experiment was performed to verify, if the crosslink product formed by HlyB-F175* was HlyA specific. We UV-irradiated cells, which expressed only Bpa-incorporated HlyB-F175* and HlyD, but no HlyA (Figure 11B). The main signal for crosslinked HlyB was still detectable upon UV treatment, meaning that HlyB-F175* predominantly did not form a covalent bond with HlyA, but with another protein in close proximity, most likely with another HlyB protomer or HlyD. Still, UV irradiation of HlyB-F175* in the presence of HlyA resulted in additional smear above the main signal which could originate from HlyB-HlyA crosslinks. Closer inspection revealed two higher molecular weight signals detectable with the HlyA antibody: the smaller signal (~190 kDa) coincided with the lower edge of the crosslink signal visible with the HlyB antibody, while the bigger signal matched with the higher molecular weight smear observed with the HlyB antibody (Figure 11C).

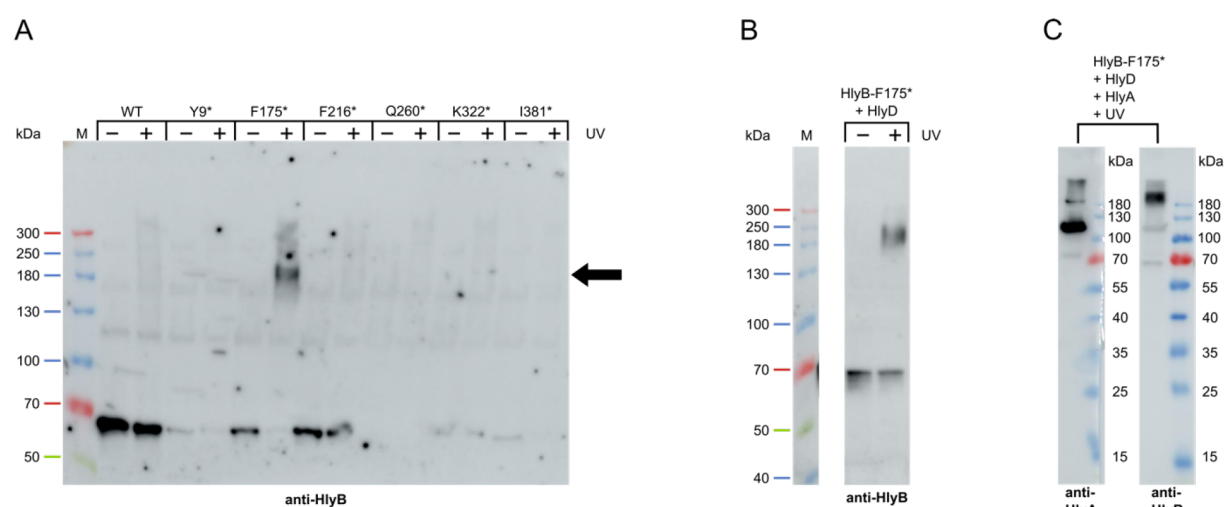


Figure 11: Photo-crosslinking of HlyB-F175*. **(A)** Immunoblot analysis of whole *E. coli* BL21(DE3) cells expressing HlyA, HlyD and HlyB* with an amber mutation at the position indicated above (WT: no amber mutation). Samples were taken 3 h after induction and either UV irradiated at 365 nm (+UV) or left untreated (-UV). The used antibody targeted HlyB. Crosslinked HlyB* is marked with an arrow. **(B)** Immunoblot analysis of whole *E. coli* BL21(DE3) cells expressing HlyB-F175* and HlyD without eGFP-HlyA supplemented with Bpa. Samples were taken 3 h after induction and either UV irradiated at 365 nm (+UV) or left untreated (-UV). The used antibody targeted HlyB. **(C)** Same as in **(B)**, but cells additionally expressed HlyA and were UV-irradiated after expression. The left membrane was incubated with an antibody targeting the secretion signal of HlyA, while the right membrane was incubated with an antibody targeting HlyB. M: Spectra Multicolor High Range Protein Ladder.

Enrichment necessary for detection of HlyB*-HlyA crosslinks

The recently published structure of the HlyB-HlyD complex shed some light on the identification of positions in the CLD and TMD of HlyB, which can crosslink to eGFP-HlyA1 (Zhao *et al.* 2022). None of the positions tested by us were among the crosslink positions detected by Zhao *et al.* Interestingly, the group could not detect higher molecular weight bands with Bpa incorporated at K322 either, but observed the formation of a crosslink when Bpa was introduced one position further at F323. We thus chose three positions within HlyB, which were shown to form crosslinks (E102*, F323* and A422*) and introduced an amber codon in HlyB. Additionally, we used the same tags and positions for enrichment of the crosslinked species as shown by Zhao *et al.* (Strep tag at the C-terminal NBD of HlyB as well as a 6xHis tag at the N-terminus of HlyD) (Zhao *et al.* 2022).

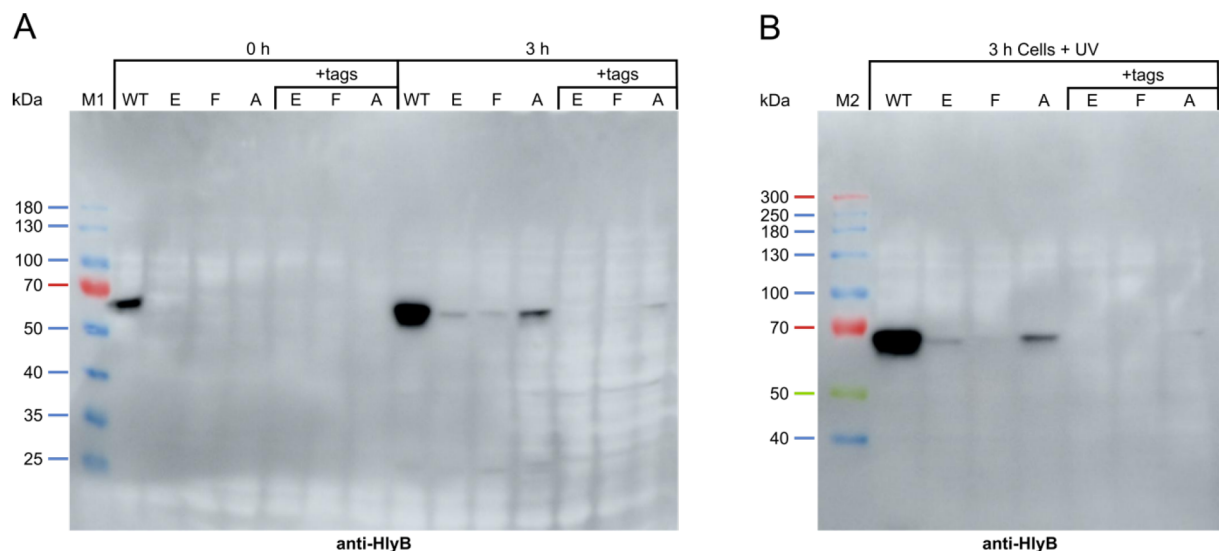


Figure 12: Expression and photo-crosslinking of published (Zhao *et al.* 2022) HlyB* amber mutants with incorporated Bpa. **(A)** Immunoblot analysis of whole *E. coli* BL21(DE3) cells expressing eGFP-HlyA, HlyD and HlyB* with an amber mutation at the position indicated above (WT: no amber mutation, E: E102*, F: F323*, A: A422*). Samples marked with "+tags" contained HlyB* with a C-terminal Strep tag and HlyD with an N-terminal 6xHis tag. Samples were taken before (0 h) and 3 h after induction (3 h). The used antibody targeted HlyB. **(B)** Samples shown in (A) were UV irradiated for 15 min at 365 nm. M1: PageRuler Prestained Protein Ladder, M2: Spectra Multicolor High Range Protein Ladder.

In comparison to unmodified wildtype HlyB, the expression of these new amber mutants was significantly reduced, with HlyB-A422* showing the most intense signal. (Figure 12A). Additionally, the introduction of the affinity tags to HlyB and HlyD further reduced the expression levels of the mutants with only a faint signal visible for HlyB-A422* while HlyB-E102* and HlyB-F323* could not be detected at all (Figure 12A).

Although all proteins necessary for formation of the secretion complex were present in the case of untagged HlyB and HlyD (Figure S4), no higher molecular weight bands could be detected upon UV irradiation (Figure 12B).

Next, the secretion efficiency of these new (untagged) amber mutants was checked. Although HlyB-E102* and HlyB-A422* (Figure S5) mutants could secrete HlyA, HlyB-F323* was not able to. We also tested the identification of crosslinked products using GFP in-gel fluorescence, but the sensitivity of this method was too low for detection of crosslinked protein from whole cells samples (data not shown). Thus, it was not possible to replicate the findings of Zhao *et al.* without the enrichment of HlyB*.

Fusion of affinity tags to HlyB affects its secretion capability

Cells expressing the affinity tagged HlyD and HlyB amber mutants showed a decreased secretion of HlyA, but it was not clear, if this effect was simply due to the lower expression level of HlyB, the incorporation of Bpa or the fusion of the affinity tags. We therefore compared the secretion efficiency of the Strep tagged HlyB and 6xHis tagged HlyD to the unmodified proteins by directly evaluating the supernatant and whole cells of secretion cultures, both adjusted to match the same optical density. Although the expression level of HlyA was identical, regardless of affinity tags, the detected amount of HlyA in the supernatant was greatly decreased for cultures of cells expressing the tagged secretion complex (Figure 13A and B). Simultaneously, the expression of HlyB-Strep and 6xHis-HlyD was also reduced when compared to the untagged variants (Figure 13C and D). However, the reduction in secreted HlyA was not proportional to the reduction of expressed HlyB and HlyD.

Thus, we expanded this evaluation of secretion efficiency by quantifying the amount of secreted HlyA as well as the amount of expressed HlyB and HlyD in cells carrying differently tagged variants of HlyB (Figure 14E). These variants included N-terminally 10xHis tagged HlyB (His-HlyB), N-terminally TwinStrep tagged HlyB (TS-HlyB) and two variants which featured two additional amino acids at their N-terminus, mimicking left-overs of affinity tagged HlyB, which was cut by a factor Xa protease (GR) or HRV 3C protease (GP) respectively. While all HlyB variants exhibited similar levels of intracellularly expressed HlyA (Figure 14B), the secretion levels of HlyA were different (Figure 14A). No secretion could be detected by His-HlyB, while the secretion by TS-

HlyB was reduced to $14\% \pm 1\%$ (Figure 14A and E). Surprisingly, the absence of HlyA in the supernatant in the case of His-HlyB was not due to missing or reduced expression of the transporter, as the expression of His-HlyB was even increased by a factor of 3.5 when compared to the untagged variant (Figure 14C and E). The expression level of TS-HlyB was reduced to $6\% \pm 1\%$ in comparison to HlyB-WT. The co-expression of HlyD mimicked the trend observed with His-HlyB and TS-HlyB respectively, as the amount of HlyD in the cells was slightly elevated in the case of His-HlyB and reduced in the case of TS-HlyB (Figure 14D and E). For HlyB variants GR and GP, secretion and expression levels for HlyA, HlyB and HlyD were comparable to the ones of HlyB-WT (Figure 14A-E). However, the amount of HlyA detected in the supernatant solely does not determine if the capability of HlyB to secrete is affected, as the differently tagged HlyB displayed different expression levels.

Normalization of the relative amount of secreted HlyA to the relative amount of expressed HlyB displayed that the construct HlyB-Strep + 6xHis-HlyD (also used by Zhao *et al.* for the structure determination of the secretion complex) has a severely reduced secretion efficiency (17% of the WT, Figure 14). Even though the expression level of TS-HlyB was even more reduced, the higher abundance of HlyA in the supernatant resulted in a secretion efficiency of $265\% \pm 52\%$ when compared to the wildtype protein without affinity tags. The presented data reveals HlyB to be highly sensitive to terminal fusion of affinity tags in terms of expression level and ability to secrete HlyA.

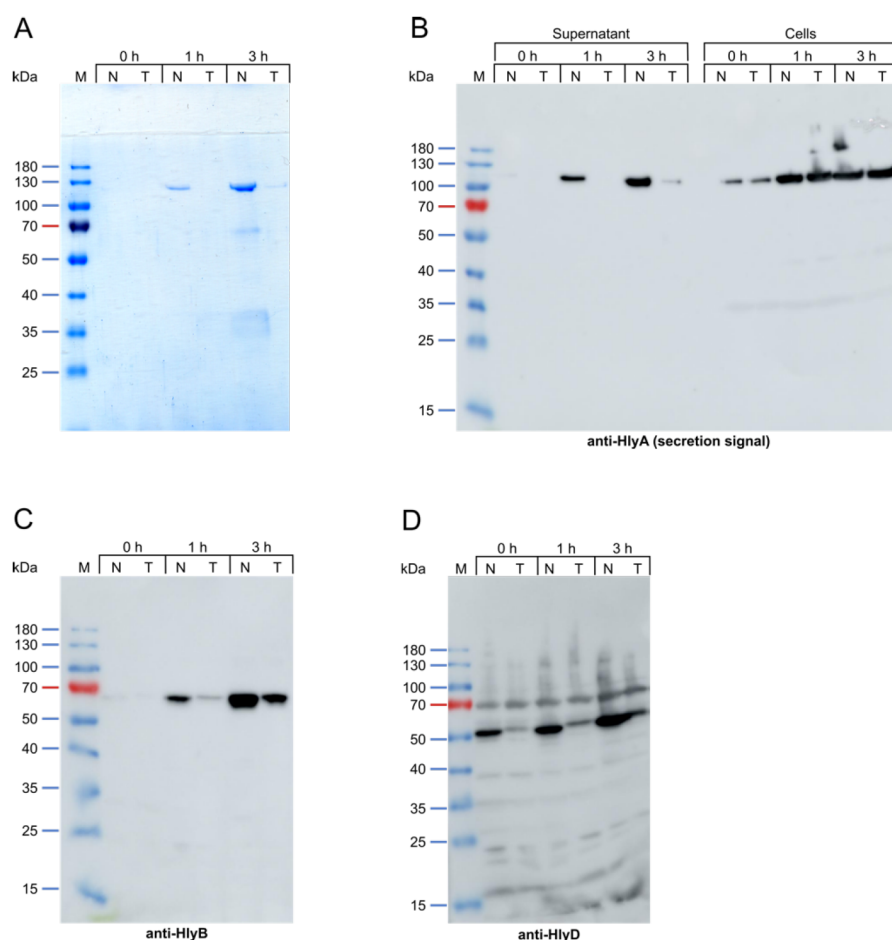


Figure 13: Effect of affinity tags on the secretion of HlyA by HlyB and HlyD. **(A)** Supernatant samples from *E. coli* BL21(DE3) cells expressing HlyA, HlyD and HlyB (N: no affinity tags fused to HlyB and HlyD, T: C-terminal Strep tag fused to HlyB and N-terminal 6xHis tag fused to HlyD) were taken before (0 h), 1 h and 3 h after induction and analyzed via SDS-PAGE **(A)** and immunoblot **(B)**. The cells used in **(A)** were analyzed via immunoblot for the presence of HlyA **(B)**, HlyB **(C)** and HlyD **(D)** with respective antibodies. The time after induction and fraction (supernatant or cells) are indicated above. M: PageRuler Prestained Protein Ladder.

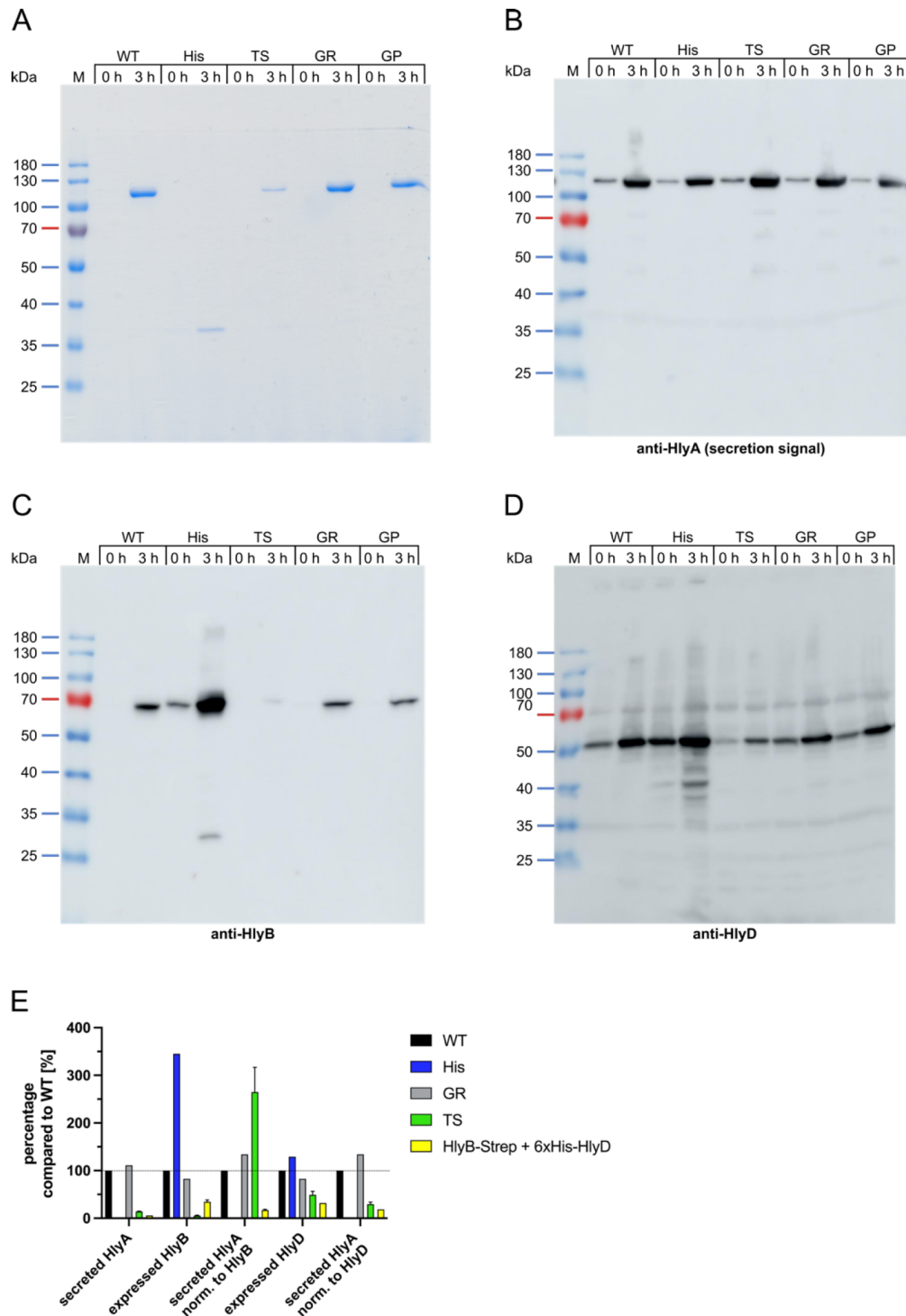


Figure 14: Quantification of HlyA secretion by HlyB and HlyD with different affinity tags. Analysis of supernatant and whole cell samples from cells expressing HlyA, HlyD and HlyB via SDS-PAGE (**A**) and immunoblots targeting HlyA (**B**), HlyB (**C**) and HlyD (**D**) with respective antibodies. The used affinity tags are indicated above (WT: no affinity tags fused to HlyB and HlyD, His: N-terminal 10xHis tag fused to HlyB, TS: N-terminal TwinStrep tag fused to HlyB, GR: dipeptide GR (mimics cleavage by factor Xa protease) fused to the N-terminus of HlyB, GP: dipeptide GP (mimics cleavage by HRV 3C protease) fused to the N-terminus of HlyB). Samples were taken before (0 h) and 3 h after induction. M: PageRuler Prestained Protein Ladder. (**E**) Expression levels of HlyB and HlyD with affinity tags and secretion level of HlyA (normalized to the amount of HlyB and HlyD) were compared to the expression and secretion level of HlyA, HlyB and HlyD without affinity tags (WT). The expression and secretion levels by C-terminally Strep tagged HlyB and N-terminally 6xHis tagged HlyD (yellow) were quantified from gels shown in Figure 13.

Discussion

The hemolysin system, as a type I secretion system, transports the eponymous substrate HlyA via its C-terminal secretion signal. At the time of this study, structural information about the associated ABC transporter HlyB was limited to the isolated C39 peptidase-like domain (CLD) and nucleotide-binding domain (NBD) (Schmitt *et al.* 2003, Lecher *et al.* 2012). For these two domains, interactions with the secretion signal of HlyA were demonstrated (Benabdelhak *et al.* 2003, Lecher *et al.* 2012). However, the structure of the transmembrane domain (TMD) of HlyB was unknown and no data on its interactions with HlyA were available. Considering that the classical ABC transporter features a substrate binding site within the TMD (Martin *et al.* 2001, Higgins and Linton 2004), we ambitiously aimed to map HlyB, especially the TMD, which forms the translocation tunnel, to determine possible contact sites with its substrate.

The incorporation of photolysine (AbK) into eGFP-HlyA was significantly less efficient when compared to Bpa and is likely an inherent attribute of the tRNA and/or aaRS (Young *et al.* 2010, Plass *et al.* 2011). We could show that the incorporation and photo-activation of the unnatural amino acid Bpa into (eGFP-)HlyA* was specific and efficient. Expression levels for Bpa-incorporated eGFP-HlyA were similar to wildtype eGFP-HlyA but reduced in the case of AbK. UAA containing HlyA was still secretable, as even HlyA with Bpa incorporated into the secretion signal could be found in the supernatant (data not shown).

Likewise, introduction of Bpa did not influence the stalling of the secretion system, as Bpa-incorporated eGFP-HlyA could be found in the membrane fraction (Lenders *et al.* 2015). This “freezing” of the secretion process should decrease the momentum of the otherwise highly dynamic secretion process (Lenders *et al.* 2016). The appearance of a HlyA dimer signal at ~270 kDa even without UV irradiation complicated the identification process, but could be eliminated with the addition of DTT to the SDS sample and/or heating of the sample to 95°C for 5 min.

Initial identification of crosslinked eGFP-HlyA using the HlyA-secretion signal specific antibody was not possible at first, as only the signal intensity of the non-crosslinked eGFP-HlyA decreased with increasing UV irradiation time. We ascribe this observation to either the destruction or the masking of the antibody epitope induced by irradiation with UV light, since aromatic amino acids are prone to photo-induced damaging and

crosslinking (Pattison and Davies 2006). This non-specific crosslinking - even in wildtype eGFP-HlyA without an amber stop codon mutation - would also explain the signals for higher molecular weight species in immunoblots using the full-length HlyA antibody. Even though the non-specific crosslinking of eGFP-HlyA made it difficult to identify Bpa-induced crosslink species of the secretion complex, we were able to show that the latter indeed occurred by quantifying the reduction in eGFP-HlyA signal intensity using the HlyA secretion signal specific antibody (see Figure 7). The HlyA full-length antibody proved to be not suitable for reliable detection of crosslinks, as multiple and smeary bands occurred after UV irradiation, also with the eGFP-HlyA-WT control. The mutational scanning and crosslinking of the N-terminus of HlyA later revealed Bpa-specific, photo-induced crosslinks with the secretion signal specific antibody (Figure 9). Ultimately, this shows the successful crosslinking of HlyA to the secretion channel and a way to map the translocation pathway of the hemolysin secretion system.

In theory, a crosslink between one copy of eGFP-HlyA (140.0 kDa) and one copy of HlyB (79.8 kDa) would result in a crosslinked product with a molecular weight of ~220 kDa, but the crosslinked species identified here were bigger (~300 kDa) and did not appear as focused protein bands but rather as a smear. Usually, only one Bpa-mediated covalent bond is expected to be formed between single copies of HlyB and eGFP-HlyA. However, two crosslinked proteins can appear different in size depending on the position of the crosslink as SDS-PAGE separates proteins based on hydrodynamic radius and not by mass. This migration behavior could be observed before with lipopolysaccharide (LPS) crosslinked to LptA, one of the proteins building up the LPS transport system (Okuda *et al.* 2012), and also with Bpa-incorporated HlyB crosslinked to eGFP-HlyA1 (Zhao *et al.* 2022). Also, with the structure of the HlyB-HlyD complex unveiled by (Zhao *et al.* 2022), some assumptions can be made: since the molecular weight of crosslinked species was higher than expected, additional proteins must be involved. Due to the fact that Bpa can form only one covalent bond to another protein, a second eGFP-HlyA is most likely crosslinked to the same HlyB molecule and would fit to the observed molecular weight of crosslinked products ($2 \times 140 \text{ kDa} + 80 \text{ kDa} = 360 \text{ kDa}$). The presence of two HlyA copies inside of the transporter is unlikely, because the narrowest part of the channel formed by HlyB is approx. 10 Å, just enough space to accommodate one α -helix. However, each HlyB carries an N-terminal CLD and a C-terminal NBD, both of which have shown to interact with HlyA (Benabdelhak *et al.* 2003, Lecher *et al.* 2012, Pourhassan *et al.* 2022). In

the structure of the inner membrane complex of (Zhao *et al.* 2022), one CLD of one HlyB protomer is interacting with HlyD from a neighboring HlyB-HlyD protomer, while the structure of the other CLD was not resolved, most likely due to high flexibility. Since the HlyB-HlyD complex structure was solved without the presence of HlyA, it is unknown, how many copies of HlyA are present at HlyB during secretion. Our crosslinking data and the observed apparent mass of crosslinked proteins suggests a sequential secretion of HlyA, similar to PCAT1 (Kieuvongngam *et al.* 2020): while one copy of eGFP-HlyA is residing in the channel formed by a dimer of HlyB, the next eGFP-HlyA is already present at the transporter, waiting to be secreted. We were not able to identify the crosslinked amino acid in HlyB, therefore we cannot narrow down, at which domain the second copy of eGFP-HlyA might be located. Immunoblots with an antibody targeting HlyB were often not sensitive enough to reliably identify HlyB of crosslinked species in whole cells, especially after irradiation with UV light. This observation could be due to the crosslinking of HlyA to the NBD, which would thereby decrease the accessibility of the epitope for the HlyB antibody. In cases when crosslinked complexes containing HlyB were detectable, molecular masses were coinciding with crosslink bands observed with the antibody targeting full-length HlyA (Figure 6E).

The occurrence of crosslinked products irrespective of the position of the introduced Bpa was unexpected. In the properly stalled complex, HlyA should start the folding process once the C-terminal part of HlyA reaches the extracellular space due to the presence of Ca^{2+} ions, impeding the sliding back of the toxin. As discussed above, crosslinking of additional eGFP-HlyA to the CLD or NBD could be possible (Benabdelhak *et al.* 2003, Lecher *et al.* 2012, Pourhassan *et al.* 2022). The positions of Bpa in crosslinked products identified with the secretion signal specific HlyA antibody during the mutational scanning of the N-terminus of HlyA (28*, 41 and 93*) could be inside of the HlyB-TMD or at the CLD/NBD when stalling the secretion complex. The TMD of HlyB has a length of ~ 70 Å (Zhao *et al.* 2022). Assuming that HlyA is an unfolded peptide chain in the TMD and that one amino acid has a length of ~ 3.6 Å (Dietz and Rief 2006), approx. 20 amino acids are located in the TMD at the same time. The number of residues within crosslink proximity increases when taking the dimensions of the NBD (length of 50 Å along the y-axis) and the CLD into account. It is therefore conceivable, that a larger number of amino acids of HlyA can crosslink to HlyB.

Investigation of the observed crosslink signals >280 kDa for eGFP-HlyA via mass spectrometry revealed the presence of peptides for eGFP-HlyA as well as HlyB and also HlyD in low quantity. Since these proteins would not migrate at >280 kDa in their monomeric form, this indicates the formation of a crosslinked species with these proteins.

Identification of the crosslinked peptides required the enrichment of the crosslinked complexes. Different purification and immunoprecipitation techniques were applied for this. Both termini seemed to be inaccessible: enrichment via the N-terminal eGFP and His tag were not expedient. Similarly, insertion of a 10xHis tag in between HlyA and its secretion signal did not show binding to Ni-NTA resin either (data not shown). The binding of GFP nanobodies to soluble eGFP-HlyA was not compromised, and the UV irradiation as a cause could be excluded as well. However, in contrast to a simple PCAT architecture (Kieuvongngam *et al.* 2020), Zhao *et al.* showed that the IMC of the hemolysin system forms a much larger complex, which might explain the binding deficiency (Zhao *et al.* 2022). The inaccessibility of antibody epitopes upon complex formation is not unusual (Johanson and McHenry 1982, Moyle *et al.* 1982). The use of two antibodies during immunoprecipitation could provide a workaround for the absent binding. Additionally, a new construct of eGFP-HlyA was generated in this study in which an affinity tag was introduced upstream of the first RTX domain. This position seemed to be exposed, as first purifications indicated the successful isolation of the complete secretion complex (data not shown).

Bpa is a commonly used UAA, also for membrane proteins (Welte *et al.* 2012, Sherman *et al.* 2018, Zhao *et al.* 2022). However, incorporation of Bpa into the ABC transporter HlyB resulted in a significantly decreased expression level. This effect could be inherent for some membrane proteins as the insertion of an amber codon into the genetic code of membrane proteins might interfere with the biogenesis. One alternative would be the expression of the HlyB amber mutants at reduced temperatures. A thereby decreased expression speed could be beneficial, as performed by Zhao *et al.* (Zhao *et al.* 2022).

Most of the HlyB amber mutants initially tested (Y9*, F216*, Q260*, K322* and I381*), exhibited an insufficient expression level and/or no formation of crosslink bands. Only HlyB-F175* showed the formation of crosslinked products. Crosslinks with a molecular weight higher than 200 kDa were detectable in the presence of HlyA with an anti-HlyB

antibody and coincided with signals visible in anti-HlyA immunoblots, proving the formation of HlyB-HlyA crosslinks. Still, the main crosslink visible at ~200 kDa occurred also in the absence of HlyA, indicating HlyB to form crosslinks with another protein. Immunoblots with an anti-HlyD antibody revealed no bands of corresponding size (data not shown), which suggested an intermolecular crosslink between two HlyB monomers. Shortly after investigating HlyB-F175*, the group of Jue Chen published the structure of the HlyB-HlyD complex with an unexpected architecture of three HlyB dimers (Zhao *et al.* 2022). There, the residue F175, even though on the upper end of the TMD, is buried too deep within the translocation channel in order to generate covalent bonds with residues of HlyD. We checked the position and orientation of F175 within the structure reported by Zhao *et al.* and indeed found several residues in a neighboring HlyB within crosslinking proximity: the HlyB dimers adopt two different conformations in the complex. Thus, depending on which of the three HlyB dimers are examined, different residues are in proximity to Bpa for crosslinking when substituted for F175 (Figure 15). The residues M389 and L393 in the TMH5 of the opposing HlyB protomer can be found in a radius of 4 Å of F175, presenting the closest residues for crosslink formation. When the threshold of the radius is increased to 5-6 Å, I390 in TMH5 and N414 in TMH6 come into consideration for crosslink partners as well. The observed crosslink bands with HlyB-F175* are therefore likely originating from two crosslinked HlyB.

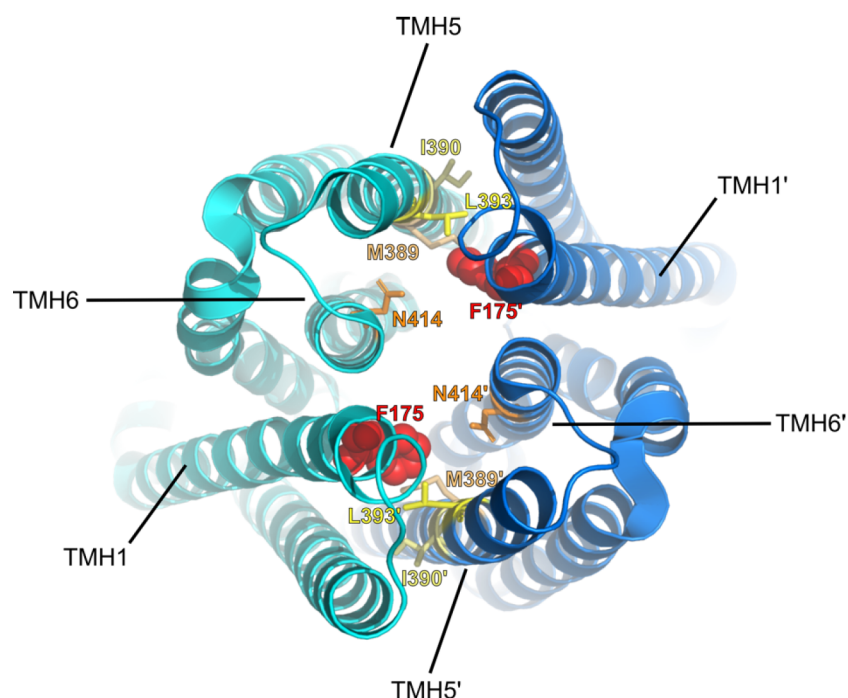


Figure 15: Possible intermolecular photo-crosslinks of HlyB-F175*. Top-down view from the periplasm on the TMDs of one HlyB dimer in cartoon representation (PDB: 7SGR) (Zhao *et al.* 2022). The transmembrane helices (TMH) of the two protomers are colored in cyan and blue and distinguished by an apostrophe ('). The residue F175 is highlighted as red spheres. Residues posing as possible crosslink partners are shown as sticks and are colored in shades ranging from yellow to orange.

HlyB already displayed a sensitivity for alterations to its genetic code, as introduction of amber stop codons greatly reduced the expression level. Upon addition of affinity tags to the termini of HlyB, not only the expression level was affected, but it also had a detrimental effect on the ability of the secretion complex to secrete HlyA. For instance, addition of a Strep tag to the C-terminus of HlyB (as used in (Zhao *et al.* 2022)) resulted in a severely decreased secretion of HlyA. Additionally, fusion of a 10xHis tag to the N-terminus of HlyB increased the expression level. Even though expression of His tagged HlyB was improved, it simultaneously rendered the transporter unable to secrete HlyA. Conversely, fusion of a TwinStrep tag to the N-terminus of HlyB greatly decreased the expression level of HlyB, but not the ability of the transporter to secrete its substrate. Depending on the protein's properties, affinity tagging of termini can affect the expression level, solubility, folding and/or activity, as observed for MRP1 from *Saccharomyces cerevisiae*, MSP1₄₂ from *Plasmodium falciparum*, hydantoinase from *Agrobacterium radiobacter* or human interferon-gamma (Huang *et al.* 2003, Lee and Altenberg 2003, Khan *et al.* 2012, Krachmarova *et al.* 2017). In case of HlyB, tagging of either terminus could affect structure and function of

the secretion complex, as the N-terminal CLD as well as the C-terminal NBD are involved in substrate recognition, stabilization of the complex and energization, all of which are critical for the secretion process (Benabdelhak *et al.* 2003, Lecher *et al.* 2012, Zhao *et al.* 2022). Therefore, to ensure isolation of the complete and fully functional secretion system, affinity tagging of HlyB is not advised. The tagging of HlyD termini could be disadvantageous as well, as the N-terminus was shown to interact with the substrate, while the C-terminus is placed between two HlyB protomers (Balakrishnan *et al.* 2001, Zhao *et al.* 2022). Instead, isolation of the complex via an affinity tag placed in HlyA (mentioned above) poses the least functional interferences.

The group of Zhao *et al.* showed the presence of “secreted” HlyA in the supernatant with the affinity-tagged complex. However, instead of assessing the presence of HlyA directly from the crude supernatant via SDS-PAGE, as in the present study here, the detected HlyA was purified from the medium via an affinity tag and detected using immunoblotting (Zhao *et al.* 2022). This makes it difficult to derive any conclusions on the secretion efficiency of the affinity tagged complex in comparison to the untagged complex. On the one hand, information on the (relative) secretion rate of HlyA is lost, on the other hand, the purified HlyA might not have been secreted, but originate from lysed cells instead.

In summary, we could show the successful incorporation of Bpa into different variants of HlyA and to some extent also HlyB. Subsequent irradiation with UV light resulted in the formation of Bpa-specific crosslinks between HlyA and HlyB. The mass of crosslinked species suggests a sequential secretion with the presence of more than one copy of HlyA at the transporter. In the stalled secretion complex, both termini of HlyA were inaccessible for conventional purification and immunoprecipitation approaches such as Ni-NTA affinity or GFP nanobody co-IP. Enrichment of the complex via affinity tagged HlyB variants is not advised, as HlyB exhibited a high sensitivity towards alterations of the termini, resulting in severe effects on the expression level of the transporter and the ability of the complex to secrete HlyA. An internal affinity tag in HlyA presents a promising candidate for pull-down of the crosslinked complex and for complete mapping of the translocation pathway, especially with the HlyA amber mutants identified here during the N-terminal mutational scanning. The complete secretion complex purified this way could also be used for structural determination e.g. via small angle X-ray scattering or cryogenic electron

microscopy. The crosslinking process could be beneficial by stabilizing the complex for these analyses.

Funding

This work was supported by the Deutsche Forschungsgemeinschaft (DFG, CRC 1208 project A01 to LS).

Acknowledgements

We thank all members of the Institute of Biochemistry for productive discussions. We are indebted to Prof. Dr. Samuel Wagner for his helpful input (Interfaculty Institute of Microbiology and Infection Medicine (IMIT), Eberhard Karls University, Tübingen). Equal thanks go to Prof. Dr. Edward Lemke for sharing of plasmids for the incorporation of photolysine (Institute of Molecular Biology, Johannes Gutenberg University, Mainz). We are thankful to Prof Dr. Irene Coin and Thore Böttke (Synthetic Protein Biochemistry, University Leipzig) for their suggestions regarding scanning mutagenesis. We also thank Dr. Nina Prescher (Institute of Molecular Medicine I, Proteome Research, University Hospital Düsseldorf, Heinrich Heine University, Düsseldorf) for help with mass spectrometry and Martina Wesemann (Institute of Biochemistry, Heinrich Heine University, Düsseldorf) for technical support. Additionally, we thank Dr. Tobias Beer for providing purified eGFP-HlyA.

Material and Methods

Bacterial strains and cloning of plasmids

During cloning procedures, *Escherichia coli* DH5 α and *E. coli* XL1-blue cells were used. *E. coli* BL21(DE3) cells were used for overexpression, crosslinking, and secretion experiments. A list of all plasmids and oligonucleotides used in this study can be found in Table 1 and Table 2 respectively. Oligonucleotides were either ordered from Eurofins Genomics or Sigma-Aldrich.

The plasmid pSUP-Bpa (Ryu and Schultz 2006) encodes six copies of an orthogonal suppressor tRNA and one copy of an aminoacyl-tRNA synthetase from *Methanocaldococcus jannaschii* for the incorporation of the UAA p-benzoyl-L-phenylalanine (Bpa) into amber stop codons (TAG).

The plasmid pEVOL-Bpa-ColA is based on pEVOL-Bpa (Chin *et al.* 2002) and encodes for one copy of the suppressor tRNA as well as two copies of the aminoacyl-tRNA synthetase from *Methanocaldococcus jannaschii* mentioned above. For plasmid compatibility, the original p15a origin of replication (ori) was exchanged to a ColA ori from pCOLADuet-1, which was cut out using the restriction sites XbaI and NheI and inserted into pEVOL-Bpa, which was cut with the same enzymes.

The incorporation of H-L-Photolysine (AbK) (Iris Biotech GmbH) was executed using the vector pEVOL-AbK-ColA, which is based on the plasmid pEvol tRNA^{pyl}/pyIRS^{AF} (Plass *et al.* 2011) and encodes for one orthogonal suppressor tRNA and two copies of an aminoacyl-tRNA synthetase from *Methanosarcina mazei*. The p15a ori was exchanged because of plasmid compatibility. The ColA-ori was amplified from pEVOL-Bpa-ColA using the primers ColA-fw and -rev, while pEvol tRNA^{pyl}/pyIRS^{AF} was amplified without its p15a ori, but with overhangs to the ColA ori sequence for Gibson assembly (Gibson 2011) using the primers pEVOL-ColA-Ins-fw and -rev.

Functionality of the crosslink setup was assessed using pSUP-Bpa in conjunction with the plasmid pSB3408. It is based on pGEX-KG-GST-SicP-SptP (Akeda and Galán 2005) and encodes for the effector protein SptP and its dedicated chaperone SicP, which is N-terminally tagged with a glutathione S-transferase (GST), from *Salmonella enterica*. SicP has an amber stop codon substitution at position F36.

Amber stop codon substitutions were introduced via PCR. Site-directed mutagenesis and design of primers was performed individually for every position, either according to the QuikChange II Site-Directed Mutagenesis Kit (Agilent) or Q5 Site-Directed Mutagenesis Kit (New England Biolabs) according to the manufacturer's protocol. For amplification either Q5 High-Fidelity DNA Polymerase, Phusion High-Fidelity DNA Polymerase (New England Biolabs) or PfuUltra II Fusion High-Fidelity DNA Polymerase (Agilent) was used. Success of the amplification was assessed via agarose gel electrophoresis using a 1% agarose gel. If necessary, DNA product was purified or isolated using either the Monarch PCR & DNA Cleanup Kit or the Monarch DNA Gel Extraction Kit (New England Biolabs). Template DNA was DpnI digested, or in case of the Q5 Site-Directed Mutagenesis approach, the PCR product was incubated with KLD enzyme mix (New England Biolabs). Subsequently, *E. coli* DH5 α or *E. coli* XL1-blue were transformed via heat-shock, plated out on 2xYT agar plates supplemented with the respective antibiotic and incubated overnight at 37°C. Single clones were transferred into 5 ml 2xYT medium supplemented with the respective antibiotic and again incubated overnight at 37°C and 180 rpm for plasmid DNA isolation on the next day using the NucleoSpin Plasmid Miniprep Kit (Macherey Nagel). Successful DNA manipulation was verified via Sanger sequencing (Microsynth Seqlab).

The amber stop codon substitution during the scanning mutagenesis of the N-terminal 194 amino acids of HlyA in eGFP-HlyA (pSOI-eGFP-HlyA-1* to -194*) was performed as described in (Sun *et al.* 2013). The AAScan tool was used in batch mode and the amber stop codon TAG set as the desired mutation. The minimum length of the primers was set to 18 bp, while the maximum length was set to 60 bp and the MinGCclamp was set to 2 with the OptimisedGCclamp option enabled. The limits for the primer melting temperatures were set to 60°C and 70°C respectively with a maximal temperature difference of 5°C between the forward and reverse primer. The minimal distance of the primers 3' end to the mutation was set to 15 bp. The length of the PCR fragments overlaps was set to be between 13 and 15 bp.

The insertion of a TwinStrep tag with varying protease cleavage sites at the N-terminus of HlyB was performed via Gibson assembly. The pK184-HlyBD plasmid was amplified using the primers stated in Table 2 and Gibson assembly was performed with the Gibson Assembly Master Mix (New England Biolabs) and according to the

manufacturer's protocol. Single clones were transferred to 5 ml 2xYT medium supplemented with kanamycin, incubated at 37°C overnight and used for plasmid isolation with subsequent sequencing.

The amino acids GR and GP in the case of pK184-GR-HlyBD and pK184-GP-HlyBD respectively were inserted by amplifying pK184-HlyBD with the primers listed in Table 2. In the case of pK184-HlyB-GStrep-6HisG-HlyD, the Strep tag at the C-terminus of HlyB was inserted by using primers HlyB-GStrep-Ins-fw and -rev, followed by insertion of the 6xHis tag at the N-terminus of HlyD using primers HlyD-6HisG-Ins-fw and -rev. Plasmids were isolated and successful modification confirmed by sequencing.

Table 1: Plasmids used in this study with detailed information for encoded genes, plasmid backbone, resistance genes, ori and promoter.

Plasmid name	Backbone	Details	Resistance	Ori	Promoter	Source
pSB3408	pGEX	Encodes for the effector SptP and its chaperone SicP from <i>S. enterica</i> with an amber mutation at F36 and an N-terminal GST tag	Amp	tac	ColE1	Gift of Samuel Wagner (Akeda and Galán 2005)
pCOLADuet-1	pET	Empty vector	Kan	T7	ColA	Novagen (Sigma-Aldrich)
pSUP-Bpa	pSUP	Encodes for six copies of the orthogonal tRNA _{Bpa} and one copy of the respective aaRS _{Bpa} for incorporation of the UAA Bpa in amber stop codons	Cm	glnS', proK	p15a	Gift of Samuel Wagner (Ryu and Schultz 2006)
pEVOL-Bpa	pEVOL	Encodes for one copy of the orthogonal tRNA _{Bpa} and two copies of the respective aaRS _{Bpa} for incorporation of the UAA Bpa in amber stop codons	Cm	araBAD	p15a	Gift of Peter Schultz (Chin <i>et al.</i> 2002)

Continuation Table 1: Plasmids used in this study with detailed information for encoded genes, plasmid backbone, resistance genes, ori and promoter.

Plasmid name	Backbone	Details	Resistance	Ori	Promoter	Source
pEVOL-Bpa-ColA	pEVOL	Encodes for one copy of the orthogonal tRNA _{Bpa} and two copies of the respective aaRS _{Bpa} for incorporation of the UAA Bpa in amber stop codons with ColA ori	Cm	araBAD	ColA	This study
pEvol tRNA ^{pyl} /pyIRS ^{AF}	pEVOL	Encodes for one copy of the orthogonal tRNA _{AbK} and two copies of the respective aaRS _{AbK} for incorporation of the UAA AbK in amber stop codons	Cm	araBAD	p15a	Gift of Edward Lemke (Plass <i>et al.</i> 2011)
pEVOL-AbK-ColA	pEVOL	Encodes for one copy of the orthogonal tRNA _{AbK} and two copies of the respective aaRS _{AbK} for incorporation of the UAA AbK in amber stop codons	Cm	araBAD	ColA	This study

Continuation Table 1: Plasmids used in this study with detailed information for encoded genes, plasmid backbone, resistance genes, ori and promoter.

Plasmid name	Backbone	Details	Resistance	Ori	Promoter	Source
pK184-HlyBD	pK184	Encodes for HlyD and HlyB	Kan	lac	p15a	(Bakkes <i>et al.</i> 2010)
pK184-HlyBD-Y9*	pK184	Encodes for HlyD and HlyB (amber mutation at Y9)	Kan	lac	p15a	This study
pK184-HlyBD-E102*	pK184	Encodes for HlyD and HlyB (amber mutation at E102)	Kan	lac	p15a	This study
pK184-HlyBD-F175*	pK184	Encodes for HlyD and HlyB (amber mutation at F175)	Kan	lac	p15a	This study
pK184-HlyBD-F216*	pK184	Encodes for HlyD and HlyB (amber mutation at F216)	Kan	lac	p15a	This study
pK184-HlyBD-Q260*	pK184	Encodes for HlyD and HlyB (amber mutation at Q260)	Kan	lac	p15a	This study
pK184-HlyBD-K322*	pK184	Encodes for HlyD and HlyB (amber mutation at K322)	Kan	lac	p15a	This study
pK184-HlyBD-F323*	pK184	Encodes for HlyD and HlyB (amber mutation at F323)	Kan	lac	p15a	This study

*: indicates position with an amber stop codon mutation

Continuation Table 1: Plasmids used in this study with detailed information for encoded genes, plasmid backbone, resistance genes, ori and promoter.

Plasmid name	Backbone	Details	Resistance	Ori	Promoter	Source
pK184-HlyBD-I381*	pK184	Encodes for HlyD and HlyB (amber mutation at I381)	Kan	lac	p15a	This study
pK184-HlyBD-A422*	pK184	Encodes for HlyD and HlyB (amber mutation at A422)	Kan	lac	p15a	This study
pK184-HlyBD-Q432*	pK184	Encodes for HlyD and HlyB (amber mutation at Q432)	Kan	lac	p15a	This study
pK184-HlyBD-E102*-tags	pK184	Encodes for HlyD (N-terminal 6xHis tag) and HlyB (amber mutation at E102 and C-terminal Strep tag)	Kan	lac	p15a	This study
pK184-HlyBD-F323*-tags	pK184	Encodes for HlyD (N-terminal 6xHis tag) and HlyB (amber mutation at F323 and C-terminal Strep tag)	Kan	lac	p15a	This study
pK184-HlyBD-A422*-tags	pK184	Encodes for HlyD (N-terminal 6xHis tag) and HlyB (amber mutation at A422 and C-terminal Strep tag)	Kan	lac	p15a	This study

*: indicates position with an amber stop codon mutation

Continuation Table 1: Plasmids used in this study with detailed information for encoded genes, plasmid backbone, resistance genes, ori and promoter.

Plasmid name	Backbone	Details	Resistance	Ori	Promoter	Source
pK184-10His-FXa-HlyBD	pK184	Encodes for HlyD and HlyB (N-terminal 10xHis tag with FXa cleavage site)	Kan	lac	p15a	(Jenewein 2008)
pK184-TS-FXa-HlyBD	pK184	Encodes for HlyD and HlyB (N-terminal TwinStrep tag with FXa protease cleavage site)	Kan	lac	p15a	This study
pK184-TS-TEV-HlyBD	pK184	Encodes for HlyD and HlyB (N-terminal TwinStrep tag with TEV protease cleavage site)	Kan	lac	p15a	This study
pK184-TS-3C-HlyBD	pK184	Encodes for HlyD and HlyB (N-terminal TwinStrep tag with 3C protease cleavage site)	Kan	lac	p15a	This study
pK184-GR-HlyBD	pK184	Encodes for HlyD and GR-HlyB (mimics TEV protease cleavage of an N-terminal affinity tag)	Kan	lac	p15a	This study
pK184-GP-HlyBD	pK184	Encodes for HlyD and GP-HlyB (mimics 3C protease cleavage of an N-terminal affinity tag)	Kan	lac	p15a	This study

*: indicates position with an amber stop codon mutation

Continuation Table 1: Plasmids used in this study with detailed information for encoded genes, plasmid backbone, resistance genes, ori and promoter.

Plasmid name	Backbone	Details	Resistance	Ori	Promoter	Source
pK184-HlyB-GStrep-6HisG-HlyD	pK184	Encodes for HlyD with an N-terminal 6xHis tag and HlyB with a C-terminal Strep tag	Kan	lac	p15a	This study
pSU2726-HlyA	pUC19	Encodes for HlyA	Amp	lac	ColE1	(Thomas <i>et al.</i> 2014)
pSU2726-HlyA-L13*	pUC19	Encodes for HlyA (amber mutation at L13*)	Amp	lac	ColE1	This study
pSU2726-HlyA-F110*	pUC19	Encodes for HlyA (amber mutation at F110*)	Amp	lac	ColE1	This study
pSU2726-HlyA-L209*	pUC19	Encodes for HlyA (amber mutation at L209*)	Amp	lac	ColE1	This study
pSU2726-HlyA-G308*	pUC19	Encodes for HlyA (amber mutation at G308*)	Amp	lac	ColE1	This study
pSU2726-HlyA-M417*	pUC19	Encodes for HlyA (amber mutation at M417*)	Amp	lac	ColE1	This study
pSU2726-HlyA-P517*	pUC19	Encodes for HlyA (amber mutation at P517*)	Amp	lac	ColE1	This study
pSU2726-HlyA-I610*	pUC19	Encodes for HlyA (amber mutation at I610*)	Amp	lac	ColE1	This study
pSU2726-HlyA-K708*	pUC19	Encodes for HlyA (amber mutation at K708*)	Amp	lac	ColE1	This study

*: indicates position with an amber stop codon mutation

Continuation Table 1: Plasmids used in this study with detailed information for encoded genes, plasmid backbone, resistance genes, ori and promoter.

Plasmid name	Backbone	Details	Resistance	Ori	Promoter	Source
pSU2726-HlyA-L810*	pUC19	Encodes for HlyA (amber mutation at L810*)	Amp	lac	ColE1	This study
pSU2726-HlyA-W914*	pUC19	Encodes for HlyA (amber mutation at W914*)	Amp	lac	ColE1	This study
pSOI-eGFP-HlyA	pBAD	Encodes for eGFP-HlyA with an N-terminal 6xHis tag	Amp	araBAD	ColE1	(Lenders <i>et al.</i> 2015)
pSOI-eGFP-HlyA-L13*	pBAD	Encodes for eGFP-HlyA (amber mutation at L13) with an N-terminal 6xHis tag	Amp	araBAD	ColE1	This study
pSOI-eGFP-HlyA-F110*	pBAD	Encodes for eGFP-HlyA (amber mutation at F110) with an N-terminal 6xHis tag	Amp	araBAD	ColE1	This study
pSOI-eGFP-HlyA-L209*	pBAD	Encodes for eGFP-HlyA (amber mutation at L209) with an N-terminal 6xHis tag	Amp	araBAD	ColE1	This study
pSOI-eGFP-HlyA-G308*	pBAD	Encodes for eGFP-HlyA (amber mutation at G308) with an N-terminal 6xHis tag	Amp	araBAD	ColE1	This study
pSOI-eGFP-HlyA-M417*	pBAD	Encodes for eGFP-HlyA (amber mutation at M417) with an N-terminal 6xHis tag	Amp	araBAD	ColE1	This study

*: indicates position with an amber stop codon mutation

Continuation Table 1: Plasmids used in this study with detailed information for encoded genes, plasmid backbone, resistance genes, ori and promoter.

Plasmid name	Backbone	Details	Resistance	Ori	Promoter	Source
pSOI-eGFP-HlyA-P517*	pBAD	Encodes for eGFP-HlyA (amber mutation at P517) with an N-terminal 6xHis tag	Amp	araBAD	ColE1	This study
pSOI-eGFP-HlyA-I610*	pBAD	Encodes for eGFP-HlyA (amber mutation at I610) with an N-terminal 6xHis tag	Amp	araBAD	ColE1	This study
pSOI-eGFP-HlyA-K708*	pBAD	Encodes for eGFP-HlyA (amber mutation at K708) with an N-terminal 6xHis tag	Amp	araBAD	ColE1	This study
pSOI-eGFP-HlyA-L810*	pBAD	Encodes for eGFP-HlyA (amber mutation at L810) with an N-terminal 6xHis tag	Amp	araBAD	ColE1	This study
pSOI-eGFP-HlyA-W914*	pBAD	Encodes for eGFP-HlyA (amber mutation at W914) with an N-terminal 6xHis tag	Amp	araBAD	ColE1	This study
pSOI-eGFP-HlyA-1* to -194*	pBAD	194 plasmids encoding for eGFP-HlyA with an N-terminal 6xHis tag; each plasmid carries one amber stop codon, ranging from aa position 1 to 194	Amp	araBAD	ColE1	This study

*: indicates position with an amber stop codon mutation

Table 2: Oligonucleotides used in this study. Overhangs for Gibson assembly are underlined. Sequences introduced and amino acids substituted through the primers are indicated in lower case. Resulting amber stop codons are shown in red. Primers for substitution via the QuikChange Site-Directed Mutagenesis strategy are termed “Amber”, while primers for substitution via the Q5 Site-Directed Mutagenesis strategy are termed “Q5”.

Name	Details	Sequence (5'→3')	Plasmids
Amber-HlyA-L13-fw Amber-HlyA-L13-rev	Substitution of amino acid L13 in HlyA with an amber stop codon for incorporation of unnatural amino acids	CAAATTAAAAGCACAtaG CAGTCTGCAAAGCAATC GATTGCTTTGCAGACTG CtaTGTGCTTTTAATTTG	pSOI-eGFP-HlyA-L13*
Amber-HlyA-F110-fw Amber-HlyA-F110-rev	Substitution of amino acid F110 in HlyA with an amber stop codon for incorporation of unnatural amino acids	GGGGAGTGACTATCTagGCACCACAATTAGAC GTCTAATTGTGGTGCctAGATAGTCACTCCCC	pSOI-eGFP-HlyA-F110*
Amber-HlyA-L209-fw Amber-HlyA-L209-rev	Substitution of amino acid L209 in HlyA with an amber stop codon for incorporation of unnatural amino acids	GTAACTCATTTTCTCAACAAtagAATACTCTGGGAAGTGATTA TAATACACTTCCCAGAGTATTctaTTGTTGAGAAAATGAGTTAAC	pSOI-eGFP-HlyA-L209*
Amber-HlyA-G308-fw Amber-HlyA-G308-rev	Substitution of amino acid G308 in HlyA with an amber stop codon for incorporation of unnatural amino acids	CTGCTGCTGCTGCctagTTAATTGCTTCTGC GCAGAAGCAATTAActaGGCAGCAGCAGCAG	pSOI-eGFP-HlyA-G308*
Amber-HlyA-M417-fw Amber-HlyA-M417-rev	Substitution of amino acid M417 in HlyA with an amber stop codon for incorporation of unnatural amino acids	CTTCAAAGCAGGCAtaGTTTGAACATGTTGC GCAACATGTTCAAA CtaTGCCTGCTTTGAAG	pSOI-eGFP-HlyA-M417*
Amber-HlyA-P517-fw Amber-HlyA-P517-rev	Substitution of amino acid P517 in HlyA with an amber stop codon for incorporation of unnatural amino acids	CGTCTGGAGAAAAAAtaGGATGAATTCCAGAAG CTTCTGGAATTCATC CtaTTTTTCTCCAGACG	pSOI-eGFP-HlyA-P517*

Continuation Table 2: Oligonucleotides used in this study. Overhangs for Gibson assembly are underlined. Sequences introduced and amino acids substituted through the primers are indicated in lower case. Resulting amber stop codons are shown in red. Primers for substitution via the QuikChange Site-Directed Mutagenesis strategy are termed “Amber”, while primers for substitution via the Q5 Site-Directed Mutagenesis strategy are termed “Q5”.

Name	Details	Sequence (5'→3')	Plasmids
Amber-HlyA-I610-fw Amber-HlyA-I610-rev	Substitution of amino acid I610 in HlyA with an amber stop codon for incorporation of unnatural amino acids	CCAGTATCGGGAA <u>tag</u> CGTATTGAGTCACACC GGTGTGACTCAATACG <u>cta</u> TTCCCGATACTGG	pSOI-eGFP-HlyA-I610*
Amber-HlyA-K708-fw Amber-HlyA-K708-rev	Substitution of amino acid K708 in HlyA with an amber stop codon for incorporation of unnatural amino acids	GTTATGAATTCACCTCATATCAATGGT <u>tAg</u> AATTTAACAGAGACTG CAGTCTCTGTAAATT <u>cTa</u> ACCATTGATATGAGTGAATTCATAAC	pSOI-eGFP-HlyA-K708*
Amber-HlyA-L810-fw Amber-HlyA-L810-rev	Substitution of amino acid L810 in HlyA with an amber stop codon for incorporation of unnatural amino acids	GGTTCAGGGAAATCT <u>tag</u> GCAAAAAATGTATTATTCGG CCGAATAATACATTTTTTGC <u>cta</u> AGAATTTCCCTGAACC	pSOI-eGFP-HlyA-L810*
Amber-HlyA-W914-fw Amber-HlyA-W914-rev	Substitution of amino acid W914 in HlyA with an amber stop codon for incorporation of unnatural amino acids	GTATTACATTCAGGAAC <u>taG</u> TTTGAAAAAGAGTCAG CTGACTCTTTTCAAA <u>Cta</u> GTTCTGAATGTAATAC	pSOI-eGFP-HlyA-W914*
Amber-HlyB-Y9-fw Amber-HlyB-Y9-rev	Substitution of amino acid Y9 in the CLD of HlyB with an amber stop codon for incorporation of unnatural amino acids	CTGATTCTTGTCATAAAATTGAT <u>TA</u> gGGGTTATACGCCCTGG CCAGGGCGTATAACCC <u>cTA</u> ATCAATTTTATGACAAGAATCAG	pK184-HlyBD-Y9*
Q5-HlyB-E102-fw Q5-HlyB-E102-rev	Substitution of amino acid E102 in the CLD of HlyB with an amber stop codon for incorporation of unnatural amino acids	TTTTGATCTG <u>tAG</u> CAGCGAAATC ATAAGATATCTGTTTGCTTCTTTAC	pK184-HlyBD-E102*, pK184-HlyBD-E102*-tags
Amber-HlyB-F175-fw Amber-HlyB-F175-rev	Substitution of amino acid F175 in the TMD of HlyB with an amber stop codon for incorporation of unnatural amino acids	GCATTAATAACCCCCCTTTT <u>Tag</u> CAGGTGGTTATGGACAAAG CTTTGTCCATAACCACCTG <u>ctA</u> AAAAAGGGGGGTTATTAATGC	pK184-HlyBD-F175*

Continuation Table 2: Oligonucleotides used in this study. Overhangs for Gibson assembly are underlined. Sequences introduced and amino acids substituted through the primers are indicated in lower case. Resulting amber stop codons are shown in red. Primers for substitution via the QuikChange Site-Directed Mutagenesis strategy are termed “Amber”, while primers for substitution via the Q5 Site-Directed Mutagenesis strategy are termed “Q5”.

Name	Details	Sequence (5'→3')	Plasmids
Amber-HlyB-F216-fw Amber-HlyB-F216-rev	Substitution of amino acid F216 in the TMD of HlyB with an amber stop codon for incorporation of unnatural amino acids	CAGCGGTTTAAGAACTTACATT <u>Tag</u> GCACATAGTACAAGTCGG CCGACTTGTA CTATGTGC <u>ct</u> AAATGTAAGTTCTTAAACCGCTG	pK184-HlyBD-F216*
Amber-HlyB-Q260-fw Amber-HlyB-Q260-rev	Substitution of amino acid Q260 in the TMD of HlyB with an amber stop codon for incorporation of unnatural amino acids	CCAGGGTAAGAGAATTAGACT <u>tAG</u> ATCCGTAATTTCTGAC GTCAGAAAATTACGGAT <u>CTa</u> GTCTAATTCTCTTACCCTGG	pK184-HlyBD-Q260*
Amber-HlyB-K322-fw Amber-HlyB-K322-rev	Substitution of amino acid K322 in the TMD of HlyB with an amber stop codon for incorporation of unnatural amino acids	GACGTCGCCTTGATGAT <u>tAG</u> TTTTTCACGGAATGC GCATTCCGTGAAAA <u>CTa</u> ATCATCAAGGCGACGTC	pK184-HlyBD-K322*
Q5-HlyB-F323-fw Q5-HlyB-F323-rev	Substitution of amino acid F323 in the TMD of HlyB with an amber stop codon for incorporation of unnatural amino acids	GATGATAAG <u>tag</u> TCACGGAATGCGGATAATC AAGGCGACGTCGCAAAATG	pK184-HlyBD-F323*, pK184-HlyBD-F323*-tags
Amber-HlyB-I381-fw Amber-HlyB-I381-rev	Substitution of amino acid I381 in the TMD of HlyB with an amber stop codon for incorporation of unnatural amino acids	CAACCATTGGTCAACAAGGA <u>tag</u> CAGTTAATACAAAAGACTGTTATG CATAACAGTCTTTTGATTAAGT <u>cta</u> TCCTTGTTGACCAATGGTTG	pK184-HlyBD-I381*
Q5-HlyB-A422-fw Q5-HlyB-A422-rev	Substitution of amino acid A422 in the TMD of HlyB with an amber stop codon for incorporation of unnatural amino acids	TCAGATTGTT <u>tag</u> CCGGTTATTCGC CCAGCAAGCATATTTAAAG	pK184-HlyBD-A422*, pK184-HlyBD-A422*-tags
Amber-HlyB-Q432-fw Amber-HlyB-Q432-rev	Substitution of amino acid Q432 in the TMD of HlyB with an amber stop codon for incorporation of unnatural amino acids	CCTTGCAAAATCTGG <u>tAG</u> GATTTCCAGCAGG CCTGCTGGAAATC <u>CTa</u> CCAGATTTGTGCAAGG	pK184-HlyBD-Q432*

Continuation Table 2: Oligonucleotides used in this study. Overhangs for Gibson assembly are underlined. Sequences introduced and amino acids substituted through the primers are indicated in lower case. Resulting amber stop codons are shown in red. Primers for substitution via the QuikChange Site-Directed Mutagenesis strategy are termed “Amber”, while primers for substitution via the Q5 Site-Directed Mutagenesis strategy are termed “Q5”.

Name	Details	Sequence (5'→3')	Plasmids
ColA-fw ColA-rev	Amplification of the ColA ori for insertion into pEvol tRNA ^{pyl} /pyIRS ^{AF} (ori exchange)	AAACGTCCTAGAAGATGCCAG TGGTGTCTCGGGAATCCGTAAAG	
pEVOL-ColA-Ins-fw pEVOL-ColA-Ins-rev	Amplification of pEvol tRNA ^{pyl} /pyIRS ^{AF} without the p15a with overhangs to ColA ori for insertion via Gibson assembly (ori exchange)	<u>TGGCATCTTCTAGGACGTTTTATTTCTAGATTCAGT</u> GCAATTTATCTCTT CAAATG <u>TTTACGGATTCCCGACACCACTCCGCTAGCGCTGATGTC</u>	pEVOL-AbK-ColA
TwinStrep-TEV-fw TwinStrep-TEV-rev	Primer pair was hybridized and used as synthetic insert in Gibson assembly for insertion of an N-terminal TwinStrep tag with TEV protease cleavage site in front of HlyB	TGGTCTCACCCACAATTCGAGAAGGGCGGTGGTTCTGGCGGTGGTTCT GGAGGTTCTCTGCCTGGAGCCACCCGCAGTTCGAAAAGGGTGGTGG TGAGAATCTTTATTTTCAGGGC GCCCTGAAAATAAAGATTCTCACCACCACCCTTTTCGAACTGCGGGTGG CTCCAGGCAGAGGAACCTCCAGAACCACCGCCAGAACCACCGCCCTTC TCGAATTGTGGGTGAGACCA	pK184-TS-TEV-HlyBD
TwinStrep-FXa-fw TwinStrep-FXa-rev	Primer pair was hybridized and used as synthetic insert in Gibson assembly for insertion of an N-terminal TwinStrep tag with FXa protease cleavage site in front of HlyB	TGGTCTCACCCACAATTCGAGAAGGGCGGTGGTTCTGGCGGTGGTTCT GGAGGTTCTCTGCCTGGAGCCACCCGCAGTTCGAAAAGGGTGGTGG TATCGAAGGCCGC GCGGCCTTCGATACCACCACCCTTTTCGAACTGCGGGTGGCTCCAGGC AGAGGAACCTCCAGAACCACCGCCAGAACCACCGCCCTTCTCGAATTG TGGGTGAGACCA	pK184-TS-FXa-HlyBD
HlyB-GStrep-Ins-fw HlyB-GStrep-Ins-rev	Insertion of a Strep tag at the C-terminus of HlyB via the primers	<u>GCAGTTTGAAAAATAACAGAAAGAACAGAAGAATATG</u> <u>GGATGGCTCCAACCGTCTGACTGTAAGTATATAAG</u>	pK184-HlyB-GStrep-6HisG-HlyD
HlyD-6HisG-Ins-fw HlyD-6HisG-Ins-rev	Insertion of a 6xHis tag at the N-terminus of HlyD via the primers	<u>CCATCATGGTAAAACATGGTTAATGGGG</u> <u>TGATGATGGTGCATATTCTTCTGTTCTTTCTG</u>	

Continuation Table 2: Oligonucleotides used in this study. Overhangs for Gibson assembly are underlined. Sequences introduced and amino acids substituted through the primers are indicated in lower case. Resulting amber stop codons are shown in red. Primers for substitution via the QuikChange Site-Directed Mutagenesis strategy are termed “Amber”, while primers for substitution via the Q5 Site-Directed Mutagenesis strategy are termed “Q5”.

Name	Details	Sequence (5'→3')	Plasmids
TwinStrep-3C-fw	Primer pair was hybridized and used as synthetic insert in Gibson assembly for insertion of an N-terminal TwinStrep tag with 3C protease cleavage site in front of HlyB	TGGTCTCACCCACAATTTCGAGAAGGGCGGTGGTTCTGGCGGTGGTTCTGG	pK184-TS-3C-HlyBD
TwinStrep-3C-rev		AGGTTCTCTGCCTGGAGCCACCCGCAGTTCGAAAAGGGTGGTGGTCTG GAAGTGCTGTTTCAGGGTCCG CGGACCCTGAAACAGCACTTCCAGACCACCACCCCTTTTCGAACTGCGGGT GGCTCCAGGCAGAGGAACCTCCAGAACCACCGCCAGAACCACCGCCCTT CTCGAATTGTGGGTGAGACCA	
HlyB-GR-fw	Forward primer for amplification of pK184-HlyBD to insert the amino acids GR in front of HlyBD	AACAGTCATGGgccgcAATTCTGATTCTTGTCATAAAATTG	pK184-GR-HlyBD
HlyB-GP-fw	Forward primer for amplification of pK184-HlyBD to insert the amino acids GP in front of HlyBD	AACAGTCATGGgtccgAATTCTGATTCTTGTC	pK184-GP-HlyBD
HlyB-GR/P-rev	Reverse primer for amplification of pK184-HlyBD to insert either the amino acids GR or GP in front of HlyBD	TCCTGTGTGAAATTGTTATC	pK184-GR-HlyBD, pK184-GP-HlyBD
pK-Ins-tsTEV-fw	Forward primer for amplification of pK184-HlyBD with overhangs to a TwinStrep-TEV tag for insertion in front of HlyB via Gibson assembly	<u>GAATCTTTATTTTCAGGGCA</u> AATTCTGATTCTTGTCATAAAATTG	pK184-TS-TEV-HlyBD
pK-Ins-tsFXa-fw	Forward primer for amplification of pK184-HlyBD with overhangs to a TwinStrep-FXa tag for insertion in front of HlyB via Gibson assembly	<u>TATCGAAGGCCGC</u> AATTCTGATTCTTGTCATAAAATTG	pK184-TS-FXa-HlyBD
pK-Ins-ts3C-fw	Forward primer for amplification of pK184-HlyBD with overhangs to a TwinStrep-3C tag for insertion in front of HlyB via Gibson assembly	<u>TGTTTCAGGGTCCGA</u> AATTCTGATTCTTGTCATAAAATTG	pK184-TS-3C-HlyBD
pK-Ins-tsXXX-rev	Reverse primer for amplification of pK184-HlyBD with overhangs to a TwinStrep tag for insertion in front of HlyB via Gibson assembly	<u>TGTGGGTGAGACCAC</u> ATGACTGTTTCCTGTGTG	pK184-TS-HlyBD plasmids with cleavage site

Solvation of unnatural amino acids

For 1 mM Bpa (molecular weight 269.29 g/mol), 2.7 mg of the UAA per 10 ml of 2xYT medium was dissolved in 11 μ l of 1 M NaOH; the mass and volume can be increased to fit the required scale. Subsequently, 2xYT medium was added stepwise with the following volumes: first 2x 11 μ l, then 4x 25 μ l. During these dilution steps, Bpa precipitates again in form of white flakes. The addition of 50 μ l 1 M NaOH again dissolves Bpa completely in the medium. The Bpa solution is filled up with 2xYT medium to 10 ml and the pH of the medium checked to ensure a neutral pH; usually the pH is ~7.5. Afterwards, the required antibiotics are added and the UAA supplemented medium can be inoculated with cells for incorporation of the UAA in the protein of choice. In case of H-L-Photolysine, 1 mM of the UAA could be solved directly in 2xYT medium.

Protein expression for crosslinking and secretion experiments

E. coli BL21(DE3) cells were made chemically competent and transformed via heat-shock. Since multiple plasmids were introduced, cells were initially transformed with one plasmid and subsequently made chemically competent again for transformation with the next plasmid. Most cells in this study contained a plasmid variant encoding for HlyB and HlyD as well as an additional plasmid encoding for a variant of HlyA. Strains carrying a plasmid with an amber stop codon substitution additionally contained a plasmid for incorporation of an unnatural amino acid.

A preculture in 5 ml of 2xYT medium was supplemented with the respective antibiotics, inoculated and incubated overnight at 37°C and 180 rpm. 20 ml of 2xYT medium in a 100 ml non-baffled flask were supplemented with antibiotics and inoculated to an OD₆₀₀ of 0.1. Cultures were grown at 37°C and 180 rpm until the OD₆₀₀ reached 1.0. At this point, SDS samples were taken and protein expression was induced by the addition of 1 mM IPTG and 6.6 mM arabinose (= 0.1% (w/v)). Simultaneously, the folding of HlyA was induced by supplementing the medium with 4 mM CaCl₂. Cultures were further incubated at 37°C and 180 rpm and SDS samples were taken regularly. After 3 h, cells were harvested by centrifugation at 4,000 xg and 4°C for 20 min. The supernatant was

discarded and cells resuspended in PBS buffer. The volume was adjusted to set the cells to an OD₆₀₀ of ~4.0 and cell suspensions were kept on ice until photo-crosslinking.

In the case of expressions in 96-well plate format, a preculture plate with 150 µl 2xYT medium supplemented with antibiotics in each well was incubated overnight at 37°C and 800 rpm. Subsequently, a fresh 96 well plate with 150 µl 2xYT medium supplemented with antibiotics and 1 mM Bpa was prepared and inoculated with 2 µl cell suspension of the preculture plate. Cells were incubated at 37°C and 800 rpm for 4 h. Afterwards, 15 µl of an inducer mix containing CaCl₂, IPTG and arabinose was added (working concentrations identical to flask expressions stated above). Cells were incubated for additional 3 h at 37°C and 800 rpm

Photo-crosslinking experiments

For *in vivo* photo-crosslinking, *E. coli* cells expressing the hemolysin T1SS with an amber stop codon mutation in HlyA or HlyB were cultivated as described above. Cells suspended in PBS buffer were placed in a petri dish and cooled using ice during irradiation. For crosslinking of proteins containing either AbK or Bpa, UV irradiation at 365 nm was performed on a benchUV 40 Lhi Transilluminator (Analytik Jena). Cells were UV irradiated for up to 45 min with the UV intensity set to “high” and the ice was replaced every 15 min. SDS samples were taken and the crosslinked cell suspension was frozen in liquid nitrogen and stored at -80°C.

Cells grown in 96 well plates were photo-crosslinked in 2xYT medium.

Co-immunoprecipitation experiments

Prior to the co-immunoprecipitation experiments, a protease inhibitor cocktail was added to the crosslinked cell suspension and cells were disrupted either by ultrasonication (MS72 ultrasonic microtip, 5 alternating cycles of 1 min ultrasonication at 50% power with ice cooling and 1 min of incubation on ice) or cell disruption (Microfluidizer M-110P, Microfluidics, 3 passes at 1.5 kbar). Cell debris was separated by centrifugation at 18,000 xg and 4°C for 30 min and membranes were isolated by centrifugation at 200,000 xg and 4°C for 90 min. The supernatant was discarded and

the membrane pellet was homogenized in PBS buffer. If not stated otherwise, membranes were solubilized with 1% (w/v) Fos-Choline-14 (FC14, Anatrace) for at least 1 h at 4°C under low agitation. Unsolubilized material was separated by centrifugation (150,000 xg, 4°C, 30 min) and the solubilized membranes were subsequently used for the co-immunoprecipitation experiments.

For immunoprecipitation via the N-terminal eGFP tag of HlyA, GFP-Trap agarose was used according to the manufacturers protocol (ChromoTek). In short, the GFP-Trap agarose slurry was resuspended and 25 µl were placed into a spin column. The slurry was washed thrice with 500 µl PBS buffer and the buffer removed in between the washing steps by centrifugation at 5,000 xg for 5 min. Solubilized membranes were diluted with PBS buffer in a 1:1 ratio and 2 ml were added to the GFP-Trap agarose beads. The mixture was incubated at 4°C for at least 1 h on an end-over-end shaker and the beads were separated from the supernatant in 500 µl steps using a spin column and centrifugation at 100 xg and RT for 30 s. An SDS sample of the flow through after this binding step was taken. The beads were washed thrice with 500 µl PBS buffer + 0.01% (w/v) FC14 and centrifugation at 100 xg and RT for 30 s. An SDS sample of the flow through after the second washing step was taken. Bound protein was eluted either by pH shift or addition of SDS sample buffer. Elution was performed using SDS sample buffer: GFP-Trap agarose beads were resuspended in 2x SDS sample buffer and the suspension was heated at 99°C for 5 min. The beads were separated by centrifugation at 2,500 xg and RT for 2 min.

The co-immunoprecipitation experiments with Ni-NTA magnetic agarose beads (Qiagen) were performed similar: membranes were isolated, solubilized and diluted as described above. The Ni-NTA magnetic agarose bead slurry was resuspended and 150 µl were taken for each sample. Beads were separated from the storage solution using a magnetic separator and equilibrated using 500 µl of PBS buffer + 5 mM imidazole + 0.01% (w/v) FC14. The solubilized membranes were supplemented with 5 mM imidazole as well and added to the agarose beads. Samples were incubated at 4°C for at least 1 h on an end-over-end shaker. Beads were separated afterwards using a magnetic separator and a sample of the supernatant was taken. Non-specifically bound protein was removed by washing the beads with PBS buffer containing 0.01% (w/v) FC14 and increasing amounts of up to 50 mM imidazole (specified in the “Results” section for each experiment) and an SDS sample of the

supernatant during these washing steps was taken as well. Bound protein was eluted by addition of 100 µl PBS buffer supplemented with 0.01% (w/v) FC14 and 250 mM imidazole and mixed with SDS sample buffer.

Liquid chromatography coupled mass spectrometric analysis

Protein containing bands were cut out from polyacrylamide gels stained with Coomassie brilliant blue and prepared for mass spectrometric analysis essentially as described (Brenig *et al.* 2020). Briefly, proteins were reduced with dithiothreitol, alkylated with iodoacetamide, overnight digested with trypsin and resulting peptides extracted from the gel and finally resuspended in 0.1% trifluoro acetic acid. Subsequently, peptides were separated using an Ultimate3000 (Thermo Fisher Scientific) nano liquid chromatography system on C18 material using a one-hour gradient and sprayed via a nano-electrospray interface in the mass spectrometer essentially as described before in (Prescher *et al.* 2021). A QExactive plus (Thermo Fisher Scientific) mass spectrometer was used to analyze eGFP-HlyA-L13*: precursor spectra were recorded and top ten intense precursors isolated by a quadrupole, fragmented by higher-energy collisional dissociation and fragment spectra recorded in the orbitrap analyzer as described (Prescher *et al.* 2021). HlyB-F175* were analyzed using an Orbitrap Fusion Lumos (Thermo Fisher Scientific) mass spectrometer using data dependent positive mode. First, precursor spectra were recorded in the orbitrap analyzer (resolution 120000, scan range 200-2000 m/z, maximum injection time 60 ms, automatic gain control target 400000). Second, 2-7 fold charged precursors were isolated by the build in quadrupole (isolation window 1.6 m/z), fragmented by higher-energy collisional dissociation and analyzed in the orbitrap (resolution 15000, scan range auto, maximum injection time 22 ms, automatic gain control target 50000). Cycle time was 2 seconds and active exclusion set to 60 seconds.

Spectra were processed by MaxQuant version 1.6.3.4 (eGFP-HlyA-L13*) or 1.6.17.0 (HlyB-F175*) for peptide identification and quantification with standard parameters if not stated otherwise. Carbamidomethylation at cysteines was considered as fixed and methionine oxidation and protein N-terminal acetylation as variable modification. Dependent on the analyzed sample, a mass shift for the incorporation of Bpa (L: +138.0106 or F: + 104.0262) was additionally considered as variable modification. Searches were carried out including UniProt KB proteome UP000002032 *E. coli* BL21

(DE3) entries downloaded on 2nd April 2019 (eGFP-HlyA-L13*) or 27th January 2021 (HlyB F175*) and additional entries for HlyA, HlyB, HlyD and TolC.

For crosslink search, raw files were converted into .mgf files by Proteome discoverer 2.4.1.15 (Thermo Fisher Scientific) and searches on base of HlyA, HlyB, HlyD and TolC entries performed with StavroX version 3.6.6.6 (Götze *et al.* 2011).

Electrophoresis, immunological detection and signal quantification

DNA samples were mixed with 6x Purple Gel Loading Dye (New England Biolabs) and subjected to a 1% agarose gel supplemented with 4 µl MIDORI Green Xtra (Nippon Genetics Europe). Gels were connected to a power supply unit for 50 min at 90 V. DNA bands were visualized on an Amersham AI680 Imager (Cytiva) using the blue epi-illumination filter.

Protein samples were subjected to an SDS-PAGE with subsequent Western blotting. Before, SDS samples were heated for 5 min to 95°C and 40 mM DTT were added after cooling the sample down to RT if not stated otherwise. Western blots were performed with a semi-dry setup using Trans-Blot Turbo (Bio-Rad). The SDS gels were stained using Quick Coomassie Stain solution (Protein Ark).

Band intensities of HlyA, HlyB or HlyD were quantified from antibody stained immunoblots and Coomassie stained gels using Fiji (Schindelin *et al.* 2012). For the detection of HlyA, either a polyclonal antibody (termed anti HlyA full-length) or an antibody specifically targeting the C-terminal secretion signal sequence (termed anti-HlyA secretion signal) was used. The antibody for detection of HlyB targeted the highly conserved NBD, while the HlyD antibody targeted the periplasmic part of the protein. The secretion level of HlyA was normalized to the expression level of HlyB or HlyD by dividing the quantified amount of HlyA by the quantified amount of HlyB or HlyD. The secretion and expression levels by/of mutant or affinity tagged proteins were then normalized to the secretion and expression level of wildtype protein by division.

Bibliography

1. Akeda, Y. and Galán, J. E. (2005). "Chaperone release and unfolding of substrates in type III secretion." Nature **437**(7060): 911-915.
2. Bakkes, P. J., Jenewein, S., Smits, S. H., Holland, I. B. and Schmitt, L. (2010). "The rate of folding dictates substrate secretion by the *Escherichia coli* hemolysin type 1 secretion system." J. Biol. Chem. **285**(52): 40573-40580.
3. Balakrishnan, L., Hughes, C. and Koronakis, V. (2001). "Substrate-triggered recruitment of the TolC channel-tunnel during type I export of hemolysin by *Escherichia coli*." J. Mol. Biol. **313**(3): 501-510.
4. Beer, T., Hänsch, S., Pfeffer, K., Smits, S. H., Weidtkamp-Peters, S. and Schmitt, L. (2021). "Quantification and surface localization of the hemolysin A type 1 secretion system at the endogenous level and under conditions of overexpression." Appl. Environ. Microbiol. **88**(3): AEM. 01896-01821.
5. Belin, D. and Puigbò, P. (2022). "Why Is the UAG (amber) stop codon almost absent in highly expressed bacterial genes?" Life **12**(3): 431.
6. Benabdelhak, H., Kiontke, S., Horn, C., Ernst, R., Blight, M. A., Holland, I. B. and Schmitt, L. (2003). "A specific interaction between the NBD of the ABC-transporter HlyB and a C-terminal fragment of its transport substrate haemolysin A." J. Mol. Biol. **327**(5): 1169-1179.
7. Berg, M., Michalowski, A., Palzer, S., Rupp, S. and Sohn, K. (2014). "An *in vivo* photo-cross-linking approach reveals a homodimerization domain of Aha1 in *S. cerevisiae*." PLoS One **9**(3): e89436.
8. Boehm, D., Welch, R. and Snyder, I. (1990). "Calcium is required for binding of *Escherichia coli* hemolysin (HlyA) to erythrocyte membranes." Infect. Immun. **58**(6): 1951-1958.
9. Böttke, T., Ernicke, S., Serfling, R., Ihling, C., Burda, E., Gurevich, V. V., Sinz, A. and Coin, I. (2020). "Exploring GPCR-arrestin interfaces with genetically encoded crosslinkers." EMBO Rep. **21**(11): e50437.
10. Brenig, K., Grube, L., Schwarzländer, M., Köhrer, K., Stühler, K. and Poschmann, G. (2020). "The proteomic landscape of cysteine oxidation that underpins retinoic acid-induced neuronal differentiation." J. Proteome. Res. **19**(5): 1923-1940.
11. Chen, S., Schultz, P. G. and Brock, A. (2007). "An improved system for the generation and analysis of mutant proteins containing unnatural amino acids in *Saccharomyces cerevisiae*." J. Mol. Biol. **371**(1): 112-122.
12. Chenal, A., Guijarro, J. I., Raynal, B., Delepierre, M. and Ladant, D. (2009). "RTX calcium binding motifs are intrinsically disordered in the absence of calcium: implication for protein secretion." J. Biol. Chem. **284**(3): 1781-1789.
13. Chin, J. W., Martin, A. B., King, D. S., Wang, L. and Schultz, P. G. (2002). "Addition of a photocrosslinking amino acid to the genetic code of *Escherichia coli*." Proc. Natl. Acad. Sci. **99**(17): 11020-11024.

14. Choi, C. P., Moon, A. S., Back, P. S., Jami-Alahmadi, Y., Vashisht, A. A., Wohlschlegel, J. A. and Bradley, P. J. (2019). "A photoactivatable crosslinking system reveals protein interactions in the *Toxoplasma gondii* inner membrane complex." PLoS Biol. **17**(10): e3000475.
15. Costa, T. R., Felisberto-Rodrigues, C., Meir, A., Prevost, M. S., Redzej, A., Trokter, M. and Waksman, G. (2015). "Secretion systems in gram-negative bacteria: structural and mechanistic insights." Nat. Rev. Microbiol. **13**(6): 343-359.
16. Delepelaire, P. (2004). "Type I secretion in gram-negative bacteria." Biochim. Biophys. Acta, Mol. Cell Res. **1694**(1-3): 149-161.
17. Dietz, H. and Rief, M. (2006). "Protein structure by mechanical triangulation." Proc. Natl. Acad. Sci. **103**(5): 1244-1247.
18. Dorman, G. and Prestwich, G. D. (1994). "Benzophenone photophores in biochemistry." Biochemistry **33**(19): 5661-5673.
19. Fu, Y. and Galán, J. E. (1998). "Identification of a specific chaperone for SptP, a substrate of the centisome 63 type III secretion system of *Salmonella typhimurium*." J. Bacteriol. **180**(13): 3393-3399.
20. Fukumura, T., Makino, F., Dietsche, T., Kinoshita, M., Kato, T., Wagner, S., Namba, K., Imada, K. and Minamino, T. (2017). "Assembly and stoichiometry of the core structure of the bacterial flagellar type III export gate complex." PLoS Biol. **15**(8): e2002281.
21. Gibson, D. G. (2011). "Enzymatic assembly of overlapping DNA fragments." Methods Enzymol. **498**: 349-361.
22. Götze, M., Pettelkau, J., Schaks, S., Bosse, K., Ihling, C. H., Krauth, F., Fritzsche, R., Kühn, U. and Sinz, A. (2011). "StavroX—a software for analyzing crosslinked products in protein interaction studies." J. Am. Soc. Mass Spectrom. **23**(1): 76-87.
23. Gray, L., Baker, K., Kenny, B., Mackmann, N., Haigh, R. and Holland, I. B. (1989). "A novel C-terminal signal sequence targets *Escherichia coli* haemolysin directly to the medium." J. Cell Sci. **1989**(Supplement_11): 45-57.
24. Harterink, M., Port, F., Lorenowicz, M. J., McGough, I. J., Silhankova, M., Betist, M. C., van Weering, J. R. T., van Heesbeen, R. G. H. P., Middelkoop, T. C., Basler, K., Cullen, P. J. and Korswagen, H. C. (2011). "A SNX3-dependent retromer pathway mediates retrograde transport of the Wnt sorting receptor Wntless and is required for Wnt secretion." Nat. Cell Biol. **13**(8): 914-923.
25. Higgins, C. F. and Linton, K. J. (2004). "The ATP switch model for ABC transporters." Nat. Struct. Mol. Biol. **11**(10): 918.
26. Hino, N., Okazaki, Y., Kobayashi, T., Hayashi, A., Sakamoto, K. and Yokoyama, S. (2005). "Protein photo-cross-linking in mammalian cells by site-specific incorporation of a photoreactive amino acid." Nat. Methods **2**(3): 201-206.
27. Hinsa, S. M., Espinosa-Urgel, M., Ramos, J. L. and O'toole, G. A. (2003). "Transition from reversible to irreversible attachment during biofilm formation by *Pseudomonas fluorescens* WCS365 requires an ABC transporter and a large secreted protein." Mol. Microbiol. **49**(4): 905-918.

28. Huang, C.-Y., Chao, Y.-P. and Yang, Y.-S. (2003). "Purification of industrial hydantoinase in one chromatographic step without affinity tag." Protein Expr. Purif. **30**(1): 134-139.
29. Jarchau, T., Chakraborty, T., Garcia, F. and Goebel, W. (1994). "Selection for transport competence of C-terminal polypeptides derived from *Escherichia coli* hemolysin: the shortest peptide capable of autonomous HlyB/HlyD-dependent secretion comprises the C-terminal 62 amino acids of HlyA." Mol. Gen. Genet. **245**(1): 53-60.
30. Jenewein, S. (2008). The *Escherichia* haemolysin transporter: a paradigm for type I secretion, Düsseldorf, Univ., Diss., 2008.
31. Johanson, K. O. and McHenry, C. S. (1982). "The beta subunit of the DNA polymerase III holoenzyme becomes inaccessible to antibody after formation of an initiation complex with primed DNA." J. Biol. Chem. **257**(20): 12310-12315.
32. Jones, H. E., Holland, I., Baker, H. L. and Campbell, A. K. (1999). "Slow changes in cytosolic free Ca^{2+} in *Escherichia coli* highlight two putative influx mechanisms in response to changes in extracellular calcium." Cell Calcium **25**(3): 265-274.
33. Kanonenberg, K., Schwarz, C. K. and Schmitt, L. (2013). "Type I secretion systems—a story of appendices." Res. Microbiol. **164**(6): 596-604.
34. Khan, F., Legler, P. M., Mease, R. M., Duncan, E. H., Bergmann-Leitner, E. S. and Angov, E. (2012). "Histidine affinity tags affect MSP142 structural stability and immunodominance in mice." Biotechnol. J. **7**(1): 133-147.
35. Kieuvongngam, V., Olinares, P. D. B., Palillo, A., Oldham, M. L., Chait, B. T. and Chen, J. (2020). "Structural basis of substrate recognition by a polypeptide processing and secretion transporter." eLife **9**.
36. Kim, H.-M., Xu, Y., Lee, M., Piao, S., Sim, S.-H., Ha, N.-C. and Lee, K. (2010). "Functional relationships between the AcrA hairpin tip region and the TolC aperture tip region for the formation of the bacterial tripartite efflux pump AcrAB-TolC." J. Bacteriol. **192**(17): 4498-4503.
37. Kloet, S. L., Makowski, M. M., Baymaz, H. I., van Voorthuijsen, L., Karemaker, I. D., Santanach, A., Jansen, P. W. T. C., Di Croce, L. and Vermeulen, M. (2016). "The dynamic interactome and genomic targets of Polycomb complexes during stem-cell differentiation." Nat. Struct. Mol. Biol. **23**(7): 682-690.
38. Koronakis, V., Koronakis, E. and Hughes, C. (1989). "Isolation and analysis of the C-terminal signal directing export of *Escherichia coli* hemolysin protein across both bacterial membranes." EMBO J. **8**(2): 595-605.
39. Krachmarova, E., Tileva, M., Lilkova, E., Petkov, P., Maskos, K., Ilieva, N., Ivanov, I., Litov, L. and Nacheva, G. (2017). "His-FLAG tag as a fusion partner of glycosylated human interferon-gamma and its mutant: gain or loss?" BioMed Res. Int. **2017**: 3018608.
40. Lecher, J., Schwarz, C. K., Stoldt, M., Smits, S. H., Willbold, D. and Schmitt, L. (2012). "An RTX transporter tethers its unfolded substrate during secretion via a unique N-terminal domain." Structure **20**(10): 1778-1787.
41. Lee, S. H. and Altenberg, G. A. (2003). "Expression of functional multidrug-resistance protein 1 in *Saccharomyces cerevisiae*: effects of N- and C-terminal affinity tags." Biochem. Biophys. Res. Commun. **306**(3): 644-649.

-
42. Lenders, M. H., Beer, T., Smits, S. H. and Schmitt, L. (2016). "In vivo quantification of the secretion rates of the hemolysin A Type I secretion system." Sci. Rep. **6**: 33275.
 43. Lenders, M. H., Weidtkamp-Peters, S., Kleinschrodt, D., Jaeger, K.-E., Smits, S. H. and Schmitt, L. (2015). "Directionality of substrate translocation of the hemolysin A Type I secretion system." Sci. Rep. **5**(1): 12470.
 44. L  toff  , S., Ghigo, J. and Wandersman, C. (1994). "Secretion of the *Serratia marcescens* HasA protein by an ABC transporter." J. Bacteriol. **176**(17): 5372-5377.
 45. Lin, D. Y.-w., Huang, S. and Chen, J. (2015). "Crystal structures of a polypeptide processing and secretion transporter." Nature **523**(7561): 425.
 46. Ludwig, A., Schmid, A., Benz, R. and Goebel, W. (1991). "Mutations affecting pore formation by haemolysin from *Escherichia coli*." Mol. Gen. Genet. **226**: 198-208.
 47. Martin, C., Higgins, C. F. and Callaghan, R. (2001). "The vinblastine binding site adopts high-and low-affinity conformations during a transport cycle of P-glycoprotein." Biochemistry **40**(51): 15733-15742.
 48. Miller, W. T. and Kaiser, E. T. (1988). "Probing the peptide binding site of the cAMP-dependent protein kinase by using a peptide-based photoaffinity label." Proc. Natl. Acad. Sci. **85**(15): 5429-5433.
 49. Moyle, W. R., Ehrlich, P. H. and Canfield, R. E. (1982). "Use of monoclonal antibodies to subunits of human chorionic gonadotropin to examine the orientation of the hormone in its complex with receptor." Proc. Natl. Acad. Sci. **79**(7): 2245-2249.
 50. Murray, C. I., Westhoff, M., Eldstrom, J., Thompson, E., Emes, R. and Fedida, D. (2016). "Unnatural amino acid photo-crosslinking of the IKs channel complex demonstrates a KCNE1: KCNQ1 stoichiometry of up to 4:4." Elife **5**: e11815.
 51. Okuda, S., Freinkman, E. and Kahne, D. (2012). "Cytoplasmic ATP hydrolysis powers transport of lipopolysaccharide across the periplasm in *E. coli*." Science **338**(6111): 1214-1217.
 52. Ostolaza, H., Soloaga, A. and Go  ni, F. M. (1995). "The binding of divalent cations to *Escherichia coli* α -haemolysin." Eur. J. Biochem. **228**(1): 39-44.
 53. Owens, T. W., Taylor, R. J., Pahil, K. S., Bertani, B. R., Ruiz, N., Kruse, A. C. and Kahne, D. (2019). "Structural basis of unidirectional export of lipopolysaccharide to the cell surface." Nature **567**(7749): 550-553.
 54. Pattison, D. I. and Davies, M. J. (2006). "Actions of ultraviolet light on cellular structures." Cancer: cell structures, carcinogens and genomic instability: 131-157.
 55. Pimenta, A., Young, J., Holland, I. and Blight, M. (1999). "Antibody analysis of the localisation, expression and stability of HlyD, the MFP component of the *E. coli* haemolysin translocator." Mol. Gen. Genet. **261**(1): 122-132.
 56. Plass, T., Milles, S., Koehler, C., Schultz, C. and Lemke, E. A. (2011). "Genetically encoded copper-free click chemistry." Angew. Chem. Int. Ed. **50**(17): 3878-3881.

57. Pourhassan, Z., Hachani, E., Spitz, O., Smits, S. H. and Schmitt, L. (2022). "Investigations on the substrate binding sites of hemolysin B, an ABC transporter, of a type 1 secretion system." Front. Microbiol. **13**: 1-15.
58. Prescher, N., Hänsch, S., Knobbe-Thomsen, C. B., Stühler, K. and Poschmann, G. (2021). "The migration behavior of human glioblastoma cells is influenced by the redox-sensitive human macrophage capping protein CAPG." Free Radic. Biol. Med. **167**: 81-93.
59. Reimann, S., Poschmann, G., Kanonenberg, K., Stühler, K., Smits, S. H. and Schmitt, L. (2016). "Interdomain regulation of the ATPase activity of the ABC transporter hemolysin B from *E. coli*." Biochem. J. **473**(16): 2471-2483.
60. Ryu, Y. and Schultz, P. G. (2006). "Efficient incorporation of unnatural amino acids into proteins in *Escherichia coli*." Nat. Methods **3**(4): 263-265.
61. Sanchez-Magraner, L., Viguera, A. R., Garcia-Pacios, M., Garcillan, M. P., Arrondo, J.-L. R., de la Cruz, F., Goni, F. M. and Ostolaza, H. (2007). "The calcium-binding C-terminal domain of *Escherichia coli* α -hemolysin is a major determinant in the surface-active properties of the protein." J. Biol. Chem. **282**(16): 11827-11835.
62. Sato, S., Mimasu, S., Sato, A., Hino, N., Sakamoto, K., Umehara, T. and Yokoyama, S. (2011). "Crystallographic study of a site-specifically cross-linked protein complex with a genetically incorporated photoreactive amino acid." Biochemistry **50**(2): 250-257.
63. Schindelin, J., Arganda-Carreras, I., Frise, E., Kaynig, V., Longair, M., Pietzsch, T., Preibisch, S., Rueden, C., Saalfeld, S. and Schmid, B. (2012). "Fiji: an open-source platform for biological-image analysis." Nat. Methods **9**(7): 676-682.
64. Schmitt, L., Benabdelhak, H., Blight, M. A., Holland, I. B. and Stubbs, M. T. (2003). "Crystal structure of the nucleotide-binding domain of the ABC-transporter haemolysin B: identification of a variable region within ABC helical domains." J. Mol. Biol. **330**(2): 333-342.
65. Sherman, D. J., Xie, R., Taylor, R. J., George, A. H., Okuda, S., Foster, P. J., Needleman, D. J. and Kahne, D. (2018). "Lipopolysaccharide is transported to the cell surface by a membrane-to-membrane protein bridge." Science **359**(6377): 798-801.
66. Simpson, B. W., Owens, T. W., Orabella, M. J., Davis, R. M., May, J. M., Trauger, S. A., Kahne, D. and Ruiz, N. (2016). "Identification of residues in the lipopolysaccharide ABC transporter that coordinate ATPase activity with extractor function." MBio **7**(5): e01729-01716.
67. Stebbins, C. E. and Galán, J. E. (2001). "Maintenance of an unfolded polypeptide by a cognate chaperone in bacterial type III secretion." Nature **414**(6859): 77-81.
68. Sun, D., Ostermaier, M. K., Heydenreich, F. M., Mayer, D., Jaussi, R., Standfuss, J. and Veprintsev, D. B. (2013). "AAscan, PCRdesign and MutantChecker: a suite of programs for primer design and sequence analysis for high-throughput scanning mutagenesis." PLoS One **8**(10): e78878.

-
69. Thanabalu, T., Koronakis, E., Hughes, C. and Koronakis, V. (1998). "Substrate-induced assembly of a contiguous channel for protein export from *E. coli*: reversible bridging of an inner-membrane translocase to an outer membrane exit pore." EMBO J. **17**(22): 6487-6496.
 70. Thomas, S., Smits, S. H. and Schmitt, L. (2014). "A simple in vitro acylation assay based on optimized HlyA and HlyC purification." Anal. Biochem. **464**: 17-23.
 71. Torres-Vargas, C. E., Kronenberger, T., Roos, N., Dietsche, T., Poso, A. and Wagner, S. (2019). "The inner rod of virulence-associated type III secretion systems constitutes a needle adapter of one helical turn that is deeply integrated into the system's export apparatus." Mol. Microbiol. **112**(3): 918-931.
 72. Vermeulen, M., Eberl, H. C., Matarese, F., Marks, H., Denissov, S., Butter, F., Lee, K. K., Olsen, J. V., Hyman, A. A., Stunnenberg, H. G. and Mann, M. (2010). "Quantitative interaction proteomics and genome-wide profiling of epigenetic histone marks and their readers." Cell **142**(6): 967-980.
 73. Wang, R., Seror, S. J., Blight, M., Pratt, J. M., Broome-Smith, J. K. and Holland, I. B. (1991). "Analysis of the membrane organization of an *Escherichia coli* protein translocator, HlyB, a member of a large family of prokaryote and eukaryote surface transport proteins." J. Mol. Biol. **217**(3): 441-454.
 74. Welch, R. (1991). "Pore-forming cytolysins of gram-negative bacteria." Mol. Microbiol. **5**(3): 521-528.
 75. Welte, T., Kudva, R., Kuhn, P., Sturm, L., Braig, D., Müller, M., Warscheid, B., Drepper, F. and Koch, H.-G. (2012). "Promiscuous targeting of polytopic membrane proteins to SecYEG or YidC by the *Escherichia coli* signal recognition particle." Mol. Biol. Cell **23**(3): 464-479.
 76. Xu, Y., Song, S., Moeller, A., Kim, N., Piao, S., Sim, S.-H., Kang, M., Yu, W., Cho, H.-S. and Chang, I. (2011). "Functional implications of an intermeshing cogwheel-like interaction between TolC and MacA in the action of macrolide-specific efflux pump MacAB-TolC." J. Biol. Chem. **286**(15): 13541-13549.
 77. Young, T. S., Ahmad, I., Brock, A. and Schultz, P. G. (2009). "Expanding the genetic repertoire of the methylotrophic yeast *Pichia pastoris*." Biochemistry **48**(12): 2643-2653.
 78. Young, T. S., Ahmad, I., Yin, J. A. and Schultz, P. G. (2010). "An enhanced system for unnatural amino acid mutagenesis in *E. coli*." J. Mol. Biol. **395**(2): 361-374.
 79. Zhao, H., Lee, J. and Chen, J. (2022). "The hemolysin A secretion system is a multi-engine pump containing three ABC transporters." Cell **185**(18): 3329-3340.

Supplementary Information

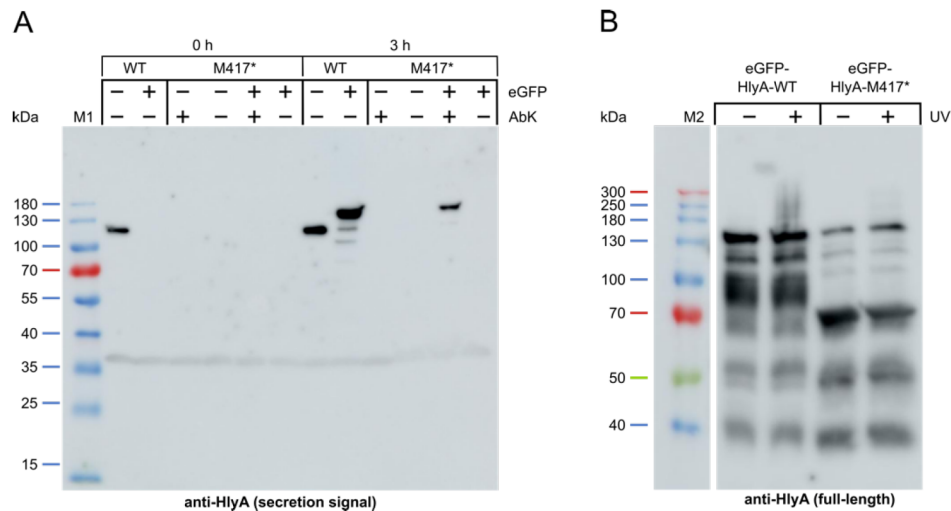


Figure S1: Expression and photo-crosslinking of HlyA* amber mutants with incorporated photolysine. **(A)** Immunoblot analysis of whole *E. coli* BL21(DE3) cells expressing HlyB, HlyD and either HlyA-M417* or HlyA without amber mutation. Samples were taken before (0 h) and 3 h after induction. The HlyA variant with (+ eGFP) or without N-terminal eGFP (- eGFP) and the addition of photolysine (AbK) is indicated above. The used antibody targeted the secretion signal of HlyA. **(B)** Immunoblot analysis of photo-crosslinked AbK samples shown in **(A)**. Samples were UV irradiated at 365 nm for 20 min (+UV) or left untreated (-UV). The used antibody targeted full-length HlyA. M1: PageRuler Prestained Protein Ladder, M2: Spectra Multicolor High Range Protein Ladder.

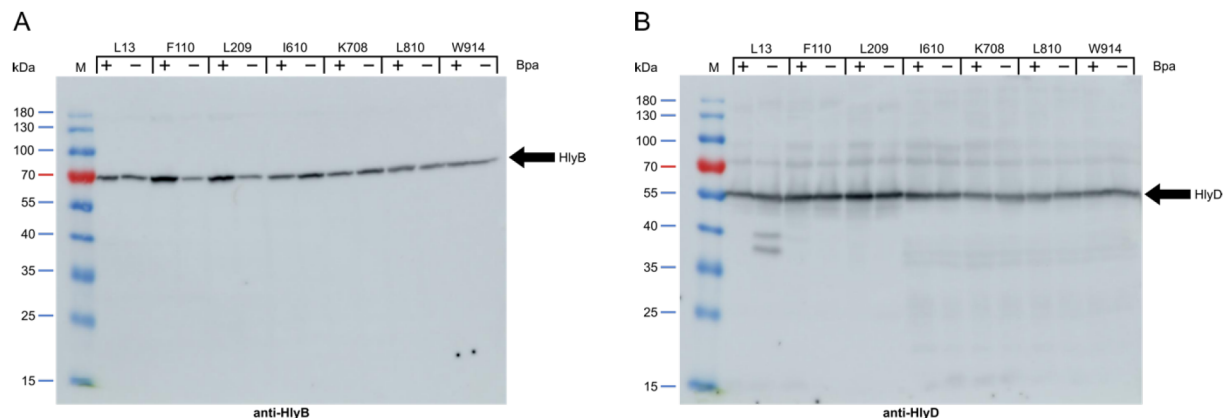


Figure S2: Immunoblot analysis of *E. coli* BL21(DE3) containing the pEVOL-Bpa amber suppression plasmid, pK184-HlyBD plasmid and an eGFP-HlyA plasmid containing an amber stop codon mutation at the position indicated on the top. Expressions were performed either with (+) or without Bpa (-) in the medium. Used antibodies targeted either HlyB **(A)** or HlyD **(B)**, the corresponding signals are marked with an arrow. M: PageRuler Prestained Protein Ladder.

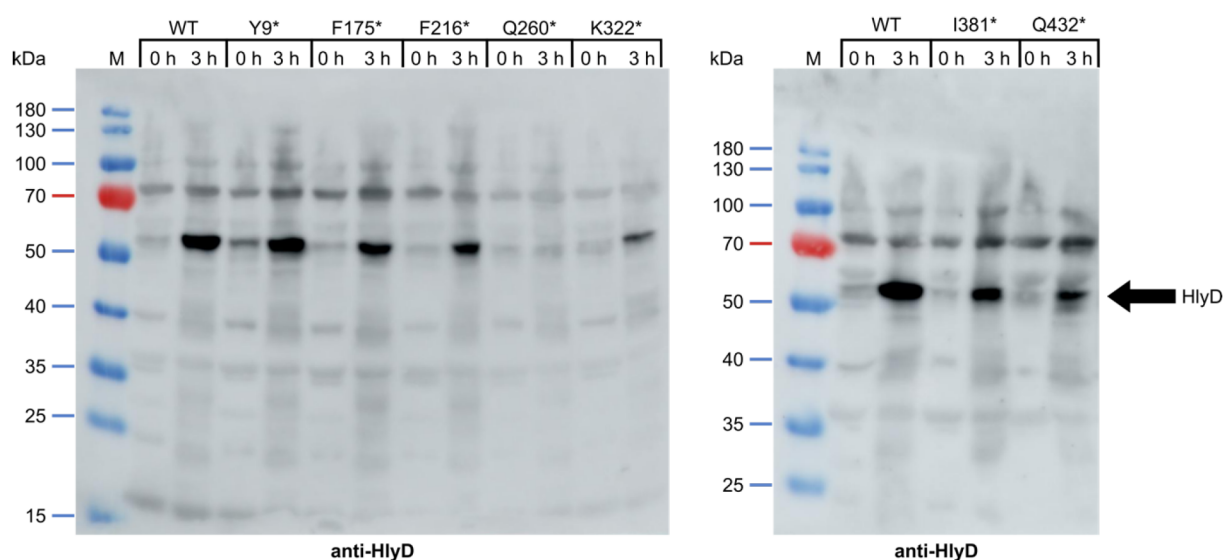


Figure S3: Expression level of HlyD in cells expressing HlyB* amber mutants with incorporated Bpa. Immunoblot analysis of whole *E. coli* BL21(DE3) cells expressing HlyD and HlyB* with an amber mutation at the position indicated above (WT: no amber mutation). Samples were taken before (0 h) and 3 h after induction. The used antibody targeted HlyD. M: PageRuler Prestained Protein Ladder.

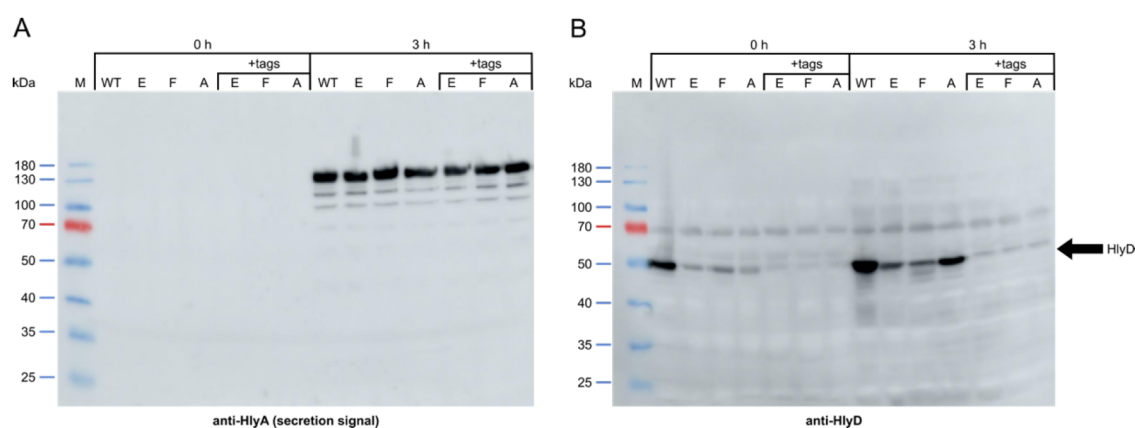


Figure S4: Expression of eGFP-HlyA and HlyD in cells expressing HlyB* amber mutants with incorporated Bpa as stated by (Zhao *et al.* 2022). Immunoblot analysis of whole *E. coli* BL21(DE3) cells expressing eGFP-HlyA, HlyD and HlyB* with an amber mutation at the position indicated above (WT: no amber mutation, E: E102*, F: F323*, A: A422*). Samples marked with “+tags” contained HlyB* with a C-terminal Strep tag and HlyD with an N-terminal 6xHis tag as mentioned in (Zhao *et al.* 2022). Samples were taken before (0 h) and 3 h after induction. The used antibody targeted the secretion signal of HlyA (A) and HlyD (B). M: PageRuler Prestained Protein Ladder.

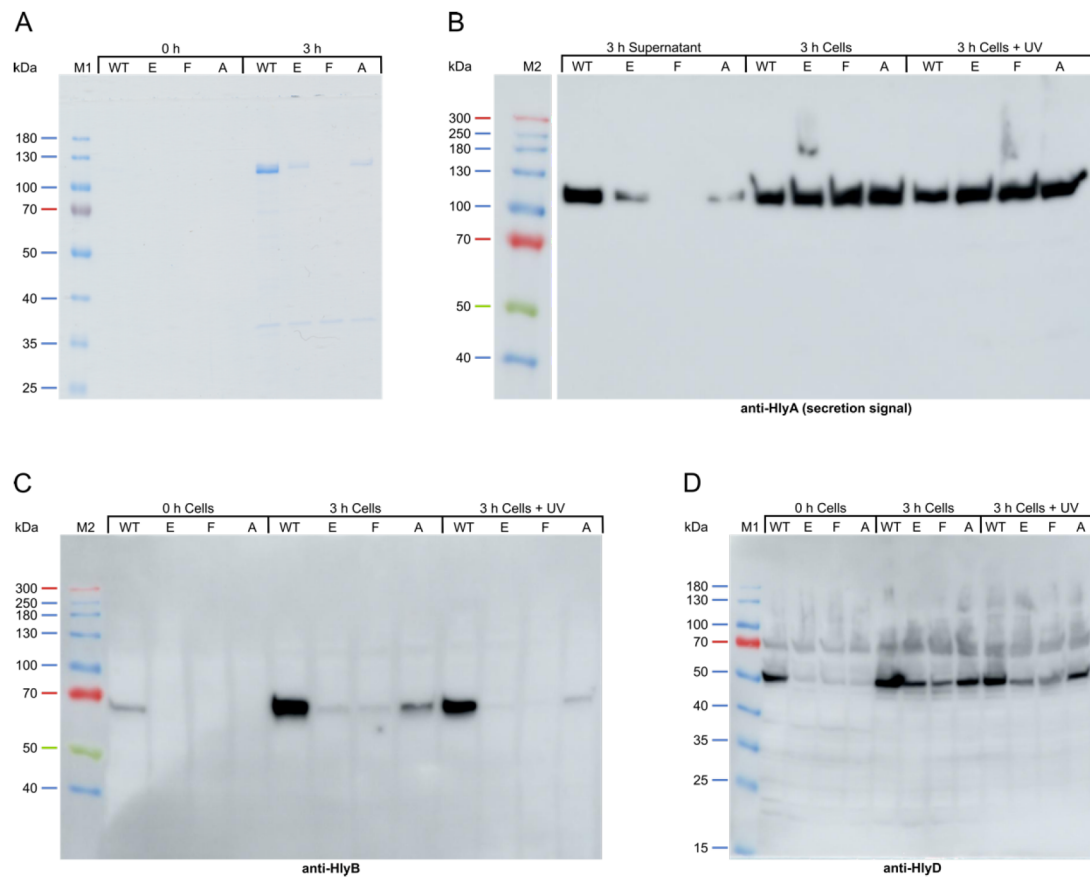


Figure S5: Secretion of HlyA by HlyB* amber mutants with incorporated Bpa as published (Zhao *et al.* 2022). HlyA, HlyD and HlyB* with an amber mutation at the position indicated above (WT: no amber mutation, E: E102*, F: F323*, A: A422*) were expressed in *E. coli* BL21(DE3). Samples were taken before (0 h) and 3 h after induction. Secretion of HlyA was analyzed via SDS-PAGE (**A**) and the presence of HlyA (**B**), HlyB (**C**) and HlyD (**D**) analyzed via immunoblot with respective antibodies. Abbreviations for the HlyB* variant are the same as in (**A**). The time after induction and fraction (cells or supernatant) are indicated above. "+UV" indicated samples which were UV irradiated at 365 nm for 15 min. M1: PageRuler Prestained Protein Ladder, M2: Spectra Multicolor High Range Protein Ladder.

3.4. Chapter 4: Type 1 secretion necessitates a tight interplay between all domains of the ABC transporter

Title:	Type 1 secretion necessitates a tight interplay between all domains of the ABC transporter
Authors:	Manuel T. Anlauf , Jens Reiners, Olivia Spitz, Eymen Hachani, Sander H.J. Smits, Lutz Schmitt
Published in:	(to be submitted)
Own proportion on this work:	75%
	Designing and cloning of plasmids
	Expression of proteins
	Secretion experiments
	Protein purification
	ATPase assays
	Data analysis and quantification
	Preparation of figures
	Writing of the manuscript

Type 1 secretion necessitates a tight interplay between all domains of the ABC transporter

Manuel T. Anlauf¹, Jens Reiners², Olivia Spitz^{1†}, Eymen Hachani¹,
Sander H.J. Smits^{1,2}, Lutz Schmitt^{1*}

¹Heinrich Heine University Düsseldorf, Faculty of Mathematics and Natural Sciences, Institute of Biochemistry, Universitätsstraße 1, 40225 Düsseldorf, Germany

²Heinrich Heine University Düsseldorf, Faculty of Mathematics and Natural Sciences, Center for Structural Studies, Universitätsstraße 1, 40225 Düsseldorf, Germany

[†]present address: INCONSULT, Duisburg, Germany

*Corresponding author: Lutz Schmitt, Heinrich Heine University Düsseldorf, Faculty of Mathematics and Natural Sciences, Institute of Biochemistry, Universitätsstraße 1, 40225 Düsseldorf, Germany, Tel.: +49 211 81-10773, E-Mail: lutz.schmitt@hhu.de

Abstract

Type I secretion systems (T1SS) facilitate the secretion of substrates in one step across both membranes of Gram-negative bacteria. A prime example is the hemolysin T1SS which secretes the toxin HlyA. Secretion is energized by the ABC transporter HlyB, which forms a complex together with the membrane fusion protein HlyD and the outer membrane protein TolC. HlyB features three domains: an N-terminal C39 peptidase-like domain (CLD), a transmembrane domain (TMD) and a C-terminal nucleotide binding domain (NBD). Here, we created chimeric transporters by swapping one or more domains of HlyB with the respective domain(s) of RtxB, a HlyB homolog from *Kingella kingae*. We tested all chimeric transporters for their ability to secrete pro-HlyA when co-expressed with HlyD. The CLD proved to be most critical, as a substitution abolished secretion. Swapping only the TMD or NBD reduced the secretion efficiency, while a simultaneous exchange abolished secretion. These results indicate that the CLD is the most critical secretion determinant, while TMD and NBD might possess additional recognition or interaction sites. This mode of recognition represents a hierarchical and extreme unusual case of substrate recognition for ABC transporters and optimal secretion requires a tight interplay between all domains.

Keywords

Type I secretion system, ABC transporter, hemolysin, substrate recognition

Introduction

Secretion, the transport of a substrate from the cytosol across the membrane to the extracellular space or even to the cytosol of the host cell, is used by bacteria for several processes, e.g. acquirement of nutrients by scavenging proteins, cell-to-cell communication via quorum sensing or infection of host cells using toxins or other virulence factors. Today, at least nine secretion systems were identified in Gram-negative bacteria¹⁻³. One of them, the type I secretion system (T1SS, reviewed in Holland *et al.*⁴) is considered to be a prototype system. It has a rather simple architecture consisting of an ATP binding cassette (ABC) transporter and a membrane fusion protein (MFP) residing in the inner membrane as well as an outer membrane protein (OMP) present in the outer membrane. Together they form a continuous channel, allowing the transport of various substrates ranging from small peptides to

huge S-layer proteins in an unfolded state in one step without the occurrence of a periplasmic intermediate⁵.

One of the best investigated T1SSs is the hemolysin system found in uropathogenic *Escherichia coli* (*E. coli*) strains^{6,7}. Its MFP is hemolysin D (HlyD), its OMP is TolC, and as a member of the T1SS sub-family 2, its ABC transporter is hemolysin B (HlyB), which contains an N-terminal C39 peptidase-like domain (CLD)⁸. Although inactive, the CLD was shown to modulate HlyB's activity and to be essential for the secretion by interacting with the C-terminal part of the substrate hemolysin A (HlyA) in its unfolded state⁸⁻¹¹. Sequence analysis revealed, that transporters involved in the secretion of Repeat in ToXin (RTX) proteins all carry such a CLD^{8,10}. Additionally, it was shown that the nucleotide binding domain (NBD) of HlyB interacts with the secretion signal of HlyA¹². A recent study identified two possible binding regions for HlyA in the NBD of HlyB as well as indications for a concerted binding of HlyA to both the CLD and NBD¹³. Only recently, the structure of the HlyB-HlyD complex was resolved by single particle cryo-EM¹⁴ and showed an unexpected stoichiometry composed of three HlyB dimers in complex with six HlyD.

HlyA is a 1,024 amino acids long pore-forming toxin and features several glycine-rich nonapeptide repeats (GG repeats), which are characteristic for the RTX domain and allow the binding of Ca²⁺ ions, which promotes the folding of the GG repeats into a β -roll¹⁵, but only in the extracellular space, since the bacterial intracellular Ca²⁺ concentration (approx. 300 nM) is several magnitudes lower than the K_D of HlyA (150 μ M)^{16,17}. HlyA is secreted via its C-terminal secretion signal, which is encoded within the last 48-60 amino acids and reaches the outside of the cell first¹⁸. Although research has focused on elucidation of common features for secretion signals of T1SS, universal conservation of the primary sequence does not exist⁴. This led to the suggestion, that the presence of a secondary structure element could be a prerequisite for a functional secretion signal. Multiple studies were performed to elucidate the presence of structural features in the signal sequence of HlyA and related proteins and the presence of an amphipathic helix was proven to be essential for the early steps of secretion¹⁹⁻²⁵.

The hemolysin system was shown to exhibit a considerable promiscuity for the secreted substrate. For instance, cells expressing *hlyBD* were able to secrete LktA from *Pasteurella haemolytica*²⁶, PaxA from *Pasteurella aerogenes*²⁷, CyaA from *Bordetella pertussis*²⁸, NodO from *Rhizobium leguminosarum*²⁹, FrpA from *Neisseria*

*meningitidis*³⁰, HlyA from *Actinobacillus pleuropneumoniae*³¹, AqxA from *Actinobacillus equuli*³² and MbxA from *Moraxella bovis*³³.

The above mentioned examples motivated us to further investigate the specificity of interactions between the substrate HlyA and the ABC transporter HlyB in this study. For this, we created different chimeras of HlyB (chHlyB) by swapping the CLD, transmembrane domain (TMD), NBD and/or combinations of these domains with the respective domain of a homologous T1SS ABC transporter from *Kingella kingae* (*K. kingae*), RtxB. *K. kingae* is a Gram-negative bacterium and an emerging pathogen infecting mainly young children, causing e.g. osteoarticular infections, septic arthritis and endocarditis³⁴⁻³⁶. Similar to *E. coli* and its hemolysin system, *K. kingae* is equipped with a T1SS and secretes the RTX protein RtxA³⁷. Secretion experiments using our chimeric transporters suggest that all three domains of HlyB seem to contain identity determinants for recognition and secretion of HlyA, with the CLD being the most critical one, suggesting a hierarchy with the individual interactions and tight interplay of the domains.

Results

In our search of suitable, homologous candidates for the domain swapping of HlyB, we applied the protein Basic Local Alignment Search Tool (pBLAST) using the primary sequence of HlyB (UniProt-ID: Q1R2T6). We specifically searched for transporters, which lacked a cysteine residue in the first 100 amino acids, as this classifies the transporter as a group 2 T1SS ABC transporter with a CLD, just like HlyB^{8,10}. After identification of such ABC transporters, the genome of the respective organism was scanned for the presence of a HlyD-like MFP using pBLAST with the sequence of HlyD (UniProt-ID: Q1R2T7) and for the presence of an RTX protein using pBLAST with the sequence of HlyA as a reference (UniProt-ID: P08715). Most organisms featured multiple proteins containing RTX motifs (noted in Supplementary Table S1). Organisms lacking an MFP or RTX protein were excluded from the list of interesting homologs. A total of 25 organisms identified were included for an alignment using Clustal Omega³⁸ (Supplementary Table S1). The resulting phylogenetic tree could be subdivided into four groups (see Supplementary Figure S1).

The ABC transporter RtxB from *K. kingae* has an identity of 71% when compared with HlyB. Taking a closer look on the domains of the ABC transporters, their TMDs and NBDs have the highest identity with 79% and 73% respectively, while the CLDs have an identity of only 48%. The toxin RtxA from *K. kingae* is composed of 956 amino acids and somewhat smaller than HlyA (1,024 amino acids), but still similar in size. The structural model for RtxA as predicted by AlphaFold2³⁹ as well as secondary structure predictions reveal an amphipathic helix similar to HlyA (Supplementary Figure S2, S3 and S4). However, the secretion signals (approx. the last 100 amino acids) of HlyA and RtxA have a very low identity of 23%, with the sequence identity of the entire proteins being not much higher (42%). The MFPs HlyD and RtxD show a similar identity level as the toxins with 40%. We chose the T1SS from *K. kingae* and RtxB as the source for the domain swapping approach of HlyB based on the level of sequence identities (Supplementary Figure S1). We also reasoned, that this combination was ideal to investigate the influence of the different ABC transporter domains on the substrate specificity without the risk of either no effect on secretion because of too high similarity, or inability to secrete with any domain combination because of too structurally different substrates.

We therefore created chimeric HlyB (chHlyB) variants by swapping one, two or all three domains with the respective domain of RtxB. The 3-letter nomenclature used for the

chimeras in this study is derived from the domains position; the first letter is designated for the N-terminal CLD, while the second and third letter represent the TMD and C-terminal NBD, respectively. The letter describes the origin of the domain, with ‘E’ being the domain from *E. coli* HlyB and ‘K’ being the one from *K. kingae* RtxB. For example, the ABC transporter ‘HlyB-EKE’ contains the N-terminal CLD and C-terminal NBD from HlyB, while the TMD is derived from RtxB. Likewise, HlyB-EEE is synonymous to HlyB and HlyB-KKK is synonymous to RtxB. A colored scheme for the transporter’s domain origin is provided above the respective SDS-PAGE and immunoblot analyses (Figure 1).

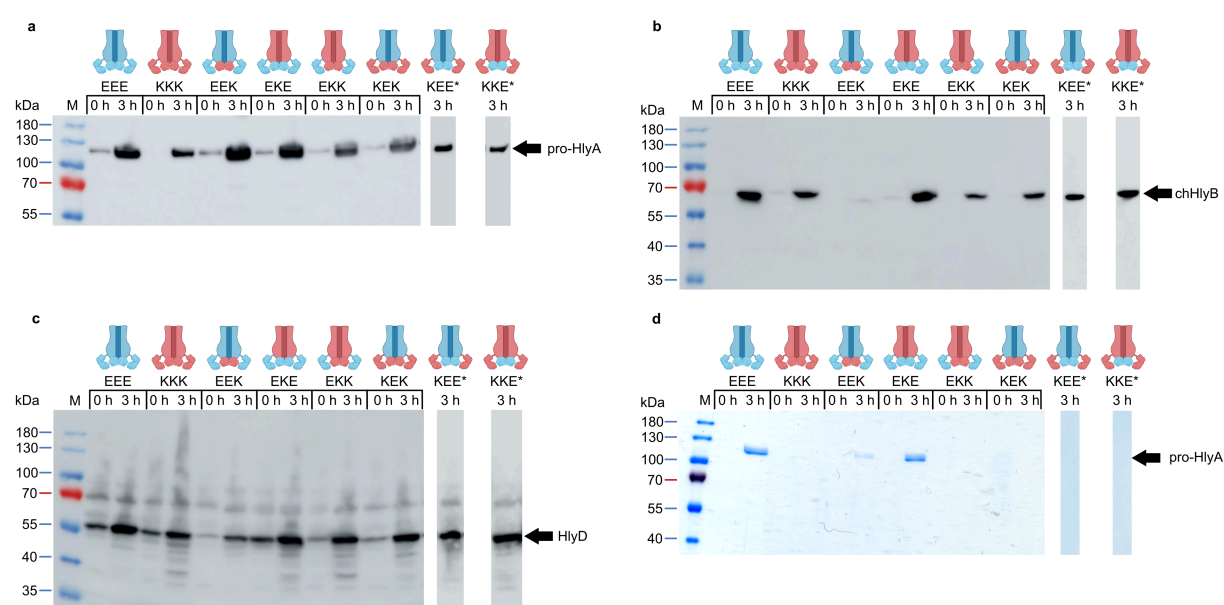


Figure 1: Secretion of pro-HlyA by chHlyB ABC transporters. Immunoblot analysis of whole *E. coli* cells expressing the indicated chHlyB show the presence of pro-HlyA (a), chHlyB (b) and HlyD (c). SDS-PAGE analysis (d) shows secreted pro-HlyA in the supernatant of *E. coli* cells expressing the different chHlyB, HlyD and pro-HlyA. The contrast of the SDS-PAGE in d was adjusted to improve visibility of secreted pro-HlyA in the case of HlyB-EEK. Schematic representation of the chHlyB variants are depicted above the respective chimera. Blue domains originate from HlyB (*E. coli*) and red domains from RtxB (*K. kingae*). Cell and supernatant samples were diluted to match the same OD₆₀₀. Note that samples marked with an asterisk are not from the same Western blot membrane. Uncropped Western blots and SDS-PAGE gels are shown in Supplementary Figure S5. M: Protein marker, the approximated molecular weight of the marker proteins is given on the left; x h: time after induction, when the samples were taken.

We tested the ability of all chHlyB and RtxB (HlyB-KKK) to secrete the inactive pro-HlyA when co-expressed with HlyD in *E. coli* BL21(DE3) and compared it to HlyB. The inactive pro-HlyA lacks the acylation of two internal lysine residues, which is installed prior to secretion by the acyltransferase HlyC⁴⁰. Immunoblot analysis targeting the secretion signal of pro-HlyA, the NBD of chHlyB or HlyD was performed to test for the expression of all proteins of the hemolysin T1SS. Only the presence of TolC was not

tested, as it is an endogenous protein and constitutively expressed in *E. coli*⁴¹⁻⁴⁴. Irrespective of the chHlyB variant, cells were able to express pro-HlyA (Figure 1a) and HlyD (Figure 1c). Cells expressing RtxB showed a slightly lower expression level of pro-HlyA. The expression level of HlyB-EEK was visibly reduced, and the co-expression of HlyD in the same cells was lower when compared to other chimeric transporters (Figure 1b). Overall, the signal intensity of transporters with the RtxB-NBD appeared reduced in comparison to transporters with the HlyB-NBD. All other cells were expressing HlyB, RtxB or chHlyB in comparable amounts. Nevertheless, not all HlyB variants were able to secrete pro-HlyA (Figure 1d). All transporter variants carrying the CLD from RtxB failed to secrete pro-HlyA. Only HlyB and the chimeras HlyB-EEK and HlyB-EKE showed a signal for pro-HlyA in the supernatant. For HlyB-EEK, the amount of secreted protein was often difficult to visualize using Coomassie staining (Figure 1d). Therefore, detection via immunoblot analysis was additionally carried out. Interestingly, exchanging either only the TMD or only the NBD of HlyB to the respective version of RtxB allowed the secretion of pro-HlyA. On the other hand, swapping both domains at the same time and only keeping the CLD of HlyB (EKK) still rendered the transporter unable to secrete pro-HlyA.

We focused on the transporters, which were competent in transporting pro-HlyA and aimed to quantify the secretion efficiencies for HlyB-EKE and HlyB-EEK in comparison to HlyB (HlyB-EEE). Since we noticed a reduced band intensity of transporters carrying the RtxB-NBD we intended to determine if the HlyB-NBD antibody recognized the NBD of RtxB with a reduced efficiency. Note that the anti-HlyB antibody was raised against the NBD of HlyB. For this, we overexpressed and purified the soluble RtxB-NBD with an N-terminal 6xHis-tag (theoretical molecular weight 27,676 Da) to homogeneity (Supplementary Table S2, Figure 2a and Supplementary Figure S7 and S8). We subjected pure HlyB-NBD and RtxB-NBD to an SDS-PAGE and quantified the intensity of the NBD signals with the HlyB-NBD antibody (Supplementary Figure S9). Even though equal amounts of protein were used in both cases, the signal intensity ratio between the RtxB-NBD and the HlyB-NBD was 0.36 ± 0.10 when using the HlyB-NBD antibody. Accordingly, the quantified secretion efficiency of HlyB-EEK was corrected using the aforementioned factor to account for the decreased recognition of the NBD from *K. kingae* by the used antibody.

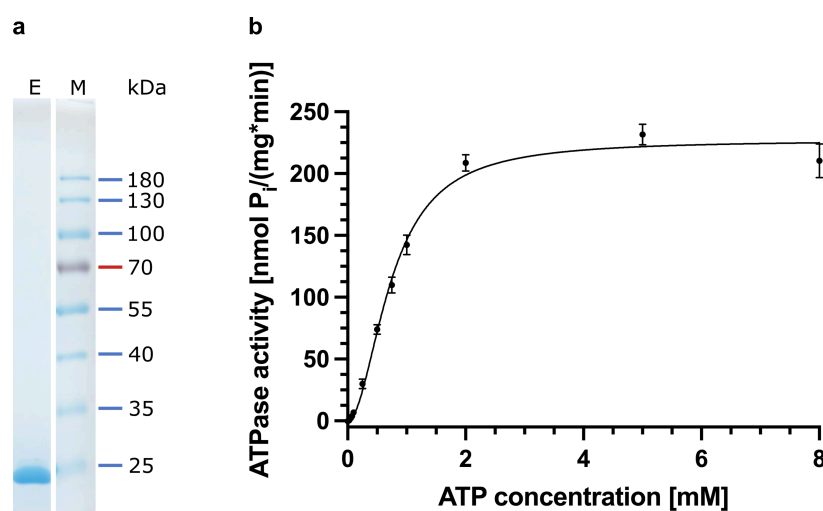


Figure 2: Analysis of purified RtxB-NBD. **(a)** SDS-PAGE analysis of purified RtxB-NBD. Shown is the elution fraction (E) after Size Exclusion Chromatography with Coomassie staining. Chromatograms of the purification and an uncropped SDS-PAGE analysis of additional samples are shown in Supplementary Figure S7. RtxB-NBD-NHis6 has a size of 27,676 Da. M: Protein marker, the approximated molecular weight of the marker proteins is given on the right. **(b)** ATPase activity of RtxB-NBD in dependency of varying ATP concentrations. The data was analyzed using the Hill equation. Shown are mean values and standard deviations as error bars of three independent experiments.

We repeated the secretion experiments with HlyB, HlyB-EKE and HlyB-EEK to determine relative secretion efficiencies. For this, we quantified the amount of pro-HlyA secreted into the supernatant (Figure 3a and b) as well as the amount of the HlyB variants in whole cells (Figure 3c). Normalizing the protein amounts of the chimeric ABC transporters as well as the secreted pro-HlyA to the ones of HlyB-EEE, and dividing the amount of secreted pro-HlyA by the amount of chHlyB in the cells, allowed the determination of relative secretion efficiencies (Figure 3d). With this approach, the secretion efficiency of HlyB-EEE was set to 1.0. For both, HlyB-EKE and HlyB-EEK, secretion was reduced by a factor of approximately three. The calculations were performed with secreted pro-HlyA quantified by immunoblot analysis (HlyB-EKE: 0.41 ± 0.22 ; HlyB-EEK: 0.35 ± 0.16) and from Coomassie stained gels (HlyB-EKE: 0.30 ± 0.20 ; HlyB-EEK: 0.30 ± 0.22). The reason for the reduced secretion of HlyB-EKE and -EEK seem to be different and synergistic, as the secretion of pro-HlyA by the chimera HlyB-EKK, in which both substitutions of the TMD and NBD were combined, was completely abolished (Figure 1).

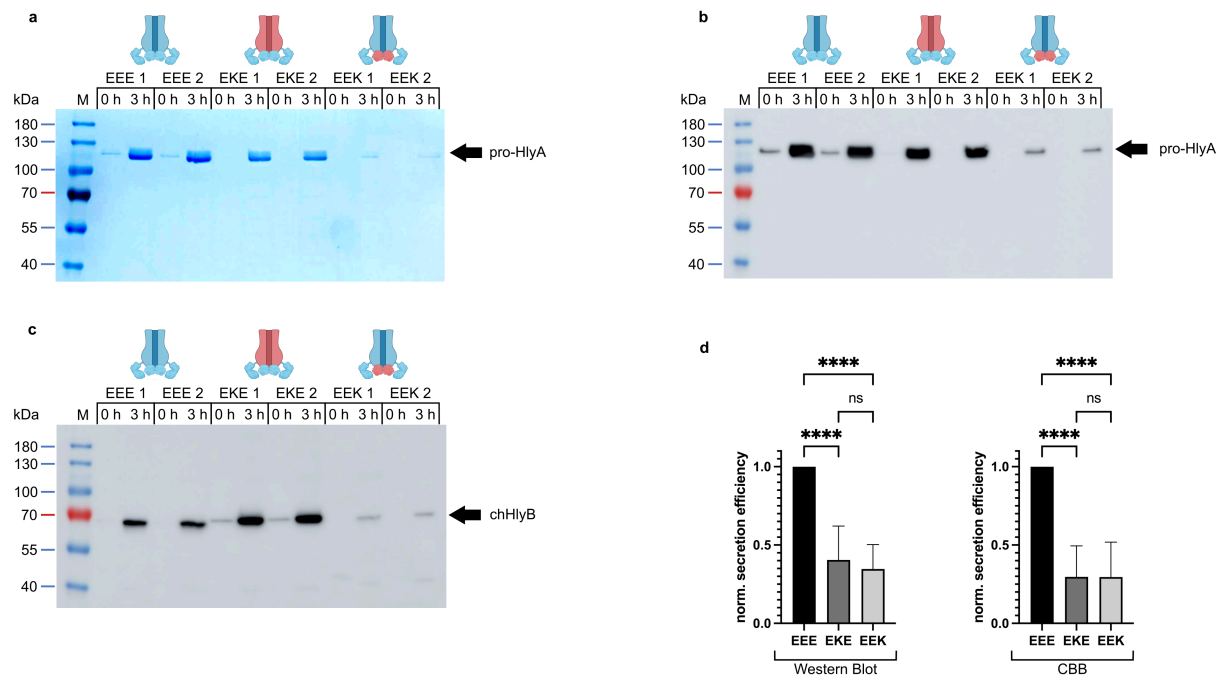


Figure 3: Quantification of chHlyB expression and pro-HlyA secretion. SDS-PAGE (a) and immunoblot analysis (b) of pro-HlyA from supernatants of *E. coli* cells expressing the indicated chHlyB and HlyD in two replicates; the used antibody targeted the secretion signal of pro-HlyA. Immunoblot (c) of whole *E. coli* cells show the amount of expressed chHlyB in two replicates; the used antibody targeted the NBD of chHlyB. The samples were diluted to match the same OD₆₀₀. The contrast of the SDS-PAGE in a was adjusted to improve visibility of secreted pro-HlyA in the case of HlyB-EEK. Schematic representation of the chHlyB variants are depicted above the respective chimera. Blue domains originate from HlyB (*E. coli*) and red domains from RtxB (*K. kingae*). The quantification revealed reduced secretion efficiencies for both HlyB-EKE (dark grey) and HlyB-EEK (light grey) by a factor of ~3 when compared to HlyB-EEE (black) (d). The left panel shows the calculations using signals from Western blots for quantifications of pro-HlyA, while the right panel shows quantifications using Coomassie stained gels (CBB). Shown are the mean values with standard deviations as error bars (n ≥ 16, biological replicates). Statistical analysis was performed using a one-way ANOVA test (****: p < 0.0001, ns: p = 0.5138 for EKE vs. EEK (Western Blot) and p = 0.9995 for EKE vs. EEK (CBB)). Uncropped Western Blots and SDS-PAGE gels are shown in Supplementary Figure S6. M: Protein marker, the approximated molecular weight of the marker proteins is given on the left; x h: time after induction, when the samples were taken.

Table 1: Kinetic parameters determined for RtxB-NBD. The maximum enzyme velocity (v_{\max}), the substrate concentration at half maximal enzyme velocity ($K_{0.5}$) as well as the Hill coefficient (h) are displayed for RtxB-NBD and compared to the parameters of HlyB-NBD¹³.

Kinetic parameter	RtxB-NBD	HlyB-NBD ¹³
v_{\max} [nmol P _i mg ⁻¹ min ⁻¹]	227.0 ± 2.9 (s.d.)	253.8 ± 7.6
$K_{0.5}$ [mM]	0.74 ± 0.02 (s.d.)	0.49 ± 0.03
h	1.96 ± 0.10 (s.d.)	1.66 ± 0.15

Next, we examined, if the reduced secretion of pro-HlyA by HlyB-EEK could be ascribed to a decreased ATP hydrolysis rate. For this, the ATPase activity of RtxB-NBD was determined colorimetrically (Figure 2b) using equation (1). The kinetic parameters are summarized in Table 1 and compared to the HlyB-NBD¹³. For RtxB-

NBD, the maximum velocity (v_{\max}) was calculated to be 227.0 ± 2.9 nmol P_i mg^{-1} min^{-1} and therefore comparable to the maximum velocity of 253.8 ± 7.6 nmol P_i mg^{-1} min^{-1} for HlyB-NBD¹³. Both the hill coefficient ($h = 1.96 \pm 0.10$) and the ATP concentration providing half the maximum velocity ($K_{0.5} = 0.74 \pm 0.02$ mM) of RtxB-NBD were slightly increased compared to HlyB-NBD ($h = 1.66 \pm 0.154$; $K_{0.5} = 0.49 \pm 0.026$ mM)¹³. Still, these differences in kinetic parameters are only minor and do not explain the major reduction in HlyA secretion efficiency of HlyB-EEK.

Discussion

The hemolysin system is often referred to as the prototypic T1SS. Its ABC transporter HlyB is enabling the active transport of the toxin HlyA by binding and hydrolyzing ATP through its NBD. The TMD is anchoring the transporter in the inner membrane and forming the translocation channel, as shown by crosslinking studies and the recently published structure of the HlyB-HlyD complex^{11,14}, while the CLD is important for substrate recognition and modulation of hydrolytic activity^{10,11}. Recent studies also showed that the NBD of HlyB is also interacting with its substrate, thus not only energizing the secretion process^{12,13}. The secretion signal sequence with a putative amphipathic helix within HlyA is of utmost importance for this interaction²⁵. HlyB has shown to exhibit at least some promiscuity in recognizing and secreting substrates²⁶⁻³³. Here, we have used chimeric transporters of the T1SS from *E. coli* and *K. kingae* to shed light onto specificity determinants within the domains of the transporter HlyB for the recognition and secretion of its substrate HlyA.

Our secretion assays highlight that the CLD is the most important specificity determinant for the secretion of HlyA (Figure 1). No pro-HlyA was detectable in supernatant samples of chHlyB, in which the CLD was exchanged to the one of RtxB, a HlyB homolog from *K. kingae*. Former investigations showed that the deletion of the CLD from HlyB renders the transporter unable to secrete¹⁰. The same study showed a specific interaction of the CLD with the unfolded RTX domain of HlyA. Even though RtxA and HlyA share the same number of GG repeats in their RTX domains and the fold of RTX domains is conserved, the premise for the CLD-substrate interaction seems to be the exact amino acid sequence. This assumption is supported by the facts, that HlyA is present in an unfolded state in the cytoplasm and that the binding of the HlyB-CLD was only observed with unfolded HlyA¹⁰, indicating that the RTX fold

itself is not recognized. Furthermore, the CLD possesses the lowest identity of all three domains when HlyB is compared to RtxB. Therefore, it is likely that the CLD evolved to specifically recognize its associated substrate and the simple presence of a CLD, even a homologous one, is not sufficient for recognition and secretion of the endogenous substrate.

The secretion experiments further revealed, that HlyB tolerated the non-simultaneous swapping of either the TMD (HlyB-EKE) or NBD (HlyB-EEK) to the respective one from RtxB (Figures 1 and 3). The single-substitutions were accompanied by a decrease of HlyA secretion with a similar factor when normalized to the expression level of the chimeric ABC transporter. Both domain swaps are likely to affect different aspects or steps of the HlyA secretion process, since combination of both substitutions into HlyB-EEK resulted in a transporter completely deficient in HlyA secretion. A lesser activity of the RtxB-NBD as a cause for the reduced secretion efficiency with HlyB-EEK is unlikely, since we purified the RtxB-NBD to homogeneity (Figures 2, S5 and S6) and the determined kinetic parameters show an activity similar to HlyB-NBD (Table 1). Admittedly, the full-length RtxB might behave differently from the isolated domain. A recent study identified binding pockets for HlyA within the NBD of HlyB and a simultaneous binding of HlyA to the CLD and NBD of HlyB¹³.

The reduced secretion efficiency of HlyB-EKE could be ascribed to additional critical interaction point(s) for HlyA within the TMD of HlyB, which are missing in the RtxB-TMD. Crosslinking studies already confirmed HlyA to travel through the channel formed by the HlyB-TMD^{11,14}. So far it is not known, if the identified positions are critical interaction points or merely residues to which HlyA is in close proximity during the passage of the TMD. The classical view of ABC transporters and their specificity suggests a substrate binding pocket within the TMD in the inward facing conformation⁴⁵. It is unlikely that the binding of HlyD to the chimeric transporter or that the multimeric complex assembly is affected: The identity of both MFPs HlyD and RtxD might be rather low with 40%. However, the cryo-EM structure of the HlyB-HlyD complex demonstrated, that the main interactions stabilizing the components in the inner membrane are provided by a cluster of acidic residues in HlyD and five basic residues in the CLD of HlyB¹⁴. Four of these five basic residues (K56, K58, R66 and R128) are also conserved in the CLD of RtxB and only one lysine, K62, is a glutamine in RtxB (Figure 4a and b). Zhao *et al.* could show that complex assembly is rather stable as single substitutions of those basic residues did not affect the secretion of

HlyA and only combinations of at least two substitutions resulted in a reduced or abolished secretion¹⁴. Additional contacts are made between the N-terminal region of HlyD and the transmembrane helices 1 and 2 of HlyB. Comparing the sequences of RtxB and HlyB, all of these residues are either identical or substituted by another hydrophobic amino acid¹⁴. Pimenta *et al.* showed that the stability of HlyD is diminishing in the absence of HlyB (or TolC), most likely because HlyD is unstable in the absence of the other proteins of the secretion complex⁴⁶. We noticed bands with smaller molecular weight for some of the chimeric transporters, but not to an extent as shown by Pimenta *et al.* or when we expressed a Strep-tagged variant of HlyD without HlyB present (Supplementary Figure S10). Furthermore, the amount of degradation did not coincide with the observed secretion behavior. For example, HlyD showed less degradation in cells expressing HlyB-KEK, -KEE and -KKE (with which secretion of pro-HlyA was abolished) when compared to cells expressing HlyB-EKE or -EKK (the former was able to secrete pro-HlyA, while the latter was not, see Figure 1c). Pimenta *et al.* noted, that HlyD is inherently prone to degradation, even in the presence of all transport components⁴⁶, and we detected degradation bands of HlyD in cells expressing the wildtype transporter HlyB as well (Figure 1c). HlyD on its own is only stably expressed when N-terminally truncated⁴⁷. We therefore conclude, that the assembly of the secretion system is not affected and that the observed secretion behavior of the chimeric transporters is due to affected interaction with the substrate.

a

```

      60           128
      |           |
HlyB - KVKQVKKTIDR...R
RtxB - KAKVVKQPISR...R
      |           |
      60           129

```

b

```

    148    160    170    200    210
    |      |      |      |      |
HlyB - II...VVSFVLQLFALI...VALSVVVVFEEIILSGL
RtxB - VI...LVSFVLQIFALI...VALLVVSLEFIMLGGL
    148    160    170    200    210

```

Figure 4: Comparative view on the CLD and TMD of HlyB and RtxB. Basic residues in the CLD (a) and hydrophobic residues in the TMD (b) of HlyB, which are involved in interactions with HlyD, are marked in yellow¹⁴. The respective residues in RtxB are highlighted as bold letters. A pairwise sequence alignment was performed using the GGSEARCH2SEQ tool³⁸.

This study used chimeric transporters of HlyB, where one or more complete domains were swapped to the RtxB domains. With this, a detailed mapping of interaction sites within HlyB to HlyA, especially within the TMD and NBD, is not possible yet. This may be achieved by substituting only specific amino acids or patches of HlyB instead. The exchange of whole domains bears the risk of a non-native domain organization, which could influence functionality of the transporter, especially for fine-tuned interactions of the NBD and TMD via for example their coupling helix. Should this interaction be affected, e.g. for chimeras HlyB-EKE or HlyB-EEK, then the use of both RtxB domains (TMD and NBD) should grant full functionality. This is not the case, as we observed the opposite and secretion with HlyB-EKK was abolished (Figure 1). Our domain swapping strategy demonstrated that HlyB shows a hierarchical substrate recognition involving all three domains with the CLD, although lacking peptidase activity, being the most important factor for the secretion of the substrate HlyA. This is an unusual mode of action, as the classical ABC transporter binding pocket is located within the TMD^{48,49}. A similar multi-domain interaction was reported for the Has system from *Serratia marcescens*⁵⁰. However, this T1SS belongs to another subgroup and works fundamentally different compared to the HlyA system⁸: i) the ABC transporter HasD has the classical architecture with no additional N-terminal domain, ii) the substrate HasA is considerably smaller (~19 kDa), which features no RTX motifs, iii) HasA is not secreted with its C-terminus first, but with its N-terminus first, iv) the secretion signal is not involved in the assembly of the secretion complex, but its disassembly, v) secretion of HasA is dependent on the general chaperone SecB, while no chaperones are known for the HlyA T1SS^{8,50,51}. The identity of the TMD also plays a role in the recognition and/or secretion of HlyA by HlyB, but to a lesser extent when compared to ABC transporters, which translocate smaller molecules, like the multidrug resistance transporters MRP1 and PDR5^{52,53} or the lipopolysaccharide transporter LptB₂FGC⁵⁴. Equally important for the secretion is the identity of the NBD. Thus, one can speculate that the substantially larger substrate HlyA (110 kDa) might have necessitated multiple recognition sites in the transporter for a controlled secretion process.

Acknowledgements

We thank all former and current members of the Institute of Biochemistry for their support and productive discussions. We are indebted to Isabelle Erenburg for initial bioinformatic work and identification of the T1SS of *K. kingae*. We also thank Cigdem Günes for preliminary work with the chimeric HlyB transporters. We acknowledge DESY (Hamburg, Germany), a member of the Helmholtz Association HGF, for the provision of experimental facilities. Parts of this research were carried out at PETRA III and we would like to thank Dmytro Soloviov (EMBL Hamburg) for the assistance in using beamline P12.

Funding

This work was supported by the Deutsche Forschungsgemeinschaft (DFG, CRC 1208 project A01 to LS). The Center for Structural studies is funded by the DFG (Grant number 417919780 and INST 208/761-1 FUGG to SS).

Author contribution

SS and LS conceived and coordinated this study. MA constructed the plasmids stated in this study and conducted expression, purification and secretion experiments. MA determined ATPase activities and secretion efficiencies. MA and OS performed sequence alignments. JR collected and analyzed the SAXS data. MA wrote the initial version of the manuscript. JR prepared Figure S8, OS prepared Figure S1, EH prepared Figure S10, MA prepared the remaining Figures. MA, SS, and LS wrote the final version of the manuscript.

Data availability

We uploaded the SAXS data to the Small Angle Scattering Biological Data Bank (SASBDB)⁵⁵, with the accession code **SASDS56**.

Competing interests

The authors declare no competing interests

Material and Methods

Bacterial strains and plasmids

Escherichia coli DH5 α cells were used for cloning, *E. coli* BL21(DE3) cells were used for overexpression, purification and secretion experiments. Plasmids and oligonucleotides used are listed in Supplementary Table S3 and S4 respectively. The gene encoding for *rtxB* was isolated from the genome of *K. kingae* ATCC 23330 (DSM 7536) and ordered from the German Collection of Microorganisms and Cell Cultures GmbH (DSMZ).

Construction of plasmids

The pK184-RtxB-HlyD plasmid as well as plasmids containing chimeric transporters were generated using Gibson assembly⁵⁶. For this, pK184-HlyBD was amplified either without the domains of *hlyB* to be exchanged or without the complete gene *hlyB*. Additionally, the gene or domains of RtxB (UniProt-ID: F5S9L7) to be inserted were amplified from the genome of *K. kingae* (DSM 7536) with overlaps to the aforementioned pK184 plasmid. The purification plasmid pPSG122-RtxB-NBD-NHis6 was constructed similarly by amplifying the backbone of pPSG122-HlyB-NBD-NHis6⁵⁷ without the *hlyB* NBD with overlaps to *rtxB* NBD. All oligonucleotides were purchased from Sigma-Aldrich and diluted in MilliQ water. All PCRs were performed using Q5 DNA polymerase with subsequent DpnI digestion and DNA purification using the Monarch PCR & DNA cleanup kit (all from New England Biolabs). The NucleoSpin plasmid miniprep kit was purchased from Macherey-Nagel and DNA sequencing performed at Microsynth Seqlab.

Protein expression for secretion experiments

E. coli BL21(DE3) chemically competent cells were first transformed⁵⁸ with pSU2726-HlyA and grown on 2xYT agar plates supplemented with 100 $\mu\text{g ml}^{-1}$ ampicillin. A mixture of transformed clones was used to generate a new batch of chemically competent *E. coli* BL21(DE3) cells for a second transformation with one of the pK184 plasmids carrying the genes for *hlyD* and (chimeric) *hlyB* or *rtxB*. Cells were grown on 2xYT agar plates supplemented with 100 $\mu\text{g ml}^{-1}$ ampicillin and 30 $\mu\text{g ml}^{-1}$ kanamycin. Single clones were used to prepare a pre-culture in 5 ml 2xYT medium and cultivated overnight (37°C and 180 rpm). The pre-culture was used to inoculate 50 ml of 2xYT medium at an OD₆₀₀ of 0.1 in a 300 ml unbaffled shaking flask. Cultures were incubated

at 37°C and 180 rpm to an OD₆₀₀ of 0.8-1.0 and protein expression induced by addition of 1 mM IPTG (isopropyl-β-D-thiogalacto-pyranoside); additionally, 4 mM CaCl₂ was added to the media to initiate folding of secreted HlyA. Expression took place for up to 3 h and 1 ml samples were taken and OD₆₀₀ was measured as well. The supernatant was separated from the cells by centrifugation for 2 min at 13,000 xg at room temperature (RT). The cells were resuspended in MilliQ water to normalize the samples in respect of their OD₆₀₀, the same was performed for the supernatants by dilution with MilliQ water. Both cells and supernatant samples were mixed with SDS sample buffer containing 40 mM DTT.

The samples were subjected to an SDS-PAGE with subsequent immunoblot analysis. Before, SDS samples were heated for 5 min to 95°C. Western blots were performed either in semi-dry (Trans-Blot Turbo, Bio-Rad) or wet blot (Criterion, Bio-Rad). The SDS-PAGE gels were stained using Quick Coomassie Stain solution (Protein Ark). Band intensities of (chimeric) HlyB or RtxB, HlyD and secreted HlyA were quantified from Western blots and Coomassie stained gels using Fiji (version 2.0.0-rc-69/1.52p)⁵⁹. Antibodies used are listed in Supplementary Table S5. Band intensities of HlyA and chHlyB from cells expressing RtxB or chimeric HlyB were normalized to the band intensity of HlyB expressing cells.

Protein expression and purification of RtxB-NBD

Expression and purification of the NBD from RtxB were performed as described previously for the NBD from HlyB⁶⁰ with slight modifications. In brief, *E. coli* BL21(DE3) was transformed with pPSG122-HlyB-NBD-NHis6 and grown on 2xYT agar plates supplemented with 100 µg ml⁻¹ ampicillin. Several clones were added to 50 ml 2xYT medium supplemented with 100 µg ml⁻¹ ampicillin for a pre-culture and incubated overnight at 37°C and 180 rpm. The pre-culture was used to inoculate 2 l of 2xYT supplemented with 100 µg ml⁻¹ ampicillin to an OD₆₀₀ of 0.1 in a 5 l baffled shaking flask. Cultures were incubated at 37°C and 160 rpm to an OD₆₀₀ of 0.6-0.8. The flasks containing the cells were cooled on ice for 20 min. Protein expression was induced by addition of 1 mM L-arabinose and expression took place for 3 h with shaking at 160 rpm and 20°C.

Cells were harvested by centrifugation at 5,488 xg for 30 min and 4°C and afterwards resuspended in buffer A1 (25 mM sodium phosphate, 100 mM potassium chloride, 10 mM imidazole, 20% (v/v) glycerol, pH 8). Cells from a total of 6 l expression were

used for purification and a cOMplete protease inhibitor cocktail (Sigma-Aldrich) as well as DNase (Sigma-Aldrich) were added. Cells were disrupted by passing them three times through a Microfluidizer M-110P (Microfluidics) at 1.5 kbar. Centrifugation for 90 min at 140,000 xg and 4°C was used to remove undisrupted cells and cell debris. The supernatant was loaded onto a 5 ml HiTrap Chelating HP column (Cytiva) which was pre-charged with Zn^{2+} and equilibrated with buffer A1. The column was washed with 50 ml buffer A until baseline absorption was reached and the elution was started with a linear gradient over 90 min using buffer A2 (25 mM sodium phosphate, 100 mM potassium chloride, 300 mM imidazole, 20% (v/v) glycerol, pH 8). Fractions containing RtxB-NBD were pooled and concentrated to a final volume of 5 ml using an Amicon Ultra-15 centrifugal filter (MWCO = 10,000 Da, Merck Millipore). The protein solution was centrifuged for 30 min at 17,000 xg and 4°C and subjected to a size exclusion chromatography using a Superdex 200 HiLoad 16/60 prep grade (Cytiva) and buffer B1 (10 mM CAPS-NaOH, 20% (v/v) glycerol, pH 10.4). Again, fractions containing pure RtxB-NBD were pooled and concentrated using an Amicon Ultra-15 centrifugal filter (MWCO = 10,000 Da, Merck Millipore). During this concentration step, the buffer was exchanged step-wise to buffer B2 (100 mM CAPS-NaOH, 20% (v/v) glycerol, pH 10.4). The protein was stored at 4°C and showed no signs of precipitation even after 4 months.

ATPase activity assays

ATPase activity was determined using a colorimetric assay as described previously⁶¹ with minor modifications. In brief, the concentrated and purified RtxB-NBD was diluted in buffer C (100 mM HEPES, 20% (v/v) glycerol, pH 7) directly before starting the reaction to a final concentration of 30 $\mu\text{g ml}^{-1}$. For each reaction, 6 μl of 50 mM MgCl_2 and 6 μl of ATP solution (final concentrations ranging from 0-8 mM in buffer C) were mixed with 18 μl of RtxB-NBD protein solution (50 $\mu\text{g ml}^{-1}$). For negative controls, buffer C was added instead of MgCl_2 . The reactions were started with the addition of the RtxB-NBD protein solution.

The ATPase reaction mixture was incubated for 90 min at 25°C and stopped by transferring 25 μl of the reaction mixture to 175 μl of pre-cooled 10 mM H_2SO_4 in a 96 well plate. Subsequently, fresh staining solution was prepared (0.096% (w/v) malachite green, 1.48% (w/v) ammonium molybdate, 0.173% (v/v) Tween-20 in 2.36 M H_2SO_4) and 50 μl were added. The solution was incubated for 9 min at RT. The amount of free

inorganic phosphate was determined by measuring the absorbance at 595 nm using a micro plate reader (iMark Microplate Reader, Bio-Rad). On the same plate, a calibration of the phosphate concentration was performed using Na₂HPO₄ with concentrations ranging from 0-500 µM. Data was analyzed using GraphPad Prism 9 Software (GraphPad) and fitted using equation (1), the Hill equation:

$$v = \frac{v_{max}[S]^h}{K_{0.5}^h + [S]^h} \quad (1)$$

Here, v corresponds to the enzyme velocity, v_{max} is the maximum enzyme velocity, $[S]$ is the substrate concentration, h is the Hill coefficient and $K_{0.5}$ is the substrate concentration, at which half of the enzymes maximum velocity is reached.

Sequence alignments

Proteins and putative T1SS homologous to the hemolysin system were identified using pBLAST⁶². The sequences that were used as a reference were taken from UniProt with the following UniProt-IDs: HlyB: Q1R2T6, HlyD: Q1R2T7, HlyA: P08715, HlyC: Q1R2T4. The alignments as well as the phylogenetic tree were created with Clustal Omega³⁸.

For comparison of the individual ABC transporter domains from HlyB and RtxB, pairwise protein sequence alignments were performed using the GGSEARCH2SEQ tool³⁸. The sequence for RtxB was taken from UniProt (UniProt-ID: F5S9L7).

Structure predictions of RtxA and HlyA using AlphaFold2

Secondary structure prediction of the secretion signal sequences of HlyA and RtxA were performed using the Quick2D tool⁶³. The helical wheel projections were performed with NetWheel⁶⁴.

The structure of HlyA from *E. coli* (UniProt-ID: P08715) was predicted using AlphaFold2³⁹ with standard settings. The structure of RtxA is accessible via the AlphaFold identifier AF-A1YKW7-F1.

References

1. Bhoite, S., Van Gerven, N., Chapman, M. R. & Remaut, H. Curli biogenesis: bacterial amyloid assembly by the type VIII secretion pathway. *EcoSal Plus* **8** (2019).
2. Costa, T. R. *et al.* Secretion systems in gram-negative bacteria: structural and mechanistic insights. *Nat. Rev. Microbiol.* **13**, 343-359 (2015).
3. Gorasia, D. G., Veith, P. D. & Reynolds, E. C. The type IX secretion system: advances in structure, function and organisation. *Microorganisms* **8**, 1173 (2020).
4. Holland, I. *et al.* Type I protein secretion-deceptively simple yet with a wide range of mechanistic variability across the family. *EcoSal Plus* **7**, 1-46 (2016).
5. Delepelaire, P. Type I secretion in gram-negative bacteria. *Biochim. Biophys. Acta, Mol. Cell Res.* **1694**, 149-161 (2004).
6. Lovell, R. & Rees, T. A filterable haemolysin from *Escherichia coli*. *Nature* **188**, 755-756 (1960).
7. Nicaud, J.-M., Mackman, N., Gray, L. & Holland, I. Regulation of haemolysin synthesis in *E. coli* determined by HLY genes of human origin. *Mol. Gen. Genet.* **199**, 111-116 (1985).
8. Kanonenberg, K., Schwarz, C. K. & Schmitt, L. Type I secretion systems—a story of appendices. *Res. Microbiol.* **164**, 596-604 (2013).
9. Lecher, J. *et al.* 1 H, 15 N and 13 C resonance assignment of the N-terminal C39 peptidase-like domain of the ABC transporter haemolysin B (HlyB). *Biomol. NMR Assign.* **5**, 199-201 (2011).
10. Lecher, J. *et al.* An RTX transporter tethers its unfolded substrate during secretion via a unique N-terminal domain. *Structure* **20**, 1778-1787 (2012).
11. Reimann, S. *et al.* Interdomain regulation of the ATPase activity of the ABC transporter hemolysin B from *E. coli*. *Biochem. J.* **473**, 2471-2483 (2016).
12. Benabdelhak, H. *et al.* A specific interaction between the NBD of the ABC-transporter HlyB and a C-terminal fragment of its transport substrate haemolysin A. *J. Mol. Biol.* **327**, 1169-1179 (2003).
13. Pourhassan, Z., Hachani, E., Spitz, O., Smits, S. H. & Schmitt, L. Investigations on the substrate binding sites of hemolysin B, an ABC transporter, of a type 1 secretion system. *Front. Microbiol.* **13**, 1-15 (2022).
14. Zhao, H., Lee, J. & Chen, J. The hemolysin A secretion system is a multi-engine pump containing three ABC transporters. *Cell* **185**, 3329-3340 (2022).
15. Bumba, L. *et al.* Calcium-driven folding of RTX domain β -rolls ratchets translocation of RTX proteins through type I secretion ducts. *Mol. Cell* **62**, 47-62 (2016).
16. Jones, H. E., Holland, I., Baker, H. L. & Campbell, A. K. Slow changes in cytosolic free Ca^{2+} in *Escherichia coli* highlight two putative influx mechanisms in response to changes in extracellular calcium. *Cell Calcium* **25**, 265-274 (1999).

17. Sanchez-Magraner, L. *et al.* The calcium-binding C-terminal domain of *Escherichia coli* α -hemolysin is a major determinant in the surface-active properties of the protein. *J. Biol. Chem.* **282**, 11827-11835 (2007).
18. Lenders, M. H. *et al.* Directionality of substrate translocation of the hemolysin A type I secretion system. *Sci. Rep.* **5**, 12470 (2015).
19. Hui, D. & Ling, V. A combinatorial approach toward analyzing functional elements of the *Escherichia coli* hemolysin signal sequence. *Biochemistry* **41**, 5333-5339 (2002).
20. Hui, D., Morden, C., Zhang, F. & Ling, V. Combinatorial analysis of the structural requirements of the *Escherichia coli* hemolysin signal sequence. *J. Biol. Chem.* **275**, 2713-2720 (2000).
21. Koronakis, V., Koronakis, E. & Hughes, C. Isolation and analysis of the C-terminal signal directing export of *Escherichia coli* hemolysin protein across both bacterial membranes. *EMBO J.* **8**, 595-605 (1989).
22. Stanley, P., Koronakis, V. & Hughes, C. Mutational analysis supports a role for multiple structural features in the C-terminal secretion signal of *Escherichia coli* haemolysin. *Mol. Microbiol.* **5**, 2391-2403 (1991).
23. Yin, Y., Zhang, F., Ling, V. & Arrowsmith, C. H. Structural analysis and comparison of the C-terminal transport signal domains of hemolysin A and leukotoxin A. *FEBS Lett.* **366**, 1-5 (1995).
24. Zhang, F., Yin, Y., Arrowsmith, C. H. & Ling, V. Secretion and circular dichroism analysis of the C-terminal signal peptides of HlyA and LktA. *Biochemistry* **34**, 4193-4201 (1995).
25. Spitz, O. *et al.* Identity determinants of the translocation signal for a type 1 secretion system. *Front. Physiol.* **12**, 1-13 (2022).
26. Chang, Y.-F., Young, R., Moulds, T. L. & Struck, D. K. Secretion of the *Pasteurella* leukotoxin by *Escherichia coli*. *FEMS Microbiol. Lett.* **60**, 169-173 (1989).
27. Kuhnert, P., Heyberger-Meyer, B., Nicolet, J. & Frey, J. Characterization of PaxA and its operon: a cohemolytic RTX toxin determinant from pathogenic *Pasteurella aerogenes*. *Infect. Immun.* **68**, 6-12 (2000).
28. Masure, H. R., Au, D. C., Gross, M. K., Donovan, M. G. & Storm, D. R. Secretion of the *Bordetella pertussis* adenylate cyclase from *Escherichia coli* containing the hemolysin operon. *Biochemistry* **29**, 140-145 (1990).
29. Scheu, A. *et al.* Secretion of the *Rhizobium leguminosarum* nodulation protein NodO by haemolysin-type systems. *Mol. Microbiol.* **6**, 231-238 (1992).
30. Thompson, S. A. & Sparling, P. The RTX cytotoxin-related FrpA protein of *Neisseria meningitidis* is secreted extracellularly by meningococci and by HlyBD+ *Escherichia coli*. *Infect. Immun.* **61**, 2906-2911 (1993).
31. Gygi, D. *et al.* Isolation of the *Actinobacillus pleuropneumoniae* haemolysin gene and the activation and secretion of the prohaemolysin by the HlyC, HlyB and HlyD proteins of *Escherichia coli*. *Mol. Microbiol.* **4**, 123-128 (1990).

32. Berthoud, H., Frey, J. & Kuhnert, P. Characterization of Aqx and its operon: the hemolytic RTX determinant of *Actinobacillus equuli*. *Vet. Microbiol.* **87**, 159-174 (2002).
33. Erenburg, I. N. *et al.* Heterologously secreted MbxA from *Moraxella bovis* induces a membrane blebbing response of the human host cell. *Sci. Rep.* **12**, 17825 (2022).
34. Gouveia, C. *et al.* *Kingella kingae* displaced *S. aureus* as the most common cause of acute septic arthritis in children of all ages. *Pediatr. Infect. Dis. J.* **40**, 623-627 (2021).
35. Principi, N. & Esposito, S. *Kingella kingae* infections in children. *BMC Infect. Dis.* **15**, 1-7 (2015).
36. Yagupsky, P., Porsch, E. & St Geme, J. W. *Kingella kingae*: an emerging pathogen in young children. *Pediatrics* **127**, 557-565 (2011).
37. Kehl-Fie, T. E. & St. Geme III, J. W. Identification and characterization of an RTX toxin in the emerging pathogen *Kingella kingae*. *J. Bacteriol.* **189**, 430-436 (2007).
38. Madeira, F. *et al.* Search and sequence analysis tools services from EMBL-EBI in 2022. *Nucleic Acids Res.* **50**, W276-W279 (2022).
39. Jumper, J. *et al.* Highly accurate protein structure prediction with AlphaFold. *Nature* **596**, 583-589 (2021).
40. Stanley, P., Packman, L. C., Koronakis, V. & Hughes, C. Fatty acylation of two internal lysine residues required for the toxic activity of *Escherichia coli* hemolysin. *Science* **266**, 1992-1996 (1994).
41. Aono, R., Tsukagoshi, N. & Yamamoto, M. Involvement of outer membrane protein TolC, a possible member of the mar-sox regulon, in maintenance and improvement of organic solvent tolerance of *Escherichia coli* K-12. *J. Bacteriol.* **180**, 938-944 (1998).
42. Gotoh, N. *et al.* Intrinsic resistance of *Escherichia coli* to mureidomycin A and C due to expression of the multidrug efflux system AcrAB-TolC: comparison with the efflux systems of mureidomycin-susceptible *Pseudomonas aeruginosa*. *J. Infect. Chemother.* **9**, 101-103 (2003).
43. Touzé, T. *et al.* Interactions underlying assembly of the *Escherichia coli* AcrAB-TolC multidrug efflux system. *Mol. Microbiol.* **53**, 697-706 (2004).
44. Swick, M. C., Morgan-Linnell, S. K., Carlson, K. M. & Zechiedrich, L. Expression of multidrug efflux pump genes *acrAB-tolC*, *mdfA*, and *norE* in *Escherichia coli* clinical isolates as a function of fluoroquinolone and multidrug resistance. *Antimicrob. Agents Chemother.* **55**, 921-924 (2011).
45. Locher, K. P. Mechanistic diversity in ATP-binding cassette (ABC) transporters. *Nat. Struct. Mol. Biol.* **23**, 487-493 (2016).
46. Pimenta, A., Young, J., Holland, I. & Blight, M. Antibody analysis of the localisation, expression and stability of HlyD, the MFP component of the *E. coli* haemolysin translocator. *Mol. Gen. Genet.* **261**, 122-132 (1999).

47. Kim, J.-S. *et al.* Crystal structure of a soluble fragment of the membrane fusion protein HlyD in a type I secretion system of Gram-negative bacteria. *Structure* **24**, 477-485 (2016).
48. Higgins, C. F. & Linton, K. J. The ATP switch model for ABC transporters. *Nat. Struct. Mol. Biol.* **11**, 918 (2004).
49. Martin, C., Higgins, C. F. & Callaghan, R. The vinblastine binding site adopts high-and low-affinity conformations during a transport cycle of P-glycoprotein. *Biochemistry* **40**, 15733-15742 (2001).
50. Masi, M. & Wandersman, C. Multiple signals direct the assembly and function of a type 1 secretion system. *J. Bacteriol.* **192**, 3861-3869 (2010).
51. Delepelaire, P. & Wandersman, C. The SecB chaperone is involved in the secretion of the *Serratia marcescens* HasA protein through an ABC transporter. *EMBO J.* **17**, 936-944 (1998).
52. Johnson, Z. L. & Chen, J. Structural basis of substrate recognition by the multidrug resistance protein MRP1. *Cell* **168**, 1075-1085 (2017).
53. Harris, A. *et al.* Structure and efflux mechanism of the yeast pleiotropic drug resistance transporter Pdr5. *Nat. Commun.* **12**, 5254 (2021).
54. Tang, X. D. *et al.* Cryo-EM structures of lipopolysaccharide transporter LptB(2)FGC in lipopolysaccharide or AMP-PNP-bound states reveal its transport mechanism. *Nat. Commun.* **10**, 4175 (2019).
55. Kikhney, A. G., Borges, C. R., Molodenskiy, D. S., Jeffries, C. M. & Svergun, D. I. SASBDB: Towards an automatically curated and validated repository for biological scattering data. *Protein Sci.* **29**, 66-75 (2020).
56. Gibson, D. G. Enzymatic assembly of overlapping DNA fragments. *Methods Enzymol.* **498**, 349-361 (2011).
57. Benabdelhak, H. *et al.* Positive co-operative activity and dimerization of the isolated ABC ATPase domain of HlyB from *Escherichia coli*. *Biochem. J.* **386**, 489-495 (2005).
58. Hanahan, D. Studies on transformation of *Escherichia coli* with plasmids. *J. Mol. Biol.* **166**, 557-580 (1983).
59. Schindelin, J. *et al.* Fiji: an open-source platform for biological-image analysis. *Nat. Methods* **9**, 676-682 (2012).
60. Zaitseva, J., Holland, I. B. & Schmitt, L. The role of CAPS buffer in expanding the crystallization space of the nucleotide-binding domain of the ABC transporter haemolysin B from *Escherichia coli*. *Acta Crystallogr. D Biol. Crystallogr.* **60**, 1076-1084 (2004).
61. Zaitseva, J. *et al.* Functional characterization and ATP-induced dimerization of the isolated ABC-domain of the haemolysin B transporter. *Biochemistry* **44**, 9680-9690 (2005).
62. Altschul, S. F., Gish, W., Miller, W., Myers, E. W. & Lipman, D. J. Basic local alignment search tool. *J. Mol. Biol.* **215**, 403-410 (1990).
63. Zimmermann, L. *et al.* A completely reimplemented MPI bioinformatics toolkit with a new HHpred server at its core. *J. Mol. Biol.* **430**, 2237-2243 (2018).

64. Mól, A. R., Castro, M. S. & Fontes, W. NetWheels: A web application to create high quality peptide helical wheel and net projections. *BioRxiv*, 416347 (2018).
65. Blanchet, C. E. *et al.* Versatile sample environments and automation for biological solution X-ray scattering experiments at the P12 beamline (PETRA III, DESY). *J. Appl. Crystallogr.* **48**, 431-443 (2015).
66. Manalastas-Cantos, K. *et al.* ATSAS 3.0: expanded functionality and new tools for small-angle scattering data analysis. *J. Appl. Crystallogr.* **54**, 343-355 (2021).
67. Konarev, P. V., Volkov, V. V., Sokolova, A. V., Koch, M. H. J. & Svergun, D. I. PRIMUS: a Windows PC-based system for small-angle scattering data analysis. *J. Appl. Crystallogr.* **36**, 1277-1282 (2003).
68. Guinier, A. Small-angle X-ray diffraction: application to the study of ultramicroscopic phenomena. *Ann. Phys.* **11**, 161-237 (1939).
69. Svergun, D. I. Determination of the regularization parameter in indirect-transform methods using perceptual criteria. *J. Appl. Crystallogr.* **25**, 495-503 (1992).
70. Svergun, D. I., Petoukhov, M. V. & Koch, M. H. Determination of domain structure of proteins from X-ray solution scattering. *Biophys. J.* **80**, 2946-2953 (2001).
71. Mirdita, M. *et al.* ColabFold: making protein folding accessible to all. *Nat. Methods* **19**, 679-682 (2022).
72. Kozin, M. B. & Svergun, D. I. Automated matching of high- and low-resolution structural models. *J. Appl. Crystallogr.* **34**, 33-41 (2001).
73. Bakkes, P. J., Jenewein, S., Smits, S. H., Holland, I. B. & Schmitt, L. The rate of folding dictates substrate secretion by the *Escherichia coli* hemolysin type 1 secretion system. *J. Biol. Chem.* **285**, 40573-40580 (2010).
74. Thomas, S., Smits, S. H. & Schmitt, L. A simple *in vitro* acylation assay based on optimized HlyA and HlyC purification. *Anal. Biochem.* **464**, 17-23 (2014).
75. Linhartová, I. *et al.* RTX proteins: a highly diverse family secreted by a common mechanism. *FEMS Microbiol. Rev.* **34**, 1076-1112 (2010).
76. Porod, G. Die Röntgenkleinwinkelstreuung von dichtgepackten kolloiden Systemen - 1 Teil. *Kolloid Z.* **124**, 83-114 (1951).
77. Fischer, H., Neto, M. D., Napolitano, H. B., Polikarpov, I. & Craievich, A. F. Determination of the molecular weight of proteins in solution from a single small-angle X-ray scattering measurement on a relative scale. *J. Appl. Crystallogr.* **43**, 101-109 (2010).
78. Rambo, R. P. & Tainer, J. A. Accurate assessment of mass, models and resolution by small-angle scattering. *Nature* **496**, 477-481 (2013).
79. Hajizadeh, N. R., Franke, D., Jeffries, C. M. & Svergun, D. I. Consensus Bayesian assessment of protein molecular mass from solution X-ray scattering data. *Sci. Rep.* **8**, 7204 (2018).
80. Molodenskiy, D. S., Svergun, D. I. & Kikhney, A. G. Artificial neural networks for solution scattering data analysis. *Structure* **30**, 900-908 (2022).

-
81. Petoukhov, M. V. & Svergun, D. I. Ambiguity assessment of small-angle scattering curves from monodisperse systems. *Acta Crystallogr. D Biol. Crystallogr.* **71**, 1051-1058 (2015).
 82. Svergun, D., Barberato, C. & Koch, M. H. J. CRY SOL - A program to evaluate X-ray solution scattering of biological macromolecules from atomic coordinates. *J. Appl. Crystallogr.* **28**, 768-773 (1995).
 83. Schrödinger, L. The PyMOL molecular graphics system, version 2.5. (2022).
 84. Jones, D. T. Protein secondary structure prediction based on position-specific scoring matrices. *J. Mol. Biol.* **292**, 195-202 (1999).
 85. Yan, R., Xu, D., Yang, J., Walker, S. & Zhang, Y. A comparative assessment and analysis of 20 representative sequence alignment methods for protein structure prediction. *Sci. Rep.* **3**, 2619 (2013).
 86. Wang, S., Peng, J., Ma, J. & Xu, J. Protein secondary structure prediction using deep convolutional neural fields. *Sci. Rep.* **6**, 18962 (2016).
 87. Klausen, M. S. *et al.* NetSurfP-2.0: Improved prediction of protein structural features by integrated deep learning. *Proteins: Struct. Funct. Bioinform.* **87**, 520-527 (2019).

SUPPLEMENTARY INFORMATION

Type 1 secretion necessitates a tight interplay between all domains of the ABC transporter

Manuel T. Anlauf¹, Jens Reiners², Olivia Spitz^{1†}, Eymen Hachani¹,
Sander H.J. Smits^{1,2}, Lutz Schmitt^{1*}

¹Heinrich Heine University Düsseldorf, Faculty of Mathematics and Natural Sciences, Institute of Biochemistry, Universitätsstraße 1, 40225 Düsseldorf, Germany

²Heinrich Heine University Düsseldorf, Faculty of Mathematics and Natural Sciences, Center for Structural Studies, Universitätsstraße 1, 40225 Düsseldorf, Germany

[†]present address: INCONSULT, Duisburg, Germany

*Corresponding author: Lutz Schmitt, Heinrich Heine University Düsseldorf, Faculty of Mathematics and Natural Sciences, Institute of Biochemistry, Universitätsstraße 1, 40225 Düsseldorf, Germany, Tel.: +49 211 81-10773, E-Mail: lutz.schmitt@hhu.de

Supplemental Material and Methods

Small Angle X-ray Scattering (SAXS)

The SAXS data was collected on the P12 beamline (PETRA III, DESY Hamburg⁶⁵). The sample to detector distance of the P12 beamline was 3.00 m, resulting in an achievable q -range of 0.03 – 4.5 nm⁻¹. The measurements were performed at 10°C with a protein concentration of 1.93 mg ml⁻¹ of RtxB-NBD. 40 frames were collected with an exposer time of 0.095 sec frame⁻¹. Data were collected on relative scale.

All used programs for data processing were part of the ATSAS Software package (Version 3.0.5)⁶⁶. Primary data reduction was performed with the program PRIMUS⁶⁷. The forward scattering $I(0)$ and the radius of gyration (R_g) were determined with the Guinier approximation⁶⁸. The program GNOM⁶⁹ was used to estimate the maximum particle dimension (D_{max}) with the pair-distribution function $p(r)$. Low resolution *ab initio* models were calculated with GASBOR⁷⁰. Superimposing of the RtxB-NBD AlphaFold2^{39,71} model was done with the program SUPCOMB⁷².

Table S1: Identity and characteristics of putative T1SS components from 25 different organisms. Proteins were identified by pBLAST search. The Number (No.) of GG repeats is displayed in form of a range and depends on how strict the RTX motif GGxGxDxUx (U being a large hydrophobic residue and x being any amino acid) is applied⁷⁵. If multiple identities and sizes for the HlyA homolog are displayed, more than one RTX protein was identified.

Organism	Identity compared to [%]			Putative RTX protein	
	HlyB	HlyD	HlyA	Size [aa]	No. of GG repeats
<i>Xylella fastidiosa</i>	61	41	37	1,814	16-18
<i>Xanthomonas axonopodis</i>	63	38	38	2,512	36-38
<i>Lysobacter antibioticus</i>	64	37	42	574	9-11
<i>Aeromonas diversa</i> CDC 2478-85	65	38	43	351	9-10
<i>Gallibacterium anatis</i>	70	49	29	2,038	5-6
<i>Avibacterium paragallinarum</i>	69	48	32	2,286	15
<i>Cronobacter malonaticus</i>	69	46	36	866	6
<i>Aggregatibacter actinomycetemcomitans</i>	84	68	50	1,051	7
<i>Mannheimia haemolytica</i>	82	61	43	953	5
<i>Bibersteinia trehalosi</i>	82	59	42	955	6
<i>Pasteurella aerogenes</i>	83	62	52	1,049	6-9
<i>Actinobacillus equuli</i> subsp. <i>Haemolyticus</i>	86	64	47	987	4
<i>Morganella morganii</i>	90	81	80	1,024	5-6
<i>Proteus vulgaris</i>	92	95	46	598	6
<i>Vibrio parahaemolyticus</i>	92	81	82	986	8-9
<i>Enterobacter cloacae</i>	98	98	97	1,024	6-7
<i>Serratia</i> sp. Leaf51	69	42	33; 34	965; 2,893	9; 12-14
<i>Cardiobacterium valvarum</i>	70	41	34; 35; 41; 49	217; 569; 665; 558	4; 8-9; 2; 5-6
<i>Vitreoscilla</i> sp. SN6	70	42	44	444	10
<i>Acinetobacter baumannii</i>	69	44	52	3,298	49-58
<i>Moraxella bovis</i>	69	41	43	927	5
<i>Kingella kingae</i>	71	40	42	956	6
<i>Alysiella crassa</i>	70	41	31	248	4
<i>Snodgrassella alvi</i>	71	45	50	895	24
<i>Neisseria</i> sp. oral taxon 020	70	43	38; 46; 49	1,605; 636; 188	14; 3-5; 4-5

Table S2: Overall SAXS Data for RtxB-NBD.

SAXS Device	P12, PETRA III, DESY Hamburg⁶⁵
Data collection parameters	
Detector	PILATUS 6 M (423.6 x 434.6 mm ²)
Detector distance (m)	3.0
Beam size	120 μ m x 200 μ m
Wavelength (nm)	0.124
Sample environment	Quartz glass capillary, 1 mm \varnothing
s range (nm ⁻¹) [‡]	0.03 – 4.5
Sample	RtxB-NBD
Organism	<i>Kingella kingae</i>
UniProt ID	F5S9L7
Mode of measurement	batch
Temperature (°C)	10
Exposure time per frame (s)	0.095 (40 Frames)
Protein buffer	100 mM HEPES pH 8.0, 10 % (v/v) Glycerol
Protein concentration (mg/ml)	1.93
Structural parameters	
<i>I</i> (0) from P(r)	0.02
<i>R</i> _g (real-space from P(r)) (nm)	2.20
s-range for GNOM fit (nm ⁻¹)	0.133 – 4.181
<i>I</i> (0) from Guinier fit	0.02
s-range for Guinier fit (nm ⁻¹)	0.133 – 0.593
<i>R</i> _g (from Guinier fit) (nm)	2.19
points from Guinier fit	1 - 160
<i>D</i> _{max} (nm)	7.60
POROD volume estimate (nm ³)	47.55
Molecular mass (kDa)	
From <i>I</i> (0)	25.77
From Qp ⁷⁶	20.36
From MoW2 ⁷⁷	21.26
From Vc ⁷⁸	24.92
Bayesian Inference ⁷⁹	23.05
From GNNOM ⁸⁰	30.70
From POROD	29.72
From sequence	27.68 (monomer) 55.36 (dimer)
Structure Evaluation	
GASBOR fit χ^2	1.082
CRY SOLfit χ^2	1.445
Ambimeter score	1.362
Software	
ATSAS Software Version ⁶⁶	3.0.5
Primary data reduction	PRIMUS ⁶⁷
Data processing	GNOM ⁶⁹
<i>Ab initio</i> modelling	GASBOR ⁷⁰
Superimposing	SUPCOMB ⁷²
Structure evaluation	AMBIMETER ⁸¹ / CRY SOL ⁸²
Model visualization	PyMOL ⁸³

[‡]s = $4\pi\sin(\theta)/\lambda$, 2θ – scattering angle, n.d. not determined

Table S3: Plasmids used in this study.

Plasmid name	Backbone	Encoded genes	Source
pK184-HlyBD	pK184	<i>hlyB</i> , <i>hlyD</i>	⁷³
pK184-HlyBD-KEE	pK184	<i>hlyB-KEE</i> , <i>hlyD</i>	This study
pK184-HlyBD-EKE	pK184	<i>hlyB-EKE</i> , <i>hlyD</i>	This study
pK184-HlyBD-EEK	pK184	<i>hlyB-EEK</i> , <i>hlyD</i>	This study
pK184-HlyBD-KKE	pK184	<i>hlyB-KKE</i> , <i>hlyD</i>	This study
pK184-HlyBD-KEK	pK184	<i>hlyB-KEK</i> , <i>hlyD</i>	This study
pK184-HlyBD-EKK	pK184	<i>hlyB-EEK</i> , <i>hlyD</i>	This study
pK184-RtxB-HlyD	pK184	<i>rtxB</i> , <i>hlyD</i>	This study
pSU2726-HlyA	pSU2726	<i>hlyA</i>	⁷⁴
pPSG122-RtxB-NBD-NHis6	pBAD18	<i>rtxB-NBD</i>	This study

Table S4: Oligonucleotides used in this study. Overhangs for Gibson assembly are underlined.

Name	Details	Sequence (5'→3')	Plasmid
lin-pK-fw lin-pK-rev pK-Ins-RtxB-fw pK-Ins-RtxB-rev	Linearization of the pK184-HlyBD plasmid without <i>hlyB</i> Amplification of <i>rtxB</i> with overhangs to pK184	CATGACTGTTTCTGTGTGAAATTG TAACAGAAAGAACAGAAGAATATGAAAC <u>CAGGAAACAGTCATG</u> GATAAACTTCTCAACCCGC <u>CTTCTGTTCTTTCTGTT</u> ACCCATTCTGTAAATCATACAAATAACG	pK184-RtxB-HlyD
RtxB-CLD-fw RtxB-CLD-rev pK-RtxB-CLD-Ins-fw pK-RtxB-CLD-Ins-rev	Amplification of <i>rtxB</i> CLD Amplification of pK184-HlyBD without <i>hlyB</i> CLD with overhangs to <i>rtxB</i> CLD	GATAAAACCTCTCAACCCGC GACAAAATCATTTTGCCTGAATATC <u>GCAAAATGATTTTGTG</u> CGTTCCCGTTCTTCTGTTG <u>GTTGAGAGGTTTTATC</u> CATGACTGTTTCTGTGTG	pK184-HlyBD-KEE
RtxB-TMD-fw RtxB-TMD-rev pK-RtxB-TMD-Ins-fw pK-RtxB-TMD-Ins-rev	Amplification of <i>rtxB</i> TMD Amplification of pK184-HlyBD without <i>hlyB</i> TMD with overhangs to <i>rtxB</i> TMD	TTAGAAGTGCTGCTGGTGTC TAACTGTGCCAAACGAATCAC <u>GTTTGGCACAGTTAT</u> GGCAGGATTTCCAGCAG <u>AGCAGCACTTCTA</u> AAAAATATTCTCCTGTATTTATAATGGCAG	pK184-HlyBD-EKE
RtxB-NBD-fw RtxB-NBD-rev pK-RtxB-NBD-Ins-fw pK-RtxB-NBD-Ins-rev	Amplification of <i>rtxB</i> NBD Amplification of pK184-HlyBD without <i>hlyB</i> NBD with overhangs to <i>rtxB</i> NBD	ATTACTTTTGAACACGTTGATTTAG CCCATTCTGTAAATCATACAAATAAC <u>TGATTACAGAATGGG</u> TAACAGAAAGAACAGAAGAATATG <u>CGTGTTCAAAAGTAAT</u> ATCACCATTAATTTCCGG	pK184-HlyBD-EEK
HlyB-CLD-fw HlyB-CLD-rev pK-HlyB-CLD-Ins-fw pK-HlyB-CLD-Ins-rev	Amplification of <i>hlyB</i> CLD Amplification of pK184-RtxB-HlyD without <i>rtxB</i> CLD with overhangs to <i>hlyB</i> CLD	GCGAATTCTGATTCTTGTCATAAAATTG GATAAGAATAATATGCCCTGATATAACG <u>GGGCATATTATCTTAT</u> CGCATCTCGCGCATCCGTG <u>AAGAATCAGAATTG</u> CCATGACTGTTTCTGTGTGAAATTGTTATCC	pK184-HlyBD-EKK
HlyB-TMD-fw HlyB-TMD-rev pK-HlyB-TMD-Ins-fw pK-HlyB-TMD-Ins-rev	Amplification of <i>hlyB</i> TMD Amplification of pK184-RtxB-HlyD without <i>rtxB</i> TMD with overhangs to <i>hlyB</i> TMD	ATTGAAACCTTGTTGTGTCTG GATTTGTGCAAGGCGAATAAC <u>GCCTTGACACAAATC</u> TGGCAGGATTTTCAGCAAG <u>CAACAAGGGTTTCA</u> ATAAAAAATGCGGCGATATTTAATCAC	pK184-HlyBD-KEK
HlyB-NBD-fw HlyB-NBD-rev pK-HlyB-NBD-Ins-fw pK-HlyB-NBD-Ins-rev	Amplification of <i>hlyB</i> NBD Amplification of pK184-RtxB-HlyD without <i>rtxB</i> NBD with overhangs to <i>hlyB</i> NBD	ATCACTTTTCGTAATATCCGTTTC GTCTGACTGTAAGTATATAAGTAAC <u>CAGTTACAGTCAGAC</u> TAACAGAAAGAACAGAAGAATATGAAAC <u>GATATTACGAAAAGTGAT</u> GTGCGCTTGAATATCGGG	pK184-HlyBD-KKE
pPSG-RtxB-NBD-Ins-fw pPSG-RtxB-NBD-Ins-rev	Amplification of pPSG122-HlyB-NBD-NHis6 without <i>hlyB</i> NBD with overhangs to <i>rtxB</i> NBD	<u>TGATTACAGAATGGG</u> TAAGAATTCGAGCTCGGTAC <u>ACGTGTTCAAAAGTAAT</u> ATCGTGATGGTGATGGTG	pPSG122-RtxB-NBD-NHis6

Table S5: List of used antibodies.

Name	Description	Host	Dilution
Anti-HlyA	Polyclonal, targets the N-terminal secretion signal of pro-HlyA, purified	Rabbit	1 : 1,000
Anti-HlyB	Polyclonal, targets the NBD of HlyB, purified	Rabbit	1 : 4,000
Anti-HlyD	Polyclonal, targets the periplasmic part of HlyD, serum	Rabbit	1 : 4,000
Anti-Rabbit-HRP	Polyclonal, targets rabbit IgG, HRP-conjugated, purified (Thermo Scientific)	Goat	1 : 20,000

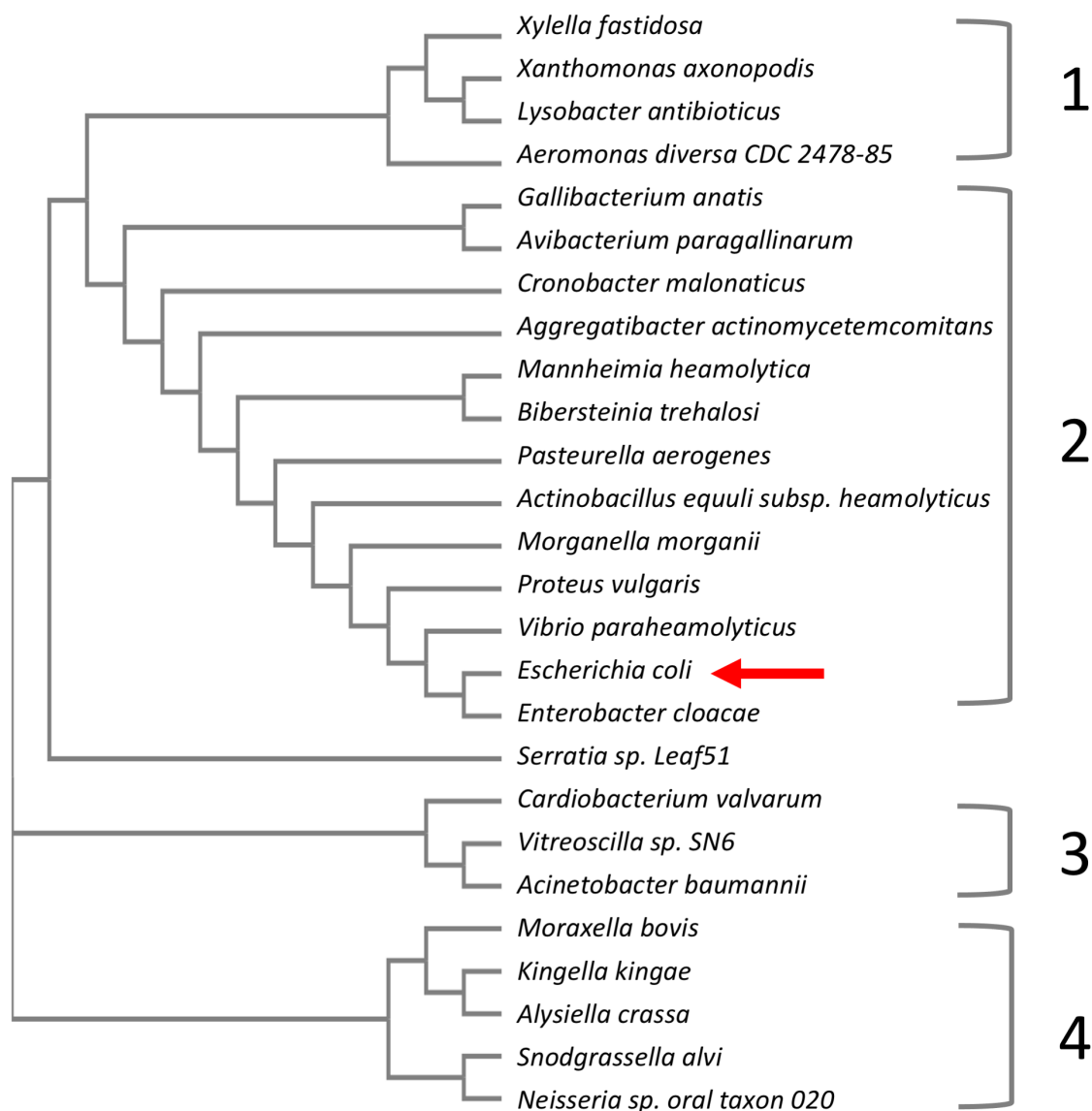


Figure S1: Phylogenetic tree of organisms containing transporters homologous to HlyB. The primary sequence of T1SS transporters from the depicted organisms was used in an alignment performed with Clustal Omega³⁸. The organisms can be divided into four groups based on their relation. *Escherichia coli* is marked with a red arrow. Note that the length of the branches does not relate to the degree of relation.

a		b	
HlyA	974 – NPLINEISKIISAAGSF – 990	RtxA	913 – GNLASTLNKLIESMASF – 929
SS_PSIPRED	HHHHHHHHHHHHH	SS_PSIPRED	HHHHHHHHHHHHH
SS_PSSPRED4	HHHHHHHHHHHHH	SS_PSSPRED4	HHHHHHHHHHHHH
SS_DEEPCNF	HHHHHHHHHHHHH	SS_DEEPCNF	HHHHHHHHHHHHH
SS_NETSURFP2	HHHHHHHHHHHHH	SS_NETSURFP2	HHHHHHHHHHHHH

Figure S2: Prediction of secondary structures in the secretion signal sequences of HlyA (**a**) and RtxA (**b**) using the Quick2D tool. SS_PSIPRED⁸⁴, SS_PSSPRED4⁸⁵, SS_DEEPCNF⁸⁶ and SS_NETSURFP2⁸⁷ are different prediction algorithms. ‘H’ indicates amino acids, which are predicted to form an α -helix.

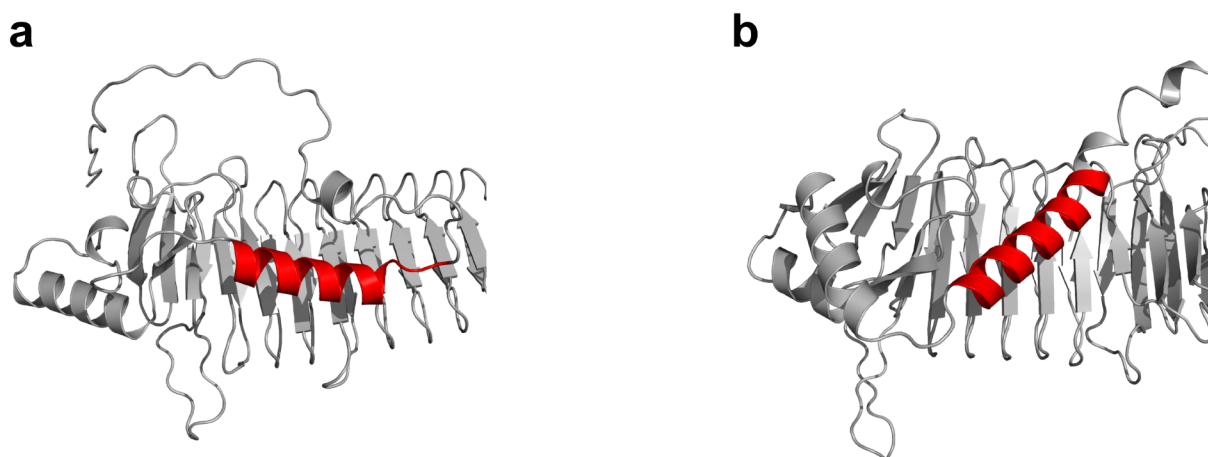


Figure S3: Models of pro-HlyA (**a**) and pro-RtxA (**b**) as predicted by AlphaFold2³⁹. The C-terminal amphipathic helix of the secretion signal sequence of both toxins is shown in red.

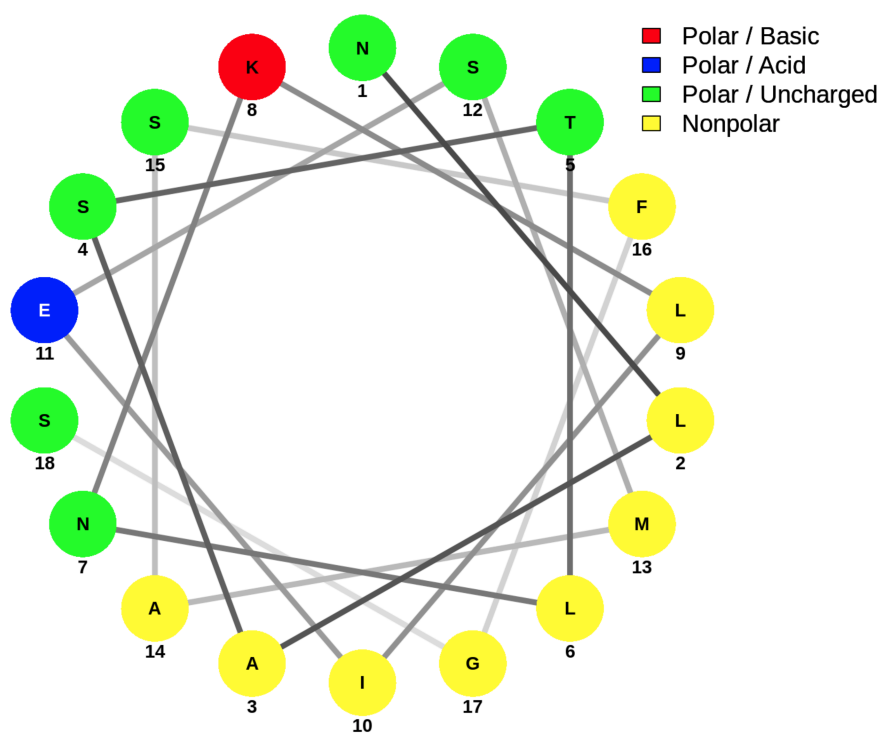


Figure S4: Helical wheel projection of the putative amphipathic helix in the secretion signal of RtxA. The image was created using NetWheel⁶⁴. Nonpolar residues are shown in yellow, polar residues in green, acidic residues in blue and basic residues in red.

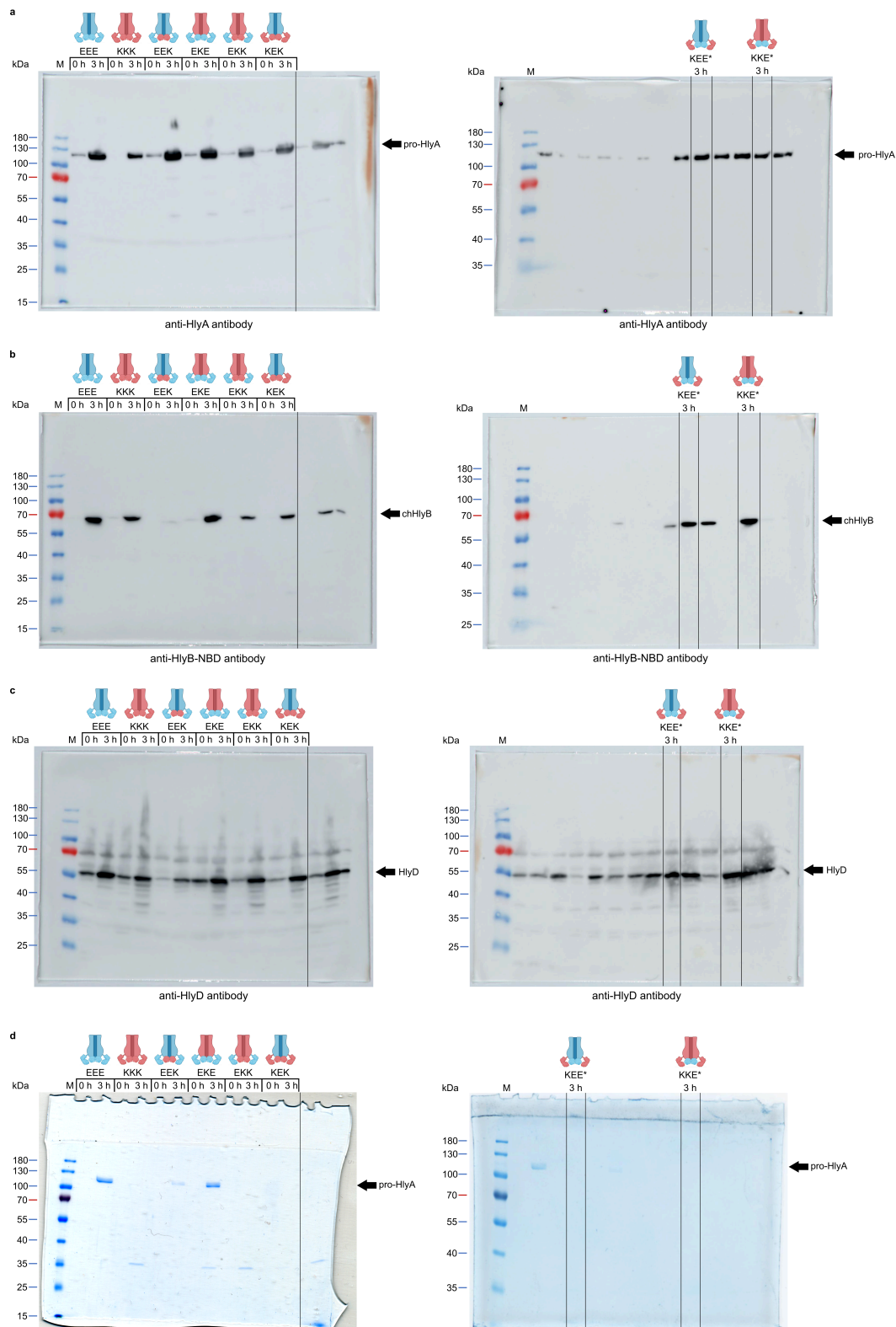


Figure S5: Uncropped Western Blots and SDS-PAGE gels shown in Figure 1. Vertical crop sides are indicated as black lines for better distinction between lanes of samples shown in the main text and lanes containing unrelated samples.

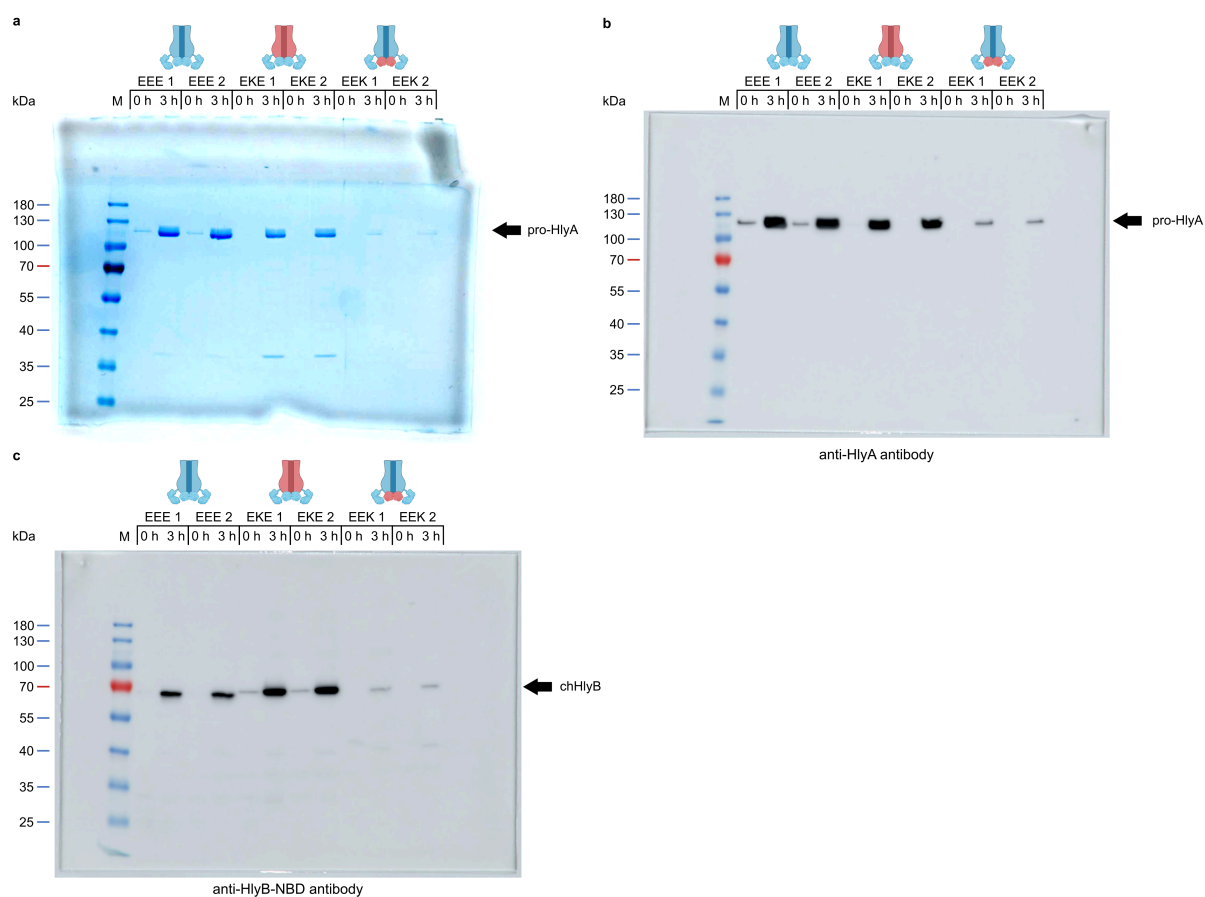


Figure S6: Uncropped Western Blots and SDS-PAGE gels shown in Figure 3.

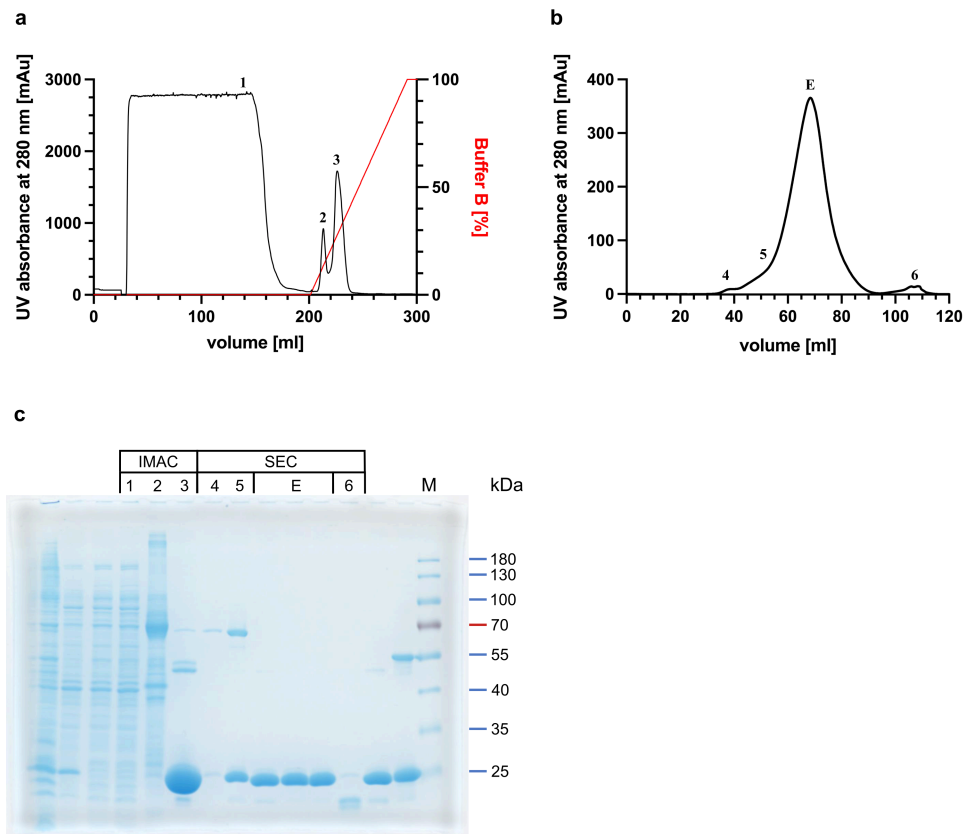


Figure S7: Purification of RtxB-NBD. The N-terminally fused 6xHis-tag allowed an immobilized metal affinity chromatography (IMAC, **a**); 1: Flow through; 2: Wash; 3: Elution. After washing to baseline, a gradient elution was performed (red, 100% Buffer = 300 mM imidazole). The elution peak was concentrated and applied to a size exclusion chromatography (SEC, **b**); 4,5,6: Contamination; E: Elution of target protein. (**c**): SDS-PAGE analysis of protein samples from IMAC and SEC with Coomassie staining. RtxB-NBD-NHis6 has a size of 27,676 Da. M: Protein marker, the approx. size of the marker proteins is given on the right.

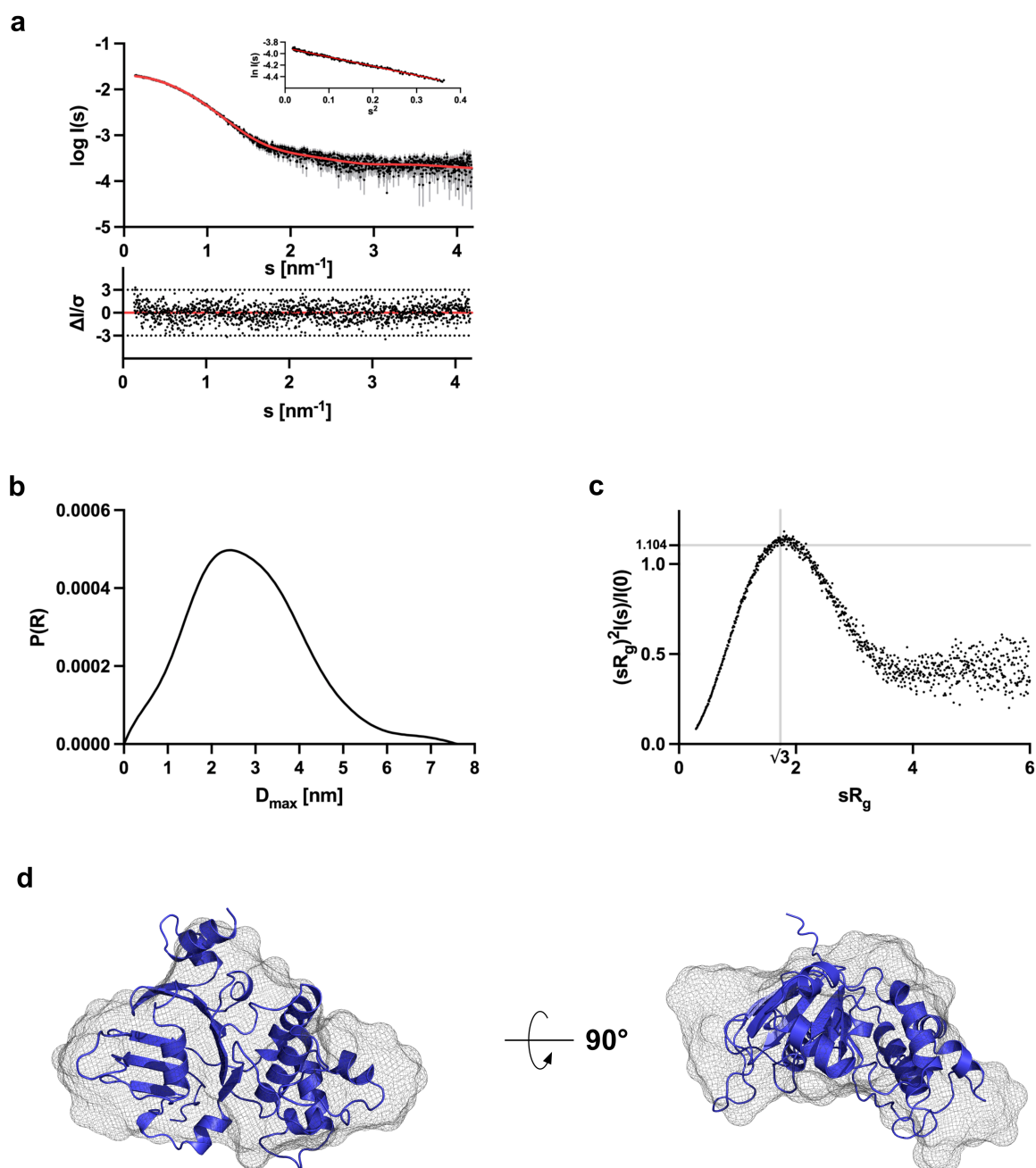


Figure S8: Small-angle X-ray scattering data from RtxB-NBD. **(a):** Scattering data of RtxB-NBD. Experimental data is shown in black dots, with grey error bars. The GASBOR *ab initio* model fit is shown as a red line, below is the residual plot of the data. The Guinier plot is added in the upper right corner. **(b):** Pair distance distribution function $p(r)$ revealed RtxB-NBD to be a folded, monomeric, almost globular particle in solution. **(c):** Dimensionless Kratky plot of RtxB-NBD showed a compact particle, as globular particles exhibit a peak at $\sqrt{3}$ with a maximum at 1.104 (marked with grey lines). **(d):** The AlphaFold2 model is shown in blue, and the GASBOR *ab-initio* envelope is shown as a grey mesh (GASBOR fit $\chi^2 = 1.082$). The unstructured N-terminus sticking out of the mesh contains the 6xHis-tag.

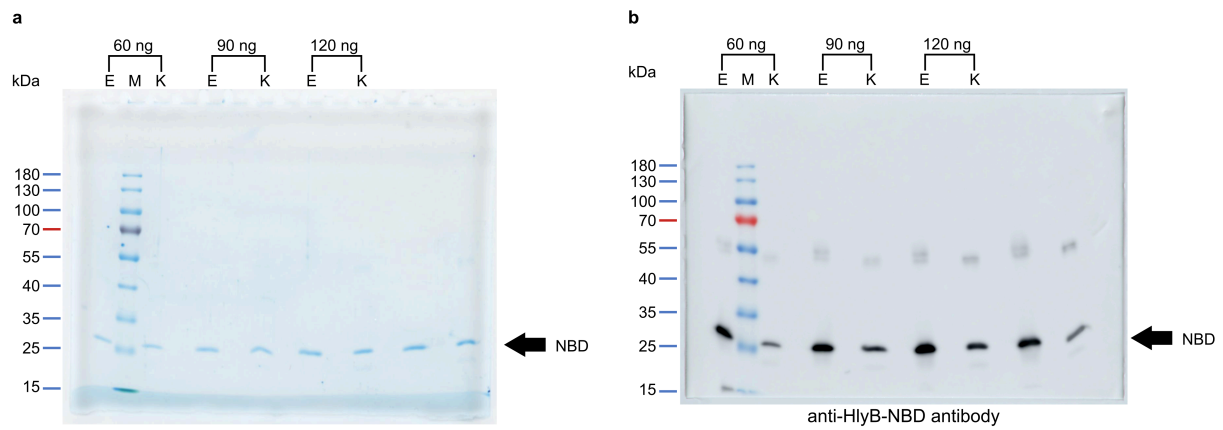


Figure S9: Comparative quantification of the NBDs from HlyB and RtxB. Equal amounts of purified protein ranging from 60-120 ng were analyzed via SDS-PAGE (a) and immunoblot using the HlyB-NBD antibody (b). The signal intensity of the HlyB-NBD antibody for RtxB-NBD was divided by the HlyB-NBD signal intensity and resulted in a factor of 0.36 ± 0.10 . M: Protein marker, the approx. size of the marker proteins is given on the left; E: HlyB-NBD; K: RtxB-NBD.

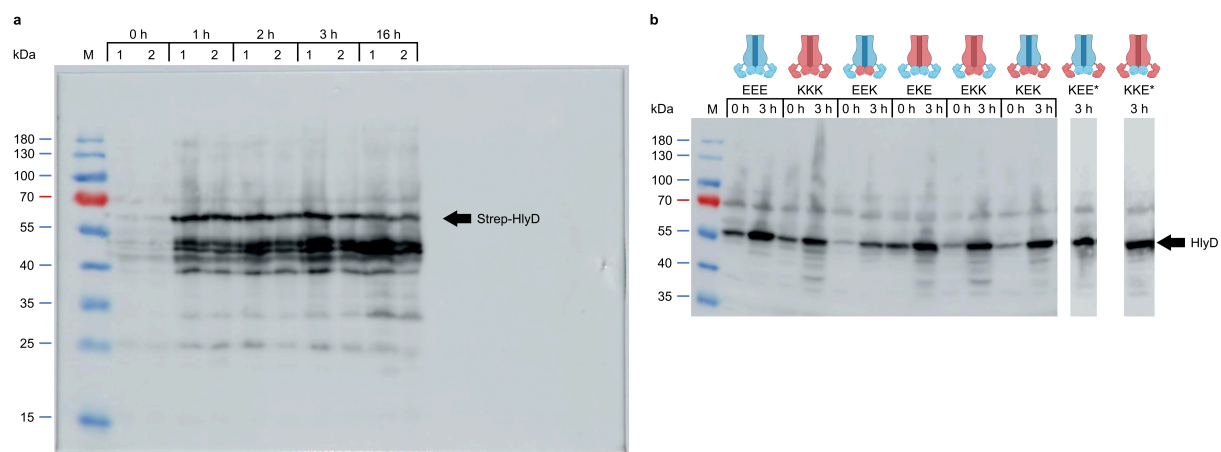


Figure S10: Degradation of HlyD. (a) Expression of Strep-tagged HlyD without the presence of HlyB in two replicates (1 & 2). Samples were taken before induction (0 h) as well as after 1 h, 2 h, 3 h and 16 h of expression. HlyD severely degrades when HlyB is not present and no secretion complex can be formed. (b) Figure 1 C from the main text is shown here for easier comparison.

4. Discussion

Since the discovery of the toxin HlyA, which is the main pathogenicity factor of uropathogenic *Escherichia coli* (UPEC) strains, great efforts were put into the structural and functional elucidation of its secretion process, making it one of the best studied T1SS (Robinson 1951, Bien *et al.* 2012). The translocation complex consists of the ATP-binding cassette (ABC) transporter HlyB and the membrane fusion protein (MFP) HlyD, both located in the inner membrane (Mackman *et al.* 1985a, Mackman *et al.* 1985b), and the outer membrane protein (OMP) TolC (Wandersman and Delepelaire 1990), forming a conduit through the inner and outer bacterial membranes.

This thesis focused on the secretion of HlyA by its ABC transporter HlyB, stability of the toxin prior to its secretion and the interactome between HlyA and HlyB. The study was divided into three aims. The first aim was to investigate whether localized translation of HlyA mRNA could be an explanation for the stability of unfolded HlyA in the cytoplasm (chapter 3.2). The second aim was the identification of amino acids in the transmembrane domain (TMD) of HlyB, which are interacting with its substrate, using unnatural amino acids as crosslinkers (chapter 3.3). In the last chapter (chapter 3.4), chimeric transporters of HlyB from *E. coli* and RtxB from *Kingella kingae* were used to gain a deeper understanding of the substrate recognition process by the ABC transporter and the influence of its different domains on substrate specificity and secretion efficiency.

4.1. What keeps HlyA stable in the cytoplasm?

The type and size of proteins secreted by T1SS differs greatly, ranging from the 6 kDa bacteriocin colicin V, 19 kDa hemophore HasA and 110 kDa toxin HlyA to the 900 kDa adhesion protein LapA (Goebel and Hedgpeth 1982, Fath *et al.* 1994, Arnoux *et al.* 1999, Hinsä *et al.* 2003). A large group of secreted proteins belong to the Repeats in ToXins (RTX) superfamily, which are exclusively secreted by T1SS and have two common properties. One is the presence of the eponymous RTX motifs (glycine- and aspartate-rich nonapeptide sequence), which are usually found in the C-terminal part of the protein and interact with the ABC transporter. These motifs start to fold only upon Ca²⁺ ion binding once the protein reaches the extracellular space (Linhartová *et al.*

2010). The other is the directional secretion via an essential, non-cleavable C-terminal secretion signal. Both these characteristics deduce the following: firstly, the substrate secretion cannot occur co-translationally, as the secretion signal needs to be present (Nicaud *et al.* 1986). Secondly, the substrate needs to be unfolded, as fusions of fast folding proteins to the N-terminus of HlyA bring the secretion system to a halt (Bakkes *et al.* 2010, Lenders *et al.* 2015). These points raise an important question: how are large, unfolded RTX proteins like HlyA kept in a stable, secretion-competent state and how is their aggregation or degradation prevented?

In case of the SecYEG transport system (Hartl *et al.* 1990) and other secretion systems, such as T3SSs (Job *et al.* 2010), T4SSs (Alvarez-Martinez and Christie 2009), T5SSs (Baud *et al.* 2009), T7SSs (Korotkova *et al.* 2014) and T8SSs (Taylor *et al.* 2016), proteins destined for transport are usually stabilized by either specialized or general chaperones like SecB or Skp. However, for RTX proteins, no chaperones involved in secretion could be identified so far (Motlova *et al.* 2020). In fact, the only T1SS known to rely on a chaperone (SecB) is the HasA secretion system from *Serratia marcescens* (Delepelaire and Wandersman 1998). However, HasA as a hemophore is a non-RTX substrate and the secretion system operates fundamentally different when compared to RTX secretion systems like the hemolysin system. While ABC transporters of T1SSs secreting RTX proteins belong without exception to the subgroup 2 of T1SSs and contain an N-terminal C39 peptidase-like domain (CLD), the HasA-associated ABC transporter HasD in contrast belongs to the subgroup 3 of T1SS and lacks an N-terminal domain (Lecher *et al.* 2012, Kanonenberg *et al.* 2013). Furthermore, the complete assembly of the hemolysin secretion complex involves the recognition of the substrate by its secretion signal and is secreted with the C-terminus first. The secretion signal of HasA on the other hand acts as a ‘releasing signal’, as it is not participating in the assembly of the complex, but rather in the disassembly. Additionally, HasA exits the cell with the N-terminus first (Masi and Wandersman 2010).

One explanation for T1SSs not necessitating cytoplasmic chaperones could be the spatially constrained expression of the substrate at the membrane. The unfolded protein would reside in the cytoplasm for only a limited time before being recognized and transported by the secretion complex. A localized translation was reported in *E. coli* for the lactose permease LacY, BglF (a protein involved in β -glucoside

transport), the Fimbrin-like protein Fiml and the 8-amino-7-oxononanoate synthase BioF (Nevo-Dinur *et al.* 2011, Kannaiah *et al.* 2019). Transcripts of those proteins were tracked using the MS2 system and accumulated close to the membranes. A similar observation was also made for the T5SS autotransporters SepA and lcsA from *Shigella flexneri*, which localized to the cell poles in the cytoplasm before and independent of secretion (Jain *et al.* 2006). Therefore, a similar translation of HlyA near the membrane was hypothesized and *hlyA* transcripts were aimed to be localized utilizing the fluorescently labeled MS2 system and *lacY* transcripts as a positive control (Nevo-Dinur *et al.* 2011). Unfortunately, localization of *lacY* transcripts did not match the published results, as the associated fluorescence showed a uniform distribution in the cytoplasm instead of the expected membrane localization, even though all necessary transcripts and proteins were present (chapter 3.2). This contradictory effect was observed irrespective of the expression level of the MS2 coat protein-eGFP fusion construct and with two different plasmid systems (pK184 and pEVOL). The original plasmids and sequences were not available and were therefore replicated based on the limited information provided in the original publication (Nevo-Dinur *et al.* 2011). Potential explanations for the discrepancy to the published results could be slight deviations in the sequence of the MS2 RNA loop or MS2 coat protein, a defective interaction of these two elements or a non-functional MS2 loop-LacY mRNA. It should also be noted, that (membrane-)localized translation of mRNAs in bacteria has been investigated for only a little more than a decade with only a few reported cases using the MS2 system (Montero Llopis *et al.* 2010, Nevo-Dinur *et al.* 2011, dos Santos *et al.* 2012, Kannaiah *et al.* 2019). The system might therefore not be as trivial to use in bacteria. Due to the ambiguous results, the possibility of a localized translation for the mRNA of HlyA could neither be confirmed nor refuted.

One other possibility for the stability of unfolded HlyA in the cytoplasm could be the RTX motifs themselves acting as intramolecular chaperones. This hypothesis is mainly fueled by the observation that RTX proteins with a reduced number of the conserved tandem repeats show a strong reduction of the intracellular protein level and secretion level, often attributed to a rapid degradation as in the case of the lipase PML from *Pseudomonas* sp. MIS38. This protein contains 12 RTX motifs and showed an increasingly reduced secretion and expression level when 7, 8, 11 and all 12 motifs were deleted (Kwon *et al.* 2002, Meier *et al.* 2007). However, the reduced secretion

level could originate from another effect than the RTX motifs acting as chaperones. Instead, recent data showed that shortening the distance between the amphipathic helix of the secretion signal and the first RTX motif decreased the secretion efficiency of HlyA as well (Pourhassan *et al.* 2022). The correct distance between these features seems to be necessary for proper and simultaneous binding of HlyA to the CLD and NBD (Benabdelhak *et al.* 2003, Lecher *et al.* 2012), before threading the C-terminus into the transporter. This concept is also supported by investigations using chimeric HlyB/RtxB transporters in this thesis (chapter 3.4), as exchanging the domain identity of HlyB with a homologous one decreased the secretion efficiency. A reduced substrate recognition or binding would explain the reduced secretion efficiency, especially with the exchange of the CLDs portraying the most severe effects.

Another possible explanation is the CLD acting as a chaperone, which has been contemplated for a long time due to several reasons. Firstly, chemical shift perturbation and pull-down experiments with HlyA1 (the C-terminal 218 residues of HlyA) showed that the CLD of HlyB interacts exclusively with the unfolded RTX motifs, but not when Ca^{2+} ions are bound to them (Lecher *et al.* 2012). Secondly, no known RTX substrate possesses a cytoplasmic chaperone, rather all RTX proteins are secreted by T1SS group 2 transporters (which contain a CLD) (Kanonenberg *et al.* 2013). Thirdly, if the transport complex is absent, RTX proteins demonstrate to either aggregate or degrade, as HlyA formed inclusion bodies when expressed without HlyBD (Thomas *et al.* 2014a) and RtxA from *Vibrio cholerae* displayed an instability when accumulating in the cytoplasm (Boardman *et al.* 2007). The photo-crosslinking studies of the HlyA T1SS (chapter 3.3) in this thesis support the possibility of the CLD acting as a chaperone. The unnatural amino acid p-Benzoyl-L-phenylalanine (Bpa) was successfully incorporated at different positions into eGFP-HlyA. Irradiation with UV light produced crosslinks to HlyB exhibiting a molecular weight of >300 kDa. This mass significantly exceeded the expected one of eGFP-HlyA:HlyB crosslinks with a ratio of 1:1 (140 kDa (eGFP-HlyA) + 80 kDa (HlyB) = 220 kDa), but would fit to an eGFP-HlyA:HlyB crosslink ratio of 2:1 (360 kDa). While one eGFP-HlyA is still present in the channel formed by HlyB and its translocation stalled, another eGFP-HlyA could already be present at the CLD of the transporter.

4.2. The HlyB CLD is a key player during HlyA secretion

A CLD-centered mode of secretion would be reminiscent to the secretion by the ABC transporter PCAT1 (Lin *et al.* 2015). However, there are some striking differences between the transport systems, which raise several questions, especially with the recently published structure of the HlyBD complex (Zhao *et al.* 2022). PCAT1 is found in *Clostridium thermocellum*, a Gram-positive bacterium, which is not part of a T1SS and therefore misses an MFP and OMP (Lin *et al.* 2015). So far, there are no indications that PCAT1 dimers form trimeric complexes in the membrane as observed for HlyB, and rather remain isolated dimers as usually observed for ABC transporters such as P-glycoprotein, Sav1866 or MacB (Dawson and Locher 2006, Aller *et al.* 2009, Fitzpatrick *et al.* 2017). The architecture of PCAT1 is almost identical to HlyB, but as the name PCAT (Peptidase-Containing ABC Transporter) suggests, it contains an active peptidase domain instead of a CLD.

Even though an inactive domain in the case of HlyB, both the CLD and peptidase domain of HlyB and PCAT1 respectively, are indispensable for substrate secretion. Without the peptidase domain, PCAT1 can neither bind CtA, nor cleave the N-terminal leader peptide for translocation of the cargo (Lin *et al.* 2015). In the case of HlyB, deletion of the CLD influences not only the regulation of the ATPase activity (Reimann *et al.* 2016), but also abolishes the secretion of HlyA completely (Lecher *et al.* 2012). The chimeric RtxB-HlyB transporters tested in this thesis revealed that the CLD is the most important specificity determinant, as a substitution with the CLD from the homologous ABC transporter RtxB still abolished the secretion of HlyA completely (chapter 3.4). Chimeric transporters with the TMD or NBD substituted with the respective domains of RtxB retained the ability to secrete HlyA, even though secretion levels were reduced by ~60%. Considering prior research as well as the structures of CtA-bound PCAT1 and the HlyBD complex, the CLD seems to have three functions. Firstly, deletion experiments revealed the CLD to have a regulatory role and to modulate the hydrolytic activity of the transporter (Reimann *et al.* 2016). Lower concentrations of HlyA1 inhibited the hydrolysis of ATP, while higher concentrations had a stimulating effect (Reimann *et al.* 2016). Furthermore, HlyB Δ CLD exhibited an increased basal ATPase activity (Reimann *et al.* 2016). Secondly, although one of the CLDs of HlyB was not resolved in the structure, it is likely to be positioned in front of the lateral gate upon substrate binding, similar to PCAT1 (Figure 16 A), threading HlyA

into HlyB for translocation. A defective recognition and/or binding of HlyA by the RtxB-CLD could impede the correct insertion of HlyA into the transport complex. Taking the findings of the crosslinking studies presented in this thesis into account (chapter 3.3), molecular weights of crosslinked eGFP-HlyA suggest a second HlyA being present at the transporter while the first one is still being secreted. The second CLD is stabilizing the oligomeric HlyBD complex via an electrostatic network with HlyD (Zhao *et al.* 2022). In this position, the CLD should still be able to bind HlyA. The structure of the HlyBD complex with bound HlyA is unknown, but the substrate-bound PCAT1 structure can be used to hypothesize an interaction mechanism between HlyA, HlyB and HlyD. Even though CtA has an N-terminal leader peptide and therefore a different secretion signal-cargo architecture than HlyA (C-terminal secretion signal), a similar binding mode is assumed for the sake of simplicity. The structures of the peptidase domain of PCAT1 and the CLD of HlyB align relatively well with a root mean square deviation (RMSD) between 1.57 Å and 1.94 Å over 151 C α atoms, depending on which CLD of the HlyBD complex is used for the superimposition (Figure 16B & C). Again, assuming that HlyA is positioned in the CLD of HlyB similar to CtA in the PCAT1 peptidase domain, the N-terminal part of HlyA would get close to the cytoplasmic part of one HlyD when the toxin binds with its RTX motifs to the CLD (Lecher *et al.* 2012).

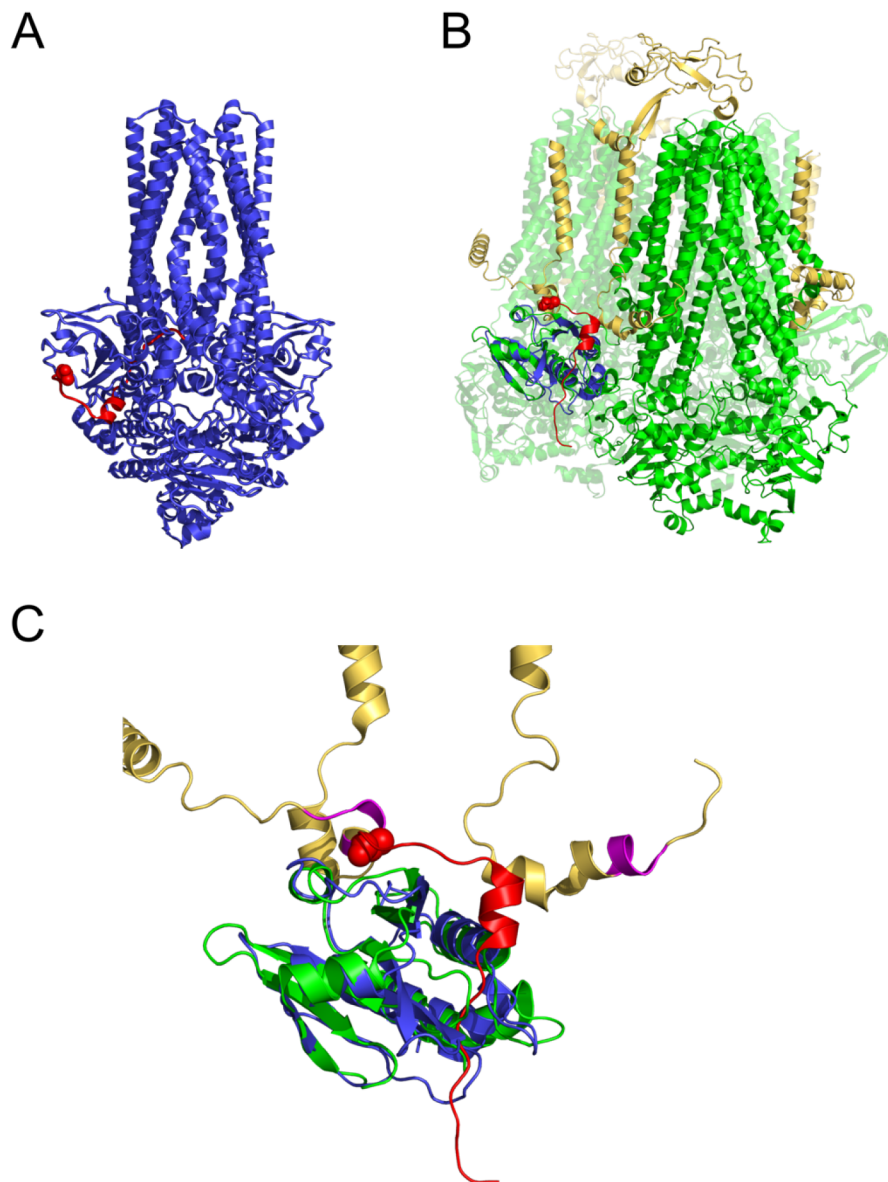


Figure 16: Possible substrate binding by one CLD of HlyB. (A) Cartoon representation of PCAT1 (blue) and the bound 'translocating' CtA (red, PDB: 6V9Z (Kieuvongngam *et al.* 2020)). The N-terminal Asn8 of CtA is shown as spheres. (B) Cartoon representation of the inner membrane complex (PDB: 7SGR (Zhao *et al.* 2022)) formed by HlyB (green) and HlyD (yellow). The peptidase domain of PCAT1 (blue) with bound CtA (red) is superimposed onto the CLD of HlyB. (C) Zoom-in on the superimposed peptidase(-like) domains shown in (B). Other domains of HlyB were removed for clarity, while the 'REKDE' motif in HlyD is colored in magenta. The figure was created with PyMOL (Schrödinger 2022).

In fact, this part of HlyD contains a cluster of charged residues ('REKDE', marked in magenta in Figure 16 C), which was shown to be essential for the recruitment of TolC and secretion of HlyA, although not essential for the binding of HlyA to HlyD (Balakrishnan *et al.* 2001). The binding of HlyA to the CLD, which is involved in inter-protomer stabilization of the HlyBD complex, and presentation to the cytoplasmic part of HlyD might be the third function of the CLD in the secretion process and could depict

a mode of action by which TolC is recruited. It is still unknown, if HlyA remains bound to the inter-protomer CLD or dissociates from it in the time frame after secretion of the first HlyA molecule and binding of the next HlyA molecule to be secreted. Earlier crosslinking studies demonstrated, that the connection between the IMC and TolC necessitates HlyA and that this connection is only temporary (Thanabalu *et al.* 1998). Dissociation of the IMC and TolC was only observed after the intracellular HlyA pool has been depleted by secretion (Thanabalu *et al.* 1998). This is in contrast to the AcrAB-TolC multidrug efflux pump, where TolC is recruited even in the absence of a substrate and remains in a resting state until the complex encounters a secretable drug molecule (Shi *et al.* 2019). It would make sense for the HlyA secretion system to remain completely assembled in order to efficiently secrete as much HlyA as possible in a given time, for as long as substrate is available in the cytoplasm. The strength and longevity of the CLD-HlyA-HlyD interaction could be deduced from the binding affinities of the respective proteins for each other. However, the dissociation constant K_D of the CLD and HlyD for HlyA are unknown. Additional research e.g. in form of isothermal titration calorimetry (ITC) or surface plasmon resonance (SPR) is necessary to determine those parameters and to further elucidate, if HlyA is only transiently bound to the CLD or remains bound for a longer time to keep TolC recruited.

4.3. The HlyB TMD as an additional interaction site

Considering the structure of the HlyBD complex, where HlyA is postulated to be secreted through the dimer interface of HlyB, some questions still remain unanswered. The most important question is: how is a large protein like HlyA mechanistically translocated? The working model for PCAT1 and its substrate CtA is the classical switch between an inward-facing-open (IFO) and an outward-facing-open (OFO) conformation (Bilsing *et al.* 2023). The transmembrane cavity of PCAT1 was calculated to be approx. 15,000 Å³, which is large enough to accommodate the 66 residue substrate CtA (estimated size: 9,000 Å³) (Kieuvongngam *et al.* 2020). Superimposition of PCAT1 with a HlyB dimer of the HlyBD complex showed a significant similarity (RMSD of 3.7 Å), therefore one HlyB dimer will have a comparable cavity volume. Indeed, using the ³V Voss Volume Voxelator tool (Voss and Gerstein 2010), the inner volume of the HlyB dimer interface was estimated to be approx. 13,500 Å³. However,

HlyA has over 15x the size of CtA and is too large to fit into the dimer cavity in its entirety, which makes the translocation by a single switch of an IFO to an OFO conformation hardly conceivable. Closure of the transporter with HlyA still inside the lateral gate and the dimer interface would hardly be possible either, as a protein chain in between the transmembrane helices would pose steric hinderances for the TMHs to move closer to each other.

Related to this issue is the question, if HlyA is transported through the HlyB dimer interface or through the central pore formed by three HlyB dimers? The central pore would surely provide more space for this large substrate. However, the crosslinking data could only show the interaction of HlyA with residues inside the HlyB dimer interface, but not with residues facing towards the central pore (Zhao *et al.* 2022). Five of the six crosslinked residues were directly located at the lateral gate, which could potentially also crosslink to HlyA when travelling through the lateral gates of HlyB and through the central pore, while only one crosslinked residue was located closer to the distal end of HlyB (Zhao *et al.* 2022). However, residues of HlyB facing the central pore did not crosslink to HlyA (Zhao *et al.* 2022). Crosslinking experiments described in this thesis (chapter 3.3) with Bpa incorporated at position F175 of HlyB (top end of HlyB facing the periplasm) produced signals with higher molecular weight (~200 kDa) even in the absence of HlyA, suggesting intermolecular crosslinks between two copies of HlyB, which form a dimer. However, crosslinking in the presence of (eGFP-)HlyA and subsequent detection with an antibody targeting the secretion signal of HlyA revealed higher molecular weight bands (>>180 kDa) as well. A crosslink to HlyA this close to the periplasmic opening of HlyB would only occur with HlyA sandwiched between both HlyB molecules and leaving the transporter onto the periplasmic bridge formed by HlyB. A crosslink between HlyA and HlyB would be rather unlikely should HlyA be transported via the central pore. These results further support the dimer interface of HlyB to be the translocation route.

But what prevents HlyA from entering the HlyB dimer through the lateral gate on the one side and exiting through the gate on the opposite side into the central pore lumen? In case of PCAT1, the opposing peptidase with the 'non-translocating CtA' is positioned in front of the lateral gate, preventing the 'translocating CtA' to leave the transporter (Lin *et al.* 2015, Kieuvongngam *et al.* 2020). In HlyB however, one CLD is positioned between neighboring protomers and stabilizes the multimeric complex,

while the position of the other CLD was not resolved due to flexibility (Zhao *et al.* 2022). For other transporters with a lateral gate, like the LPS translocating transporters MsbA and LptB₂FGC, exit through the opposing gate does not pose a problem as the substrate would simply leave the transporter and another substrate could enter afterwards. MsbA and LptB₂FGC feature residues inside the cavity, which recognize and bind LPS for translocation (Hamad *et al.* 2012, Bertani *et al.* 2018, Padayatti *et al.* 2019). For HlyB though, entry into the central pore cavity does not seem to occur and could potentially even clog the secretion system, preventing any further HlyA translocation.

One possibility is, that the TMD exhibits a gating-like mechanism, where HlyA would be recognized only via the C-terminal secretion signal and threaded through the lateral gate into the dimer interface, preventing the substrate from exiting through the lateral gate on the opposing side and into the central pore cavity. This scenario is supported by secretion experiments with the HlyA T1SS, which showed some promiscuity for their native substrate and the identity of the N-terminal part of the substrate being less important. Fusions of HlyA1 (23 kDa) to slow-folding MalE variants (396 residues, 43 kDa) or the intestinal fatty acid binding protein IFABP (132 residues, 15 kDa) could still be secreted by HlyBD-TolC, although the latter fusion demonstrated a reduced secretion level (Bakkes *et al.* 2010, Schwarz *et al.* 2012).

The second possibility is, that the TMD features binding or interaction sites within the cavity and not (only) at the entry gate to guide the substrate during translocation. Data supporting this scenario comes e.g. from secretion experiments with fusion proteins of PrtB, an RTX motif-containing protease secreted by a T1SS in *Erwinia chrysanthemi*, and N-terminal fragments of LacZ, HlyA, or CyaA (Létoffé and Wandersman 1992). Depending on the size of the fusion protein, some could be secreted with solely the secretion signal, while some fusion proteins also required the RTX motifs. Interestingly, the presence of the RTX motifs was not essential for the secretion of smaller truncations of PrtB but necessary to allow the secretion of larger fusion proteins of PrtB (Létoffé and Wandersman 1992). Secretion of larger Type I substrates could therefore occur similar to a power-stroke mechanism in which the GG repeats of the RTX motif serve as recognition points, while smaller substrates would not need these motifs, as they could be secreted in only one or a few power strokes. It should be noted though, that the respective ABC transporter PrtE is, similar to HasD, classified as a T1SS

transporter of group 3 and therefore lacks an N-terminal CLD or peptidase domain. The substrate recognition and secretion might take place in a (slightly) different manner with the TMD playing a more important role, when compared to secretion systems with an N-terminal appendix, since a complete domain usually involved in substrate recognition is missing.

Secretion experiments with chimeric transporters using domains of RtxB, a homologous transporter from *Kingella kingae*, revealed the TMD of HlyB to be more important than merely providing a Teflon cage through which HlyA is threaded (chapter 3.4). Exchange of the HlyB TMD with the RtxB TMD caused a decrease in HlyA secretion by ~70% (chapter 3.4). Since a similar effect was observed for chimeric transporters, where the HlyB NBD was exchanged to the RtxB NBD (chapter 3.4), and since binding of HlyA to the NBD was reported before (Benabdelhak *et al.* 2003, Pourhassan *et al.* 2022), this suggests that HlyA is recognized and bound by the TMD as well. Since the whole TM domain was exchanged, a differentiation between the two possibilities of substrate recognition (via residues at the lateral gate or via residues within the cavity) is not possible yet. The exchange/mutation of single transmembrane helices or residues forming the lateral gate or the cavity would enable a more differentiated statement. Photo-crosslinking of the hemolysin secretion system using the unnatural amino acid Bpa (chapter 3.3) suggests that a second HlyA is in close proximity to the TMD when stalled during secretion. As identification of the crosslinked residues in HlyA and HlyB was not possible due to the inaccessibility of both HlyA termini in the stalled complex (chapter 3.3), it is still questionable, if the TMD of HlyB is interacting only with the C-terminal part of its substrate during the initial step(s) of secretion or with the entire molecule throughout the whole secretion process. However, the usage of a novel eGFP-HlyA construct with an internal affinity tag introduced into a flexible loop, which would be exposed once the RTX motifs fold upon reaching the extracellular space, showed the successful isolation of all hemolysin complex proteins (HlyA, HlyB, HlyD and TolC) in initial tests (data not shown). With this, all means are now in hand to not only map the translocation path of HlyA within HlyB, but also to structurally analyze the stalled complex in a whole e.g. via Small Angle X-ray Scattering (SAXS) or cryo Electron Microscopy (cryo-EM).

4.4. The NBD: more than a powerhouse

As the name ATP-binding cassette transporter suggests, their key characteristic is the ability to bind (and hydrolyze) ATP to power the transport of substrates. This property is derived from the nucleotide binding domains, often referred to as ‘motor domains’ (Oswald *et al.* 2006, Hollenstein *et al.* 2007), found in every ABC transporter. These domains are highly conserved, due to a variety of motifs essential for the coordination and hydrolysis of ATP like the Walker A and B motifs and the signature motif, to only name a few (see section 1.4.2).

It is therefore not surprising, that ABC transporters from T1SSs show a relatively high identity. Of the 25 ABC transporters identified in homologous systems, the lowest identity to HlyB was 61% for the T1SS transporter from *Xylella fastidiosa* (chapter 3.4). Comparing the isolated NBDs of those transporters, identities to HlyB were even higher with 68% for the transporter from *Xylella fastidiosa* or 86% for the transporter from *Kingella kingae*. Likewise, the fold and structure of NBDs is highly conserved (Hollenstein *et al.* 2007) as could also be shown by the SAXS model of the RtxB-NBD (chapter 3.4) The SAXS envelope of RtxB-NBD was fitting well to its AlphaFold2 model, which in turn has an RMSD of 1.2 Å when compared with the crystal structure of HlyB-NBD. Still, an exchange of the NBD from HlyB with the RtxB-NBD resulted in a reduction of HlyA secretion by ~70% (chapter 3.4). Besides the energization of the secretion process, NBDs have an additional function in T1SS as they exhibit binding sites for the substrate (Benabdelhak *et al.* 2003). The recently identified binding sites within the HlyB-NBD (Pourhassan *et al.* 2022) are also largely conserved in the RtxB-NBD, except for F518 in binding site 1 (leucine in RtxB) and V675, E677 and L697 in binding site 2 (alanine, aspartate and tyrosine respectively in RtxB). This raises the question, if these amino acid changes are the cause for the reduced secretion or if additional interacting amino acids on the surface of the NBD exist, which were not identified yet. Alternatively, not the binding of HlyA to the NBD could be compromised, but rather the interdomain crosstalk of the NBD to the other domains within HlyB.

4.5. Secretion of HlyA and the multiple interactions between hemolysin proteins

The investigation of the chimeric transporters in this thesis (chapter 3.4) showed that all three domains of the ABC transporter confer specificity for the secreted substrate and a concerted interplay exists between the HlyB domains. Changing one or more domains of HlyB to the respective domain found in the homologous ABC transporter of *K. kingae*, RtxB, decreased the secretion efficiency of HlyA. Additionally, judging from the molecular weight of eGFP-HlyA:HlyB crosslinks from stalled complexes (>300 kDa, chapter 3.3), multiple copies of HlyA are present at one ABC transporter.

The CLD represents a central hub for HlyA secretion. Both deletion (Lecher *et al.* 2012) and even substitution with a CLD from a homologous transporter (RtxB, identity of CLDs: 48%, chapter 3.4) completely abolished the secretion of HlyA. The latter observation is rather surprising, since most research articles refer to the work of (Lecher *et al.* 2012) and state the CLD of HlyB to interact with the RTX motifs of HlyA. With the RTX motif being highly conserved throughout substrates of T1SSs group 2, one would expect the CLDs to be somewhat interchangeable. Although the study of (Lecher *et al.* 2012) narrowed down the CLD to interact with unfolded HlyA2 (residues 807-966 of HlyA), it never actually showed the interaction of CLDs with the conserved GG repeat sequence themselves (Lecher *et al.* 2012). It is therefore conceivable that the CLD interacts with a less conserved region close to the GG repeats, which confers substrate specificity. The severe effect of CLD alterations on the secretion could be explained by a dual mode of action in complex assembly and substrate secretion: in a first step, one CLD (positioned in between two HlyB protomers) binds to the RTX motif of one HlyA copy and presents it to the 'REKDE' motif of HlyD (Balakrishnan *et al.* 2001, Lecher *et al.* 2012), which in turn promotes the recruitment of TolC to the IMC and formation of the complete secretion system (Thanabalu *et al.* 1998, Balakrishnan *et al.* 2001) (Figure 17 step 1). HlyD and TolC interact in a tip-to-tip manner via the conserved DLA and VGL/T motifs, respectively (see section 1.4.3). The other CLD (not resolved in the HlyB-HlyD structure (Zhao *et al.* 2022)) would then position itself in front of the open, lateral gate similar to PCAT1 and thread a second copy of HlyA into the transporter with the C-terminal secretion signal of HlyA reaching the extracellular space first (Figure 17 step 2). The recognition of HlyA and correct placement into the

HlyB dimer interface is ensured by secondary binding sides within the TMD and NBD, with the secretion signal initially binding to the NBD (Benabdelhak *et al.* 2003, Pourhassan *et al.* 2022). If the binding of HlyA to the different domains occurs in a step-wise or simultaneous manner is so far unclear. The distance between the secretion signal and (first) GG repeat in the substrate acts as a molecular ruler for efficient secretion. The binding sides within the TMD and NBD are either stronger conserved within transporters of T1SSs group 2 or less important for the secretion, as chimeric transporters with a TMD or NBD from RtxB (identity of TMDs and NBDs: 79% and 73% respectively) were still able to secrete HlyA with approx. 30% efficiency each (chapter 3.4).

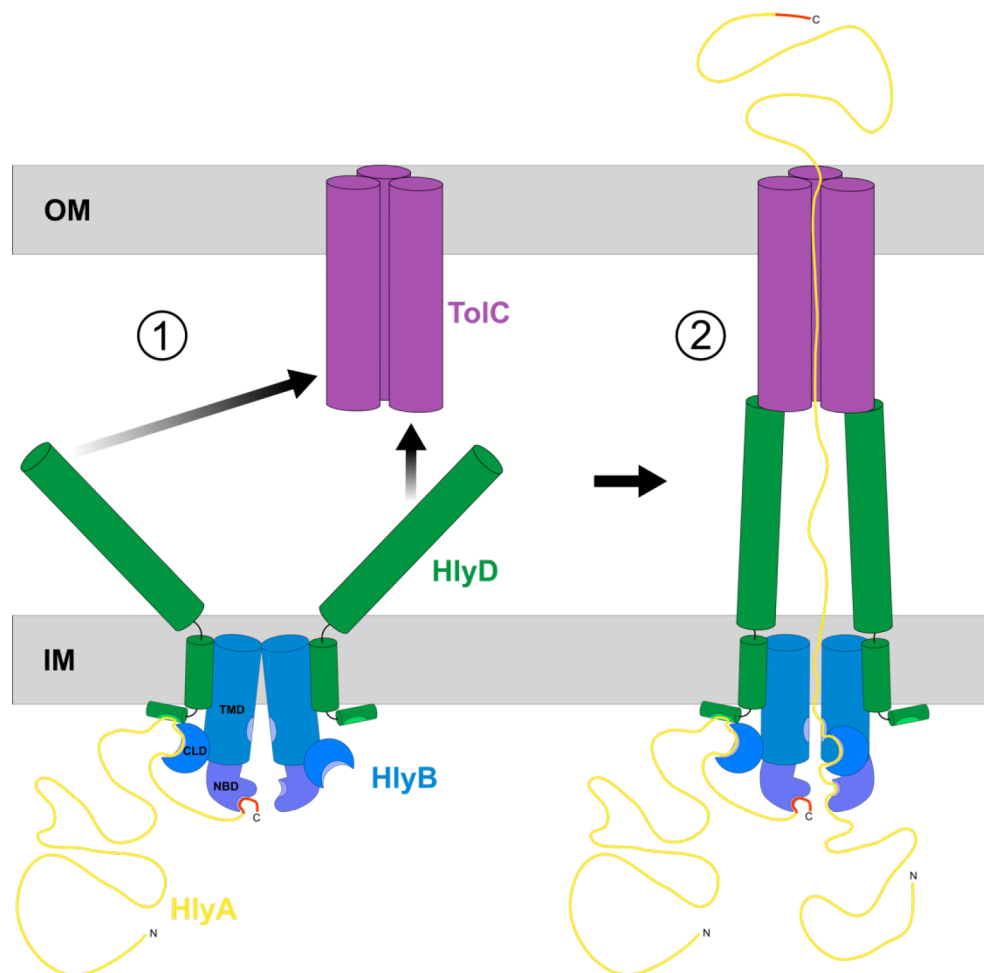


Figure 17: Suggested interactions between HlyB domains and other Hly proteins during complex formation and secretion. (1) The C-terminal secretion signal (red) of HlyA (yellow) is recognized by the nucleotide binding domain (NBD) of HlyB (blue shades) while the RTX motif is bound to the C39 peptidase-like domain (CLD), which presents HlyA to the 'REKDE' motif of HlyD (green). This promotes the recruitment of TolC (purple) in the outer membrane (OM) to the complex in the inner membrane (IM). (2) Formation of the complete secretion complex allows the ATP-dependent translocation of a second HlyA molecule, which interacts with the CLD, NBD and transmembrane domain (TMD) of HlyB during secretion. Note that only one HlyB dimer and two HlyD of the multimeric secretion complex are shown for simplicity.

The NBD of HlyB was shown to interact with the secretion signal of HlyA in earlier studies (Benabdelhak *et al.* 2003), and two possible binding pockets were recently discovered (Pourhassan *et al.* 2022). The simultaneous exchange of the TMD and NBD from HlyB with the respective domains from RtxB showed an additive effect, since the chimeric transporter HlyB-EKK showed no secretion of HlyA (chapter 3.4). A tight interplay between the ABC transporter's domains and an ordered recognition of the substrate or transfer in between the domains seem necessary for effective secretion. This is also supported by secretion experiments with truncated HlyA variants and *in silico* measurements, which suggested a concurrent binding of the C-terminal secretion signal and first GG repeat of HlyA to the NBD and CLD of HlyB, respectively (Pourhassan *et al.* 2022).

Additionally, the mentioned interactions involving HlyB seem to be rather sensitive, as the fusion of some affinity tags to the termini of HlyB greatly affect the amount of expressed HlyB and/or decrease the amount of secreted HlyA, indicating e.g. a defective complex formation or defective substrate recognition (chapter 3.3). Fusion of a 10xHis tag to the N-terminus of HlyB led to a greatly increased expression of HlyB, but the transporter was not able to secrete HlyA. Conversely, N-terminal fusion of a TwinStrep tag to HlyB greatly decreased the expression level of the transporter, but not its ability to secrete HlyA. Addition of a Strep tag to the C-terminus of HlyB (used for structure determination by Zhao *et al.* in 2022) did not only decrease the expression level of HlyB, but the (normalized) secretion of HlyA was reduced to 17% when compared to the untagged ABC transporter (chapter 3.3). The influence of affinity tags on the characteristics of proteins is a known, but often overlooked effect. Depending on the protein, alterations to the expression level, folding and biological activity can occur. For MRP1 from *Saccharomyces cerevisiae*, fusion of a His tag or FLAG tag to the N-terminus reduced protein expression in comparison to C-terminal fusion constructs (Lee and Altenberg 2003), while N-terminally tagged Hydantoinase from *Agrobacterium radiobacter* was reported to be less active when compared to the wild-type protein and even inactive, when the affinity tag was placed at the C-terminus (Huang *et al.* 2003). In a similar fashion, human interferon-gamma was shown to be 100 times less active when it featured an N-terminal 6xHis-FLAG tag (Krachmarova *et al.* 2017) and the small oomycete apoplastic effector SCF96 exhibited a differentiated ability to induce plant cell death, depending on the type and position of the tag (Jin *et*

al. 2023). Sensitivity of affinity tags was also reported for other ABC transporters, e.g. heterologous expression of PDR2 and PDR8 from *Arabidopsis thaliana* in *E. coli* was not possible with a CBP-6xHis tag fused to the C-terminus and only detectable in cells when the tag was placed at the N-terminus (Gräfe *et al.* 2019). In general, alterations on proteins characteristics are often observed when tags are located at positions important for interaction/function. In case of HlyB, all domains were shown to be involved in secretion of the substrate (chapter 3.4) and/or stabilization of the complex, which makes the purification of functional HlyB challenging. Tag-fusion at the C-terminal NBD does not seem to (completely) abolish NBD dimerization, since the purified HlyB-Strep-His-HlyD complex was able to hydrolyze ATP (Zhao *et al.* 2022), therefore recognition of HlyA might be affected. Tag-fusion at the N-terminal NBD on the other hand does not (completely) abolish the recognition of HlyA, since addition of HlyA to purified His-HlyB was still able to modulate the ATPase activity of HlyB (Reimann *et al.* 2016, Kanonenberg *et al.* 2019), but might interfere with the oligomerization of HlyB and HlyD. Either way, removal of the affinity tag after purification should be undertaken for structural and functional analyses with purified HlyB, as constructs mimicking HlyB after protease cleavage (HlyB-GR and HlyB-GP, chapter 3.3) behaved like wild-type HlyB in respect to expression and secretion.

5. Bibliography

1. Abramson, J., Iwata, S. and Kaback, H. R. (2004). "Lactose permease as a paradigm for membrane transport proteins." Mol. Membr. Biol. **21**(4): 227-236.
2. Akopyan, K., Edgren, T., Wang-Edgren, H., Rosqvist, R., Fahlgren, A., Wolf-Watz, H. and Fallman, M. (2011). "Translocation of surface-localized effectors in type III secretion." Proc. Natl. Acad. Sci. **108**(4): 1639-1644.
3. Al-Dulaimi, T. H., Bunyan, I. A. and Banimuslem, T. A. (2022). "Genotypic assay to determine some virulence factors of uropathogenic *E. coli* (UPEC) isolates." Int. J. Health Sci. **6**(S4): 1593-1604.
4. Alami, M., Lüke, I., Deitermann, S., Eisner, G., Koch, H.-G., Brunner, J. and Müller, M. (2003). "Differential interactions between a twin-arginine signal peptide and its translocase in *Escherichia coli*." Mol. Cell **12**(4): 937-946.
5. Alav, I., Kobylka, J., Kuth, M. S., Pos, K. M., Picard, M., Blair, J. M. A. and Bavro, V. N. (2021). "Structure, assembly, and function of tripartite efflux and type 1 secretion systems in gram-negative bacteria." Chem. Rev. **121**(9): 5479-5596.
6. Albers, R. W., Siegel, G. J. and Xie, Z.-J. (2012). Membrane transport. Basic neurochemistry, Elsevier: 73-94.
7. Alberts, B., Johnson, A., Lewis, J., Raff, M., Roberts, K. and Walter, P. (2002). Membrane transport of small molecules and the electrical properties of membranes. Molecular Biology of the Cell, Garland Science: 597-640.
8. Alfano, J. R. and Collmer, A. (2004). "Type III secretion system effector proteins: double agents in bacterial disease and plant defense." Annu. Rev. Phytopathol. **42**: 385-414.
9. Aller, S. G., Yu, J., Ward, A., Weng, Y., Chittaboina, S., Zhuo, R., Harrell, P. M., Trinh, Y. T., Zhang, Q. and Urbatsch, I. L. (2009). "Structure of P-glycoprotein reveals a molecular basis for poly-specific drug binding." Science **323**(5922): 1718-1722.
10. Alvarez-Martinez, C. E. and Christie, P. J. (2009). "Biological diversity of prokaryotic type IV secretion systems." Microbiol. Mol. Biol. Rev. **73**(4): 775-808.
11. Alvira, S., Watkins, D. W., Troman, L., Allen, W. J., Lorrigan, J. S., Degliesposti, G., Cohen, E. J., Beeby, M., Daum, B. and Gold, V. A. (2020). "Inter-membrane association of the Sec and BAM translocons for bacterial outer-membrane biogenesis." eLife **9**: e60669.
12. Aly, K. A. and Baron, C. (2007). "The VirB5 protein localizes to the T-pilus tips in *Agrobacterium tumefaciens*." Microbiology **153**(11): 3766-3775.
13. Amro, J., Black, C., Jemouai, Z., Rooney, N., Daneault, C., Zeytuni, N., Ruiz, M., Bui, K. H. and Baron, C. (2023). "Cryo-EM structure of the *Agrobacterium tumefaciens* T-pilus reveals the importance of positive charges in the lumen." Structure **31**(4): 375-384.e374.

14. Arends, K., Celik, E.-K., Probst, I., Goessweiner-Mohr, N., Fercher, C., Grumet, L., Soellue, C., Abajy, M. Y., Sakinc, T., Broszat, M., Schiwon, K., Koraimann, G., Keller, W. and Grohmann, E. (2013). "TraG encoded by the pIP501 type IV secretion system is a two-domain peptidoglycan-degrading enzyme essential for conjugative transfer." J. Bacteriol. **195**(19): 4436-4444.
15. Arnoux, P., Haser, R., Izadi, N., Lecroisey, A., Delepierre, M., Wandersman, C. and Czjzek, M. (1999). "The crystal structure of HasA, a hemophore secreted by *Serratia marcescens*." Nat. Struct. Biol. **6**(6): 516-520.
16. Bakkes, P. J., Jenewein, S., Smits, S. H., Holland, I. B. and Schmitt, L. (2010). "The rate of folding dictates substrate secretion by the *Escherichia coli* hemolysin type 1 secretion system." J. Biol. Chem. **285**(52): 40573-40580.
17. Balakrishnan, L., Hughes, C. and Koronakis, V. (2001). "Substrate-triggered recruitment of the TolC channel-tunnel during type I export of hemolysin by *Escherichia coli*." J. Mol. Biol. **313**(3): 501-510.
18. Bansal-Mutalik, R. and Nikaido, H. (2014). "Mycobacterial outer membrane is a lipid bilayer and the inner membrane is unusually rich in diacyl phosphatidylinositol dimannosides." Proc. Natl. Acad. Sci. **111**(13): 4958-4963.
19. Baud, C., Hodak, H., Willery, E., Drobecq, H., Loch, C., Jamin, M. and Jacob-Dubuisson, F. (2009). "Role of DegP for two-partner secretion in *Bordetella*." Mol. Microbiol. **74**(2): 315-329.
20. Bay, D. C. and Turner, R. J. (2016). Small multidrug resistance efflux pumps. Efflux-Mediated Antimicrobial Resistance in Bacteria: Mechanisms, Regulation and Clinical Implications. X.-Z. Li, C. A. Elkins and H. I. Zgurskaya. Cham, Springer International Publishing: 45-71.
21. Beckham, K. S. H., Ritter, C., Chojnowski, G., Ziemianowicz, D. S., Mullanpudi, E., Rettel, M., Savitski, M. M., Mortensen, S. A., Kosinski, J. and Wilmanns, M. (2021). "Structure of the mycobacterial ESX-5 type VII secretion system pore complex." Sci. Adv. **7**(26): eabg9923.
22. Beer, T., Hänsch, S., Pfeffer, K., Smits, S. H., Weidtkamp-Peters, S. and Schmitt, L. (2021). "Quantification and surface localization of the hemolysin A type 1 secretion system at the endogenous level and under conditions of overexpression." Appl. Environ. Microbiol. **88**(3): AEM. 01896-01821.
23. Benabdelhak, H., Kiontke, S., Horn, C., Ernst, R., Blight, M. A., Holland, I. B. and Schmitt, L. (2003). "A specific interaction between the NBD of the ABC-transporter HlyB and a C-terminal fragment of its transport substrate haemolysin A." J. Mol. Biol. **327**(5): 1169-1179.
24. Bennion, D., Charlson, E. S., Coon, E. and Misra, R. (2010). "Dissection of β -barrel outer membrane protein assembly pathways through characterizing BamA POTRA 1 mutants of *Escherichia coli*." Mol. Microbiol. **77**(5): 1153-1171.
25. Benz, R., Döbereiner, A., Ludwig, A. and Goebel, W. (1992). "Haemolysin of *Escherichia coli*: comparison of pore-forming properties between chromosome and plasmid-encoded haemolysins." FEMS Microbiol. Immunol. **5**(1-3): 55-62.
26. Berks, B. C., Sargent, F. and Palmer, T. (2000). "The Tat protein export pathway." Mol. Microbiol. **35**(2): 260-274.

27. Bernstein, H. D. (2019). "Type V secretion in gram-negative bacteria." EcoSal Plus **8**(2): 10.1128/ecosalplus.ESP-0031-2018.
28. Bertani, B. and Ruiz, N. (2018). "Function and biogenesis of lipopolysaccharides." EcoSal Plus **8**(1): 10.1128/ecosalplus. ESP-0001-2018.
29. Bertani, B. R., Taylor, R. J., Nagy, E., Kahne, D. and Ruiz, N. (2018). "A cluster of residues in the lipopolysaccharide exporter that selects substrate variants for transport to the outer membrane." Mol. Microbiol. **109**(4): 541-554.
30. Beveridge, T. J. (1999). "Structures of gram-negative cell walls and their derived membrane vesicles." J. Bacteriol. **181**(16): 4725-4733.
31. Bhoite, S., Van Gerven, N., Chapman, M. R. and Remaut, H. (2019). "Curli biogenesis: bacterial amyloid assembly by the type VIII secretion pathway." EcoSal Plus **8**(2): 10.1128/ecosalplus.esp-0037-2018.
32. Bien, J., Sokolova, O. and Bozko, P. (2012). "Role of uropathogenic *Escherichia coli* virulence factors in development of urinary tract infection and kidney damage." Int. J. Nephrol. **2012**: 1-15.
33. Bilsing, F. L., Anlauf, M. T., Hachani, E., Khosa, S. and Schmitt, L. (2023). "ABC transporters in bacterial nanomachineries." Int. J. Mol. Sci. **24**(7): 6227.
34. Birtalan, S. C., Phillips, R. M. and Ghosh, P. (2002). "Three-dimensional secretion signals in chaperone-effector complexes of bacterial pathogens." Mol. Cell **9**(5): 971-980.
35. Boardman, B. K., Meehan, B. M. and Satchell, K. J. F. (2007). "Growth phase regulation of *vibrio cholerae* RTX toxin export." J. Bacteriol. **189**(5): 1827-1835.
36. Bouley, J., Condemine, G. and Shevchik, V. E. (2001). "The PDZ domain of OutC and the N-terminal region of OutD determine the secretion specificity of the type II out pathway of *Erwinia chrysanthemi*." J. Mol. Biol. **308**(2): 205-219.
37. Bountra, K., Hagelueken, G., Choudhury, H. G., Corradi, V., El Omari, K., Wagner, A., Mathavan, I., Zirah, S., Yuan Wahlgren, W. and Tieleman, D. P. (2017). "Structural basis for antibacterial peptide self-immunity by the bacterial ABC transporter McjD." EMBO J. **36**(20): 3062-3079.
38. Boyer, F., Fichant, G., Berthod, J., Vandenbrouck, Y. and Attree, I. (2009). "Dissecting the bacterial type VI secretion system by a genome wide in silico analysis: what can be learned from available microbial genomic resources?" BMC Genomics **10**(104): 1-14.
39. Boyer, P. D. (1997). "The ATP synthase—a splendid molecular machine." Annu. Rev. Biochem. **66**(1): 717-749.
40. Bunduc, C. M., Fahrenkamp, D., Wald, J., Ummels, R., Bitter, W., Houben, E. N. G. and Marlovits, T. C. (2021). "Structure and dynamics of a mycobacterial type VII secretion system." Nature **593**(7859): 445-448.
41. Cabelli, R. J., Chen, L., Tai, P. C. and Oliver, D. B. (1988). "SecA protein is required for secretory protein translocation into *E. coli* membrane vesicles." Cell **55**(4): 683-692.
42. Cambronne, E. D. and Roy, C. R. (2007). "The *Legionella pneumophila* lcmSW complex interacts with multiple Dot/Icm effectors to facilitate type IV translocation." PLoS Path. **3**(12): e188.

43. Carruthers, A. (1990). "Facilitated diffusion of glucose." Physiol. Rev. **70**(4): 1135-1176.
44. Cascales, E. and Christie, P. J. (2004). "Definition of a bacterial type IV secretion pathway for a DNA substrate." Science **304**(5674): 1170-1173.
45. Cescau, S., Debarbieux, L. and Wandersman, C. (2007). "Probing the *in vivo* dynamics of type I protein secretion complex association through sensitivity to detergents." J. Bacteriol. **189**(5): 1496-1504.
46. Chaddock, A. M., Mant, A., Karnauchov, I., Brink, S., Herrmann, R. G., Klösgen, R. and Robinson, C. (1995). "A new type of signal peptide: central role of a twin-arginine motif in transfer signals for the delta pH-dependent thylakoidal protein translocase." EMBO J. **14**(12): 2715-2722.
47. Chen, M., Shi, X., Yu, Z., Fan, G., Serysheva, I. I., Baker, M. L., Luisi, B. F., Ludtke, S. J. and Wang, Z. (2022). "*In situ* structure of the AcrAB-TolC efflux pump at subnanometer resolution." Structure **30**(1): 107-113. e103.
48. Chernyatina, A. A. and Low, H. H. (2019). "Core architecture of a bacterial type II secretion system." Nat. Commun. **10**(1): 5437.
49. Cherradi, Y., Schiavolin, L., Moussa, S., Meghraoui, A., Meksem, A., Biskri, L., Azarkan, M., Allaoui, A. and Botteaux, A. (2013). "Interplay between predicted inner-rod and gatekeeper in controlling substrate specificity of the type III secretion system." Mol. Microbiol. **87**(6): 1183-1199.
50. Cherrak, Y., Flaugnatti, N., Durand, E., Journet, L. and Cascales, E. (2019). "Structure and activity of the type VI secretion system." Microbiol. Spectr. **7**(4): 10.1128/microbiolspec.psib-0031-2019.
51. Cherrak, Y., Rapisarda, C., Pellarin, R., Bouvier, G., Bardiaux, B., Allain, F., Malosse, C., Rey, M., Chamot-Rooke, J., Cascales, E., Fronzes, R. and Durand, E. (2018). "Biogenesis and structure of a type VI secretion baseplate." Nat. Microbiol. **3**(12): 1404-1416.
52. Chervaux, C. and Holland, I. (1996). "Random and directed mutagenesis to elucidate the functional importance of helix II and F-989 in the C-terminal secretion signal of *Escherichia coli* hemolysin." J. Bacteriol. **178**(4): 1232-1236.
53. Choudhury, D., Thompson, A., Stojanoff, V., Langermann, S., Pinkner, J., Hultgren, S. J. and Knight, S. D. (1999). "X-ray structure of the FimC-FimH chaperone-adhesin complex from uropathogenic *Escherichia coli*." Science **285**(5430): 1061-1066.
54. Christensen, L. F. B., Schafer, N., Wolf-Perez, A., Madsen, D. J. and Otzen, D. E. (2019). Bacterial amyloids: biogenesis and biomaterials. Biological and Bio-inspired Nanomaterials: Properties and Assembly Mechanisms. S. Perrett, A. K. Buell and T. P. J. Knowles. Singapore, Springer Singapore: 113-159.
55. Christie, P. J. (2016). "The mosaic type IV secretion systems." EcoSal Plus **7**(1): 10.1128/ecosalplus.ESP-0020-2015.
56. Claxton, D. P., Jagessar, K. L. and Mchaourab, H. S. (2021). "Principles of alternating access in multidrug and toxin extrusion (MATE) transporters." J. Mol. Biol. **433**(16): 166959.

57. Cline, K. and Mori, H. (2001). "Thylakoid Δ pH-dependent precursor proteins bind to a cpTatC–Hcf106 complex before Tha4-dependent transport." J. Cell Biol. **154**(4): 719-730.
58. Cortajarena, A. L., Goñi, F. M. and Ostolaza, H. (2001). "Glycophorin as a receptor for *Escherichia coli* α -Hemolysin in erythrocytes." J. Biol. Chem. **276**(16): 12513-12519.
59. Costa, T. R., Felisberto-Rodrigues, C., Meir, A., Prevost, M. S., Redzej, A., Trokter, M. and Waksman, G. (2015). "Secretion systems in gram-negative bacteria: structural and mechanistic insights." Nat. Rev. Microbiol. **13**(6): 343-359.
60. Cunnac, S., Lindeberg, M. and Collmer, A. (2009). "*Pseudomonas syringae* type III secretion system effectors: repertoires in search of functions." Curr. Opin. Microbiol. **12**(1): 53-60.
61. Dassa, E. and Bouige, P. (2001). "The ABC of ABCs: a phylogenetic and functional classification of ABC systems in living organisms." Res. Microbiol. **152**(3-4): 211-229.
62. Davidson, A. L. and Sharma, S. (1997). "Mutation of a single MalK subunit severely impairs maltose transport activity in *Escherichia coli*." J. Bacteriol. **179**(17): 5458-5464.
63. Dawson, R. J. P. and Locher, K. P. (2006). "Structure of a bacterial multidrug ABC transporter." Nature **443**(7108): 180-185.
64. Deitermann, S., Sprie, G. S. and Koch, H.-G. (2005). "A dual function for SecA in the assembly of single spanning membrane proteins in *Escherichia coli*." J. Biol. Chem. **280**(47): 39077-39085.
65. Delepelaire, P. and Wandersman, C. (1998). "The SecB chaperone is involved in the secretion of the *Serratia marcescens* HasA protein through an ABC transporter." EMBO J. **17**(4): 936-944.
66. Deng, W., Marshall, N. C., Rowland, J. L., McCoy, J. M., Worrall, L. J., Santos, A. S., Strynadka, N. C. J. and Finlay, B. B. (2017). "Assembly, structure, function and regulation of type III secretion systems." Nat. Rev. Microbiol. **15**(6): 323-337.
67. DiGiuseppe Champion, P. A., Champion, M. M., Manzanillo, P. and Cox, J. S. (2009). "ESX-1 secreted virulence factors are recognized by multiple cytosolic AAA ATPases in pathogenic mycobacteria." Mol. Microbiol. **73**(5): 950-962.
68. dos Santos, V. T., Bisson-Filho, A. W. and Gueiros-Filho, F. J. (2012). "DivIVA-mediated polar localization of ComN, a posttranscriptional regulator of *Bacillus subtilis*." J. Bacteriol. **194**(14): 3661-3669.
69. Driessen, A. J. M., Manting, E. H. and van der Does, C. (2001). "The structural basis of protein targeting and translocation in bacteria." Nat. Struct. Biol. **8**(6): 492-498.
70. Du, D., Wang, Z., James, N. R., Voss, J. E., Klimont, E., Ohene-Agyei, T., Venter, H., Chiu, W. and Luisi, B. F. (2014). "Structure of the AcrAB–TolC multidrug efflux pump." Nature **509**(7501): 512.

71. Du, M., Yuan, Z., Werneburg, G. T., Henderson, N. S., Chauhan, H., Kovach, A., Zhao, G., Johl, J., Li, H. and Thanassi, D. G. (2021). "Processive dynamics of the usher assembly platform during uropathogenic *Escherichia coli* P pilus biogenesis." Nat. Commun. **12**(1): 5207.
72. Duong, F. and Wickner, W. (1997). "Distinct catalytic roles of the SecYE, SecG and SecDFyajC subunits of preprotein translocase holoenzyme." EMBO J. **16**(10): 2756-2768.
73. Duquesne, S., Destoumieux-Garz n, D., Peduzzi, J. and Rebuffat, S. (2007). "Microcins, gene-encoded antibacterial peptides from enterobacteria." Nat. Prod. Rep. **24**(4): 708-734.
74. Durand, E., Cambillau, C., Cascales, E. and Journet, L. (2014). "VgrG, Tae, Tle, and beyond: the versatile arsenal of type VI secretion effectors." Trends Microbiol. **22**(9): 498-507.
75. Durand, E., Nguyen, V. S., Zoued, A., Logger, L., Péhau-Arnaudet, G., Aschtgen, M.-S., Spinelli, S., Desmyter, A., Bardiaux, B., Dujeancourt, A., Roussel, A., Cambillau, C., Cascales, E. and Fronzes, R. (2015). "Biogenesis and structure of a type VI secretion membrane core complex." Nature **523**(7562): 555-560.
76. Eicher, T., Seeger, M. A., Anselmi, C., Zhou, W., Brandstätter, L., Verrey, F., Diederichs, K., Faraldo-G mez, J. D. and Pos, K. M. (2014). "Coupling of remote alternating-access transport mechanisms for protons and substrates in the multidrug efflux pump AcrB." eLife **3**: e03145.
77. El-Kirat-Chatel, S., Beaussart, A., Boyd, C. D., O'Toole, G. A. and Dufrêne, Y. F. (2014). "Single-cell and single-molecule analysis deciphers the localization, adhesion, and mechanics of the biofilm adhesin LapA." ACS Chem. Biol. **9**(2): 485-494.
78. Erenburg, I. N., Hänsch, S., Chacko, F. M., Hamacher, A., Wintgens, S., Stuhldreier, F., Poschmann, G., Spitz, O., Stühler, K. and Wesselborg, S. (2022). "Heterologously secreted MbxA from *Moraxella bovis* induces a membrane blebbing response of the human host cell." Sci. Rep. **12**(1): 17825.
79. Espinosa, A. and Alfano, J. R. (2004). "Disabling surveillance: bacterial type III secretion system effectors that suppress innate immunity." Cell. Microbiol. **6**(11): 1027-1040.
80. Evans, M. L., Chorell, E., Taylor, J. D., Åden, J., Götheson, A., Li, F., Koch, M., Sefer, L., Matthews, S. J. and Wittung-Stafshede, P. (2015). "The bacterial curli system possesses a potent and selective inhibitor of amyloid formation." Mol. Cell **57**(3): 445-455.
81. Fath, M. J., Zhang, L. H., Rush, J. and Kolter, R. (1994). "Purification and characterization of colicin V from *Escherichia coli* culture supernatants." Biochemistry **33**(22): 6911-6917.
82. Fitzpatrick, A. W. P., Llabrés, S., Neuberger, A., Blaza, J. N., Bai, X.-C., Okada, U., Murakami, S., van Veen, H. W., Zachariae, U., Scheres, S. H. W., Luisi, B. F. and Du, D. (2017). "Structure of the MacAB–TolC ABC-type tripartite multidrug efflux pump." Nat. Microbiol. **2**: 17070.

83. Galán, J. E., Lara-Tejero, M., Marlovits, T. C. and Wagner, S. (2014). "Bacterial type III secretion systems: specialized nanomachines for protein delivery into target cells." Annu. Rev. Microbiol. **68**(1): 415-438.
84. Galán, J. E. and Wolf-Watz, H. (2006). "Protein delivery into eukaryotic cells by type III secretion machines." Nature **444**(7119): 567-573.
85. Gilson, L., Mahanty, H. K. and Kolter, R. (1990). "Genetic analysis of an MDR-like export system: the secretion of colicin V." EMBO J. **9**(12): 3875-3884.
86. Glavier, M., Puvanendran, D., Salvador, D., Decossas, M., Phan, G., Garnier, C., Frezza, E., Cece, Q., Schoehn, G., Picard, M., Taveau, J. C., Dauray, L., Broutin, I. and Lambert, O. (2020). "Antibiotic export by MexB multidrug efflux transporter is allosterically controlled by a MexA-OprM chaperone-like complex." Nat. Commun. **11**(1): 4948.
87. Glew, M. D., Veith, P. D., Chen, D., Gorasia, D. G., Peng, B. and Reynolds, E. C. (2017). "PorV is an outer membrane shuttle protein for the type IX secretion system." Sci. Rep. **7**(1): 8790.
88. Goebel, W. and Hedgpeth, J. (1982). "Cloning and functional characterization of the plasmid-encoded hemolysin determinant of *Escherichia coli*." J. Bacteriol. **151**(3): 1290-1298.
89. Gohlke, U., Pullan, L., McDevitt, C. A., Porcelli, I., De Leeuw, E., Palmer, T., Saibil, H. R. and Berks, B. C. (2005). "The TatA component of the twin-arginine protein transport system forms channel complexes of variable diameter." Proc. Natl. Acad. Sci. **102**(30): 10482-10486.
90. Goldsmith, J. A., DiVenere, A. M., Maynard, J. A. and McLellan, J. S. (2022). "Structural basis for non-canonical integrin engagement by *Bordetella* adenylate cyclase toxin." Cell Rep. **40**(7): 111196.
91. Gorasia, D. G., Silva, I. L., Butler, C. A., Chabalier, M., Doan, T., Cascales, E., Veith, P. D. and Reynolds, E. C. (2022). "Protein interactome analysis of the type IX secretion system identifies PorW as the missing link between the PorK/N ring complex and the Sov translocon." Microbiol. Spectr. **10**(1): e01602-01621.
92. Gorasia, D. G., Veith, P. D., Hanssen, E. G., Glew, M. D., Sato, K., Yukitake, H., Nakayama, K. and Reynolds, E. C. (2016). "Structural insights into the PorK and PorN components of the *Porphyromonas gingivalis* type IX secretion system." PLoS Path. **12**(8): e1005820.
93. Goyal, P., Krasteva, P. V., Van Gerven, N., Gubellini, F., Van den Broeck, I., Troupiotis-Tsaïlaki, A., Jonckheere, W., Péhau-Arnaudet, G., Pinkner, J. S., Chapman, M. R., Hultgren, S. J., Howorka, S., Fronzes, R. and Remaut, H. (2014). "Structural and mechanistic insights into the bacterial amyloid secretion channel CsgG." Nature **516**(7530): 250-253.
94. Grabowicz, M. (2019). "Lipoproteins and their trafficking to the outer membrane." EcoSal Plus **8**(2): 10.1128/ecosalplus. ESP-0038-2018.
95. Gräfe, K., Shanmugarajah, K., Zobel, T., Weidtkamp-Peters, S., Kleinschrodt, D., Smits, S. H. and Schmitt, L. (2019). "Cloning and expression of selected ABC transporters from the *Arabidopsis thaliana* ABCG family in *Pichia pastoris*." PLoS One **14**(1): e0211156.

96. Gram, C. (1884). "Ueber die isolirte Färbung der Schizomyceten in Schnitt-und Trockenpräparaten." Fortschritte der Medizin **2**: 185-189.
97. Grudnik, P., Bange, G. and Sinning, I. (2009). "Protein targeting by the signal recognition particle." Biol. Chem. **390**(8): 775-782.
98. Hamad, M. A., Di Lorenzo, F., Molinaro, A. and Valvano, M. A. (2012). "Aminoarabinose is essential for lipopolysaccharide export and intrinsic antimicrobial peptide resistance in *Burkholderia cenocepacia*." Mol. Microbiol. **85**(5): 962-974.
99. Hammar, M., Bian, Z. and Normark, S. (1996). "Nucleator-dependent intercellular assembly of adhesive curli organelles in *Escherichia coli*." Proc. Natl. Acad. Sci. **93**(13): 6562-6566.
100. Hammer, N. D., McGuffie, B. A., Zhou, Y., Badtke, M. P., Reinke, A. A., Brännström, K., Gestwicki, J. E., Olofsson, A., Almqvist, F. and Chapman, M. R. (2012). "The C-terminal repeating units of CsgB direct bacterial functional amyloid nucleation." J. Mol. Biol. **422**(3): 376-389.
101. Hammer, N. D., Schmidt, J. C. and Chapman, M. R. (2007). "The curli nucleator protein, CsgB, contains an amyloidogenic domain that directs CsgA polymerization." Proc. Natl. Acad. Sci. **104**(30): 12494-12499.
102. Hancock, R. (1987). "Role of porins in outer membrane permeability." J. Bacteriol. **169**(3): 929-933.
103. Hartl, F.-U., Lecker, S., Schiebel, E., Hendrick, J. P. and Wickner, W. (1990). "The binding cascade of SecB to SecA to SecYE mediates preprotein targeting to the *E. coli* plasma membrane." Cell **63**(2): 269-279.
104. Havarstein, L. S., Diep, D. B. and Nes, I. F. (1995). "A family of bacteriocin ABC transporters carry out proteolytic processing of their substrates concomitant with export." Mol. Microbiol. **16**(2): 229-240.
105. Henderson, I. R., Navarro-Garcia, F., Desvaux, M., Fernandez, R. C. and Ala'Aldeen, D. (2004). "Type V protein secretion pathway: the autotransporter story." Microbiol. Mol. Biol. Rev. **68**(4): 692-744.
106. Hennell James, R., Deme, J. C., Kjær, A., Alcock, F., Silale, A., Lauber, F., Johnson, S., Berks, B. C. and Lea, S. M. (2021). "Structure and mechanism of the proton-driven motor that powers type 9 secretion and gliding motility." Nat. Microbiol. **6**(2): 221-233.
107. Hinsä, S. M., Espinosa-Urgel, M., Ramos, J. L. and O'toole, G. A. (2003). "Transition from reversible to irreversible attachment during biofilm formation by *Pseudomonas fluorescens* WCS365 requires an ABC transporter and a large secreted protein." Mol. Microbiol. **49**(4): 905-918.
108. Hobbs, E. C., Yin, X., Paul, B. J., Astarita, J. L. and Storz, G. (2012). "Conserved small protein associates with the multidrug efflux pump AcrB and differentially affects antibiotic resistance." Proc. Natl. Acad. Sci. **109**(41): 16696-16701.
109. Holland, I., Peherstorfer, S., Kanonenberg, K., Lenders, M., Reimann, S. and Schmitt, L. (2016). "Type I protein secretion-deceptively simple yet with a wide range of mechanistic variability across the family." EcoSal Plus **7**(1): 1-46.

110. Holland, I. B., Schmitt, L. and Young, J. (2005). "Type 1 protein secretion in bacteria, the ABC-transporter dependent pathway." Mol. Membr. Biol. **22**(1-2): 29-39.
111. Hollenstein, K., Dawson, R. J. and Locher, K. P. (2007). "Structure and mechanism of ABC transporter proteins." Curr. Opin. Struct. Biol. **17**(4): 412-418.
112. Hospenthal, M. K., Zyla, D., Costa, T. R. D., Redzej, A., Giese, C., Lillington, J., Glockshuber, R. and Waksman, G. (2017). "The cryoelectron microscopy structure of the type 1 chaperone-usher pilus rod." Structure **25**(12): 1829-1838.e1824.
113. Huang, C.-Y., Chao, Y.-P. and Yang, Y.-S. (2003). "Purification of industrial hydantoinase in one chromatographic step without affinity tag." Protein Expr. Purif. **30**(1): 134-139.
114. Hui, D. and Ling, V. (2002). "A combinatorial approach toward analyzing functional elements of the *Escherichia coli* hemolysin signal sequence." Biochemistry **41**(17): 5333-5339.
115. Hui, D., Morden, C., Zhang, F. and Ling, V. (2000). "Combinatorial analysis of the structural requirements of the *Escherichia coli* hemolysin signal sequence." J. Biol. Chem. **275**(4): 2713-2720.
116. Hunte, C., Screpanti, E., Venturi, M., Rimon, A., Padan, E. and Michel, H. (2005). "Structure of a Na⁺/H⁺ antiporter and insights into mechanism of action and regulation by pH." Nature **435**(7046): 1197-1202.
117. Hyland, C., Vuillard, L., Hughes, C. and Koronakis, V. (2001). "Membrane interaction of *Escherichia coli* hemolysin: flotation and insertion-dependent labeling by phospholipid vesicles." J. Bacteriol. **183**(18): 5364-5370.
118. Ieva, R. and Bernstein, H. D. (2009). "Interaction of an autotransporter passenger domain with BamA during its translocation across the bacterial outer membrane." Proc. Natl. Acad. Sci. **106**(45): 19120-19125.
119. Ieva, R., Skillman, K. M. and Bernstein, H. D. (2008). "Incorporation of a polypeptide segment into the β -domain pore during the assembly of a bacterial autotransporter." Mol. Microbiol. **67**(1): 188-201.
120. Issartel, J.-P., Koronakis, V. and Hughes, C. (1991). "Activation of *Escherichia coli* prohaemolysin to the mature toxin by acyl carrier protein-dependent fatty acylation." Nature **351**(6329): 759-761.
121. Jain, S., van Ulsen, P., Benz, I., Schmidt, M. A., Fernandez, R., Tommassen, J. and Goldberg, M. B. (2006). "Polar localization of the autotransporter family of large bacterial virulence proteins." J. Bacteriol. **188**(13): 4841-4850.
122. Janas, E., Hofacker, M., Chen, M., Gompf, S., van der Does, C. and Tampé, R. (2003). "The ATP hydrolysis cycle of the nucleotide-binding domain of the mitochondrial ATP-binding cassette transporter Mdl1p." J. Biol. Chem. **278**(29): 26862-26869.

123. Jarchau, T., Chakraborty, T., Garcia, F. and Goebel, W. (1994). "Selection for transport competence of C-terminal polypeptides derived from *Escherichia coli* hemolysin: the shortest peptide capable of autonomous HlyB/HlyD-dependent secretion comprises the C-terminal 62 amino acids of HlyA." Mol. Gen. Genet. **245**(1): 53-60.
124. Jin, J.-H., Zhou, X., Liu, W., Zhang, Z.-H., Huang, S.-X., Zhao, W.-J. and Chen, X.-R. (2023). "Influence of affinity tags and tobacco PR1a signal peptide on detection, purification and bioactivity analyses of the small oomycete apoplastic effectors." Biotechnol. Lett. **45**(1): 115-124.
125. Job, V., Matteï, P.-J., Lemaire, D., Attree, I. and Dessen, A. (2010). "Structural basis of chaperone recognition of type III secretion system minor translocator proteins." J. Biol. Chem. **285**(30): 23224-23232.
126. Jones, C. H., Pinkner, J. S., Nicholes, A. V., Slonim, L. N., Abraham, S. N. and Hultgren, S. J. (1993). "FimC is a periplasmic PapD-like chaperone that directs assembly of type 1 pili in bacteria." Proc. Natl. Acad. Sci. **90**(18): 8397-8401.
127. Jones, H. E., Holland, I., Baker, H. L. and Campbell, A. K. (1999). "Slow changes in cytosolic free Ca^{2+} in *Escherichia coli* highlight two putative influx mechanisms in response to changes in extracellular calcium." Cell Calcium **25**(3): 265-274.
128. Jorgensen, S. E., Hammer, R. F. and Wu, G. K. (1980). "Effects of a single hit from the alpha hemolysin produced by *Escherichia coli* on the morphology of sheep erythrocytes." Infect. Immun. **27**(3): 988-994.
129. Journet, L., Agrain, C., Broz, P. and Cornelis, G. R. (2003). "The needle length of bacterial injectisomes is determined by a molecular ruler." Science **302**(5651): 1757-1760.
130. Junker, M., McDonnell, A., Berger, B., Li, T., Zheng, N. and Clark, P. (2009). "Vectorial transport and folding of an autotransporter virulence protein during outer membrane secretion." Mol. Microbiol. **71**(5): 1323-1332.
131. Junker, M., Schuster, C. C., McDonnell, A. V., Sorg, K. A., Finn, M. C., Berger, B. and Clark, P. L. (2006). "Pertactin β -helix folding mechanism suggests common themes for the secretion and folding of autotransporter proteins." Proc. Natl. Acad. Sci. **103**(13): 4918-4923.
132. Kannaiah, S., Livny, J. and Amster-Choder, O. (2019). "Spatiotemporal organization of the *E. coli* transcriptome: translation independence and engagement in regulation." Mol. Cell **76**(4): 574-589.
133. Kanonenberg, K., Schwarz, C. K. and Schmitt, L. (2013). "Type I secretion systems—a story of appendices." Res. Microbiol. **164**(6): 596-604.
134. Kanonenberg, K., Smits, S. H. J. and Schmitt, L. (2019). "Functional reconstitution of HlyB, a type I secretion ABC transporter, in Saposin-A nanoparticles." Sci Rep **9**(1): 8436.
135. Kapitein, N., Bönnemann, G., Pietrosiuk, A., Seyffer, F., Hausser, I., Locker, J. K. and Mogk, A. (2013). "ClpV recycles VipA/VipB tubules and prevents non-productive tubule formation to ensure efficient type VI protein secretion." Mol. Microbiol. **87**(5): 1013-1028.

136. Kenny, B., Chervaux, C. and Holland, I. B. (1994). "Evidence that residues –15 to –46 of the haemolysin secretion signal are involved in early steps in secretion, leading to recognition of the translocator." Mol. Microbiol. **11**(1): 99-109.
137. Kenny, B., Taylor, S. and Holland, I. B. (1992). "Identification of individual amino acids required for secretion within the haemolysin (HlyA) C-terminal targeting region." Mol. Microbiol. **6**(11): 1477-1489.
138. Kieuvongngam, V., Olinares, P. D. B., Palillo, A., Oldham, M. L., Chait, B. T. and Chen, J. (2020). "Structural basis of substrate recognition by a polypeptide processing and secretion transporter." eLife **9**.
139. Kim, J.-S., Song, S., Lee, M., Lee, S., Lee, K. and Ha, N.-C. (2016). "Crystal structure of a soluble fragment of the membrane fusion protein HlyD in a type I secretion system of gram-negative bacteria." Structure **24**(3): 477-485.
140. Klein, R. D., Shu, Q., Cusumano, Z. T., Nagamatsu, K., Gualberto, N. C., Lynch, A. J. L., Wu, C., Wang, W., Jain, N., Pinkner, J. S., Amarasinghe, G. K., Hultgren, S. J., Frieden, C. and Chapman, M. R. (2018). "Structure-function analysis of the curli accessory protein CsgE defines surfaces essential for coordinating amyloid fiber formation." mBio **9**(4): 10.1128/mbio.01349-01318.
141. Kobylka, J., Kuth, M. S., Müller, R. T., Geertsma, E. R. and Pos, K. M. (2020). "AcrB: a mean, keen, drug efflux machine." Ann. N. Y. Acad. Sci. **1459**(1): 38-68.
142. Komar, J., Alvira, S., Schulze, R. J., Martin, R., Lycklama a Nijeholt, J. A., Lee, S. C., Dafforn, T. R., Deckers-Hebestreit, G., Berger, I., Schaffitzel, C. and Collinson, I. (2016). "Membrane protein insertion and assembly by the bacterial holo-translocon SecYEG–SecDF–YajC–YidC." Biochem. J. **473**(19): 3341-3354.
143. Kopcho, N., Chang, G. and Komives, E. A. (2019). "Dynamics of ABC transporter P-glycoprotein in three conformational states." Sci. Rep. **9**(1): 15092.
144. Koronakis, V., Koronakis, E. and Hughes, C. (1989). "Isolation and analysis of the C-terminal signal directing export of *Escherichia coli* hemolysin protein across both bacterial membranes." EMBO J. **8**(2): 595-605.
145. Koronakis, V., Sharff, A., Koronakis, E., Luisi, B. and Hughes, C. (2000). "Crystal structure of the bacterial membrane protein TolC central to multidrug efflux and protein export." Nature **405**(6789): 914.
146. Korotkova, N., Freire, D., Phan, T. H., Ummels, R., Creekmore, C. C., Evans, T. J., Wilmanns, M., Bitter, W., Parret, A. H. A., Houben, E. N. G. and Korotkov, K. V. (2014). "Structure of the *Mycobacterium tuberculosis* type VII secretion system chaperone EspG5 in complex with PE25–PPE41 dimer." Mol. Microbiol. **94**(2): 367-382.
147. Krachmarova, E., Tileva, M., Lilkova, E., Petkov, P., Maskos, K., Ilieva, N., Ivanov, I., Litov, L. and Nacheva, G. (2017). "His-FLAG tag as a fusion partner of glycosylated human interferon-gamma and its mutant: gain or loss?" BioMed Res. Int. **2017**: 3018608.

148. Kulkarni, S. S., Zhu, Y., Brendel, C. J. and McBride, M. J. (2017). "Diverse C-terminal sequences involved in *Flavobacterium johnsoniae* protein secretion." J. Bacteriol. **199**(12): 10.1128/jb.00884-00816.
149. Kwon, H.-J., Haruki, M., Morikawa, M., Omori, K. and Kanaya, S. (2002). "Role of repetitive nine-residue sequence motifs in secretion, enzymatic activity, and protein conformation of a family I. 3 lipase." J. Biosci. Bioeng. **93**(2): 157-164.
150. Lally, E. T., Kieba, I. R., Sato, A., Green, C. L., Rosenbloom, J., Korostoff, J., Wang, J. F., Shenker, B. J., Ortlepp, S., Robinson, M. K. and Billings, P. C. (1997). "RTX toxins recognize a $\beta 2$ integrin on the surface of human target cells." J. Biol. Chem. **272**(48): 30463-30469.
151. Lasica, A. M., Goulas, T., Mizgalska, D., Zhou, X., de Diego, I., Ksiazek, M., Madej, M., Guo, Y., Guevara, T., Nowak, M., Potempa, B., Goel, A., Sztukowska, M., Prabhakar, A. T., Bzowska, M., Widziolek, M., Thøgersen, I. B., Enghild, J. J., Simonian, M., Kulczyk, A. W., Nguyen, K.-A., Potempa, J. and Gomis-Rüth, F. X. (2016). "Structural and functional probing of PorZ, an essential bacterial surface component of the type-IX secretion system of human oral-microbiomic *Porphyromonas gingivalis*." Sci. Rep. **6**(1): 37708.
152. Lauber, F., Deme, J. C., Lea, S. M. and Berks, B. C. (2018). "Type 9 secretion system structures reveal a new protein transport mechanism." Nature **564**(7734): 77-82.
153. Lecher, J., Schwarz, C. K., Stoldt, M., Smits, S. H., Willbold, D. and Schmitt, L. (2012). "An RTX transporter tethers its unfolded substrate during secretion via a unique N-terminal domain." Structure **20**(10): 1778-1787.
154. Lee, H. C. and Bernstein, H. D. (2001). "The targeting pathway of *Escherichia coli* presecretory and integral membrane proteins is specified by the hydrophobicity of the targeting signal." Proc. Natl. Acad. Sci. **98**(6): 3471-3476.
155. Lee, M., Jun, S.-Y., Yoon, B.-Y., Song, S., Lee, K. and Ha, N.-C. (2012). "Membrane fusion proteins of type I secretion system and tripartite efflux pumps share a binding motif for TolC in gram-negative bacteria." PLOS ONE **7**(7): e40460.
156. Lee, P.-C. and Rietsch, A. (2015). "Fueling type III secretion." Trends Microbiol. **23**(5): 296-300.
157. Lee, S. H. and Altenberg, G. A. (2003). "Expression of functional multidrug-resistance protein 1 in *Saccharomyces cerevisiae*: effects of N- and C-terminal affinity tags." Biochem. Biophys. Res. Commun. **306**(3): 644-649.
158. Lenders, M. H., Beer, T., Smits, S. H. and Schmitt, L. (2016). "*In vivo* quantification of the secretion rates of the hemolysin A type I secretion system." Sci. Rep. **6**: 33275.
159. Lenders, M. H., Weidtkamp-Peters, S., Kleinschrodt, D., Jaeger, K.-E., Smits, S. H. and Schmitt, L. (2015). "Directionality of substrate translocation of the hemolysin A type I secretion system." Sci. Rep. **5**(1): 12470.
160. Leo, J. C., Grin, I. and Linke, D. (2012). "Type V secretion: mechanism (s) of autotransport through the bacterial outer membrane." Philos. Trans. R. Soc. Lond., Ser. B: Biol. Sci. **367**(1592): 1088-1101.

161. Leone, P., Roche, J., Vincent, M. S., Tran, Q. H., Desmyter, A., Cascales, E., Kellenberger, C., Cambillau, C. and Roussel, A. (2018). "Type IX secretion system PorM and gliding machinery GldM form arches spanning the periplasmic space." Nat. Commun. **9**(1): 429.
162. L  toff  , S., Ghigo, J. and Wandersman, C. (1994). "Secretion of the *Serratia marcescens* HasA protein by an ABC transporter." J. Bacteriol. **176**(17): 5372-5377.
163. L  toff  , S. and Wandersman, C. (1992). "Secretion of CyaA-PrtB and HlyA-PrtB fusion proteins in *Escherichia coli*: involvement of the glycine-rich repeat domain of *Erwinia chrysanthemi* protease B." J. Bacteriol. **174**(15): 4920-4927.
164. Li, Y. G., Hu, B. and Christie, P. J. (2019). "Biological and structural diversity of type IV secretion systems." Microbiol. Spectr. **7**(2): 1-10.
165. Lim, K. B., Walker, C. R. B., Guo, L., Pellett, S., Shabanowitz, J., Hunt, D. F., Hewlett, E. L., Ludwig, A., Goebel, W. and Welch, R. A. (2000). "*Escherichia coli* α -hemolysin (HlyA) is heterogeneously acylated *in vivo* with 14-, 15-, and 17-carbon fatty acids." J. Biol. Chem. **275**(47): 36698-36702.
166. Lin, D. Y.-w., Huang, S. and Chen, J. (2015). "Crystal structures of a polypeptide processing and secretion transporter." Nature **523**(7561): 425.
167. Lindberg, F., Tennent, J., Hultgren, S., Lund, B. and Normark, S. (1989). "PapD, a periplasmic transport protein in P-pilus biogenesis." J. Bacteriol. **171**(11): 6052-6058.
168. Linhartov  , I., Bumba, L., Ma   n, J., Basler, M., Osi  ka, R., Kamanov  , J., Proch  zkov  , K., Adkins, I., Hejnov  -Holubov  , J. and Sad  lkov  , L. (2010). "RTX proteins: a highly diverse family secreted by a common mechanism." FEMS Microbiol. Rev. **34**(6): 1076-1112.
169. Llosa, M. and Alkorta, I. (2017). Coupling Proteins in Type IV Secretion. Type IV Secretion in Gram-Negative and Gram-Positive Bacteria, Springer International Publishing: 143-168.
170. Lobedanz, S., Bokma, E., Symmons, M. F., Koronakis, E., Hughes, C. and Koronakis, V. (2007). "A periplasmic coiled-coil interface underlying TolC recruitment and the assembly of bacterial drug efflux pumps." Proc. Natl. Acad. Sci. **104**(11): 4612-4617.
171. Lopez-Castilla, A., Thomassin, J.-L., Bardiaux, B., Zheng, W., Nivaskumar, M., Yu, X., Nilges, M., Egelman, E. H., Izadi-Pruneyre, N. and Francetic, O. (2017). "Structure of the calcium-dependent type 2 secretion pseudopilus." Nat. Microbiol. **2**(12): 1686-1695.
172. Low, H. H., Gubellini, F., Rivera-Calzada, A., Braun, N., Connery, S., Dujeancourt, A., Lu, F., Redzej, A., Fronzes, R., Orlova, E. V. and Waksman, G. (2014). "Structure of a type IV secretion system." Nature **508**(7497): 550-553.
173. Ludwig, A., Benz, R. and Goebel, W. (1993). "Oligomerization of *Escherichia coli* haemolysin (HlyA) is involved in pore formation." Mol. Gen. Genet. **241**(1): 89-96.

174. Ludwig, A., Schmid, A., Benz, R. and Goebel, W. (1991). "Mutations affecting pore formation by haemolysin from *Escherichia coli*." Mol. Gen. Genet. **226**: 198-208.
175. Lüke, I., Handford, J. I., Palmer, T. and Sargent, F. (2009). "Proteolytic processing of *Escherichia coli* twin-arginine signal peptides by LepB." Arch. Microbiol. **191**: 919-925.
176. Luo, Q., Yang, X., Yu, S., Shi, H., Wang, K., Xiao, L., Zhu, G., Sun, C., Li, T. and Li, D. (2017). "Structural basis for lipopolysaccharide extraction by ABC transporter LptB₂FG." Nat. Struct. Mol. Biol. **24**(5): 469-474.
177. Macé, K., Vadakkepat, A. K., Redzej, A., Lukyanova, N., Oomen, C., Braun, N., Ukleja, M., Lu, F., Costa, T. R. D., Orlova, E. V., Baker, D., Cong, Q. and Waksman, G. (2022). "Cryo-EM structure of a type IV secretion system." Nature **607**(7917): 191-196.
178. Mackman, N., Nicaud, J.-M., Gray, L. and Holland, I. (1985a). "Genetical and functional organisation of the *Escherichia coli* haemolysin determinant 2001." Mol. Gen. Genet. **201**: 282-288.
179. Mackman, N., Nicaud, J.-M., Gray, L. and Holland, I. (1985b). "Identification of polypeptides required for the export of haemolysin 2001 from *E. coli*." Mol. Gen. Genet. **201**: 529-536.
180. Madej, M., Nowakowska, Z., Ksiazek, M., Lasica, A. M., Mizgalska, D., Nowak, M., Jacula, A., Bzowska, M., Scavenius, C. and Enghild, J. J. (2021). "PorZ, an essential component of the type IX secretion system of *Porphyromonas gingivalis*, delivers anionic lipopolysaccharide to the PorU sortase for transpeptidase processing of T9SS cargo proteins." MBio **12**(1): 10.1128/mbio.02262-02220.
181. Masi, M. and Wandersman, C. (2010). "Multiple signals direct the assembly and function of a type 1 secretion system." J. Bacteriol. **192**(15): 3861-3869.
182. Masin, J., Osickova, A., Jurnecka, D., Klimova, N., Khaliq, H., Sebo, P. and Osicka, R. (2020). "Retargeting from the CR3 to the LFA-1 receptor uncovers the adenylyl cyclase enzyme-translocating segment of *Bordetella* adenylate cyclase toxin." J. Biol. Chem. **295**(28): 9349-9365.
183. Meier, R., Drepper, T., Svensson, V., Jaeger, K.-E. and Baumann, U. (2007). "A calcium-gated lid and a large β -roll sandwich are revealed by the crystal structure of extracellular lipase from *Serratia marcescens*." J. Biol. Chem. **282**(43): 31477-31483.
184. Meuskens, I., Saragliadis, A., Leo, J. C. and Linke, D. (2019). "Type V secretion systems: an overview of passenger domain functions." Front. Microbiol. **10**: 1163.
185. Mizgalska, D., Goulas, T., Rodríguez-Banqueri, A., Veillard, F., Madej, M., Małecka, E., Szczesniak, K., Ksiazek, M., Widziołek, M., Guevara, T., Eckhard, U., Solà, M., Potempa, J. and Gomis-Rüth, F. X. (2021). "Intermolecular latency regulates the essential C-terminal signal peptidase and sortase of the *Porphyromonas gingivalis* type-IX secretion system." Proc. Natl. Acad. Sci. **118**(40): e2103573118.

186. Moayeri, M. and Welch, R. A. (1994). "Effects of temperature, time, and toxin concentration on lesion formation by the *Escherichia coli* hemolysin." Infect. Immun. **62**(10): 4124-4134.
187. Monjarás Fera, J. V., Lefebvre, M. D., Stierhof, Y.-D., Galán, J. E. and Wagner, S. (2015). "Role of autocleavage in the function of a type III secretion specificity switch protein in *Salmonella enterica* serovar Typhimurium." MBio **6**(5): 10.1128/mbio. 01459-01415.
188. Montero Llopis, P., Jackson, A. F., Sliusarenko, O., Surovtsev, I., Heinritz, J., Emonet, T. and Jacobs-Wagner, C. (2010). "Spatial organization of the flow of genetic information in bacteria." Nature **466**(7302): 77-81.
189. Mori, H. and Cline, K. (2002). "A twin arginine signal peptide and the pH gradient trigger reversible assembly of the thylakoid Δ pH/Tat translocase." J. Cell Biol. **157**(2): 205-210.
190. Morova, J., Osicka, R., Masin, J. and Sebo, P. (2008). "RTX cytotoxins recognize β_2 integrin receptors through N-linked oligosaccharides." Proc. Natl. Acad. Sci. **105**(14): 5355-5360.
191. Motlova, L., Klimova, N., Fiser, R., Sebo, P. and Bumba, L. (2020). "Continuous assembly of β -roll structures is implicated in the Type I-dependent secretion of large Repeat-in-Toxins (RTX) proteins." J. Mol. Biol. **432**(20): 5696-5710.
192. Nagai, H., Cambronne, E. D., Kagan, J. C., Amor, J. C., Kahn, R. A. and Roy, C. R. (2005). "A C-terminal translocation signal required for Dot/Icm-dependent delivery of the *Legionella* RalF protein to host cells." Proc. Natl. Acad. Sci. **102**(3): 826-831.
193. Naskar, S., Hohl, M., Tassinari, M. and Low, H. H. (2021). "The structure and mechanism of the bacterial type II secretion system." Mol. Microbiol. **115**(3): 412-424.
194. Navarro-Garcia, F., Ruiz-Perez, F., Cataldi, Á. and Larzábal, M. (2019). "Type VI secretion system in pathogenic *Escherichia coli*: structure, role in virulence, and acquisition." Front. Microbiol. **10**: 1-17.
195. Nenninger, A. A., Robinson, L. S., Hammer, N. D., Epstein, E. A., Badtke, M. P., Hultgren, S. J. and Chapman, M. R. (2011). "CsgE is a curli secretion specificity factor that prevents amyloid fibre aggregation." Mol. Microbiol. **81**(2): 486-499.
196. Nevo-Dinur, K., Nussbaum-Shochat, A., Ben-Yehuda, S. and Amster-Choder, O. (2011). "Translation-independent localization of mRNA in *E. coli*." Science **331**(6020): 1081-1084.
197. Nguyen, V. S., Douzi, B., Durand, E., Roussel, A., Cascales, E. and Cambillau, C. (2018). "Towards a complete structural deciphering of type VI secretion system." Curr. Opin. Struct. Biol. **49**: 77-84.
198. Nicaud, J.-M., Mackman, N., Gray, L. and Holland, I. (1985). "Characterisation of HlyC and mechanism of activation and secretion of haemolysin from *E. coli* 2001." FEBS Lett. **187**(2): 339-344.

199. Nicaud, J.-M., Mackman, N., Gray, L. and Holland, I. (1986). "The C-terminal, 23 kDa peptide of *E. coli* haemolysin 2001 contains all the information necessary for its secretion by the haemolysin (Hly) export machinery." FEBS Lett. **204**(2): 331-335.
200. Nikaido, H. (1992). "Porins and specific channels of bacterial outer membranes." Mol. Microbiol. **6**(4): 435-442.
201. Nikaido, H. (2003). "Molecular basis of bacterial outer membrane permeability revisited." Microbiol. Mol. Biol. Rev. **67**(4): 593-656.
202. Nikaido, H. and Pagès, J.-M. (2012). "Broad-specificity efflux pumps and their role in multidrug resistance of gram-negative bacteria." FEMS Microbiol. Rev. **36**(2): 340-363.
203. Nishiyama, K.-i., Mizushima, S. and Tokuda, H. (1993). "A novel membrane protein involved in protein translocation across the cytoplasmic membrane of *Escherichia coli*." EMBO J. **12**(9): 3409-3415.
204. Nivaskumar, M. and Francetic, O. (2014). "Type II secretion system: a magic beanstalk or a protein escalator." Biochim. Biophys. Acta, Mol. Cell Res. **1843**(8): 1568-1577.
205. Noegel, A., Rdest, U., Springer, W. and Goebel, W. (1979). "Plasmid cistrons controlling synthesis and excretion of the exotoxin α -haemolysin of *Escherichia coli*." Mol. Gen. Genet. **175**(3): 343-350.
206. Ogasawara, H., Yamamoto, K. and Ishihama, A. (2011). "Role of the biofilm master regulator CsgD in cross-regulation between biofilm formation and flagellar synthesis." J. Bacteriol. **193**(10): 2587-2597.
207. Orfanoudaki, G. and Economou, A. (2014). "Proteome-wide subcellular topologies of *E. coli* polypeptides database (STEPdb)." Mol. Cell. Proteomics **13**(12): 3674-3687.
208. Osickova, A., Khaliq, H., Masin, J., Jurnecka, D., Sukova, A., Fiser, R., Holubova, J., Stanek, O., Sebo, P. and Osicka, R. (2020). "Acyltransferase-mediated selection of the length of the fatty acyl chain and of the acylation site governs activation of bacterial RTX toxins." J. Biol. Chem. **295**(28): 9268-9280.
209. Oswald, C., Holland, I. B. and Schmitt, L. (2006). "The motor domains of ABC-transporters." Naunyn-Schmiedeberg's Arch. Pharmacol. **372**(6): 385-399.
210. Oswald, C., Tam, H.-K. and Pos, K. M. (2016). "Transport of lipophilic carboxylates is mediated by transmembrane helix 2 in multidrug transporter AcrB." Nat. Commun. **7**(1): 13819.
211. Padayatti, P. S., Lee, S. C., Stanfield, R. L., Wen, P.-C., Tajkhorshid, E., Wilson, I. A. and Zhang, Q. (2019). "Structural insights into the lipid A transport pathway in MsbA." Structure **27**(7): 1114-1123.e1113.
212. Panahandeh, S., Maurer, C., Moser, M., DeLisa, M. P. and Müller, M. (2008). "Following the path of a twin-arginine precursor along the TatABC translocase of *Escherichia coli*." J. Biol. Chem.

213. Park, Y.-J., Lacourse, K. D., Cambillau, C., DiMaio, F., Mougous, J. D. and Veesler, D. (2018). "Structure of the type VI secretion system TssK–TssF–TssG baseplate subcomplex revealed by cryo-electron microscopy." Nat. Commun. **9**(1): 5385.
214. Patrick, M., Korotkov, K. V., Hol, W. G. J. and Sandkvist, M. (2011). "Oligomerization of EpsE coordinates residues from multiple subunits to facilitate ATPase activity." J. Biol. Chem. **286**(12): 10378-10386.
215. Pavlova, O., Peterson, J. H., Ieva, R. and Bernstein, H. D. (2013). "Mechanistic link between β barrel assembly and the initiation of autotransporter secretion." Proc. Natl. Acad. Sci. **110**(10): E938-E947.
216. Perkins, H. (2012). Microbial cell walls and membranes, Springer Science & Business Media.
217. Peterson, J. H., Tian, P., Ieva, R., Dautin, N. and Bernstein, H. D. (2010). "Secretion of a bacterial virulence factor is driven by the folding of a C-terminal segment." Proc. Natl. Acad. Sci. **107**(41): 17739-17744.
218. Peterson, J. H., Woolhead, C. A. and Bernstein, H. D. (2003). "Basic amino acids in a distinct subset of signal peptides promote interaction with the signal recognition particle." J. Biol. Chem. **278**(46): 46155-46162.
219. Phan, G., Remaut, H., Wang, T., Allen, W. J., Pirker, K. F., Lebedev, A., Henderson, N. S., Geibel, S., Volkan, E., Yan, J., Kunze, M. B. A., Pinkner, J. S., Ford, B., Kay, C. W. M., Li, H., Hultgren, S. J., Thanassi, D. G. and Waksman, G. (2011). "Crystal structure of the FimD usher bound to its cognate FimC–FimH substrate." Nature **474**(7349): 49-53.
220. Pimenta, A., Young, J., Holland, I. and Blight, M. (1999). "Antibody analysis of the localisation, expression and stability of HlyD, the MFP component of the *E. coli* haemolysin translocator." Mol. Gen. Genet. **261**(1): 122-132.
221. Pineau, C., Guschinskaya, N., Robert, X., Gouet, P., Ballut, L. and Shevchik, V. E. (2014). "Substrate recognition by the bacterial type II secretion system: more than a simple interaction." Mol. Microbiol. **94**(1): 126-140.
222. Pomowski, A., Zumft, W. G., Kroneck, P. M. and Einsle, O. (2011). "N₂O binding at a [4Cu: 2S] copper–sulphur cluster in nitrous oxide reductase." Nature **477**(7363): 234-237.
223. Pourhassan, Z., Hachani, E., Spitz, O., Smits, S. H. and Schmitt, L. (2022). "Investigations on the substrate binding sites of hemolysin B, an ABC transporter, of a type 1 secretion system." Front. Microbiol. **13**: 1-15.
224. Prieß, M., Göddeke, H., Groenhof, G. and Schäfer, L. V. (2018). "Molecular mechanism of ATP hydrolysis in an ABC transporter." ACS Cent. Sci. **4**(10): 1334-1343.
225. Prigent-Combaret, C., Brombacher, E., Vidal, O., Ambert, A., Lejeune, P., Landini, P. and Dorel, C. (2001). "Complex regulatory network controls initial adhesion and biofilm formation in *Escherichia coli* via regulation of the *csgD* gene." J. Bacteriol. **183**(24): 7213-7223.
226. Raetz, C. and Dowhan, W. (1990). "Biosynthesis and function of phospholipids in *Escherichia coli*." J. Biol. Chem. **265**(3): 1235-1238.

-
227. Rapisarda, C., Cherrak, Y., Kooger, R., Schmidt, V., Pellarin, R., Logger, L., Cascales, E., Pilhofer, M., Durand, E. and Fronzes, R. (2019). "In situ and high-resolution cryo-EM structure of a bacterial type VI secretion system membrane complex." EMBO J. **38**(10): e100886.
228. Reimann, S., Poschmann, G., Kanonenberg, K., Stühler, K., Smits, S. H. and Schmitt, L. (2016). "Interdomain regulation of the ATPase activity of the ABC transporter hemolysin B from *E. coli*." Biochem. J. **473**(16): 2471-2483.
229. Renault, M. G., Zamarreno Beas, J., Douzi, B., Chabalier, M., Zoued, A., Brunet, Y. R., Cambillau, C., Journet, L. and Cascales, E. (2018). "The gp27-like hub of VgrG serves as adaptor to promote Hcp tube assembly." J. Mol. Biol. **430**(18, Part B): 3143-3156.
230. Ristow, L. C., Tran, V., Schwartz, K. J., Pankratz, L., Mehle, A., Sauer, J.-D. and Welch, R. A. (2019). "The extracellular domain of the β_2 integrin β subunit (CD18) is sufficient for *Escherichia coli* hemolysin and *Aggregatibacter actinomycetemcomitans* leukotoxin cytotoxic activity." mBio **10**(4): 10.1128/mbio.01459-01419.
231. Rivera-Calzada, A., Famelis, N., Llorca, O. and Geibel, S. (2021). "Type VII secretion systems: structure, functions and transport models." Nat. Rev. Microbiol. **19**(9): 567-584.
232. Robinson, G. (1951). "The haemolysin of bacterium coli." Microbiology **5**(4): 788-792.
233. Samudrala, R., Heffron, F. and McDermott, J. E. (2009). "Accurate prediction of secreted substrates and identification of a conserved putative secretion signal for type III secretion systems." PLoS Path. **5**(4): e1000375.
234. Sanchez-Magraner, L., Viguera, A. R., Garcia-Pacios, M., Garcillan, M. P., Arrondo, J.-L. R., de la Cruz, F., Goni, F. M. and Ostolaza, H. (2007). "The calcium-binding C-terminal domain of *Escherichia coli* α -hemolysin is a major determinant in the surface-active properties of the protein." J. Biol. Chem. **282**(16): 11827-11835.
235. Santin, Y. G., Doan, T., Lebrun, R., Espinosa, L., Journet, L. and Cascales, E. (2018). "In vivo TssA proximity labelling during type VI secretion biogenesis reveals TagA as a protein that stops and holds the sheath." Nat. Microbiol. **3**(11): 1304-1313.
236. Saraogi, I. and Shan, S.-o. (2014). "Co-translational protein targeting to the bacterial membrane." Biochim. Biophys. Acta, Mol. Cell Res. **1843**(8): 1433-1441.
237. Sauer, F. G., Futterer, K., Pinkner, J. S., Dodson, K. W., Hultgren, S. J. and Waksman, G. (1999). "Structural basis of chaperone function and pilus biogenesis." Science **285**(5430): 1058-1061.
238. Sauv  , V., Bruno, S., Berks, B. C. and Hemmings, A. M. (2007). "The SoxYZ complex carries sulfur cycle intermediates on a peptide swinging arm." J. Biol. Chem. **282**(32): 23194-23204.
239. Schiebel, E., Driessen, A. J., Hartl, F.-U. and Wickner, W. (1991). " $\Delta\mu\text{H}^+$ and ATP function at different steps of the catalytic cycle of preprotein translocase." Cell **64**(5): 927-939.

240. Schmitt, L., Benabdelhak, H., Blight, M. A., Holland, I. B. and Stubbs, M. T. (2003). "Crystal structure of the nucleotide-binding domain of the ABC-transporter haemolysin B: identification of a variable region within ABC helical domains." J. Mol. Biol. **330**(2): 333-342.
241. Schmitt, L. and Tampé, R. (2002). "Structure and mechanism of ABC transporters." Curr. Opin. Struct. Biol. **12**(6): 754-760.
242. Schrödinger, L. (2022). "The PyMOL molecular graphics system, version 2.5."
243. Schulein, R., Guye, P., Rhomberg, T. A., Schmid, M. C., Schröder, G., Vergunst, A. C., Carena, I. and Dehio, C. (2005). "A bipartite signal mediates the transfer of type IV secretion substrates of *Bartonella henselae* into human cells." Proc. Natl. Acad. Sci. **102**(3): 856-861.
244. Schwarz, C. K., Landsberg, C. D., Lenders, M. H., Smits, S. H. and Schmitt, L. (2012). "Using an *E. coli* type 1 secretion system to secrete the mammalian, intracellular protein IFABP in its active form." J. Biotechnol. **159**(3): 155-161.
245. Seeger, M. A., Schiefner, A., Eicher, T., Verrey, F., Diederichs, K. and Pos, K. M. (2006). "Structural asymmetry of AcrB trimer suggests a peristaltic pump mechanism." Science **313**(5791): 1295-1298.
246. Senior, A. E., Al-Shawi, M. K. and Urbatsch, I. L. (1995). "The catalytic cycle of P-glycoprotein." FEBS Lett. **377**(3): 285-289.
247. Sennhauser, G., Amstutz, P., Briand, C., Storchenegger, O. and Grütter, M. G. (2007). "Drug export pathway of multidrug exporter AcrB revealed by DARPin inhibitors." PLoS Biol. **5**(1): e7.
248. Sennhauser, G., Bukowska, M. A., Briand, C. and Grütter, M. G. (2009). "Crystal structure of the multidrug exporter MexB from *Pseudomonas aeruginosa*." J. Mol. Biol. **389**(1): 134-145.
249. Shevchik, V. E., Robert-Baudouy, J. and Condemine, G. (1997). "Specific interaction between OutD, an *Erwinia chrysanthemi* outer membrane protein of the general secretory pathway, and secreted proteins." EMBO J. **16**(11): 3007-3016.
250. Shi, X., Chen, M., Yu, Z., Bell, J. M., Wang, H., Forrester, I., Villarreal, H., Jakana, J., Du, D. and Luisi, B. F. (2019). "*In situ* structure and assembly of the multidrug efflux pump AcrAB-TolC." Nat. Commun. **10**(1): 2635.
251. Shinoda, T., Ogawa, H., Cornelius, F. and Toyoshima, C. (2009). "Crystal structure of the sodium–potassium pump at 2.4 Å resolution." Nature **459**(7245): 446-450.
252. Short, E. C. and Kurtz, H. J. (1971). "Properties of the hemolytic activities of *Escherichia coli*." Infect. Immun. **3**(5): 678-687.
253. Shu, Q., Krezel, A. M., Cusumano, Z. T., Pinkner, J. S., Klein, R., Hultgren, S. J. and Frieden, C. (2016). "Solution NMR structure of CsgE: structural insights into a chaperone and regulator protein important for functional amyloid formation." Proc. Natl. Acad. Sci. **113**(26): 7130-7135.
254. Siliakus, M. F., van der Oost, J. and Kengen, S. W. (2017). "Adaptations of archaeal and bacterial membranes to variations in temperature, pH and pressure." Extremophiles **21**: 651-670.

-
255. Smith, P. C., Karpowich, N., Millen, L., Moody, J. E., Rosen, J., Thomas, P. J. and Hunt, J. F. (2002). "ATP binding to the motor domain from an ABC transporter drives formation of a nucleotide sandwich dimer." *Mol. Cell* **10**(1): 139-149.
256. Smith, T. J., Font, M. E., Kelly, C. M., Sondermann, H. and O'Toole, G. A. (2018). "An N-terminal retention module anchors the giant adhesin LapA of *Pseudomonas fluorescens* at the cell surface: a novel subfamily of type I secretion systems." *J. Bacteriol.* **200**(8): e00734-00717.
257. Sohlenkamp, C. and Geiger, O. (2015). "Bacterial membrane lipids: diversity in structures and pathways." *FEMS Microbiol. Rev.* **40**(1): 133-159.
258. Soltes, G. R., Martin, N. R., Park, E., Sutterlin, H. A. and Silhavy, T. J. (2017). "Distinctive roles for periplasmic proteases in the maintenance of essential outer membrane protein assembly." *J. Bacteriol.* **199**(20): 10.1128/jb. 00418-00417.
259. Spitz, O., Erenburg, I. N., Beer, T., Kanonenberg, K., Holland, I. B. and Schmitt, L. (2019). "Type I secretion systems—one mechanism for all?" *Microbiol. Spectr.* **7**(2): 1-9.
260. Spitz, O., Erenburg, I. N., Kanonenberg, K., Peherstorfer, S., Lenders, M. H., Reiners, J., Ma, M., Luisi, B. F., Smits, S. H. and Schmitt, L. (2022). "Identity determinants of the translocation signal for a type 1 secretion system." *Front. Physiol.* **12**: 1-13.
261. Stanley, P., Koronakis, V., Hardie, K. and Hughes, C. (1996). "Independent interaction of the acyltransferase HlyC with two maturation domains of the *Escherichia coli* toxin HlyA." *Mol. Microbiol.* **20**(4): 813-822.
262. Stanley, P., Koronakis, V. and Hughes, C. (1991). "Mutational analysis supports a role for multiple structural features in the C-terminal secretion signal of *Escherichia coli* haemolysin." *Mol. Microbiol.* **5**(10): 2391-2403.
263. Stanley, P., Packman, L. C., Koronakis, V. and Hughes, C. (1994). "Fatty acylation of two internal lysine residues required for the toxic activity of *Escherichia coli* hemolysin." *Science* **266**(5193): 1992-1996.
264. Steudle, A., Spann, D., Pross, E., Shanmugam, S. K., Dalbey, R. E. and Kuhn, A. (2021). "Molecular communication of the membrane insertase YidC with translocase SecYEG affects client proteins." *Sci. Rep.* **11**(1): 3940.
265. Stillwell, W. (2013). *An introduction to biological membranes: from bilayers to rafts*. Academic Press.
266. Su, C.-C., Li, M., Gu, R., Takatsuka, Y., McDermott, G., Nikaido, H. and Yu, E. W. (2006). "Conformation of the AcrB multidrug efflux pump in mutants of the putative proton relay pathway." *J. Bacteriol.* **188**(20): 7290-7296.
267. Symmons, M. F., Bokma, E., Koronakis, E., Hughes, C. and Koronakis, V. (2009). "The assembled structure of a complete tripartite bacterial multidrug efflux pump." *Proc. Natl. Acad. Sci.* **106**(17): 7173-7178.
268. Tam, H.-K., Malviya, V. N., Foong, W.-E., Herrmann, A., Malloci, G., Ruggerone, P., Vargiu, A. V. and Pos, K. M. (2020). "Binding and transport of carboxylated drugs by the multidrug transporter AcrB." *J. Mol. Biol.* **432**(4): 861-877.

269. Tamura, N., Murakami, S., Oyama, Y., Ishiguro, M. and Yamaguchi, A. (2005). "Direct interaction of multidrug efflux transporter AcrB and outer membrane channel TolC detected via site-directed disulfide cross-linking." Biochemistry **44**(33): 11115-11121.
270. Taylor, J. D., Hawthorne, W. J., Lo, J., Dear, A., Jain, N., Meisl, G., Andreasen, M., Fletcher, C., Koch, M., Darvill, N., Scull, N., Escalera-Maurer, A., Sefer, L., Wenman, R., Lambert, S., Jean, J., Xu, Y., Turner, B., Kazarian, S. G., Chapman, M. R., Bubeck, D., de Simone, A., Knowles, T. P. J. and Matthews, S. J. (2016). "Electrostatically-guided inhibition of Curli amyloid nucleation by the CsgC-like family of chaperones." Sci. Rep. **6**(1): 24656.
271. Thanabalu, T., Koronakis, E., Hughes, C. and Koronakis, V. (1998). "Substrate-induced assembly of a contiguous channel for protein export from *E. coli*: reversible bridging of an inner-membrane translocase to an outer membrane exit pore." EMBO J. **17**(22): 6487-6496.
272. Thanassi, D. G., Saulino, E. T. and Hultgren, S. J. (1998). "The chaperone/usheer pathway: a major terminal branch of the general secretory pathway." Curr. Opin. Microbiol. **1**(2): 223-231.
273. Thomas, C., Aller, S. G., Beis, K., Carpenter, E. P., Chang, G., Chen, L., Dassa, E., Dean, M., Duong Van Hoa, F., Ekiert, D., Ford, R., Gaudet, R., Gong, X., Holland, I. B., Huang, Y., Kahne, D. K., Kato, H., Koronakis, V., Koth, C. M., Lee, Y., Lewinson, O., Lill, R., Martinoia, E., Murakami, S., Pinkett, H. W., Poolman, B., Rosenbaum, D., Sarkadi, B., Schmitt, L., Schneider, E., Shi, Y., Shyng, S.-L., Slotboom, D. J., Tajkhorshid, E., Tieleman, D. P., Ueda, K., Váradi, A., Wen, P.-C., Yan, N., Zhang, P., Zheng, H., Zimmer, J. and Tampé, R. (2020). "Structural and functional diversity calls for a new classification of ABC transporters." FEBS Lett. **594**(23): 3767-3775.
274. Thomas, C. and Tampé, R. (2018). "Multifaceted structures and mechanisms of ABC transport systems in health and disease." Curr. Opin. Struct. Biol. **51**: 116-128.
275. Thomas, S., Bakkes, P. J., Smits, S. H. and Schmitt, L. (2014a). "Equilibrium folding of pro-HlyA from *Escherichia coli* reveals a stable calcium ion dependent folding intermediate." Biochim. Biophys. Acta **1844**(9): 1500-1510.
276. Thomas, S., Holland, I. B. and Schmitt, L. (2014b). "The type 1 secretion pathway—the hemolysin system and beyond." Biochim. Biophys. Acta, Mol. Cell Res. **1843**(8): 1629-1641.
277. Tikhonova, E. B. and Zgurskaya, H. I. (2004). "AcrA, AcrB, and TolC of *Escherichia coli* form a stable intermembrane multidrug efflux complex." J. Biol. Chem. **279**(31): 32116-32124.
278. Tomasek, D. and Kahne, D. (2021). "The assembly of β -barrel outer membrane proteins." Curr. Opin. Microbiol. **60**: 16-23.
279. Tomblin, G., Bartholomew, L. A., Tyndall, G. A., Gimi, K., Urbatsch, I. L. and Senior, A. E. (2004). "Properties of P-glycoprotein with mutations in the "catalytic carboxylate" glutamate residues." J. Biol. Chem.

-
280. Tottey, S., Waldron, K. J., Firbank, S. J., Reale, B., Bessant, C., Sato, K., Cheek, T. R., Gray, J., Banfield, M. J. and Dennison, C. (2008). "Protein-folding location can regulate manganese-binding versus copper- or zinc-binding." Nature **455**(7216): 1138-1142.
281. Touzé, T., Eswaran, J., Bokma, E., Koronakis, E., Hughes, C. and Koronakis, V. (2004). "Interactions underlying assembly of the *Escherichia coli* AcrAB–TolC multidrug efflux system." Mol. Microbiol. **53**(2): 697-706.
282. Trokter, M., Felisberto-Rodrigues, C., Christie, P. J. and Waksman, G. (2014). "Recent advances in the structural and molecular biology of type IV secretion systems." Curr. Opin. Struct. Biol. **27**: 16-23.
283. Troman, L. and Collinson, I. (2021). "Pushing the envelope: the mysterious journey through the bacterial secretory machinery, and beyond." Front. Microbiol. **12**.
284. Tsukazaki, T. (2018). "Structure-based working model of SecDF, a proton-driven bacterial protein translocation factor." FEMS Microbiol. Lett. **365**(12): 1-9.
285. Tsutsumi, K., Yonehara, R., Ishizaka-Ikeda, E., Miyazaki, N., Maeda, S., Iwasaki, K., Nakagawa, A. and Yamashita, E. (2019). "Structures of the wild-type MexAB–OprM tripartite pump reveal its complex formation and drug efflux mechanism." Nat. Commun. **10**(1): 1520.
286. Urbatsch, I. L., Sankaran, B., Weber, J. and Senior, A. E. (1995). "P-glycoprotein is stably inhibited by vanadate-induced trapping of nucleotide at a single catalytic site." J. Biol. Chem. **270**(33): 19383-19390.
287. Vaccaro, L., Scott, K. A. and Sansom, M. S. (2008). "Gating at both ends and breathing in the middle: conformational dynamics of TolC." Biophys. J. **95**(12): 5681-5691.
288. Valeva, A., Walev, I., Kemmer, H., Weis, S., Siegel, I., Boukhallouk, F., Wassenaar, T. M., Chavakis, T. and Bhakdi, S. (2005). "Binding of *Escherichia coli* hemolysin and activation of the target cells is not receptor-dependent." J. Biol. Chem. **280**(44): 36657-36663.
289. Veith, P., Glew, M., Gorasia, D., Cascales, E. and Reynolds, E. (2022). "The type IX secretion system and its role in bacterial function and pathogenesis." J. Dent. Res. **101**(4): 374-383.
290. Veith, P. D., Nor Muhammad, N. A., Dashper, S. G., Likić, V. A., Gorasia, D. G., Chen, D., Byrne, S. J., Catmull, D. V. and Reynolds, E. C. (2013). "Protein substrates of a novel secretion system are numerous in the bacteroidetes phylum and have in common a cleavable C-terminal secretion signal, extensive post-translational modification, and cell-surface attachment." J. Proteome Res. **12**(10): 4449-4461.
291. Vergani, P., Lockless, S. W., Nairn, A. C. and Gadsby, D. C. (2005). "CFTR channel opening by ATP-driven tight dimerization of its nucleotide-binding domains." Nature **433**(7028): 876-880.
292. Verger, D., Miller, E., Remaut, H., Waksman, G. and Hultgren, S. (2006). "Molecular mechanism of P pilus termination in uropathogenic *Escherichia coli*." EMBO Rep. **7**(12): 1228-1232.

293. Vergunst, A. C., van Lier, M. C., den Dulk-Ras, A., Grosse Stüve, T. A., Ouwehand, A. and Hooykaas, P. J. (2005). "Positive charge is an important feature of the C-terminal transport signal of the VirB/D4-translocated proteins of *Agrobacterium*." Proc. Natl. Acad. Sci. **102**(3): 832-837.
294. Vollmer, W., Blanot, D. and De Pedro, M. A. (2008). "Peptidoglycan structure and architecture." FEMS Microbiol. Rev. **32**(2): 149-167.
295. Voss, N. R. and Gerstein, M. (2010). "3V: cavity, channel and cleft volume calculator and extractor." Nucleic Acids Res. **38**(Web Server issue): W555-562.
296. Wandersman, C. and Delepelaire, P. (1990). "TolC, an *Escherichia coli* outer membrane protein required for hemolysin secretion." Proc. Natl. Acad. Sci. **87**(12): 4776-4780.
297. Wang, J., Brackmann, M., Castaño-Díez, D., Kudryashev, M., Goldie, K. N., Maier, T., Stahlberg, H. and Basler, M. (2017). "Cryo-EM structure of the extended type VI secretion system sheath–tube complex." Nat. Microbiol. **2**(11): 1507-1512.
298. Wang, X., Peterson, J. H. and Bernstein, H. D. (2021). "Bacterial outer membrane proteins are targeted to the Bam complex by two parallel mechanisms." MBio **12**(3): 10.1128/mbio.00597-00521.
299. Wang, X., Smith, D. R., Jones, J. W. and Chapman, M. R. (2007). "*In vitro* polymerization of a functional *Escherichia coli* amyloid protein." J. Biol. Chem. **282**(6): 3713-3719.
300. Wang, Y., Wang, R., Jin, F., Liu, Y., Yu, J., Fu, X. and Chang, Z. (2016). "A supercomplex spanning the inner and outer membranes mediates the biogenesis of β -barrel outer membrane proteins in bacteria." J. Biol. Chem. **291**(32): 16720-16729.
301. Wang, Z., Fan, G., Hryc, C. F., Blaza, J. N., Serysheva, I. I., Schmid, M. F., Chiu, W., Luisi, B. F. and Du, D. (2017). "An allosteric transport mechanism for the AcrAB-TolC multidrug efflux pump." eLife **6**: e24905.
302. Weirich, J., Bräutigam, C., Mühlenkamp, M., Franz-Wachtel, M., Macek, B., Meuskens, I., Skurnik, M., Leskinen, K., Bohn, E. and Autenrieth, I. (2017). "Identifying components required for OMP biogenesis as novel targets for anti-infective drugs." Virulence **8**(7): 1170-1188.
303. Whitfield, C. and Trent, M. S. (2014). "Biosynthesis and export of bacterial lipopolysaccharides." Annu. Rev. Biochem. **83**: 99-128.
304. Whitney, J. C., Beck, C. M., Goo, Y. A., Russell, A. B., Harding, B. N., De Leon, J. A., Cunningham, D. A., Tran, B. Q., Low, D. A., Goodlett, D. R., Hayes, C. S. and Mougous, J. D. (2014). "Genetically distinct pathways guide effector export through the type VI secretion system." Mol. Microbiol. **92**(3): 529-542.
305. Wild, J., Altman, E., Yura, T. and Gross, C. A. (1992). "DnaK and DnaJ heat shock proteins participate in protein export in *Escherichia coli*." Genes Dev. **6**(7): 1165-1172.
306. Wilkens, S. (2015). "Structure and mechanism of ABC transporters." F1000Prime Rep. **7**.

-
307. Yan, N. (2015). "Structural biology of the major facilitator superfamily transporters." Annu. Rev. Biophys. **44**(1): 257-283.
308. Yan, Z., Yin, M., Chen, J. and Li, X. (2020). "Assembly and substrate recognition of curli biogenesis system." Nat. Commun. **11**(1): 1-10.
309. Yin, Y., Zhang, F., Ling, V. and Arrowsmith, C. H. (1995). "Structural analysis and comparison of the C-terminal transport signal domains of hemolysin A and leukotoxin A." FEBS Lett. **366**(1): 1-5.
310. Yousefian, N., Ornik-Cha, A., Poussard, S., Decossas, M., Berbon, M., Daury, L., Taveau, J.-C., Dupuy, J.-W., Đorđević-Marquardt, S. and Lambert, O. (2021). "Structural characterization of the EmrAB-TolC efflux complex from *E. coli*." Biochim. Biophys. Acta **1863**(1): 183488.
311. Zaitseva, J., Jenewein, S., Jumpertz, T., Holland, I. B. and Schmitt, L. (2005). "H662 is the linchpin of ATP hydrolysis in the nucleotide-binding domain of the ABC transporter HlyB." EMBO J. **24**(11): 1901-1910.
312. Zaitseva, J., Oswald, C., Jumpertz, T., Jenewein, S., Wiedenmann, A., Holland, I. B. and Schmitt, L. (2006). "A structural analysis of asymmetry required for catalytic activity of an ABC-ATPase domain dimer." EMBO J. **25**(14): 3432-3443.
313. Zechner, E. L., Lang, S. and Schildbach, J. F. (2012). "Assembly and mechanisms of bacterial type IV secretion machines." Philos. Trans. R. Soc. Lond., Ser. B: Biol. Sci. **367**(1592): 1073-1087.
314. Zhang, F., Yin, Y., Arrowsmith, C. H. and Ling, V. (1995). "Secretion and circular dichroism analysis of the C-terminal signal peptides of HlyA and LktA." Biochemistry **34**(13): 4193-4201.
315. Zhang, M., Shi, H., Zhang, X., Zhang, X. and Huang, Y. (2020). "Cryo-EM structure of the nonameric CsgG-CsgF complex and its implications for controlling curli biogenesis in Enterobacteriaceae." PLoS Biol. **18**(6): e3000748.
316. Zhao, H., Lee, J. and Chen, J. (2022). "The hemolysin A secretion system is a multi-engine pump containing three ABC transporters." Cell **185**(18): 3329-3340.
317. Zheng, J. and Leung, K. Y. (2007). "Dissection of a type VI secretion system in *Edwardsiella tarda*." Mol. Microbiol. **66**(5): 1192-1206.
318. Zoued, A., Brunet, Y. R., Durand, E., Aschtgen, M.-S., Logger, L., Douzi, B., Journet, L., Cambillau, C. and Cascales, E. (2014). "Architecture and assembly of the type VI secretion system." Biochim. Biophys. Acta, Mol. Cell Res. **1843**(8): 1664-1673.
319. Zoued, A., Durand, E., Santin, Y. G., Journet, L., Roussel, A., Cambillau, C. and Cascales, E. (2017). "TssA: the cap protein of the type VI secretion system tail." Bioessays **39**(10): 1600262.
320. Zwama, M., Yamasaki, S., Nakashima, R., Sakurai, K., Nishino, K. and Yamaguchi, A. (2018). "Multiple entry pathways within the efflux transporter AcrB contribute to multidrug recognition." Nat. Commun. **9**(1): 124.

6. List of Abbreviations

Å	Ångstrom
aaRS	aminoacyl-tRNA synthetase
ABC	ATP-binding cassette
ACP	acyl carrier protein
AbK	3'-Azibutyl-N-carbamoyl-lysine (= photolysine)
A-LPS	A-lipopolysaccharide
ATP	adenosine triphosphate
AU	airy unit
BAM	β-barrel assembly machinery
bp	base pair
Bpa	p-benzoyl-L-phenylalanine
chHlyB	chimeric HlyB
CBB	coomassie brilliant blue
cDNA	complementary DNA
CL	cardiolipin
CLD	C39 peptidase-like domain
co-IP	co-immunoprecipitation
cryo-EM	cryogenic electron microscopy
cryo-ET	cryogenic electron tomography
CTD	C-terminal domain
Da	dalton
DAP	2,6-diaminopimelic acid

DNA	deoxyribonucleic acid
DTT	dithiotreithol
<i>E. coli</i>	<i>Escherichia coli</i>
eGFP	enhanced green fluorescent protein
EMSA	electrophoresis mobility shift assay
<i>et al.</i>	<i>et alii</i> (and others)
FC14	fos-choline-14
gDNA	genomic DNA
GG repeats	glycine-rich repeats
GST	glutathione S-transferase
GTP	guanosine triphosphate
IFO	inward facing open
IM	inner membrane
IMAC	immobilized metal ion affinity chromatography
IMC	inner membrane complex
IPTG	isopropyl- β -D-thiogalacto-pyranoside
HlyA	hemolysin A
HlyA*	HlyA amber mutant
HlyA1	C-terminal 218 amino acids of HlyA
HlyB	hemolysin B
HlyB*	HlyB amber mutant
HlyC	hemolysin C
HlyD	hemolysin D
HRV	human rhinovirus

List of Abbreviations

kbar	kilobar
K _D	dissociation constant
kDa	kilodalton
<i>K. kingae</i>	<i>Kingella kingae</i>
Lol	localization of lipoproteins
LPS	lipopolysaccharide
M	molar
MARTX	multifunctional autoprocessing repeats in toxins
MATE	multidrug and toxin extrusion
MBP	maltose binding protein
MCP	MS2 coat protein
MCS	multiple cloning site
MDa	megadalton
MFP	membrane fusion protein
MFS	major facilitator superfamily
mg	milligram
min	minutes
ml	milliliter
mM	nanomolar
mRNA	messenger RNA
MWCO	molecular weight cut-off
NAG	<i>N</i> -acetylglucosamine
NAM	<i>N</i> -acetylmuramic acid
NBD	nucleotide-binding domain

NBS	nucleotide-binding site
Ni-NTA	nickel nitrilotriacetic acid
nm	nanometer
nM	nanomolar
OD ₆₀₀	optical density at 600 nm
OFO	outward facing open
OM	outer membrane
OMC	outer membrane complex
OMCC	outer membrane core complex
OMP	outer membrane protein
ori	origin of replication
PA	phosphatidic acid
pBLAST	protein basic local alignment search tool
PBS	phosphate buffered saline
PCAT	peptidase-containing ABC transporter
PCR	polymerase chain reaction
PDB	protein data bank
PE	phosphatidylethanolamine
PFA	paraformaldehyde
PG	phosphatidylglycerol
PI	phosphatidylinositol
P _i	inorganic phosphate
PMF	proton motif force
PP	periplasm

List of Abbreviations

PS	phosphatidylserine
RMSD	root mean square deviation
RNA	ribonucleic acid
RND	resistance-nodulation-division
rRNA	ribosomal RNA
RT	room temperature
rpm	rotations per minute
RTX	repeats in toxins
SAXS	small angle X-ray scattering
Sct	unified secretion and cellular translocation
SEC	size exclusion chromatography
Sec	general secretion
SDS-PAGE	sodium dodecyl sulfate polyacrylamide gel electrophoresis
sec	second
SMR	small multidrug resistance
SRP	signal recognition particle
SPR	surface plasmon resonance
Tat	twin-arginine translocation
TC	transporter component
TMD	transmembrane domain
TMH	transmembrane helix
tRNA	transfer RNA
TTC	tail tube/sheath complex
T1SS	type I secretion system

T2SS	type II secretion system
T3SS	type III secretion system
T4CP	type IV coupling protein
T4SS	type IV secretion system
T5SS	type V secretion system
T6SS	type VI secretion system
T7SS	type VII secretion system
T8SS	type VIII secretion system
T9SS	type IX secretion system
UAA	unnatural amino acid
UPEC	uropathogenic <i>Escherichia coli</i>
UV	ultraviolet
WT	wildtype
°C	degrees Celsius
μl	microliter
μM	micromolar
μs	microsecond

7. List of Figures

Figure 1: General secretion pathways in bacteria.....	5
Figure 2: Structural organization of an RND system and T1SS.....	10
Figure 3: Structural organization of a T2SS.....	12
Figure 4: Structural organization of a T3SS.....	14
Figure 5: Structural organization of a T4SS.....	16
Figure 6: Structural organization of secretion systems spanning the outer membrane.....	17
Figure 7: Structural organization of a T6SS.....	19
Figure 8: Structural organization of a T7SS.....	20
Figure 9: Structural organization of a T9SS.....	23
Figure 10: Structural features of HlyA and CyaA.....	27
Figure 11: Conserved motifs of the HlyB-NBD (PDB: 1XEF).....	29
Figure 12: Architecture of the HlyB-HlyD complex and related transport systems.....	31
Figure 13: Architecture and interaction of membrane fusion proteins (MFP).....	33
Figure 14: Conformational changes of the outer membrane protein TolC.....	35
Figure 15: Schematic overview of the HlyA secretion mechanism.....	36
Figure 16: Possible substrate binding by one CLD of HlyB.....	218
Figure 17: Suggested interactions between HlyB domains and other Hly proteins during complex formation and secretion.....	225

8. Acknowledgements

Zuallererst möchte ich mich bei meinem Doktorvater Prof. Dr. Lutz Schmitt bedanken. Vielen Dank Lutz, dass ich unter Deinen Fittichen an diesem spannenden, wenn auch herausfordernden Projekt arbeiten durfte. Ich weiß es sehr zu schätzen, dass Deine Tür sprichwörtlich immer offen stand, und man mit Dir immer über alles sprechen konnte. Danke für Deine großartigen Ideen, aber auch dafür, dass Du mir den Freiraum gegeben hast, eigene Ideen und Ansätze auszuprobieren. Danke auch für das Ermöglichen, gerade so noch vor dem ganzen „Corona-Chaos“ auf Konferenz gehen zu können. Dein Optimismus und Deine Leidenschaft, trotz aller Herausforderungen und Hürden, ist wirklich legendär. Bleib immer so, und ich hoffe, dass ein wenig davon auf mich abfärben konnte.

Ein weiteres großes „Dankeschön“ geht an Prof. Dr. Sander Smits. Sander, ich mag Deine unkomplizierte, ehrliche und direkte Art. Deine kritischen Fragen und Diskussionen in den *subgroup meetings* und Seminaren waren wirklich hilfreich. Danke für Deine frischen Ideen und die Motivation für alle Projekte. Du hast eine unvergleichlich mitreißende und sympathische Art, insbesondere auch in der Lehre, die ich wirklich bewundernswert finde. Immer wenn Du gut-gelaunt-summend über die Gänge gelaufen bist, hat es mir ein Schmunzeln aufs Gesicht gezaubert.

Wenn ich das Biochemie-Studium und die Zeit an der Universität reflektiere, darf eine Person nicht vergessen werden: PD Dr. Ulrich Schulte. Uli, es ist schwer, sich die Düsseldorfer Biochemie ohne Dich vorzustellen. Ich werde Dir für Deine herzliche und faire Betreuung vom Bachelor bis zur Promotion, die erstklassige Organisation der Praktika und Vergabe fähiger Bachelorstudentinnen immer dankbar sein. Du bist viel zu früh von uns gegangen, aber ich werde dein Lachen nie vergessen.

Prof. Dr. Michael Feldbrügge möchte ich für die freundliche Übernahme des Korreferats danken. Deine Betrachtung der Projekte aus einem anderen Blickwinkel war wichtig und hilfreich. Danke für deine Expertise im Bereich *mRNA imaging*. An dieser Stelle möchte ich mich auch bei Dr. Kira Müntjes für die Bereitstellung von Plasmiden bedanken.

Wo wir gerade bei Expertise sind: Ich möchte mich herzlich bei Prof. Dr. Samuel Wagner bedanken, welcher eine große Hilfe und Ideenquelle rund um die unnatürlichen Aminosäuren war. Ebenso dankbar bin ich Prof. Dr. Stefanie

Weidtkamp-Peters. Deine Hilfe und Betreuung bei der Fluoreszenzmikroskopie war super und wegweisend. Auch möchte ich Dr. Gereon Poschmann für die Analyse der Massenspektrometrie danken.

Dann möchte ich zunächst allen ehemaligen Kollegen des Instituts für Biochemie danken, die mir bereits im Master ein warmes „Willkommen“ gegeben haben und zu Beginn der Promotion eine große Hilfe waren: Ganz besonders möchte ich meiner Master-Betreuerin Dr. Olivia Spitz danken. Oli, Du bist wirklich einzigartig – but in a good way. Mit Dir war es wirklich nie langweilig. Ich hätte mir keine bessere Betreuerin vorstellen können, die mich in die Membranproteinforschung eingeführt hat. Wir haben uns sofort super verstanden, und ich habe sehr gerne für Dich und mit Dir am Typ 1 System und den Homologen geforscht. Sei es über unsere Projekte oder Videospiele, man konnte sich mit Dir immer super unterhalten, gerne auf der Couch mit einem frischen Kaffee.

Dr. Tobias „Papabär“ Beer. Es war mir eine Ehre auch mit Dir am Hämolsin System gearbeitet zu haben. Wenn es um neue, interessante Publikationen, eine neue Methode oder die neuesten Memes ging: Als „Adoptivkind“ des Lab29 wusste ich, zu wem ich gehen konnte. Man konnte mit Dir immer wunderbar fachsimpeln und nebenbei jede Menge unnützes Wissen ansammeln. Danke auch für die Aufnahme in die Whiskey-Gruppe und das Montagabendliche Alumni-Treffen, ich hoffe, wir können diese spaßige Runde noch lange beibehalten. In diesem Zuge möchte ich Dr. Michael Lenders und Dr. Sven Reimann danken, zwei Veteranen der Montagabend-Runde und Typ-1-Gruppe (aka „die alte Riege“). Auch wenn Ihr schon länger aus dem Labor raus seid und ich Euch nur einmal im Bachelor in Aktion erleben konnte (Michael: „Was wollen die sch*ß Studenten hier oben?“. Sven: „Mensch Michael!“), wart Ihr mir direkt sympathisch und man konnte Euch auch Jahre später immer noch mit Fragen rund um Typ 1 löchern. Danke dafür, und bis Montag!

Auch Teil der Montagabendlichen Runde und jemand, der mich seit dem ersten Biochemie Praktikum geprägt hat: The One-and-Only, der Fürst der Finsternis, Dr. Marcel Lagedroste. Deine Betreuung während der Praktika ist immer noch die Beste während des gesamten Studiums gewesen. Damals hätte ich nicht damit gerechnet, dass ein Praktikumsbetreuer eine NBD EQ-Mutante mit Lee Sin verbinden würde (LOL, im doppelten Sinne). Du bist wirklich ein Alleskönner und Vorbild: Super intelligent, fleißig und es gab kaum eine Methode oder ein Gerät, zu der Du keinen

Tipp parat hattest. Man konnte Dich immer zu Allem fragen. Es war mir eine Ehre, mit Florestan als junge Padawane Deine Verantwortung für die Äktas übernommen zu haben. Auch wir hören uns Montag!

Auch möchte ich Dr. Kerstin Kanonenberg und Dr. Isabelle Erenburg danken. Rund um die Aufreinigung von HlyB, HlyA, den Malachitgrün-Assay und die homologen Systeme, Eure Erfahrung war wirklich hilfreich. Also, thank you Dr. Zohreh Pourhassan. It was nice to work with you, discuss new ideas, mutants for the hemolysin system and cloning techniques.

Dr. Tim Kroll, Dr. Martin Prescher, und mein Namensvetter Dr. Manuel Wagner. Euch nenne ich zusammen als „Drug-resistance Boys“. Wenn mal irgendwas mit dem Cell-Disruptor oder den Äktas nicht lief oder ein SEC-MALS brauchte, konnte man sich auf Euch verlassen. Auch abseits der Arbeit waren die Whiskey-tastings und LAN-Parties mit Euch echt klasse. Danke für die schöne Zeit.

Dr. Julia Schumacher, Deine Kreativität im Labor wie für Doktorwagen und -hüte war erstaunlich. Und wenn man mal tatkräftige Unterstützung brauchte, egal ob bei der Reparatur von Egal-was oder handwerkliches Geschick bei den Doktorwagen: Dr. Jens Reiners war Der Mann dafür. Vielen Dank auch für Deine SAXS Analysen.

Dr. Alexandra Bork, Feby Chacko, Julia Gottstein und Vivien Knospe. Danke für die schöne Arbeitsatmosphäre, kulinarischen Erkundungen und (ich nenne es mal) „Abenteuer an der Äkta“ =).

Stefanie Gala Marti und Lea-Marie Nentwig, die „PDR Ladies“. Danke für die schöne Zeit mit Euch. Steffi, wir haben uns damals im Master zusammen im selben Labor mit den ATPasen rumgeschlagen... und Du zusätzlich noch mit Tim. Es hat Spaß gemacht mit Dir nach dem „schönsten“ Western Blot zu eifern – alles natürlich rein objektiv. Danke auch, dass Du (und natürlich Valentin) mich an Magic herangeführt habt. Ich hoffe, wir können die Commander Runden noch lange aufrechterhalten – eines Tages vielleicht sogar mit Amelie ;) . Lea, ich weiß noch, wie Du damals deine Bachelorarbeit bei Steffi gemacht hast. Schön, dass du für den Master und schließlich auch für die Promotion zurückgekommen bist. Das Institut hat mit Dir eine wirklich liebe und kompetente Forscherin gewonnen. Wissenschaftliche (und unwissenschaftliche) Gespräche mit Dir waren immer eine Freude. Ich weiß, ich habe die Verantwortung der Kaffeekasse bei Dir in die richtigen Hände gelegt, Du packst das! Auch die

Einführung Deines „Eimers“ ist klasse. Sorge dafür, dass immer einer vorrätig ist, man weiß ja nie, wann es etwas zu feiern (oder zu trösten) gibt. Ich wünsche Dir viel Erfolg! Nun jemand, bei dem ich glücklich bin, ihn zu meinen besten Freunden zählen zu können: Florestan Bilsing. Du warst der erste andere Biochemiker, der mich damals an der Uni angesprochen hat. Danke, dass ich Teil einer tollen (wenn nicht sogar der besten) Studien- und Freundesgruppe in der Biochemie sein durfte. Ich weiß, ich kann manchmal etwas *socially awkward* sein. Danke deshalb, dass Du es trotzdem mit mir so lange ausgehalten hast. Wir sind das ganze Studium über durch dick und dünn gegangen. Zusammen haben wir die Äktas (und damit praktisch das ganze Institut) am Laufen gehalten. Wir waren Leidensgenossen in **dem einen** Projekt. Sich gegenseitig die Schulter zu leihen, wenn ein Experiment mal wieder nicht geklappt hat, ließ so manche schwierige Zeit besser aushalten. Dein Input war immer hilfreich, sei es eine kritische Frage oder eine Idee für ein weiteres Kontrollexperiment. Danke für diese wundervolle Zeit, und ich wünsche Dir das allerbeste auf Deinem weiteren Weg. Du bist einer der kompetentesten und engagiertesten Wissenschaftler, die ich kenne. Du wirst es noch weit bringen, das weiß ich.

Eymen Hachani, danke für die angenehme Arbeitsatmosphäre. Mit Dir rumzublödeln war wirklich erheiternd. Schön, dass auch Du dich nicht vom Hämolysin System hast unterkriegen lassen und mit HlyD am Ball geblieben bist. Pass gut auf das MALS auf. Auch Dir alles Gute und viel Erfolg. Mashallah!

Hans Hannig, auch wir kennen uns seit dem ersten Semester. Schön, dass auch Du so lange durchgehalten hast. Die Gespräche rund um Proteinstrukturen und Mutanten, PyMOL, den täglichen Laborwahnsinn und Videospiele waren wirklich erheiternd. Ich bin gespannt auf die VanW Struktur, lass da bloß nicht nach ;) .

I also want to thank our best PostDoc, Dr. Sakshi Khosa. Awesome to have you back in the team. Thank you for all the nice discussions, encouraging words and all the help and advices during my final steps. Thank you for all the proofreading and always being honest. You are a really kind person. And don't be afraid of cloning. It might be voodoo, but it is easy voodoo ;) .

Besonderer Dank geht an unser TA-Team, die alles am Laufen halten, Martina Wesemann und Silke Mavaro. Martina, ohne Dich würde das Institut vermutlich implodieren. Egal um was es ging: Man findet mal wieder eine Chemikalie oder ein Gerät nicht, es ist etwas kaputt gegangen oder es musste etwas bestellt werden. Du

warst immer für einen da. Danke für die Tipps und Hilfe beim Klonieren der unzähligen Mutanten. Hoffentlich kannst Du noch viele Jahre über das Institut wachen. Der Tag, an dem Du gehst, wird ein trauriger Tag für das Institut sein. Auch Dir danke ich Silke, für die Organisation und Hilfe mit dem Gentechnik-Papierkram. Und wenn mal wieder die Kompis zur Neige gingen: Auf Dich konnte man sich verlassen.

Ich danke auch allen Neuzugängen im Institut für die schönen letzten Monate im Labor: Lars Bostelmann-Arp, Sergiy Gan, Cigdem Günes, Christian Mammen, Kira Tantsur und Neele Wolff. Ich weiß noch, wie ich viele von Euch damals in meinem ersten „Biochemie II“ bzw. „Faszination Biochemie“ Praktikum betreut habe. Insbesondere meiner Nachfolgerin Cigdem wünsche ich viel Glück und alles Gute mit Ihren Projekten. Ebenso danke ich unseren neuen Nachwuchsgruppenleitern Dr. Miriam Kutsch und Dr. Marten Exterkate für die schöne Zeit und Gespräche. Ich wünsche Euch viel Erfolg sowie fleißige, kompetente und – was noch viel wichtiger ist – nette Doktoranden und/oder PostDocs. Ich wünsche außerdem unserem neuen Studiengangskoordinator Dr. Jan Stindt alles Gute. Du trittst in große Fußstapfen, aber Du wirst das Biochemie Studium in Düsseldorf bestimmt mit vielen frischen Ideen bereichern.

Unseren Sekretärinnen Mathilde Blum, Tatjana Platz und Corinna Franzkowiak danke ich für die Hilfe mit und das Abnehmen von dem ganzen Papierkram, von dem man als Labor-Mensch nun so wirklich gar keine Ahnung hatte.

Many thanks and all the best to the “Synthetic Membrane Systems” group of Prof Dr. Alexej Kedrov. It was an unusual sight to see a PI working right next to his PhD students. Keep up the enthusiasm, and thank you for all the advices and plasmids, when I needed a new ori for compatibility. Maryna Löwe, Deine Photoshop-Künste sind wirklich legendär und Einblicke in *membrane crowding* waren super interessant. Ich wünsche Dir alles Gute auf deinem weiteren Weg. Michael Kamel, thank you for the help with the gradient station, density gradient centrifugation and learning the most important arabic words with you and Athanasios. All the best to you! Athanasios Papadopoulos, ich erinnere mich noch, wie Du damals im ersten Semester das ZellMol Biologie Tutorium geleitet hast. Du warst damals schon super sympathisch. Wissenschaftliche und auch alle anderen Diskussion mit Dir sind immer interessant. Es ist schön, Dich auch in Zukunft „Kollege“ nennen zu dürfen.

Nicht zu vergessen, möchte ich mich auch bei meinen Studentinnen bedanken, die mich tatkräftig unterstützt haben: Meike Wagner, Vanessa Averin, Marie-Luise Johanningmann, Francesca Grant und Julia Speckmaier. Ich hoffe, ich habe Euch nicht zu sehr mit meinem Perfektionismus und den Verständnisfragen getriezt, ich habe es wirklich nur gut gemeint. Ich hoffe, dass Ihr während eurer Zeit bei mir einiges gelernt habt.

Vielen Dank auch an den SFB1208, der diese Arbeit finanziert hat, für all die Expertise seiner Mitglieder und Einblicke in die Membranforschung. Ganz besonderer Dank geht dabei an unsere Koordinatorin, Dr. Cordula Kruse. Cordula, danke für das Organisieren aller Konferenzen, Retreats, Kurse etc. Du hast das super gemacht. Entschuldige bitte, wenn ich mal wieder vergessen habe, die Unterlagen vom TAC Meeting abzugeben. Ups ;)

Besonderer Dank geht auch an meine Freunde, bei denen ich während der Promotion Rückhalt finden konnte. Gary und Robert, die ich nun schon seit der Grundschule kenne: Ich bin froh, Euch als Freunde zu haben. Auch die oben bereits erwähnte beste „Holland Urlaub“ Studiengruppe soll hier erwähnt werden: Nora, Alex, Anne, Florestan (nochmal), Lea, Leonie, Niklas, Maurice und Vivian. Die Zeit mit Euch während dem Studium war wirklich eine der schönsten, die ich je hatte. Hoffentlich können wir den jährlichen Urlaubs-Ausflug beibehalten!

Mein größter Dank geht zum Schluss an meine Familie: Ein riesiges Dankeschön an meine Eltern Dorothee und Hans-Bernhard für die bedingungslose Liebe und Unterstützung. Egal was war, ich konnte (und kann) mich immer auf Euch verlassen. Ihr habt mir so viel während dem Studium geholfen und so viel Last von den Schultern genommen, vielen lieben Dank! Auch ein großes Danke an meinen Bruder Benedikt. Wir sind zwar nicht immer einer Meinung, trotzdem konnte ich mich während des Studiums immer auf Deine Hilfe verlassen.

Ich danke außerdem allen Menschen, die hier zwar nicht namentlich erwähnt sind, auf deren Unterstützung ich dennoch zählen konnte und beim Gelingen dieser Arbeit geholfen haben.

9. Curriculum vitae

Personal Data

Name: Manuel Tobias Anlauf

Date of Birth: 29.03.1994

Place of Birth: Duisburg, Germany

e-Mail: manuel.anlauf@uni-duesseldorf.de

University Education

since Jan 2019 **Doctorate**

Heinrich Heine University Düsseldorf

Institute of Biochemistry

Supervisor Prof. Dr. Lutz Schmitt

Thesis: *Mutational and functional investigation of hemolysin A secretion in Escherichia coli*

Oct 2016 – Nov 2018 **Master of Science, Biochemistry** (overall grade 1.2)

Heinrich Heine University Düsseldorf

Institute of Biochemistry

Prof. Dr. Lutz Schmitt

Thesis: *Characterization of the ABC transporter of the hemolysin A type I secretion system via homologous proteins*

Oct 2013 – Sep 2016 **Bachelor of Science, Biochemistry** (overall grade 1.7)

Heinrich Heine University Düsseldorf

Institute of Biochemistry

Prof. Dr. Vlada B. Urlacher

Thesis: *Enhancement of copper content in bacterial laccases*

School Education

Aug 2004 – Jun 2013 General qualification for university entrance (Abitur),
overall grade 1.3

Reinhard-und-Max-Mannesmann-Gymnasium in
Duisburg, Germany

Participation at scientific conferences

Sep 2022 GBM Fall conference 2022 “Molecular basis of life”,
Düsseldorf, Germany (poster presentation)

Mar 2022 3rd International CRC1208 conference “Dynamic in
Membrane Systems”, Düsseldorf, Germany (poster
presentation)

Sep 2021 CRC1208 Internal Retreat 2021, Krefeld, Germany (oral
presentation)

Mar 2020 8th FEBS Special Meeting on ATP-Binding cassette
(ABC) proteins: “From Multidrug Resistance to Genetic
Disease”, Innsbruck, Austria (poster presentation)

Mar 2019 2nd International CRC1208 conference “Dynamics of
Membrane Systems”, Düsseldorf, Germany (poster
presentation)

10. Declaration

Ich versichere an Eides statt, dass die vorliegende Dissertation von mir selbstständig und ohne unzulässige fremde Hilfe unter Beachtung der „Grundsätze zur Sicherung guter wissenschaftlicher Praxis an der Heinrich-Heine-Universität Düsseldorf“ erstellt worden ist. Diese Dissertation wurde in der vorgelegten oder in ähnlicher Form noch bei keiner anderen Institution eingereicht. Ich habe bisher keine erfolglosen oder erfolgreichen Promotionsversuche unternommen.

(Ort, Datum)

Manuel Anlauf